

Theoretical Studies on Selected Organic Chalcogen Systems

By

Rahul Kumar

CHEM01201404024

Bhabha Atomic Research Centre, Mumbai

A thesis submitted to the

Board of Studies in Chemical Sciences

In partial fulfilment of requirements

for the Degree of

DOCTOR OF PHILOSOPHY

of

HOMI BHABHA NATIONAL INSTITUTE

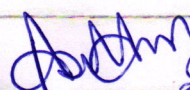
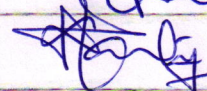
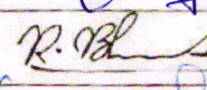
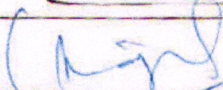
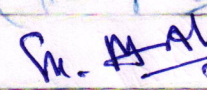
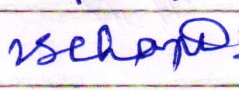


June, 2020

Homi Bhabha National Institute

Recommendations of the Viva Voce Committee

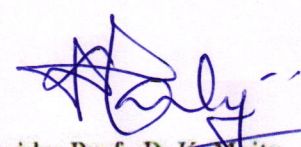
As members of the Viva Voce Committee, we certify that we have read the dissertation prepared by Mr. Rahul Kumar entitled "Theoretical Studies on Selected Organic Chalcogen Systems" and recommend that it may be accepted as fulfilling the thesis requirement for the award of Degree of Doctor of Philosophy.

Composition	Name	Signature with date
Chairman	Prof. A. K. Arya	 27/05/20
Convener (Guide)	Prof. D. K. Maity	 27/05/2020
External Examiner	Prof. R. B. Sunoj, IIT Bombay	 27/5/20
Member-1	Prof. C. Majumder	 27/05/20
Member-2	Prof. Musharaf Ali	 27/5/20
Member-3	Prof. KRS. Chandrakumar	 27/05/2020

Final approval and acceptance of this thesis is contingent upon the candidate's submission of the final copies of the thesis to HBNI.

I/We hereby certify that I/we have read this thesis prepared under my/our direction and recommend that it may be accepted as fulfilling the thesis requirement.

Date: 27 May 2020
Place: Mumbai


Guide: Prof. D. K. Maity

STATEMENT BY AUTHOR

This dissertation has been submitted in partial fulfilment of requirements for an advanced degree at Homi Bhabha National Institute (HBNI) and is deposited in the Library to be made available to borrowers under rules of the HBNI.

Brief quotations from this dissertation are allowable without special permission, provided that accurate acknowledgement of source is made. Requests for permission for extended quotation from or reproduction of this manuscript in whole or in part may be granted by the Competent Authority of HBNI when in his or her judgment the proposed use of the material is in the interests of scholarship. In all other instances, however, permission must be obtained from the author.

Rahul Kumar

Rahul Kumar

DECLARATION

I, hereby declare that the investigation presented in the thesis has been carried out by me. The work is original and has not been submitted earlier as a whole or in part for a degree/diploma at this or any other Institution / University.

Rahul Kumar

Rahul Kumar

List of Publications arising from the thesis

Journals:

1. “Effect of Excess Electron on Structure, Bonding and Spectral Properties of Sulfur/Selenium Based Dichalcogen Systems”, Rahul Kumar and Dilip Kumar Maity, *International Journal of Quantum Chemistry*, **2017**, 119, e25855 (Cover page article).
- *2. “Pulse Radiolysis and Computational Studies on a Pyrrolidinium Dicyanamide Ionic Liquid: Detection of the Dimer Radical Anion”, Laboni Das, Rahul Kumar, Dilip Kumar Maity, Soumyakanti Adhikari Surajdevprakash B. Dhiman and James F. Wishart, *Journal of Physical Chemistry A*, **2018**, 122, 3148-3155.
3. “Structure, Stability and Spectral Properties of Seleno[n]helicenes (n=1-10)”, Rahul Kumar and Dilip Kumar Maity, *New Journal of Chemistry*, **2020**, 44, 428-441.
4. “End substituted thiahelicenes for electronic device applications”, Rahul Kumar and Dilip Kumar Maity, *International Journal of Quantum Chemistry*, **2020**, (revised and submitted).
5. “A DFT study on molecular structure and electronic properties of novel tellurophene based helicenes”, Rahul Kumar and Dilip Kumar Maity, *Journals for physical chemistry and chemical physics*. **2020**, (revised & submitted).
6. “Band gaps of chalcogen based [n]helicenes (chalcogen = S, Se and Te) at the polymer limit predicted using oligomer approach”, Rahul Kumar and Dilip Kumar Maity, **2020** (under preparation).

*Not included in the thesis.

Conferences:

1. Rahul Kumar and Dilip Kumar Maity, "Theoretical Studies on Radical cations of β -Oligomers of Selenium, *DAE-BRNS Symposium on Selenium Chemistry & Biology (SSCB)*, November 9-11, 2017, Mumbai, India.
2. Rahul Kumar and Dilip Kumar Maity, Theoretical Studies on Radical cations of β -Oligomers of Furan, Thiophene & Selenophene, *14th DAE-BRNS Biennial Trombay Symposium on Radiation & Photochemistry (TSRP)*, January 3-7, 2018, Mumbai, India.
3. Rahul Kumar and Dilip Kumar Maity, Theoretical Studies on S/Se Based Dichalcogenides with an Excess Electron: Insight on Structure, Stability, Bonding and Spectral Properties, *DAE-BRNS 7th Interdisciplinary Symposium on Materials Chemistry (ISMC)*, December 4-8, 2018, Mumbai, India.
4. Rahul Kumar and Dilip Kumar Maity, Comparative Study on Electronic Properties of Thia[n]helicene and Seleno[n]helicene ($n=1-10$), *The First DAE Computational Chemistry Symposium, (DAE-CCS)*, November 7-9, 2019, Mumbai, India.
5. Rahul Kumar and Dilip Kumar Maity, A Theoretical Study on Excited State Properties of Tellurium Based β -Helicenes, *15th DAE-BRNS Biennial Trombay Symposium on Radiation & Photochemistry (TSRP)*, January 5-9, 2020, Mumbai, India.

Rahul Kumar

Rahul Kumar

Dedicated to Family, Teachers, and Friends

ACKNOWLEDGMENT

I would like to express my deepest gratitude to my supervisor **Dr. Dilip Kumar Maity** for his valuable guidance, patience, encouragement and the freedom given to me in carrying out research. Apart from the scientific knowledge, the discipline, which I learned from my supervisor is indispensable to my growth as a Ph.D. student and as a person. I considered myself to be honoured and fortunate to be associated with him.

Besides my Ph.D. guide, I would like to thank the rest of my doctoral committee members: Chairman of the committee, Dr. Ashok Kumar Arya, Dr. Chiranjib Majumder, Dr. KRS. Chandrakumar, and Dr. Sk. Musharaf Ali. Their insightful comments, encouragement and their hard questions, incited me to widen my research from various perspectives.

I would like to thank my friends and fellow graduate students, Dr. Ashish S., Dr. Abhishek K., Dr. Anshu S., Dr. Sankarrao C., Dr. Parvathi K., Alok D., Kartik K., Dr. Vinod B., Dr. Tribeni R., Dr. Anuj S., Deepika A., Rakhee Y., Dr. Arohi D., Sriram K., Bharat B., Taslim S., Viswa T., and Akash C., for the many fruitful discussions and merry memories.

It was my parents who first instilled in me the motivation for learning and their hard work has prepared me for higher education. Special thank goes to my mother Mrs. Mukesh Devi and my father Mr. Vinesh Kumar. It is impossible for me to finish this thesis without their support, encouragement and sacrifice. Thanks to my brother Mr. Sonu Kumar, my sister Mrs. Sudha Ojha and my dear friends for their constant support, love and care. I would like to thank my entire family for supporting emotionally throughout this journey and my life in general.

CONTENTS

	Page No.
Abstract	xii
List of Figures.....	xviii
List of Tables	xxi
CHAPTER 1 Introduction	1
1.1 Overview of thiophene based optical materials	2
1.2 Overview of selenophene based optical materials	4
1.3 Overview of tellurophene based optical materials	5
1.4 Molecular spectroscopy along with quantum-based calculations to design novel materials for device applications.....	6
1.5 Chalcogen based helical systems for optoelectronic device applications	7
1.6 Overview of diaryl dichalcogenides (S, Se and Te) based antioxidant systems	9
1.7 Motivation of the thesis	10
1.8 Brief overview of thesis	11
CHAPTER 2 Theoretical Background.....	16
2.1 Born-Oppenheimer Approximation	17
2.2 Theoretical model chemistry	18
2.3 Hartree-Fock Approximation.....	19
2.4 Post HF methods	23
2.4.1 Møller-Plesset (MP) perturbation theory	23
2.5 Coupled Cluster Theory	23
2.6 Density Functional Theory	24
2.6.1 Local Density Approximations (LDA), Generalized Gradient Approximation Functional (GGA), Hybrid Functionals	27
2.7 Basis Sets	28

2.8	Self-Consistent Reaction Field theories: Effect of Solvation.....	30
2.9	Geometry Optimization and Hessian calculations	31
2.10	Molecular Orbitals	34
2.11	Time-dependent density functional theory	34
2.12	Periodic Boundary Calculations for Band gap and Band structure	35
 CHAPTER 3 Structures, Stability and Spectral Properties of Thia[n]helicene (n=1-10) and their Corresponding Radical Cations..... 37		
3.1	Introduction.....	37
3.2	Theoretical Methods.....	39
3.3	Results and Discussions	40
3.3.1	Structure for thia[n]helicenes, [n]TH, n=1-10 in DCM solvent.....	40
3.3.2	Ionization energies for thia[n]helicenes, [n]TH, n=1-10 in DCM solvent	46
3.3.3	HOMO-LUMO gap for thia[n]helicenes, [n]TH, n=1-10 in DCM solvent.....	48
3.3.4	Structure for radical cations of thia[n]helicenes, [n]TH ⁺ , n=1-10 in DCM solvent.....	50
3.3.5	HOMO-LUMO energy gap for thia[n]helicenes radical cation, [n]TH ⁺ , n=1-10 in DCM solvent	57
3.3.6	Excited state electronic spectra for radical cations of thia[n]helicenes, [n]TH ⁺ , n=1-10 in DCM	58
3.3.7	Dimerization of neutral and radical cation of thia[7]helicene in DCM solvent...	64
3.4	Conclusions.....	70
 CHAPTER 4 Effect of Size on Structures, Stability and Spectral Properties of Seleno[n]helicenes (n=1-10) and their Corresponding Radical Cations..... 72		
4.1	Introduction.....	72
4.2	Theoretical Methods.....	74
4.3	Results and Discussions	75

4.3.1	Most stable structures of seleno[n]helicenes, [n]SH, n=1-10 in DCM solvent	75
4.3.2	Ionization energies of seleno[n]helicenes, [n]SH, n=1-10 in DCM solvent	80
4.3.3	Energy gap of seleno[n]helicenes, [n]SH, n=1-10 in DCM solvent	81
4.3.4	Most stable structures of radical cations of seleno[n]helicenes, [n]SH ⁺ , n=1-10	82
4.3.5	Energy gap for radical cations of seleno[n]helicenes, [n]SH ⁺ , n=1-10	89
4.3.6	Excited state electronic spectra for radical cations of seleno[n]helicenes, [n]SH ⁺ , n=1-10 in gas phase and in DCM.....	91
4.3.7	Dimerization of neutral and radical cation of thia[7]helicene in DCM solvent ...	96
4.4	Conclusions.....	101

CHAPTER 5 Comparative Study on Band Gap of Chalcogen (S, Se and Te) based β -Helicenes and Spectral Properties of their Corresponding Radical Cations102

5.1	Introduction.....	102
5.2	Computational methods.....	104
5.3	Results and Discussions	106
5.3.1	Structure for neutral telluro[n]helicene, [n]TeH, n=1-10 in DCM solvent.....	106
5.3.2	Comparison of ionization energies (IE) of thia[n]helicenes, seleno[n]helicenes and telluro[n]helicenes (n=1-10) in DCM solvent.....	111
5.3.3	Comparison of HOMO-LUMO energy gap of thia[n]helicenes, seleno[n]helicenes and telluro[n]helicenes (n=1-10) in DCM solvent	113
5.3.4	Most stable structures of telluro[n]helicene radical cations, [n]TeH ⁺ , n=1-10, in DCM solvent	114
5.3.5	PBC-DFT calculation for band gap of thia[n]helicenes, seleno[n]helicenes, and telluro[n]helicenes (n=1-10).....	119
5.3.6	Excited-state electronic spectra for telluro[n]helicenes radical cation, n=1-10 in DCM solvent	121
5.3.7	Dimerization of neutral and radical cation of telluro[7]helicene in DCM solvent.....	124

5.4	Conclusions.....	127
 CHAPTER 6: Effect of Excess Electron on Structure, Bonding and Spectral Properties of Diaryl Based Dichalcogen (S, Se and Te) Systems129		
6.1	Introduction.....	129
6.2	Theoretical Methods.....	132
6.3	Results and Discussions	133
6.3.1	Structures of (Ph-Ch) ₂ ^{•-} radical anions (Ch = S, Se, & Te).....	135
6.3.2	Effect of electron-donating ortho-substituted groups: Structures of (o-R-PhCh) ₂ ^{•-} radical anions (Ch = S, Se & Te; R= CH ₃ & OH).....	142
6.3.3	Effect of electron-withdrawing ortho-substituted group: Structures of (o-R-Ph-Ch) ₂ ^{•-} radical anions (Ch = S, Se & Te; R = NO ₂).....	148
6.3.4	Effect of geometrical flexibility: Structures of (o-PhCH ₂ -Ch) ₂ ^{•-} radical anions (Ch = S, Se & Te).....	152
6.3.5	Stability of (R-Ch) ₂ ^{•-} radical anions (Ch = S, Se & Te; R=Ph, o-CH ₃ -Ph, o-HO-Ph, o-NO ₂ -Ph, and PhCH ₂) in water medium	155
6.3.6	Excited state for (R-Ch) ₂ ^{•-} radical anions (Ch = S, Se & Te; R=Ph, o-CH ₃ -Ph, and o-HO-Ph) systems	161
6.3.7	Frontier molecular orbital for the (o-CH ₃ -Ph-Te) ₂ ^{•-} radical anionics system....	165
6.4	Conclusions.....	167
 CHAPTER 7: Summary and Future Perspectives.....168		
REFERENCES.....		171

List of Figures

- Figure 3.1** Most stable structures of neutral thia[n]helicenes, [n]TH, n=1-10 a) [1]TH, b) [2]TH, c) [3]TH, e) [4]TH, f) [5]TH, g) [6]TH, h) [7]TH, i) [8]TH, j) [9]TH and k) [10]TH, with selected geometrical parameters calculated at B3LYP-D/6-311++G(d,p) level of theory in DCM solvent. d) is the most stable structure of thia[3]helicene calculated at MP2 is /6-311++G(d,p) level of theory in DCM solvent. 45
- Figure 3.2** Most stable structures (a-j) for radical cation of thia[n]helicenes, [n]TH^{•+}, n=1-10 a) [1]TH^{•+}, b) [2]TH^{•+}, c) [3]TH^{•+}, d) [4]TH^{•+}, e) [5]TH^{•+}, f) [6]TH^{•+}, g) [7]TH^{•+}, h) [8]TH^{•+}, i) [9]TH^{•+}, and j) [10]TH^{•+} with selected geometrical parameters calculated at B3LYP-D/6-311++G(d,p) level of theory in DCM solvent. 54
- Figure 3.3** Spin density plot for thia[n]helicene radical cation at B3LYP-D/6-311++G(d,p) level of theory in DCM solvent with contour cutoff= 0.002 a.u. 56
- Figure 3.4** Simulated UV-Vis spectra for radical cations of thia[n]helicenes, n[TH]^{•+} a) n=1-5 and b) 6-10 in DCM solvent following TDDFT procedure at CAM-B3LYP/6-311++G(d,p) level of theory. 60
- Figure 3.5** Selected molecular orbital plots (a1-c2) for radical cations of thia[n]helicenes, a1) H orbital of [1]TH^{•+}, a2) L orbital of [1]TH^{•+}, a3) H-2 orbital of [1]TH^{•+}, b1) H-1 orbital of [3]TH^{•+}, b2) L orbital of [3]TH^{•+} c1) H-4 orbital of [7]TH^{•+}, c2) L orbital of [7]TH^{•+}, and c3) H-1 orbital of [7]TH^{•+} based on most stable structures in DCM solvent. The figures are taken at isovalue of 0.002 a.u. 62
- Figure 3.6** Most stable π -dimeric structure of a) neutral unsubstituted thia[7]helicene monomer b) neutral substituted thia[7]helicene monomer, c) radical cation of unsubstituted thia[7]helicene monomer, d) radical cation of substituted thia[7]helicene monomer, e) unsubstituted thia[7]helicene monomer radical cation with PF₆⁻ counter ions, f) end substituted thia[7]helicene monomer radical cation with PF₆⁻ counter ions. Calculated at B3LYP-D/6-311++G(d,p) level of theory in DCM solvent. 67
- Figure 4.1** Most stable structures (a-j) of neutral seleno[n]helicenes, [n]SH, n=1-10 a) [1]SH, b) [2]SH, c) [3]SH, d) [4]SH, e) [5]SH, f) [6]SH, g) [7]SH, h) [8]SH, i) [9]SH, and j) [10]SH, with selected geometrical parameters calculated at B3LYP-D/6-311++G(d,p) level of theory in DCM solvent. 79
- Figure 4.2** Most stable structures (a-j) for radical cation of end substituted seleno[n]helicenes [n]SH^{•+}, n=1-10 a) [1]SH^{•+}, b) [2]SH^{•+}, c) [3]SH^{•+}, d) [4]SH^{•+}, e) [5]SH^{•+}, f) [6]SH^{•+}, g) [7]SH^{•+}, h) [8]SH^{•+}, i) [9]SH^{•+}, and j) [10]SH^{•+}, with selected geometrical parameters calculated at B3LYP-D/6-311++G(d,p) level of theory in DCM solvent. 86
- Figure 4.3** Spin density plot for the radical cation of end substituted seleno[7]helicene at the B3LYP-D/6-311++G(d,p) level of theory in DCM solvent with contour cutoff = 0.004 a.u. 88
- Figure 4.4** UV-Vis spectra for radical cations of end substituted seleno[n]helicenes in DCM solvent, [1]SH^{•+}, a) n=1-5 and b) n=6-10 following TDDFT procedure at CAM-B3LYP/6-311++G(d,p) level of theory. 93
- Figure 4.5** Selected molecular orbital diagram of most stable structures of seleno[n]helicenes, [n]SH^{•+} n=1,3,7 a1) H-2 orbital of [1]SH^{•+}, a2) L orbital of [1]SH^{•+}, b1) H orbital of [3]SH^{•+}, b2) L orbital of [3]TH^{•+}, c1) H-5 orbital of [7]SH^{•+}, c2) L orbital of [7]SH^{•+}, and c3) H-1 orbital

of [7]SH⁺ calculated at B3LYP-D/6-311++G(d,p) level of theory in DCM solvent. The figures are taken at isovalue of 0.002 a.u..... 94

Figure 4.6 Most stable π -dimeric structure of a) neutral unsubstituted seleno[7]helicene monomer, b) neutral substituted seleno[7]helicene monomer, c) radical cation of unsubstituted seleno[7]helicene monomer, d) radical cation of substituted seleno[7]helicene monomer, e) radical cation of unsubstituted seleno[7]helicene monomer with PF₆⁻ counter anion, f) radical cation of substituted seleno[7]helicene monomer with PF₆⁻ counter anion. Calculated at B3LYP-D/6-311++G(d,p) level of theory in DCM solvent.....98

Figure 5.1 Most stable structures of (a-j) telluro[n]helicenes, [n]TeH, n=1-10, a) [1]TeH, b) [2]TeH, c) [3]TeH, d) [4]TeH, e) [5]TeH, f) [6]TeH, g) [7]TeH, h) [8]TeH, i) [9]TeH, and j) [10]TeH, with with selected geometrical parameters calculated at B3LYP-D functional with 6-311++G(d,p) basis set for H, C, Si, Br atoms and 3-21G basis set for Te atoms in DCM solvent. 109

Figure 5.2 Comparison of the calculated ionization energies (in eV) of thia[n]helicenes, seleno[n]helicenes and telluro[n]helicenes at B3LYP-D level of theory in DCM solvent. 6-311++G(d,p) basis set for S, Se, H, C, Br, Si atoms and 3-21G basis set for Te atom is used for the all calculations..... 112

Figure 5.3 Comparison of calculated HOMO-LUMO energy gap (in eV) of thia[n]helicenes, seleno[n]helicenes and telluro[n]helicenes at B3LYP-D level of theory in DCM solvent. 6-311++G(d,p) basis set for S, Se, H, C, Br, Si atoms atoms and 3-21G basis set for Te atom is used for the all calculations. 114

Figure 5.4 Most stable structures (a-j) of telluro[n]helicenes radical cation, [n]TeH⁺, n=1-10, a) [1]TeH⁺, b) [2]TeH⁺, c) [3]TeH⁺, d) [4]TeH⁺, e) [5]TeH⁺, f) [6]TeH⁺, g) [7]TeH⁺, h) [8]TeH⁺, i) [9]TeH⁺, and j) [10]TeH⁺ with selected geometrical parameters calculated at B3LYP-D with 6- 311++G(d,p) basis set for H, C, Si, and Br atoms and 3-21G basis set for Te atoms in DCM solvent..... 117

Figure 5.5 Comparison of calculated band gap for thia[n]helicenes, seleno[n]helicenes, and telluro[n]helicenes calculated using PBC-BLYP method with periodic boundary condition. 3-21G basis is for Te atoms and for all other atoms 6-31G(d) basis set is used with periodic boundary condition (PBC)..... 120

Figure 5.6 UV-Vis spectra for radical cations of end substituted telluro[n]helicenes, [n]TeH⁺ in DCM solvent, a) n=1-5 and b) n=6-10 c) comparison of calculated UV-Visible spectra of [7]TH⁺, [7]SH⁺ and [7]TeH⁺. TDDFT procedure is applied to generate the UV-Vis spectra calculated using CAM-B3LYP functional with 6-311++G(d,p) basis set for H, C, S, Se, Br, Si atoms and 3-21G for Te atoms. 123

Figure 5.7 Most stable π -dimeric structure of a) neutral unsubstituted telluro[7]helicene monomer, b) neutral end substituted telluro[7]helicene monomer, c) unsubstituted telluro[7]helicene monomer radical cation, d) end substituted telluro[7]helicene monomer radical cation, e) unsubstituted telluro[7]helicene monomer radical cation with PF₆⁻ counter ions, f) end substituted telluro[7]helicene monomer radical cation with PF₆⁻ counter ions Calculated at B3LYP-D functional with 6- 311++G(d,p) basis set for H, C, Si, Br, P, F atoms and 3-21G basis set for Te atoms in DCM solvent..... 126

Figure 6.1 a) Most stable structure of (PhS)₂^{•-} radical anion in the gas phase, b) second possible structure of (PhS)₂^{•-} radical anion in the gas phase, c) most stable structure of (PhS)₂^{•-} radical anion in water medium, d) most stable structure of (PhSe)₂^{•-} radical anion in water medium,

and e) most stable structure of $(\text{PhTe})_2^{\bullet-}$ radical anion in water medium. Method: MP2 level of theory with 6-311++G(d,p) basis set for H, C, S, and Se atoms and 3-21G* for Te atoms. ΔE represents the relative energy of the higher energy structure with respect to the most stable one.

..... 141

Figure 6.2 Most stable structures in water medium, a) $(\text{o-CH}_3\text{-PhS})_2^{\bullet-}$ radical anion, b) $(\text{o-CH}_3\text{-PhSe})_2^{\bullet-}$ radical anion, c) $(\text{o-CH}_3\text{-PhTe})_2^{\bullet-}$ radical anion, d) $(\text{o-HO-PhS})_2^{\bullet-}$ radical anion, e) $(\text{o-HO-PhSe})_2^{\bullet-}$ radical anion, and f) $(\text{o-HO-PhTe})_2^{\bullet-}$ radical anion. Method: MP2 level of theory, Basis set: 6-311++G(d,p) for H, C, O, S, Se atoms and 3-21G* for Te atoms..... 147

Figure 6.3 Most stable structures in water medium, a) $(\text{o-NO}_2\text{-PhS})_2^{\bullet-}$ radical anion, b) $(\text{o-NO}_2\text{-PhSe})_2^{\bullet-}$ radical anion and, c) $(\text{o-NO}_2\text{-PhTe})_2^{\bullet-}$ radical anion Method: MP2 level of theory, Basis set: 6-311++G(d,p) for H, C, N, O, S, Se atoms and 3-21G* for Te atoms.... 151

Figure 6.4 Most stable structures in water medium, a) $(\text{PhCH}_2\text{S})_2^{\bullet-}$ radical anion, b) $(\text{PhCH}_2\text{Se})_2^{\bullet-}$ radical anion, and c) $(\text{PhCH}_2\text{Te})_2^{\bullet-}$ radical anion, Method: MP2 level of theory, Basis set: 6-311++G(d,p) for H, C, S, Se atoms and 3-21G* for Te atoms. 154

Figure 6.5 UV-Vis spectra calculated at CAM-B3LYP level of theory, a) $(\text{PhCh})_2^{\bullet-}$ (Ch = S, Se & Te) radical anions in water medium (b) $(\text{o-CH}_3\text{-PhCh})_2^{\bullet-}$ radical anions in water medium, c) $(\text{PhCh})_2^{\bullet-} \cdot 2\text{H}_2\text{O}$. Basis set: 6-311++G(d,p) for C, H, O, S and Se atoms and 3-21G* for Te atoms. 164

Figure 6.6 Molecular orbital diagrams for $(\text{o-CH}_3\text{-PhTe})_2^{\bullet-}$ calculated at MP2 level of theory with 3-21G* basis for Te atoms and 6-311++G(d,p) for all other atoms in water medium. (HDOMO = highest doubly occupied molecular orbital and LSOMO = lowest singly occupied molecular orbital. Molecular orbital diagrams are plotted with contour cut-off value of 0.04 a.u..... 166

List of Tables

Table 3.1 Selected geometrical parameters of neutral thia[n]helicenes, [n]TH n=1-10 calculated at B3LYP-D /6-311++G(d,p) level of theory in gas phase. Values in the braces show corresponding geometrical parameters neutral thia[n]helicenes, n=1-10 in DCM solvent. Bold-faced values in third braces are calculated at B3LYP/6-311++G(d,p) level of theory in DCM solvent.	42
Table 3.2 Calculated ionization energy (in eV) of thia[n]helicenes, [n]TH, n=1-10 in gas phase applying different theoretical methods. Values in the braces are the corresponding energy in DCM solvent.....	47
Table 3.3 Calculated HOMO-LUMO energy gap (in eV) of thia[n]helicenes, [n]TH, n=1-10 in the gas phase. Values in the braces are the corresponding energy gaps of neutral thia[n]helicenes in DCM solvent. Data shown in bold faces are the experimental values from the literature.	49
Table 3.4 Selected geometrical parameters for radical cations of thia[n]helicenes, [n]TH ⁺ n=1-10 calculated at B3LYP-D /6-311++G(d,p) level of theory in gas phase. Values in the braces show corresponding geometrical parameters for radical cations of thia[n]helicenes, n=1-10 in DCM solvent. Bold-faced values in third braces are calculated at B3LYP/6-311++G(d,p) level of theory in DCM solvent.....	52
Table 3.5 Calculated HDOMO-LSOMO energy gap (in eV) for radical cations of thia[n]helicenes, [n]TH ⁺ , n=1-10 in DCM solvent. Values in the braces are the corresponding LSOMO-LUMO gaps for radical cations of thia[n]helicenes in DCM solvent. HDOMO refers to the highest doubly occupied molecular orbital, LSOMO stands for the lowest singly occupied molecular orbital and LUMO stands for the lowest unoccupied molecular orbital. 57	57
Table 3.6 Calculated excited state data for the radical cations of thia[n]helicenes, [n]TH ⁺ (n=1-10) in DCM solvent considering CAM-B3LYP/6-311++G(d,p) level of theory under TDDFT formalism.	57
Table 4.1 Selected geometrical parameters of neutral end substituted seleno[n]helicenes, n=1-10 calculated at B3LYP-D/6-311++G(d,p) level of theory in gas phase. Values in the first braces show corresponding geometrical parameters of neutral end substituted seleno[n]helicenes, n=1-10 in DCM solvent. Bold faced values in third braces are calculated at B3LYP/6-311++G(d,p) level of theory in DCM solvent.	77
Table 4.2 Calculated ionization energies (in eV) of neutral seleno[n]helicenes, [n]SH, n=1-10 in the gas phase applying different theoretical methods. Values in braces are corresponding ionization energies in DCM solvent.....	81
Table 4.3 Calculated HOMO-LUMO energy gap (in eV) of neutral seleno[n]helicenes, [n]SH, n = 1-10 in gas phase. Values in braces are corresponding energy gap of neutral seleno[n]helicenes in DCM solvent.	82
Table 4.4 Selected geometrical parameters of end substituted seleno[n]helicenes radical cation, n=1-10 calculated at B3LYP-D/6-311++G(d,p) level of theory in gas phase. Values in the first braces show corresponding geometrical parameters of end substituted seleno[n]helicenes radical cation, n=1-10 in DCM solvent. Bold faced values in third braces are calculated at B3LYP/6-311++G(d,p) level of theory in DCM solvent.	84

Table 4.5 Calculated HOMO-LUMO and LUMO-LUMO energy gap (in eV) for radical cations of seleno[n]helicenes, [n]SH ⁺ , n=1-10 in DCM solvent. Values in the braces are corresponding LUMO-LUMO energy gap for radical cations of seleno[n]helicenes, [n]SH ⁺ in DCM solvent.....	90
Table 4.6 Calculated excited state data for radical cations of seleno[n]helicenes [n]SH ⁺ , n=1-10 in DCM solvent considering CAM-B3LYP/6-311++G(d,p) level of theory under TDDFT formalism. Value in the braces are excited state data for radical cations of seleno[n]helicenes [n]SH ⁺ , n=1-10 in DCM solvent considering same level of theory.	92
Table 5.1 Selected geometrical parameters of neutral end substituted telluro[n]helicenes, n=1-10 calculated at B3LYP-D with 6-311++G(d,p) basis set for H, C, Si, and Br atoms and 3-21G basis set for Te atoms in DCM solvent. The value in the braces are calculated at B3LYP functional with the same basis set in DCM solvent.	107
Table 5.2 Calculated ionization energies (in eV) of telluro[n]helicenes, [n]TeH, n=10 in DCM solvent.	111
Table 5.3 Calculated HOMO-LUMO energy gap (in eV) of neutral telluro[n]helicenes, [n]TeH (n=1-10) in DCM solvent.	113
Table 5.4 Selected geometrical parameters of neutral end substituted telluro[n]helicenes radical cation, n=1-10 calculated at B3LYP-D with 6-311++G(d,p) basis set for H, C, Si, and Br atoms and 3-21G basis set for Te atoms in DCM solvent. The value in the braces are calculated at B3LYP functional with same basis set in DCM solvent.....	115
Table 5.5 Direct Band gap (in eV) of thia[n]helicenes ([n]TH), seleno[n]helicenes ([n]SH), and telluro[n]helicenes ([n]TeH), n=1-10 calculated using PBC-BLYP method with periodic boundary condition. 3-21G basis is being used for Te atom and 6-31G(d) basis set for all other atoms are considered.	119
Table 6.1 Selected geometrical and molecular parameters of diphenyl dichalcogenides, (PhS) ₂ (Ch = Se and Te) in at the different levels of theory. Values in the braces show the parameters for the systems in presence of an excess electron (PhS) ₂ ^{•-}	137
Table 6.2 Selected geometrical and molecular parameters of diphenyl dichalcogenides, (PhCh) ₂ (Ch = Se and Te) in at the different levels of theory. Values in the braces show the parameters for the systems in presence of an excess electron (PhCh) ₂ ^{•-}	138
Table 6.3 Selected geometrical and molecular parameters of diphenyl dichalcogenides, (o-CH ₃ -PhCh) ₂ (Ch = S, Se and Te) in water medium at the different levels of theory. Values in the braces show the parameters for the systems in presence of an excess electron (o-CH ₃ -PhCh) ₂ ^{•-}	144
Table 6.4 Selected geometrical and molecular parameters of diphenyl dichalcogenides, (o-HO-PhCh) ₂ (Ch = S, Se and Te) in water medium at the different levels of theory. Values in the braces show the parameters for the systems in presence of an excess electron (o-HO-PhCh) ₂ ^{•-}	145
Table 6.5 Selected geometrical and molecular parameters of (o-NO ₂ -PhCh) ₂ (Ch = S, Se and Te) in water medium at the different levels of theory. Values in the braces show the parameters for the systems in the presence of an excess electron (o-NO ₂ -PhCh) ₂ ^{•-}	150

Table 6.6 Selected geometrical and molecular parameters of diphenyl disulfide, (PhCH ₂ Ch) ₂ (S, Se and Te) in water medium at the different levels of theory. Values in the braces show the parameters for the systems in presence of an excess electron (Ph CH ₂ Ch) ₂ ^{•-}	153
Table 6.7 Energy data for neutral (o-R-Ph-Ch) ₂ (Ch = S, Se and Te; R = H, CH ₃ , and OH; Ch = S, Se and Te) in water medium at the different levels of theory. Values in the braces show the energy data for the systems in presence of an excess electron.	157
Table 6.8 Energy data for neutral (o-NO ₂ -Ph-Ch) ₂ (Ch = S, Se and Te), and (PhCH ₂ Ch) ₂ in water medium at the different levels of theory. Values in the braces show the energy data for the systems in presence of an excess electron.	158
Table 6.9 Excited state data for (RCh) ₂ ^{•-} (Ch = S, Se & Te: R = Ph, and o-CH ₃ -Ph) and (PhCh) ₂ ^{•-} .2H ₂ O radical anions in water medium.	162

CHAPTER 7

Summary and Future Perspectives

This thesis is a significant contribution to the progress of thiophene, selenophene, and tellurophene based helical systems in optoelectronic device applications. Extended π -conjugation with unique molecular structures, these systems have suitable electronic properties for optical applications in neutral as well as in their radical cationic state. Comparative studies on chalcogen based β -helicenes (Chalcogen = S, Se and Te) show that energy gap of these systems decreases not only as the number of rings increases but also as the size and polarization of chalcogen atoms increases. Band gaps of telluro[n]helicenes (3.3-1.8 eV) calculated applying periodic boundary conditions based method are lower than those of corresponding thia[n]helicenes (3.8-3.0 eV) and seleno[n]helicenes (3.6-2.4 eV) systems. Excited-state study for radical cations of substituted thiophene, selenophene and tellurophene based helicenes in DCM solvent elucidates that these systems strongly absorb in visible and near NIR region of electromagnetic spectrum. Thus, these systems may find their applications in NIR devices. Optical absorption bands obtained in UV-Visible spectra for telluro[7]helicene radical cation have stronger absorption compared to the peaks obtained for thia[7]helicene and seleno[7]helicene radical cations in DCM solvent. The stability of these substituted chalcogen based helical systems in neutral and radical cationic state is another crucial aspect that has been evoked in this work. Substituted neutral thia[n]helicenes and seleno[n]helicenes have very low probability of dimerization in non-polar solvent. This dimerization probability is much lower in substituted radical cations of thia[n]helicenes and seleno[n]helicenes. In the presence of counter ion PF_6^- this dimerization probability is further reduced. Though dimerization probability in telluro[7]helicene radical cation is more than that of the corresponding

thia[7]helicene and seleno[n] helicene radical cations, this dimerization probability is further reduced in the presence of counter ion, PF_6^- .

This study provides a strategy for fine-tuning energy gap by replacing individual chalcogen atoms or changing the numbers of aromatic rings of helicenes systems. This work definitely benefits the thiophene, selenophene and tellurophene chemistry researchers and chalcogen chemistry as a whole. As the future aspects, the mixed helicene systems formed by coupling and fusion of thiophene, selenophene and tellurophene may also provide novel candidates for device applications. As these theoretical results are providing novel candidates for optical applications, this work can serve as a motivating ground for future experimental investigations.

In addition to selected chalcogen based helical systems for device applications, a model for understanding the antioxidant behaviour of diaryl dichalcogenides (S, Se and Te) radical anions is also included in this thesis. Due to partial interactions of pi orbitals from two phenyl rings, the most stable structures of diaryl dichalcogenides radical anion shows pi-pi stacking between two phenyl rings except in dibenzyl dichalcogenides radical anion in water medium. Binding energies for dichalcogenides radical anion increases as the size and polarizability of chalcogen atom increases. Use of macroscopic (solvation model based on solute density) and discrete solvent models to consider the effect of aqueous medium further increases the reliability of present work. A useful strategy for modulation of antioxidant properties of diaryl dichalcogenides is by introducing the electron-donating groups at ortho-position in phenyl rings. On substituting the electron-donating groups at the ortho position of the phenyl rings, the binding energies of the radical anions are increased compared to the unsubstituted radical anion. However, binding energies of the radical anions are decreased compared to the unsubstituted radical anion on substituting the electron withdrawing group at the ortho position

of phenyl rings. The binding energies of dibenzyl dichalcogenides radical anion are calculated to be lower than their corresponding diphenyl dichalcogenides radical anion. These observations indicate that geometrical flexibility does not play a significant role to stabilize these radical anions and electronic effects are expected to play a major role to stabilize/destabilize these systems. It is expected that these diaryl based diselenide and ditelluride systems can provide potential antioxidant molecules to encounter the oxidative stress responsible for several human disorders. Introduction the electron-donating groups at para-position in phenyl rings may become an alternate possible strategy for modulation of antioxidant properties of diaryl dichalcogenides. This can further expand the knowledge model for understanding the antioxidant behaviour of these systems.

In the future, the studies on the measurement of antioxidant activity can be carried to calculate the kinetics data of the reaction between free radicals and dichalcogen based antioxidant systems. In-vitro and in-vivo experimental studies may be carried out to decide on a suitable dichalcogen based antioxidant system

REFERENCES

- (1) Lin, Y.; Zhan, X. Oligomer Molecules for Efficient Organic Photovoltaics. *Acc. Chem. Res.* **2016**, *49* (2), 175-183.
- (2) Ostroverkhova, O. Organic Optoelectronic Materials: Mechanisms and Applications. *Chem. Rev.* **2016**, *116* (22), 13279-13412.
- (3) Cicoira, B. F.; Santato, C. Organic Light Emitting Field Effect Transistors : Advances and Perspectives. *Adv. Funct. Mater.* **2007**, *17* (17), 3421-3434.
- (4) Gidron, O.; Bendikov, M. α -Oligofurans: An Emerging Class of Conjugated Oligomers for Organic Electronics. *Angew. Chem. Int. Ed.* **2014**, *53* (10), 2546-2555.
- (5) Cinar, M. E.; Ozturk, T. Thienothiophenes, Dithienothiophenes, and Thienoacenes: Syntheses, Oligomers, Polymers, and Properties. *Chem. Rev.* **2015**, *115* (9), 3036-3140.
- (6) Böttger-Hiller, F.; Mehner, A.; Anders, S.; Kroll, L.; Cox, G.; Simon, F.; Spange, S. Sulphur-Doped Porous Carbon from a Thiophene-Based Twin Monomer. *Chem. Commun.* **2012**, *48* (85), 10568–10570.
- (7) Miyaura, K.; Miyata, Y.; Thendie, B.; Yanagi, K.; Kitaura, R.; Yamamoto, Y.; Arai, S.; Kataura, H.; Shinohara, H. Extended-Conjugation π -Electron Systems in Carbon Nanotubes. *Sci. Rep.* **2018**, *8* (1), 2-7.
- (8) Barbarella, G.; Melucci, M.; Sotgiu, G. The Versatile Thiophene: An Overview of Recent Research on Thiophene-Based Materials. *Adv. Mater.* **2005**, *17* (13), 1581-1593.
- (9) Barbarella, G.; Favaretto, L.; Sotgiu, G.; Zambianchi, M.; Bongini, A.; Arbizzani, C.; Mastragostino, M.; Anni, M.; Gigli, G.; Cingolani, R. Tuning Solid-State Photoluminescence Frequencies and Efficiencies of Oligomers Containing One Central Thiophene-S,S-Dioxide Unit. *J. Am. Chem. Soc.* **2000**, *122* (48), 11971-11978.
- (10) Gigli, G.; Inanäs, O.; Anni, M.; De Vittorio, M.; Cingolani, R.; Barbarella, G.; Favaretto, L. Multicolor Oligothiophene-Based Light-Emitting Diodes. *Appl. Phys. Lett.* **2001**, *78* (11), 1493-1495.
- (11) Pasini, M.; Destri, S.; Porzio, W.; Botta, C.; Giovanella, U. Electroluminescent Poly(Fluorene-Co-Thiophene-S,S-Dioxide): Synthesis, Characterisation and Structure-Property Relationships. *J. Mater. Chem.* **2003**, *13* (4), 807-813.
- (12) McCullough, R. D. The Chemistry of Conducting Polythiophenes. *Adv. Mater.* **1998**, *10* (2), 1-44.
- (13) Liu, J.; Sheina, E.; Kowalewski, T.; McCullough, R. D. Tuning the Electrical Conductivity and Self-Assembly of Regioregular Polythiophene by Block

- Copolymerization: Nanowire Morphologies in New Di- and Triblock Copolymers. *Angew. Chem. Int. Ed.* **2002**, *41* (2), 329-332.
- (14) Nicolas, Y.; Blanchard, P.; Levillain, E.; Allain, M.; Mercier, N.; Roncali, J. Planarized Star-Shaped Oligothiophenes with Enhanced π -Electron Delocalization. *Org. Lett.* **2004**, *6* (2), 273-276.
 - (15) Su, Y. Z.; Lin, J. T.; Tao, Y. T.; Ko, C. W.; Lin, S. C.; Sun, S. S. Amorphous 2,3-Substituted Thiophenes: Potential Electroluminescent Materials. *Chem. Mater.* **2002**, *14* (4), 1884-1890.
 - (16) Ponomarenko, S. A.; Kirchmeyer, S.; Elschner, A.; Huisman, B. H.; Karbach, A.; Drechsler, D. Star-Shaped Oligothiophenes for Solution-Processible Organic Field-Effect Transistors. *Adv. Funct. Mater.* **2003**, *13* (8), 591-596.
 - (17) Xia, C.; Fan, X.; Locklin, J.; Advincula, R. C.; Gies, A.; Nonidez, W. Characterization, Supramolecular Assembly, and Nanostructures of Thiophene Dendrimers. *J. Am. Chem. Soc.* **2004**, *126* (28), 8735-8743.
 - (18) Chung, T.-C.; Kaufman, J. H.; Heeger, A. J.; Wudl, F. Charge Storage in Doped Poly(Thiophene): Optical and Electrochemical Studies. *Phys. Rev. B* **1984**, *30* (2), 702-710.
 - (19) Lubis, P.; Saito, M. Band Gap Design of Thiophene Polymers Based on Density Functional Theory. *Jpn. J. Appl. Phys.* **2014**, *53* (6), 071602 (1-7).
 - (20) Kaloni, T. P.; Giesbrecht, P. K.; Schreckenbach, G.; Freund, M. S. Polythiophene: From Fundamental Perspectives to Applications. *Chem. Mater.* **2017**, *29* (24), 10248-10283.
 - (21) Mehmood, U.; Al-Ahmed, A.; Hussein, I. A. Review on Recent Advances in Polythiophene Based Photovoltaic Devices. *Renew. Sust. Energ. Rev.* **2016**, *57*, 550-561.
 - (22) Nielsen, C. B.; McCulloch, I. Recent Advances in Transistor Performance of Polythiophenes. *Prog. Polym. Sci.* **2013**, *38* (12), 2053-2069.
 - (23) Tyler McQuade, D.; Pullen, A. E.; Swager, T. M. Conjugated Polymer-Based Chemical Sensors. *Chem. Rev.* **2000**, *100* (7), 2537-2574.
 - (24) Zhang, X.; Côté, A. P.; Matzger, A. J. Synthesis and Structure of Fused α -Oligothiophenes with up to Seven Rings. *J. Am. Chem. Soc.* **2005**, *127* (30), 10502-10503.
 - (25) Fichou, D. Structural Order in Conjugated Oligothiophenes and Its Implications on Opto-Electronic Devices. *J. Mater. Chem.* **2000**, *10* (3), 571-588.
 - (26) McClure, S. A.; Buriak, J. M.; Dilabio, G. A. Transport Properties of Thiophenes: Insights from Density-Functional Theory Modeling Using Dispersion-Correcting Potentials. *J. Phys. Chem. C* **2010**, *114* (24), 10952-10961.

- (27) Lin, P. P.; Zhang, S. F.; Zhang, N. X.; Fan, J. X.; Ji, L. F.; Guo, J. F.; Ren, A. M. Theoretical Study on the Charge Transport Properties of Three Series of Dicyanomethylene Quinoidal Thiophene Derivatives. *Phys. Chem. Chem. Phys.* **2019**, *21* (6), 3044-3058.
- (28) Hendriksen, B. L. M.; Martin, F.; Qi, Y.; Mauldin, C.; Vukmirovic, N.; Ren, J.; Wormeester, H.; Katan, A. J.; Altoe, V.; Aloni, S.; et al. Electrical Transport Properties of Oligothiophene-Based Molecular Films Studied by Current Sensing Atomic Force Microscopy. *Nano Lett.* **2011**, *11* (10), 4107-4112.
- (29) Nguyen, T. L.; Lee, T. H.; Gautam, B.; Park, S. Y.; Gundogdu, K.; Kim, J. Y.; Woo, H. Y. Single Component Organic Solar Cells Based on Oligothiophene-Fullerene Conjugate. *Adv. Funct. Mater.* **2017**, *27* (39), 1-9.
- (30) Liu, J.; Li, R.; Si, X.; Zhou, D.; Shi, Y.; Wang, Y.; Jing, X.; Wang, P. Oligothiophene Dye-Sensitized Solar Cells. *Energy Environ. Sci.* **2010**, *3* (12), 1924-1928.
- (31) Osuna, R. M.; Ruiz Delgado, M. C.; Hernández, V.; López Navarrete, J. T.; Vercelli, B.; Zotti, G.; Novoa, J. J.; Suzuki, Y.; Yamaguchi, S.; Henssler, J. T.; et al. Oxidation of End-Capped Pentathienoacenes and Characterization of Their Radical Cations. *Chem. Eur. J.* **2009**, *15* (45), 12346-12361.
- (32) Tateno, M.; Takase, M.; Iyoda, M.; Komatsu, K.; Nishinaga, T. Steric Control in the π -Dimerization of Oligothiophene Radical Cations Annulated with Bicyclo[2.2.2]Octene Units. *Chem. Eur. J.* **2013**, *19* (17), 5457-5467.
- (33) Mazzio, K. A.; Yuan, M.; Okamoto, K.; Luscombe, C. K. Oligoselenophene Derivatives Functionalized with a Diketopyrrolopyrrole Core for Molecular Bulk Heterojunction Solar Cells. *ACS Appl. Mater. Interfaces* **2011**, *3* (2), 271-278.
- (34) Ibanez, J. G.; Rincón, M. E.; Gutierrez-Granados, S.; Chahma, M.; Jaramillo-Quintero, O. A.; Frontana-Uribe, B. A. Conducting Polymers in the Fields of Energy, Environmental Remediation, and Chemical-Chiral Sensors. *Chem. Rev.* **2018**, *118* (9), 4731-4816.
- (35) Sung, M. J.; Luzio, A.; Park, W. T.; Kim, R.; Gann, E.; Maddalena, F.; Pace, G.; Xu, Y.; Natali, D.; de Falco, C.; et al. High-Mobility Naphthalene Diimide and Selenophene-Vinylene-Selenophene-Based Conjugated Polymer: N-Channel Organic Field-Effect Transistors and Structure-Property Relationship. *Adv. Funct. Mater.* **2016**, *26* (27), 4984-4997.
- (36) Lee, J.; Han, A.; Kim, J.; Kim, Y.; Oh, J. H.; Yang, C. Solution-Processable Ambipolar Diketopyrrolopyrrole-Selenophene Polymer with Unprecedentedly High Hole and Electron Mobilities. *J. Am. Chem. Soc.* **2012**, *134* (51), 20713-20721.
- (37) Karabay, B.; Pekel, L. C.; Cihaner, A. A Pure Blue to Highly Transmissive Electrochromic Polymer Based on Poly(3,4-Propylenedioxy-selenophene) with a High Optical Contrast Ratio. *Macromolecules* **2015**, *48* (5), 1352-1357.

- (38) Li, X. C.; Sirringhaus, H.; Garnier, F.; Holmes, A. B.; Moratti, S. C.; Feeder, N.; Clegg, W.; Teat, S. J.; Friend, R. H. A Highly π -Stacked Organic Semiconductor for Thin Film Transistors Based on Fused Thiophenes. *J. Am. Chem. Soc.* **1998**, *120* (9), 2206-2207.
- (39) Zade, S. S.; Bendikov, M. From Oligomers to Polymer: Convergence in the HOMO-LUMO Gaps of Conjugated Oligomers. *Org. Lett.* **2006**, *8* (23), 5243-5246.
- (40) Zade, S. S.; Zamoshchik, N.; Bendikov, M. Oligo- and Polyselenophenes: A Theoretical Study. *Chem. Eur. J.* **2009**, *15* (34), 8613–8624.
- (41) Patra, A.; Bendikov, M. Polyselenophenes. *J. Mater. Chem.* **2010**, *20* (3), 422-433.
- (42) Okamoto, T.; Kudoh, K.; Wakamiya, A.; Yamaguchi, S. General Synthesis of Thiophene and Selenophene-Based Heteroacenes. *Org. Lett.* **2005**, *7* (23), 5301–5304.
- (43) Janan, S. H.; A. Hasan, A. Influence of Thickness on Electrical and Optical Properties of Tellurium Thin Films Deposited by Chemical Spray Pyrolysis. *Int. J. Appl. Math. Elec.* **2015**, *3* (2), 96-101.
- (44) Edwards, D. F.; Mercado, M. Ultimate Sensitivity and Practical Performance of the Tellurium Photoconductive Detector. *Infrared Phys.* **1961**, *1* (1), 17-20.
- (45) Zhang, M.; Su, H. C.; Rheem, Y.; Hangarter, C. M.; Myung, N. V. A Rapid Room-Temperature NO₂ Sensor Based on Tellurium-SWNT Hybrid Nanostructures. *J. Phys. Chem. C* **2012**, *116* (37), 20067-20074.
- (46) Wu, X.; Lv, L.; Hu, L.; Shi, Q.; Peng, A.; Huang, H. The Synthesis and Optoelectronic Applications for Tellurophene-Based Small Molecules and Polymers. *Chem. Phys. Chem.* **2019**, *20* (20), 2600-2607.
- (47) Shida, N.; Nishiyama, H.; Zheng, F.; Ye, S.; Seferos, D. S.; Tomita, I.; Inagi, S. Redox Chemistry of π -Extended Tellurophenes. *Commun. Chem.* **2019**, *2* (1), 124 (1-9).
- (48) Ozkilinc, O.; Kayi, H. Effect of Chalcogen Atoms on the Electronic Band Gaps of Donor-Acceptor-Donor Type Semiconducting Polymers: A Systematic DFT Investigation. *J. Mol. Model.* **2019**, *25* (6) 167 (1-16).
- (49) Manion, J. G.; Ye, S.; Proppe, A. H.; Laramée, A. W.; Mckeown, G. R.; Kynaston, E. L.; Kelley, S. O.; Sargent, E. H.; Seferos, D. S. Examining Structure-Property-Function Relationships in Thiophene, Selenophene, and Tellurophene Homopolymers. *ACS Appl. Energy Mater.* **2018**, *1* (9), 5033-5042.
- (50) Al-Hashimi, M.; Han, Y.; Smith, J.; Bazzi, H. S.; Alqaradawi, S. Y. A.; Watkins, S. E.; Anthopoulos, T. D.; Heeney, M. Influence of the Heteroatom on the Optoelectronic Properties and Transistor Performance of Soluble Thiophene-, Selenophene- and Tellurophene-Vinylene Copolymers. *Chem. Sci.* **2016**, *7* (2), 1093-1099.
- (51) Ye, S.; Janasz, L.; Zajackowski, W.; Manion, J. G.; Mondal, A.; Marszalek, T.; Andrienko, D.; Müllen, K.; Pisula, W.; Seferos, D. S. Self-Organization and Charge

Transport Properties of Selenium and Tellurium Analogues of Polythiophene. *Macromol. Rapid Commun.* **2019**, *40* (1), 1-8.

- (52) Mata, R. A.; Suhm, M. A. Benchmarking Quantum Chemical Methods: Are We Heading in the Right Direction? *Angew. Chem. Int. Ed.* **2017**, *56* (37), 11011-11018.
- (53) De Visser, S. P. Getting Started in Computational Quantum Chemistry. *Frontiers in Chemistry*; **2013**; Vol. 1, pp 14.
- (54) Pretsch, E.; Bühlmann, P.; Affolter, C. *Structure Determination of Organic Compounds*, Fourth Ed.; Springer-Verlag Berlin Heidelberg, **2009**.
- (55) Ma, T.; Kapustin, E. A.; Yin, S. X.; Liang, L.; Zhou, Z.; Niu, J.; Li, L. H.; Wang, Y.; J., S.; Li, J.; W. Xiaoge.; Wang, W. D.; Wang, W.; Sun J.; Yaghi, O. M. 3,6. *Single-Crystal x-Ray Diffraction Structures of Covalent Organic Frameworks*; 2018; Vol. 361.
- (56) Lennox, D. H. X-Ray Powder Diffraction Patterns of Some Organic Compounds. *Anal. Chem.* **1957**, *29* (10), 1433-1435.
- (57) Osunas, R. M.; Ortiz, R. P.; Okamoto, T.; Suzuki, Y.; Yamaguchi, S.; Hernández, V.; Navarrete, J. T. L. Thiophene- and Selenophene-Based Heteroacenes: Combined Quantum Chemical DFT and Spectroscopic Raman and UV-Vis-NIR Study. *J. Phys. Chem. B* **2007**, *111* (26), 7488-7496.
- (58) Shen, Y.; Chen, C. F. Helicenes: Synthesis and Applications. *Chem. Rev.* **2012**, *112* (3), 1463-1535.
- (59) Meisenheimer, J.; Witte, K. Reduction von 2-Nitronaphtalin. *Chem. Ber.* **1903**, *36* (4), 4153-4164.
- (60) Wang, D. Z.; Katz, T. J.; Golen, J.; Rheingold, A. L. Diels-Alder Additions of Benzyne within Helicene Skeletons. *J. Org. Chem.* **2004**, *69* (22), 7769-7771.
- (61) Rajca, A.; Miyasaka, M. Synthesis and Characterization of Novel Chiral Conjugated Materials. In *Functional Organic Materials*; **2007**; pp 547–581.
- (62) Liu, Q.; Gao, X.; Zhong, H.; Song, J.; Wang, H. Planar Heptathienoacenes Based on Unsymmetric Dithieno[3,2-b:3',4'-d]Thiophene: Synthesis and Photophysical Properties. *J. Org. Chem.* *2016*, **2016**, *81*, 8612-8616.
- (63) Shen, Y.; Chen, C.-F. Helicenes : Synthesis and Applications. *Chem. Rev.* **2012**, *112*, 1463-1535.
- (64) Zhang, S.; Liu, X.; Li, C.; Li, L.; Song, J.; Shi, J.; Morton, M.; Rajca, S.; Rajca, A.; Wang, H. Thiophene-Based Double Helices: Syntheses, X-Ray Structures, and Chiroptical Properties. *J. Am. Chem. Soc.* **2016**, *138* (31), 10002-10010.
- (65) Rajca, A.; Wang, H.; Pink, M.; Rajca, S. Annelated Heptathiophene: A Fragment of a Carbon–sulfur Helix. *Angew. Chem. Int. Ed.* **2000**, *39* (24), 4655-4657.

- (66) Rajca, A.; Miyasaka, M.; Pink, M.; Wang, H.; Rajca, S. Helically Annelated and Cross-Conjugated Oligothiophenes: Asymmetric Synthesis, Resolution, and Characterization of a Carbon-Sulfur [7]Helicene. *J. Am. Chem. Soc.* **2004**, *126* (46), 15211-15222.
- (67) Zak, J. K.; Miyasaka, M.; Rajca, S.; Lapkowski, M.; Rajca, A. Radical Cation of Helical, Cross-Conjugated β -Oligothiophene. *J. Am. Chem. Soc.* **2010**, *132* (10), 3246-3247.
- (68) Xu, W.; Wu, L.; Fang, M.; Ma, Z.; Shan, Z.; Li, C.; Wang, H. Diseleno[2,3-b:3',2'-d]Selenophene and Diseleno[2,3-b:3',2'-d] Thiophene: Building Blocks for the Construction of [7]Helicenes. *J. Org. Chem.* **2017**, *82* (20), 11192-11197.
- (69) Wang, Y.; Zhang, H.; Pink, M.; Olankitwanit, A.; Rajca, S.; Rajca, A. Radical Cation and Neutral Radical of Aza-Thia[7]helicene with SOMO–HOMO Energy Level Inversion. *J. Am. Chem. Soc.* **2016**, *138*(23), 7298-7304
- (70) Kumar, R.; Maity, D. K. Structure, Stability and Spectral Properties of Seleno[n] helicenes (n = 1-10). *New J. Chem.* **2019**, *44* (2), 428-441.
- (71) Zaccaria, F.; Wolters, L. P. Insights on Selenium and Tellurium Diaryldichalcogenides : A Benchmark DFT Study. *J. Comput. Chem.* **2016**, *37* (18), 1672-1680.
- (72) Maity, D. K. Structure, Bonding, and Spectra of Cyclic Dithia Radical Cations: A Theoretical Study. *J. Am. Chem. Soc.* **2002**, *124* (28), 8321–8328.
- (73) Maity, D. K. Sigma Bonded Radical Cation Complexes : A Theoretical Study. *J. Phys. Chem. A* **2002**, *106* (23), 5716-5721.
- (74) Monney, N. P.; Bally, T.; Yamamoto, T.; Glass, R. S. Spectroscopic Evidence for Through-Space Arene-Sulfur-Arene Bonding Interaction in m-Terphenyl Thioether Radical Cations. *J. Phys. Chem. A* **2015**, *119* (52), 12990-12998.
- (75) Joshi, R.; Ghanty, T. K.; Naumov, S.; Mukherjee, T. Structural Investigation of Asymmetrical Dimer Radical Cation System (H₂O-H₂S)⁺: Proton-Transferred or Hemi-Bonded? *J. Phys. Chem. A* **2007**, *111* (12), 2362-2367.
- (76) Wakamiya, A.; Nishinaga, T.; Komatsu, K. 1,2-Dithiin Annelated with Bicyclo[2.2.2]Octene Frameworks. One-Electron and Two-Electron Oxidations and Formation of a Novel 2,3,5,6-Tetrathiabicyclo[2.2.2]Oct-7-Ene Radical Cation with Remarkable Stability Owing to a Strong Transannular Interaction. *J. Am. Chem. Soc.* **2002**, *124* (50), 15038-15050.
- (77) Pogocki, D.; Serdiuk, K.; Schneich, C. Computational Characterization of Sulfur-Oxygen Three-Electron-Bonded Radicals in Methionine and Methionine-Containing Peptides: Important Intermediates in One-Electron Oxidation Processes. *J. Phys. Chem. A* **2003**, *107* (36), 7032-7042.
- (78) Asuka, W. Dandan, F. Spectroscopic Observation of Two-Center Three- Electron Bonded (Hemi-Bonded) Structures of (H₂S)_n⁺ Clusters in the Gas Phase. *Chem. Sci.* **2017**, *8* (4), 2667-2670.

- (79) Zhang, S.; Wang, X.; Su, Y.; Qiu, Y.; Zhang, Z.; Wang, X. Isolation and Reversible Dimerization of a Selenium-Selenium Three-Electron σ -Bond. *Nat. Commun.* **2014**, 5 (1), 1-7.
- (80) Asmus, K.-D.; Bahnemann, D.; Fischer, C.-H.; Veltwisch, D. Structure and Stability of Radical Cations from Cyclic and Open-Chain Dithia Compounds in Aqueous Solutions. *J. Am. Chem. Soc.* **1979**, 101 (18), 5322-5329.
- (81) Gámez, J. a; Yáñez, M. Is Se-Se Bond Cleavage the Most Favourable Process in Electron Attachment to Diselenides? The Importance of Asymmetry. *Chem. Commun.* **2011**, 47 (13), 3939-3941.
- (82) Manuel, Y. Electron Attachment to Diselenides Revisited : Se-Se Bond Cleavage Is Neither Adiabatic nor the Most Favorable Process. *J. Chem. Theory Comput.* **2011**, 7 (6), 1726-1735.
- (83) Asmus, K. D.; Bahnemann, D.; Fischer, C. H. H.; Veltwisch, D. Structure and Stability of Radical Cations from Cyclic and Open-Chain Dithia Compounds in Aqueous Solutions. *J. Am. Chem. Soc.* **1979**, 101 (18), 5322-5329.
- (84) Szabo, A.; Ostlund, N. S. *Modern Quantum Chemistry: Introduction to Advanced Electronic Structure Theory*, Macmillan.; Dover Publications: Mineola, New York, **1982**.
- (85) Mayer, I. *Simple Theorems, Proofs, and Derivations in Quantum Chemistry*; Springer Science & Business Media, **2003**.
- (86) Pople, J. A. Nobel Lecture: Quantum Chemical Models. *Rev. Mod. Phys.* **1999**, 71 (5), 1267-1274.
- (87) Koch, W.; Holthausen, M. C. *A Chemist's Guide to Density Functional Theory*, Second Ed.; John Wiley & Sons: New Work, **2015**.
- (88) Becke, A. D. Density-Functional Thermochemistry . III . The Role of Exact Exchange. *J. Chem. Phys.* **1993**, 98 (7), 5648-5652.
- (89) Vosko, S. H.; Wilk, L.; Nusair, M. Accurate Spin-Dependent Electron Liquid Correlation Energies for Local Spin Density Calculations: A Critical Analysis. *Can. J. Phys* **1980**, 58 (8), 1200-1211.
- (90) Zhao, Y.; Truhlar, D. G. Density Functionals with Broad Applicability in Chemistry. *Acc. Chem. Res.* **2008**, 41 (2), 157-167.
- (91) Check, C. E.; Gilbert, T. M. Progressive Systematic Underestimation of Reaction Energies by the B3LYP Model as the Number of C– C Bonds Increases: Why Organic Chemists Should Use Multiple DFT Models for Calculations Involving Polycarbon Hydrocarbons. *J. Org. Chem.* **2005**, 70 (24), 9828-9834.
- (92) Wodrich, M. D.; Corminboeuf, C.; Schleyer, P. von R. Systematic Errors in Computed

- Alkane Energies Using B3LYP and Other Popular DFT Functionals. *Org. Lett.* **2006**, 8 (17), 3631-3634.
- (93) Tsipis, A. C.; Orpen, A. G.; Harvey, J. N. Substituent Effects and the Mechanism of Alkene Metathesis Catalyzed by Ruthenium Dichloride Catalysts. *Dalton Trans.* **2005**, 17, 2849-2858.
- (94) Grimme, S. Semiempirical GGA-Type Density Functional Constructed with a Long-Range Dispersion Correction. *J. Comput. Chem.* **2006**, 27 (15), 1787-1799.
- (95) Grimme, S.; Antony, J.; Ehrlich, S.; Krieg, H. A Consistent and Accurate Ab Initio Parametrization of Density Functional Dispersion Correction (DFT-D) for the 94 Elements H-Pu. *J. Chem. Phys.* **2010**, 132 (15), 154104-154118.
- (96) Chai, J.-D.; Head-Gordon, M. Long-Range Corrected Hybrid Density Functionals with Damped Atom-Atom Dispersion Corrections. *Phys. Chem. Chem. Phys.* **2008**, 10 (44), 6615-6620.
- (97) Jensen, F. *Introduction to Computational Chemistry*; John Wiley & Sons Ltd., **2007**.
- (98) Hariharan, P. C.; Pople, J. A. The Influence of Polarization Functions on Molecular Orbital Hydrogenation Energies. *Theoretica chimica acta* **1973**, 28 (3), 213-222.
- (99) Woon, D. E.; Dunning Jr, T. H. Gaussian Basis Sets for Use in Correlated Molecular Calculations. III. The Atoms Aluminum through Argon. *J. Chem. Phys.* **1993**, 98 (2), 1358-1371.
- (100) Dunning Jr, T. H. Gaussian Basis Sets for Use in Correlated Molecular Calculations. I. The Atoms Boron through Neon and Hydrogen. *J. Chem. Phys.* **1989**, 90 (2), 1007-1023.
- (101) Gillis, J. *Methods in Computational Physics. Physics Today*. Academic, New York **1965**.
- (102) Onsager, L. Electric Moments of Molecules in Liquids. *J. Am. Chem. Soc.* **1936**, 58 (8), 1486-1493.
- (103) Tomasi, J.; Mennucci, B.; Cammi, R. Quantum Mechanical Continuum Solvation Models. *Chem. Rev.* **2005**, 105 (8), 2999-3093.
- (104) Marenich, A. V.; Cramer, C. J.; Truhlar, D. G. Universal Solvation Model Based on Solute Electron Density and on a Continuum Model of the Solvent Defined by the Bulk Dielectric Constant and Atomic Surface Tensions. *J. Phys. Chem. B* **2009**, 113 (18), 6378-6396.
- (105) Scalmani, G.; Frisch, M. J. Continuous Surface Charge Polarizable Continuum Models of Solvation . I. General Formalism. *J. Chem. Phys.* **2010**, 132 (11), 114110–114115.
- (106) Schlegel, H. B. Optimization of Equilibrium Geometries and Transition Structures. *J. Comput. Chem.* **1982**, 3 (2), 214-218.

- (107) Makov, G.; Payne, M. C. Periodic Boundary Conditions in Ab Initio Calculations. *Phys. Rev. B* **1995**, *51* (7), 4014-4022.
- (108) Mishra, A.; Ma, C. Q.; Bäuerle, P. Functional Oligothiophenes: Molecular Design for Multidimensional Nanoarchitectures and Their Applications. *Chem. Rev.* **2009**, *109* (3), 1141-1176.
- (109) Cicoira, F.; Santato, C. Organic Light Emitting Field Effect Transistors: Advances and Perspectives. *Adv. Funct. Mater.* **2007**, *17* (17), 3421-3434.
- (110) Grimsdale, A. C.; Chan, K. L.; Martin, R. E.; Jokisz, P. G.; Holmes, A. B. Synthesis of Light-Emitting Conjugated Polymers for Applications in Electroluminescent Devices. *Chem. Rev.* **2009**, *109* (3), 897-1091.
- (111) Zou, Y.; Najari, A.; Berrouard, P.; Beaupre, S. A Thieno[3,4-c]Pyrrole-4,6-Dione-Based Copolymer for Efficient Solar Cells. *J. Am. Chem. Soc.* **2010**, *132* (15), 5330-5331.
- (112) Zhang, F.; Wu, D.; Xu, Y.; Feng, X. Thiophene-Based Conjugated Oligomers for Organic Solar Cells. *J. Mater. Chem.* **2011**, *21* (44), 17590-17600.
- (113) Mushrush, M.; Facchetti, A.; Lefenfeld, M.; Katz, H. E.; Marks, T. J.; Technologies, L.; Mountain, A. V.; Hill, M. Easily Processable Phenylene-Thiophene-Based Organic Field-Effect Transistors and Solution-Fabricated Nonvolatile Transistor Memory Elements. *J. Am. Chem. Soc.* **2003**, *125* (31), 9414-9423.
- (114) Wang, C.; Dong, H.; Hu, W.; Liu, Y.; Zhu, D. Semiconducting π -Conjugated Systems in Field-Effect Transistors: A Material Odyssey of Organic Electronics. *Chem. Rev.* **2012**, *112* (4), 2208-2267.
- (115) Rudberg, E.; Salek, P.; Helgaker, T.; Ågren, H. Calculations of Two-Photon Charge-Transfer Excitations Using Coulomb-Attenuated Density-Functional Theory. *J. Chem. Phys.* **2005**, *123* (18), 184108 (1-8).
- (116) Peach, M. J. G.; Helgaker, T.; Salek, P.; Keal, T. W.; Lutnaes, O. B.; Tozer, D. J.; Handy, N. C. Assessment of a Coulomb-Attenuated Exchange-Correlation Energy Functional. *Phys. Chem. Chem. Phys.* **2006**, *8* (5), 558-562.
- (117) Frisch, M. J.; Trucks, G. W.; Schlegel, H. B.; Scuseria, G. E.; Robb, M. A.; Cheeseman, J. R.; Scalmani, G.; Barone, V.; Petersson, G. A.; Nakatsuji, H.; Li, X.; Caricato, M.; Marenich, A. V.; Bloino, J.; Janesko, B. G.; Gomperts, R.; Mennucci, B.; Hratchian, H. P.; Ortiz, J. V.; Izmaylov, A. F.; Sonnenberg, J. L.; Williams-Young, D.; Ding, F.; Lipparini, F.; Egidi, F.; Goings, J.; Peng, B.; Petrone, A.; Henderson, T.; Ranasinghe, D.; Zakrzewski, V. G.; Gao, J.; Rega, N.; Zheng, G.; Liang, W.; Hada, M.; Ehara, M.; Toyota, K.; Fukuda, R.; Hasegawa, J.; Ishida, M.; Nakajima, T.; Honda, Y.; Kitao, O.; Nakai, H.; Vreven, T.; Throssell, K.; Montgomery, J. A., Jr.; Peralta, J. E.; Ogliaro, F.; Bearpark, M. J.; Heyd, J. J.; Brothers, E. N.; Kudin, K. N.; Staroverov, V. N.; Keith, T. A.; Kobayashi, R.; Normand, J.; Raghavachari, K.; Rendell, A. P.; Burant, J. C.; Iyengar, S. S.; Tomasi, J.; Cossi, M.; Millam, J. M.; Klene, M.; Adamo, C.; Cammi, R.; Ochterski, J. W.; Martin, R. L.; Morokuma, K.; Farkas, O.; Foresman, J. B.; Gaussian

- (118) Suzuki, Y.; Yamaguchi, S.; Henssler, J. T.; Matzger, A. J. Oxidation of End-Capped Penta Thienoacenes and Characterization of Their Radical Cations. *Chem. Eur. J.* **2009**, *15* (45), 12346–12361.
- (119) Ie, Y.; Okamoto, Y.; Tone, S.; Aso, Y. Synthesis, Properties, and π -Dimer Formation of Oligothiophenes Partially Bearing Orthogonally Fused Fluorene Units. *Chem. Eur. J.* **2015**, *21* (46), 16688-16695.
- (120) Krossing, I.; Raabe, I. Noncoordinating Anions-Fact or Fiction? A Survey of Likely Candidates. *Angew. Chem. Int. Ed.* **2004**, *43* (16), 2066-2090.
- (121) Mazzio, K. A.; Yuan, M.; Okamoto, K.; Luscombe, C. K. Oligoselenophene Derivatives Functionalized with a Diketopyrrolopyrrole Core for Molecular Bulk Heterojunction Solar Cells. *ACS Appl. Mater. Interfaces* **2011**, *3* (2), 271-278.
- (122) Lee, J.; Han, A.; Kim, J.; Kim, Y.; Oh, J. H.; Yang, C. Solution-Processable Ambipolar Diketopyrrolopyrrole–Selenophene Polymer with Unprecedentedly High Hole and Electron Mobilities. *J. Am. Chem. Soc.* **2012**, *134* (51), 20713-20721.
- (123) Patra, A.; Wijsboom, Y. H.; Leitus, G.; Bendikov, M. Tuning the Band Gap of Low-Band-Gap Polyselenophenes and Polythiophenes: The Effect of the Heteroatom. *Chem. Mater.* **2011**, *23* (3), 896-906.
- (124) Izawa, T.; Miyazaki, E.; Takimiya, K. Solution-Processible Organic Semiconductors Based on Selenophene-Containing Heteroarenes, 2,7-Dialkyl[1]Benzoselenopheno[3,2-b][1]Benzoselenophenes (Cn-BSBSs): Syntheses, Properties, Molecular Arrangements, and Field-Effect Transistor Characteristics. *Chem. Mater.* **2009**, *21* (5), 903-912.
- (125) Xu, W.; Wang, M.; Ma, Z.; Shan, Z.; Li, C.; Wang, H. Selenophene-Based Heteroarenes: Synthesis, Structures, and Physicochemical Behaviors. *J. Org. Chem.* **2018**, *83* (19), 12154-12163.
- (126) Pu, S.; Hou, J.; Xu, J.; Nie, G.; Zhang, S.; Shen, L.; Xiao, Q. Electrosyntheses of Freestanding and Conducting Polyselenophene Films. *Mater. Lett.* **2005**, *59* (8-9), 1061–1065.
- (127) Haid, S.; Mishra, A.; Uhrich, C.; Pfeiffer, M.; Bäuerle, P. Dicyanovinylene-Substituted Selenophene-Thiophene Co-Oligomers for Small-Molecule Organic Solar Cells. *Chem. Mater.* **2011**, *23* (20), 4435-4444.
- (128) Nishinaga, T.; Komatsu, K. Persistent π Radical Cations: Self-Association and Its Steric Control in the Condensed Phase. *Org. Biomol. Chem.* **2005**, *3* (4), 561-569.
- (129) Chivers, T.; Laitinen, R. S. Tellurium: A Maverick among the Chalcogens. *Chem. Soc. Rev* **2015**, *44* (7), 1725–1739.
- (130) Wadt, W. R.; Hay, P. J. Ab Initio Effective Core Potentials for Molecular Calculations.

- Potentials for Main Group Elements Na to Bi. *J. Chem. Phys.* **1985**, 82 (1), 284-298.
- (131) Check, C. E.; Faust, T. O.; Bailey, J. M.; Wright, B. J.; Gilbert, T. M.; Sunderlin, L. S. Addition of Polarization and Diffuse Functions to the LANL2DZ Basis Set for P-Block Elements. *J. Phys. Chem. A* **2001**, 105 (34), 8111-8116.
- (132) Weigend, F.; Ahlrichs, R. Balanced Basis Sets of Split Valence, Triple Zeta Valence and Quadruple Zeta Valence Quality for H to Rn: Design and Assessment of Accuracy. *Phys. Chem. Chem. Phys.* **2005**, 7 (18), 3297-3305.
- (133) Weigend, F. Accurate Coulomb-Fitting Basis Sets for H to Rn. *Phys. Chem. Chem. Phys.* **2006**, 8 (9), 1057-1065.
- (134) Erbay, T. G.; Aviyente, V.; Salman, S. How Substitution Tunes the Electronic and Transport Properties of Oligothiophenes, Oligoselenophenes and Oligotellurophenes. *Synth. Met.* **2015**, 210, 236-244.
- (135) Kumar, R.; Maity, D. K. Effect of Excess Electron on Structure, Bonding, and Spectral Properties of Sulfur/Selenium Based Dichalcogen Systems. *Int. J. Quantum Chem.* **2019**, 119 (7), e25855.
- (136) Gamez, J. a; Yáñez, M. Asymmetry and Electronegativity in the Electron Capture Activation of the Se-Se Bond: $\Sigma^*(\text{Se-Se})$ vs $\Sigma^*(\text{Se-X})$. *J. Chem. Theory Comput.* **2010**, 6 (10), 3102–3112.
- (137) Yan, M. [FAAF][−] (A = O, S, Se, Te) or How Electrostatic Interactions Influence the Nature of the Chemical Bond. *J. Chem. Theory Comput.* **2013**, 9 (12), 5211-5215.
- (138) Guo, Y.; Alvarado, S. R.; Barclay, J. D.; Vela, J. Shape-Programmed Nanofabrication : Understanding the Reactivity of Dichalcogenide Precursors. *ACS Nano* **2013**, 7 (4), 3616-3626.
- (139) Li, H.; O'Connor, P. B. Electron Capture Dissociation of Disulfide, Sulfur-Selenium, and Diselenide Bound Peptides. *J. Am. Soc. Mass Spectrom.* **2012**, 23 (11), 2001-2010.
- (140) Jacquemin, D.; Perpète, E. A.; Ciofini, I.; Adamo, C. On the TD-DFT UV/Vis Spectra Accuracy: The Azoalkanes. *Theor. Chem. Acc.* **2008**, 120 (4–6), 405-410.
- (141) Berry, J. F. Two-Center/Three-Electron Sigma Half-Bonds in Main Group and Transition Metal Chemistry. *Acc. Chem. Res.* **2016**, 49 (1), 27-34.
- (142) Champagne, M. H.; Mullins, M. W.; Colson, A.; Sevilla, M. D. Electron Spin Resonance Evidence for Intra- and Intermolecular $\Sigma\sigma^*$ Bonding In Methionine Radicals : Relative Stabilities of S-Cl , S-Br , S-N , and S-S Three-Electron Bonds. *J. Phys. Chem.* **1991**, 95 (17), 6487-6493.
- (143) Grimme, S.; Ehrlich, S.; Goerigk, L. Effect of the Damping Function in Dispersion Corrected Density Functional Theory. *J. Comput. Chem.* **2011**, 32 (7), 1456-1465.

- (144) Allen, F. H. The Cambridge Structural Database: A Quarter of a Million Crystal Structures and Rising. *Acta Cryst. B* **2002**, 58 (3), pp 380-388.
- (145) Nicovich, J. M.; Kreutter, K. D.; Van Dijk, C. A.; Wine, P. H. Temperature-Dependent Kinetics Studies of the Reactions $\text{Br}(2\text{P}_{3/2}) + \text{H}_2\text{S} \leftrightarrow \text{SH} + \text{HBr}$ and $\text{Br}(2\text{P}_{3/2}) + \text{CH}_3\text{SH} \leftrightarrow \text{CH}_3\text{S} + \text{HBr}$. Heats of Formation of SH and CH_3S Radicals. *J. Phys. Chem.* **1992**, 96 (6), 2518-2528.
- (146) Heverly-Coulson, G. S.; Boyd, R. J. Systematic Study of the Performance of Density Functional Theory Methods for Prediction of Energies and Geometries of Organoselenium Compounds. *J. Phys. Chem. A* **2011**, 115 (18), 4827-4831.
- (147) Fuller, A. L.; Scott-Hayward, L. A. S.; Li, Y.; Bühl, M.; Slawin, A. M. Z.; Woollins, J. D. Automated Chemical Crystallography. *J. Am. Chem. Soc.* **2010**, 132 (16), 5799-5802.
- (148) Bortoli, M.; Tiezza, M. D.; Muraro, C.; Saielli, G.; Orian, L. The ^{125}Te Chemical Shift of Diphenyl Ditelluride: Chasing Conformers over a Flat Energy Surface. *molecules* **2019**, 24 (7), 1-18.
- (149) D'Antonio, P.; George, C.; Lowrey, A. H.; Karle, J. Electron Diffraction Investigation of Dimethyl Diselenide. *J. Chem. Phys.* **1971**, 55 (3), 1071-1075.
- (150) Groner, P.; Gillies, C. W.; Gillies, J. Z.; Zhang, Y.; Block, E. Microwave Structural Studies of Organoselenium Compounds 1. Microwave Spectra, Molecular Structure, and Methyl Barrier to Internal Rotation of Dimethyl Diselenide. *J. Mol. Spectrosc.* **2004**, 226 (2), 169-181.
- (151) Torsello, M.; Pimenta, A. C.; Wolters, L. P.; Moreira, I. S.; Orian, L.; Polimeno, A. General AMBER Force Field Parameters for Diphenyl Diselenides and Diphenyl Ditellurides. *J. Phys. Chem. A* **2016**, 120 (25), 4389-4400.
- (152) Bortoli, M.; Zaccaria, F.; Tiezza, M. D.; Bruschi, M.; Guerra, C. F.; Matthias Bickelhaupt, F.; Orian, L. Oxidation of Organic Diselenides and Ditellurides by H_2O_2 for Bioinspired Catalyst Design. *Phys. Chem. Chem. Phys.* **2018**, 20 (32), 20874-20885.

ABSTRACT

In the present work, selected chalcogens (S, Se, and Te) based organic systems are studied in detail using electronic structure theory-based calculations. This work includes the chalcogen based flexible π -conjugated helical systems which may be very important in future as organic optoelectronic devices. Further, the present study also provides a model system to find suitable antioxidant based on diaryl dichalcogenides radical anions.

The theoretical calculations predict that the thia[n]helicenes systems are non-planar and flexible when the number of thiophene rings are three or more. As expected, HOMO-LUMO energy gap decreases as the number of thiophenes ring increases. Further, band gap calculated applying periodic boundary conditions (PBC) for neutral thia[n]helicenes shows that band gap decreases as the number of thiophene rings increases. Excited-state studies show that the radical cations generated from thia[n]helicenes have strong absorption in near infrared region (NIR) region. A case study on unsubstituted thia[7]helicene radical cation shows that the radical cation generated from its corresponding neutral thia[7]helicene system has a very low probability of dimerization in non-polar solvent. Calculations suggest that seleno[n]helicenes have lower energy gaps in comparison to the energy gaps of their corresponding thia[n]helicenes. Similarly, band gaps of seleno[n]helicenes are lower than those of corresponding thia[n]helicenes systems calculated applying periodic boundary conditions-based methods. The electronic spectral studies show that the radical cations generated from seleno[n]helicenes have strong absorption in near-infrared region (NIR) region. In addition, case study on seleno[7]helicene radical cation shows that the extent of dimerization is less in comparison to thia[7]helicene radical cation. This dimerization probability is less in the presence of counter ion PF_6^- . Comparative studies on chalcogen based β -helicenes (chalcogen

= S, Se and Te) show that energy gap of these systems decreases as the size and polarization of chalcogen atoms increases. It is worth mentioning that the band gap of higher size telluro[n]helicenes ($n > 6$) lies in NIR region. IR peaks obtained in UV-Visible spectra for telluro[7]helicene radical cation have stronger absorption compared to the IR peaks obtained for thia[7]helicene and seleno[7]helicene radical cations in DCM solvent. Moreover, the case study on telluro[7]helicene radical cation shows that these systems have a lower tendency for dimerization.

The present thesis also includes model systems based on diaryl dichalcogenides radical anions in search of a suitable antioxidant system. The effect of an excess electron on geometry, nature of bonding and stability of diaryl dichalcogenides, namely, $(RCh)_2^{\bullet-}$ ($Ch = S, Se \& Te$; $R = Ph, PhCH_2, o-NO_2-Ph, o-HO-Ph, \& o-CH_3-Ph$.) radical anions is studied. One electron reduction of neutral diaryl dichalcogenides leads to the formation of two-center three-electron (2c-3e) bonded radical anionic systems. These diaryl dichalcogenides radical anions show pi-pi stacking of two phenyl rings in water medium. They have high electron affinity in water medium and their corresponding neutral systems have a strong ability to capture electron efficiently suggesting their antioxidant property. Present calculations indicate that among all $(RCh)_2^{\bullet-}$ radical anions, the $(o-CH_3-Ph-Te)_2^{\bullet-}$ and $(o-CH_3-Ph-Se)_2^{\bullet-}$ systems are suitable antioxidant in water medium. The UV-Vis spectral studies show that in water medium diaryl dichalcogenides radical anions strongly absorb in visible region. The origin of the strong absorption bands in the visible region are assigned to the $\sigma \rightarrow \sigma^*$ type electronic transition.

CHAPTER 1

Introduction

Organic molecules with extended conjugation have received considerable attention for applications in electronic and photonic devices like solar cells^{1,2}, organic light-emitting diodes (OLEDs)², and organic field-effect transistors (OFETs)³. Stability, suitable HOMO-LUMO gap, strong optical absorption in the desired region, and suitable bandgap range are among the requirements in molecular systems for finding applications as efficient photoelectric and optical devices.⁴ The various methods are available in the literature that can be used to tune the energy gap in these systems. Some of the popular methods that serve this purpose are extending the conjugation of heterocyclic rings, inclusion and replacement of heteroatoms, chemical functionalization, doping, and changing their shape (e.g., converting a film into nanotubes) etc.⁵⁻⁷ A longer effective conjugation length along with rigid planarity increases their charge carrier mobility and thereby enhance their charge transport characteristics.

Along with these methods the nature of coupling and fusion of heterocyclic rings has become an important tool to produce wide varieties of high-performance materials for modern technological applications. Electrical conductivity and luminescence of conjugated systems depend on the overlap of p atomic orbitals which further depends on the conformations adopted, the presence of heteroatoms and effective conjugated framework.⁵ Thus, a detailed theoretical and experimental studies on structure-property relationships in the various conformations of heteroatom-based oligomer and polymeric systems are always subject of interest.

In the past decades, the use of sulfur, selenium and tellurium-based compounds for applications as optical devices has grown significantly due to their appropriate molecular, electronic and

optical properties. The present chapter covers studies reported in the literature on the use of thiophene, selenophene and tellurophene based systems as optical materials. It also discusses opportunities and challenges with these chalcogen based organic systems. Finally, it presents motivation of the work, organization of the thesis and future scope in a precise manner.

1.1 Overview of thiophene based optical materials

Thiophene is an inexpensive material and can even be obtained as a by-product of petroleum distillations.⁸ Importantly, thiophene can be functionalized in α and β positions to sulfur or at the sulfur atoms itself.^{5,8-11} A great deal of diversity is found in the chemical structures of thiophene based materials. Thus, thiophene based regio-regular oligomer and polymer with different functionalization can be prepared in linear to branched type and also in star-shapes.¹²⁻¹⁶ In addition to that, thiophene based dendrimers are also reported in the literature.¹⁷ The important reason behind the continuous creation of so many thiophene-based structures is that they allow fine-tuning of desirable electronic properties for optoelectronics. An interesting example of fine-tuning of the energy gap is that the linear polymerization of thiophene rings produces α -polythiophenes which has the band gap with a value of ~ 2.0 eV.¹⁸ The band gap of α -polythiophenes is approximately three times lower than the band gap of the single thiophene ring.¹⁹ In addition, conducting polymers based on α -polythiophenes produce changes in their colour and conductivity by twisting their polymeric backbone and disrupting conjugation when subjected to changes in temperature, solvent, and applied potential.²⁰ Thus, thiophene based systems not only are crucial as low energy devices^{21,22} but also as sensors that can provide a range of optical and electronic responses.²³ Further, thiophene based α -oligomers formed by coupling and condensation of a few numbers of thiophene monomers are also prominent semiconducting materials.²⁴ In particular, functionalized α -sexithiophene has been

used as an efficient material for active layer deposition to produce high-performance organic electronic devices and as models for understanding polythiophenes.²⁴ These α -oligothiophenes have rigid structures with an extended π -conjugation which could increase the intermolecular interactions in the solid as well as in solution state.^{24,25} The presence of multiple short intermolecular S...S contacts in α -oligothiophenes can enhance their transport properties^{26–28} as well as improve their solar efficiency^{29,30}. The strong π -conjugation in these α -oligothiophene leads to strong intermolecular interactions, and due to these intermolecular interactions, π -dimerization becomes an inherent property of conjugated α -oligothiophenes and their corresponding radical cations.^{31,32} It is worth mentioning that dimerization affects spectral features, energy gap and stability, which limits the utility and performance of these systems. Therefore, it is obvious that varying the positions of sulfur atoms significantly affects the performances of the device. However, some possible solutions can be used to avoid dimerization in this type of systems. The intermolecular interactions in these systems can be suppressed when these α -oligothiophenes are functionalized with sterically demanding structural units. An example of this type of modification is that dimerization of α -oligothiophene radical cations can be sterically controlled by annelation of this system with bicyclo[2.2.2]octene (abbreviated as BCO) units.^{31,32} Presence of large substituents like trimethylsilyl (TMS) and triisopropylsilyl (TIPS) at the terminal positions in α -oligothiophenes can significantly hinder dimerization. Such steric modifications are commonly employed to prevent the dimerization in these systems. However, the use of thiophene based cross-conjugated flexible systems is often ignored as reported in the literature.²⁴ The possible reason for this can be due to the lower solubility of flexible systems in comparison to their linear-shaped systems. However, using the solubilizing substituent like TMS and TIPS at the terminal

positions may be a possible synthetic strategy to overcome this lower solubility issue in these flexible systems.

1.2 Overview of selenophene based optical materials

In general, selenophene based systems are crucial in the fields of the electronic device. Selenophene based conjugated systems are widely used as bulk heterojunction (BHJ) solar cells³³, chemical-chiral sensors³⁴, organic field-effect transistor³⁵, high-performance complementary metal-oxide circuits (CMOC)³⁶, and highly transmissive electrochromic polymer.³⁷ In contrast to polythiophene, the polyselenophene are less explored due to its poor solubility and poor electrical properties. For example, the conductivities of doped polythiophenes films are in the range of 10-100 S cm⁻¹ and 10⁻⁴-10⁻² S cm⁻¹ for doped polyselenophenes.³⁸ Further, it is reported in the literature that iodine-doped oligoselenophenes exhibit the conductivities comparable to their doped oligothiophenes analogous. According to the literature, the majority of the thiophene-based oligomers have high charge carrier mobilities but often do not absorb strongly in the longer wavelengths of the solar spectrum. However, use of functionalized oligoselenophenes can lower the band gap as well as improve the overall solar device efficiencies. Interestingly, the experimentally reported HOMO-LUMO gap are changes from 2.0 eV for polythiophene³⁹ to 1.9 eV for polyselenophene.⁴⁰ Thus, it is obvious that due to large size and polarizable nature of Se than S, systems based on selenophene may attribute stronger π -conjugation. Larger and more polarizable nature of selenium atoms increases intermolecular interactions between oligomer backbones which in turn improve the p-type conductivity and mobilities in selenophene based π -conjugated systems. In addition to that, conformational flexibility in selenophene based systems are similar to their thiophene based systems.⁴¹ Thus, this conformational flexibility always provides an option to prepare modified

and novel selenophene based π -conjugated systems. Presence of selenium instead of sulfur in conjugated systems affects not only on the electronic structures but also on the solid-state structures.⁴² However, strong π -conjugation due to presence of selenium atoms in these selenophene based π -conjugated systems leads to strong intermolecular interactions and thus enhance the chance of intermolecular π -dimerization. But, use of flexible selenophene based systems along with solubilizing substituent at the terminal positions can decrease the probability of intermolecular π -dimerization and also improve their solubility. This makes selenophene based systems more attractive candidates for applications as optical materials compared to their thiophene based analogues.

1.3 Overview of tellurophene based optical materials

Tellurium based systems are used in various devices, including thin-film transistors⁴³, infrared detectors⁴⁴, and NO₂ sensors.⁴⁵ Tellurium is a metalloid and can form hypervalent coordination complexes. Along with that, tellurophene containing conjugated oligo- and polymers exhibit stronger interchain interaction that can be used to control the structure and electronic properties further. For example, polytellurophenes have a narrow HOMO-LUMO gap and thus the optical absorptions are red-shifted compared to their polythiophenes and polyselenophenes.⁴⁶ Thus, the replacement of S and Se by Te in an organic system can increase the strength of intermolecular interactions and decrease the HOMO-LUMO gaps and may be better suitable for organic electronic device applications.^{47–51} It is reported in the literature that the incorporation of Te atoms does not affect the processability of these materials if the carbon content level is not compromised. This approach of substitution of the heavier atom to its electronically similar lighter atoms can provide several new features. Some of these features are broader photon absorption and higher crystallinity.⁴⁶ Further, the tellurophene based

conjugated systems may exhibit efficient singlet to triplet intersystem crossing and increase the exciton diffusion lengths.⁴⁶ However, opportunities always come with challenges. The challenges in the synthetic chemistry of tellurophene based systems have hindered their fast development.

1.4 Molecular spectroscopy along with quantum-chemical calculations to design novel materials for device applications

To develop new and improved molecular materials for optical device applications, molecular spectroscopy along with quantum-chemical calculations are now essential tools.^{52–54} These methods are useful in establishing structure-property relationships in organic materials. When experimental spectroscopic data are combined with reliable quantum chemical calculations, it is possible to calculate precise molecular parameters which may be helpful to find suitable candidates for optoelectronic materials. If only experimental techniques are considered, this process of selection of appropriate systems for device applications can become a very tedious and difficult task. Some of the critical experiment techniques are as follows. 1) Single-crystal X ray diffraction data can provide the exact atomic positions, bond lengths, bond angles and dihedral angles.^{54,55} However, some additional bulk characterization methods must be used to get the identity and purity of a compound, 2) X-ray powder diffraction can provide valuable information on unit cell dimensions and phase identification of a crystalline material^{54,56}, 3) Raman frequencies and intensities provided by Raman spectroscopy can directly give the information about the π -conjugated framework of organic materials⁵⁷, 4) IR spectroscopy provide important frequency ranges, appearance of the vibration and absorptions for functional groups⁵⁴, and 5) Ultraviolet-visible spectroscopy is helpful to find absorption or reflectance of the molecular systems in the ultraviolet to visible range.⁵⁴ Optical absorption band, and in

particular the position of λ_{max} and lifetimes ($t_{1/2}$) of these bands may be used to provide indirect information on the nature and bonds strength formed in neutral and open-shell π -conjugated systems and 6) Electron Spin Resonance (ESR) offers valuable information on the nature of bonding in open-shell π -conjugated and can be used to study stability of these systems generated in solution phase. The above-mentioned experimental techniques in combination with quantum chemical methods, can become an indispensable tool to characterize the organic materials. First-principle quantum chemical calculations in the framework of the density functional theory (DFT) are well suited to model extended π -conjugated systems. With the easy availability of powerful and affordable parallel computer systems, electronic structure calculations of reasonably large systems are often routine these days. Moreover, efficient parallel version of computer programs are also available with good scaling for such calculations. Electronic structure calculations can predict geometrical parameters, atomic charges, dipole moments, IR and UV-Vis spectra with reasonable accuracy. Thus, understanding structure-property relationship of a large molecular systems is possible by theoretical calculations and such studies can provide excellent input to design novel systems for finding applications as optical electronic devices.

1.5 Chalcogen based helical systems for optoelectronic device applications

In general, the helicene term refers to the system that adopts a non-planar helical shape when aromatic or heteroaromatic rings are ortho-condensed.⁵⁸ Due to steric interactions in these π -conjugated systems, they get distorted into helices and become intrinsically chiral. In 1903, Jakob Meisenheimer reported the first helicene structure which was prepared by reduction of 2-nitronaphthalene.⁵⁹ Ever since several methods are being developed for synthesizing helicenes with different lengths and substituents. It is well reported in the literature that helicity

is a critical factor that can affect the electronic properties as well as solid-state self-organization of such systems.^{58,60,61}

Thia[n]helicene is a kind of carbon-sulfur helicene in which thiophene units are cross-conjugated and fused to form helical structures.^{62–65} After the successful synthesis of thia[3]helicene and thia[7]helicene, these systems attracted renewed attention because of their flexible shape and unusually strong optical properties.^{65,66} In these β -oligothiophenes, sulfur atoms are positioned at the molecular periphery. The presence of short intermolecular S...S contacts enhances transport properties by increasing the effective dimensionality in the electronic structure. The relevant examples are improved mobility in organic field-effect transistors, formation of neutral organic metals organic conductor-to-semiconductor phase transformations and increased critical temperatures inorganic superconductors. Furthermore, cross-conjugated π -systems have attracted recent attention because of their unusually robust optical properties; however, the studies of their electronic properties are in the early stages. Thia[7]helicene is fairly stable at room temperature (~ 11 h).⁶⁶ Thia[7]helicene system has a relatively large optical band gap, ~ 3.5 eV.⁶⁷ An exceptional structural property of this thia[7]helicene is recently explored. This shows that configurationally stable radical of thia[7]helicene can be easily generated via electrochemical one-electron oxidation in a non-polar solvent. The generated thia[7]helicene radical is stable up to ~ 15 min at room temperature.⁶⁷ The reason of this stability of open-shell radical cation may lie in its helical structure. The generated radical cation has strong absorption in NIR region; thus they can act as a substrate for making the detector for NIR region.⁶⁷ Recently, synthesis and crystal structures of new kinds of selenophene based helical organic functional materials are also reported in the literature.⁶⁸ However, structure-property relationship studies on thiophene and selenophene based helical structures are still at infant stages.^{62–65,67–70} No systematic

computational studies are reported on such helicenes systems either. To the best of the knowledge, no such effort is reported in the literature for tellurium based helicene systems. Thus, the use of quantum chemical methods to study such chalcogen based helical systems is the present subject of interest in search of novel high-performance optical materials.

1.6 Overview of diaryl dichalcogenides (S, Se and Te) based antioxidant systems

Sulfur and selenium based diaryl dichalcogenides are eco-friendly oxidation agents. Thus, these systems are receiving considerable attention in organic synthesis as well as in pharmaceutical chemistry.⁷¹ Along with these systems, their tellurium-based derivatives are also appealing drugs due to their antioxidant properties. After the discovery of ebselen which is a cyclic selenenyl amides, the antioxidant activity of diphenyl diselenides was established in 1989.⁷¹ It is reported in the literature that antioxidant activity of diaryl diselenides can be modulated by inserting suitable ring substituents.⁷¹ Further, tellurium analogues of diaryl diselenides are also being used as anticancer drugs.⁷¹ These diphenyl ditellurides have comparable toxicity to their selenium-based analogues.⁷¹ The antioxidant nature of sulfur and selenium based diaryl dichalcogenides can be due to the ability to donate an electron in their anionic state in the solution phase. Along with the ability to donate an electron, the anionic diaryl dichalcogenides should possess sufficient stability in the aqueous medium. One electron reduction of neutral dichalcogenides may lead to the formation of two-center three-electron (2c-3e) bonded radical anion systems.^{72–80} Having two electrons in the highest bonding sigma orbital and one electron in the lowest antibonding sigma orbital results in the formation of a half bond (bond order = 0.5) and hence these 2c-3e bond is also known as hemi bond or half bond. The typical symbol for such anionic systems is $(RCh \cdot \cdot ChR)^{\cdot -}$ in which Ch denotes S, Se,

Te etc and R denotes -Ph, -CH₃, and other functional groups.⁸¹⁻⁸³ Despite of the claimed antioxidant nature of these molecules, no systematic studies on the structural and electronic properties of diphenyl dichalcogenides are available in the literature. Thus, a model system to study the antioxidant nature of these diphenyl dichalcogenides can provide valuable information that might be used for rational drug design.

1.7 Motivation of the thesis

The recent decade has witnessed helicene based multiple molecular systems arising from the ortho-condensation of polycyclic aromatics rings. It is reported in the literature that the wide majority of helicenes are formed either by ortho-condensation aromatic rings like benzene, naphthalene, phenanthrene, and naphthol or by combination of benzene with heteroaromatic rings like thiophene/selenophene. But, the reports on helicenes systems formed by ortho-condensation of thiophene, selenophene and tellurophene rings rarely appear in the literature. Further, these helicene systems may have unique structural, spectral, and optical features. The majority of radical cations are very short-lived due to the problem of dimerization. However, the use of bulky solubilizing substituents like TMS and bulky substituents like Br at terminal positions can be a possible strategy to overcome this problem. The radical cations generated from their corresponding neutral helical system may have stronger absorptions in the NIR region. Therefore, it is interesting to investigate the structure-property relationship in these helical molecules in their neutral as well as in their radical cationic state. Further, replacing higher chalcogen atom can strongly affect the electronic features of these helical molecules. Thus, a comprehensive structure-property relationship on neutral radical cations of these thiophene, selenophene and tellurophene based helical systems can provide valuable guidance that can be beneficial to design novel molecules for device applications. Thus, the aim of this

thesis is to perform a theoretical investigation on molecular and electronic properties of substituted chalcogen based helical systems in their neutral and radical cationic state. A comparative study on molecular and electronic properties of neutral and radical cations of thiophene, selenophene and tellurophene based helical systems will be useful for understanding the effect of size and polarization of chalcogen atoms.

Radical anionic systems of diaryl dichalcogenides (S, Se and Te) are expected to have sufficient stability in the aqueous medium and the ability to donate an electron. In addition to that, their antioxidant activity can be modulated by inserting suitable substituents at various positions in phenyl ring. Therefore, systematic theoretical studies on these radical anionic systems having different substituents at different positions of the phenyl ring can provide information to design a suitable candidate as antioxidant. Thus, the aim of the thesis is also to make a comparative theoretical study of various diaryl dichalcogenides (S, Se and Te) with suitable substituents at suitable positions.

1.8 Brief overview of thesis

This thesis aims to understand to molecular structures and electronic properties of selected chalcogen based [n]helicenes (Chalcogen = S, Se and Te; n=1-10) in the gas phase and in DCM solvent. Further, the work also includes the study of molecular structures and electronic properties of chalcogen based [n]helicene radical cationic systems. Most of these helical systems are novel and may be useful in optical device applications. A comprehensive theoretical investigation on their molecular and electronic properties in the aqueous medium is performed on selected diaryl dichalcogenides (S, Se and Te) based radical anionic systems to understand their antioxidant behaviour. Based on the binding energies of these diaryl dichalcogenide (S, Se and Te) radical anions and electron affinity in their neutral state, a model

for understanding the antioxidant behaviour is also proposed in this thesis. The thesis is divided into seven chapters. The second chapter gives an overview of the theoretical methods used in the thesis. The third chapter deals with the structures, stability, ionization energies, energy gap of thia[n]helicenes (n=1-10) in the gas phase and in DCM solvent. The benchmark studies are performed to decide upon a suitable level of theory is provided in this chapter. The minimum energy structures of thia[n]helicenes radical cation are also calculated in the gas phase as well in DCM solvent. Geometrical parameters for the minimum energy structures are compared with available single crystal X-Ray data. Excited-state study for radical cations of thia[n]helicene shows that these systems strongly absorb in NIR region in DCM solvent. UV-Vis spectral data generated are also compared with available experimental data. A case study on π -dimers of neutral and radical cation of thia[7]helicene is also performed considering both unsubstituted and end substituted case to check the extent of π -dimerization process in the presence and absence of PF_6^- counter anion in DCM solvent.

The fourth chapter reports the selenium analogues of thia[n]helicenes which can be named as seleno[n]helicenes. They are the first reported selenophene β -helical systems of this type motivated from their corresponding thia[n]helicenes. Due to the unavailability of single-crystal X-Ray and spectral data the methods used for thia[n]helicene systems are used to get structures, stability, ionization energies, energy gap and UV-Visible spectra of seleno[n]helicenes (n=1-10) in the gas phase and in DCM solvent. Excited-state study for radical cations of seleno[n]helicenes in DCM solvent shows that these systems strongly absorb in NIR region. A case study on π -dimers on π -dimer unsubstituted and end substituted radical cations of seleno[7]helicene in presence and absence of PF_6^- counter anion are also performed to understand the extent of π -dimerization process in DCM solvent.

The fifth chapter deals with first reported telluro[n]helicene systems motivated from their corresponding thia[n]helicenes. This chapter mainly discuss the effects of size of chalcogen atom on ionization energy, HOMO-LUMO energy gap and band gap of neutral chalcogen (chalcogen= S, Se and Te) based β -helicenes (n=1-10). Due to the unavailability of X-Ray and spectral data on telluro[n]helicene systems, comparative studies with experimental data could not be performed to decide on a suitable theoretical method for electronic structure calculations. Thus, the methods used for thia[n]helicenes systems are also applied on these systems to calculate structure, stability, ionization energy, energy gap and UV-Vis spectra of telluro[n]helicenes (n=1-10) in the gas phase and in DCM solvent. Periodic boundary condition based DFT (PBC-DFT) calculations are performed to predict the direct band gap for these chalcogen based neutral [n]helicenes. Excited-state study for radical cations of telluro[n]helicene in DCM solvent shows that these systems absorb strongly in NIR region of electromagnetic spectrum. The intensity of these bands is larger than the corresponding thia- and seleno- [n]helicenes. A case study on π -dimers on π -dimer unsubstituted and end substituted radical cations of telluro[7]helicene in presence and absence of PF_6^- counter anion is also performed to understand the extent of π -dimerization process in DCM solvent. Overall, these thiophene/selenophene/tellurophene based helical systems are identified as potential candidates to be useful in organic electronic devices.

Sulfur selenium and tellurium based radical anionic systems of diaryl dichalcogenides are known to have strong antioxidant properties. In addition to that antioxidant activity of these systems can be modulated by inserting suitable substituents at phenyl rings. Chapter six provides a model system for understanding the antioxidant behaviour of dichalcogen systems. Benchmarking study is carried out to decide upon a suitable level of theory. The minimum energy structures for neutral and diaryl dichalcogenides radical anions are calculated in the gas

phase as well in the water medium. Geometrical parameters for the minimum energy structures are compared with available X-Ray data and microwave structural data. Based on the stability and high electron affinity (corresponding neutral) in water medium, the high antioxidant systems are identified. These studies may serve as a model for understanding the antioxidant behaviour of these dichalcogen radical anionic systems.

In chapter seven, the conclusions drawn from the work carried out in the present thesis and future scope related to this topic of research is briefly discussed. This thesis is a significant contribution to the progress of thiophene, selenophene and tellurophene based helical systems for applications in the optoelectronic device. These systems have suitable electronic properties in neutral as well as in their radical cationic state having extended π -conjugation with unique molecular structure. The stability of these substituted chalcogen based helical systems in neutral and radical cations is another important aspect that is evoked in this work. As these theoretical results provide novel candidates for optical applications, this work can serve as a motivating ground for future experimental investigations. This thesis has opened the way to use quantum chemical calculations on molecular systems to explore suitable systems for organic devices.

In addition to selected chalcogen based helical systems for device applications, a model for understanding the antioxidant behavior of diaryl dichalcogenides (S, Se and Te) radical anions is also included in this thesis. A useful strategy for modulation of antioxidant properties of diaryl dichalcogenides is to introduce an electron donating or an electron withdrawing group at ortho-position of phenyl rings. Use of macroscopic and discrete solvent models to consider the effect of aqueous medium further increases the reliability of present work. As these theoretical results suggest suitable antioxidant candidates, the studies on measurement of

antioxidant activity can be carried out to measure the rates of the reaction between free radicals and dichalcogen based antioxidant systems in future. Experimental studies (in-vitro and in-vivo) may be performed to decide on a suitable dichalcogen based antioxidant system in the future.

CHAPTER 2

Theoretical Background

This thesis deals with the Theoretical studies on selected organic chalcogen systems in the quest for novel systems for electronic devices. The present thesis also includes the designing of a model system to find out a suitable antioxidant among selected diaryl dichalcogenides radical anions. Thus, before going into the actual work, this chapter provides a brief and structured theoretical background for the calculations.

Time independent Schrödinger wave equation, $\hat{H} \Psi = E \Psi$ plays a crucial role in predicting the electronic structures of atoms, molecules and solids.⁸⁴ \hat{H} is the Hamiltonian operator, Ψ indicates the mathematical wave function representing the state of a molecule in terms of the coordinates and E denotes the total energy as the eigen value of that particular state for given molecular systems. The molecular Hamiltonian \hat{H} can be expressed as by the following expression in atomic units.

$$\hat{H} = - \sum_{i=1}^N \frac{1}{2} \nabla_i^2 - \sum_{i=1}^N \frac{1}{2M_a} \nabla_i^2 - \sum_{i=1}^N \sum_{a=1}^M \frac{Z_a}{r_{ia}} + \sum_{i=1}^N \sum_{j>i}^N \frac{1}{r_{ij}} + \sum_{a=1}^M \sum_{b>a}^M \frac{Z_a Z_b}{R_{ab}} \quad 2.1$$

The first two terms in the above equation correspond to the kinetic energy of electrons (\hat{T}_e) and nuclei (\hat{T}_n) respectively while the remaining three terms represent coulombic electron-nuclear attraction (\hat{V}_{ne}), the repulsive potential of the electron-electron (\hat{V}_{ee}) and the inter-nuclear repulsion potentials (\hat{V}_{nn}) respectively. The negative and positive sign terms given in equation 2.1 show the attractive and repulsive nature of the interactions respectively. The Hamiltonian in equation (2.1) takes form as given below.

$$\hat{H} = \hat{T}_e + \hat{T}_n + \hat{V}_{ne} + \hat{V}_{ee} + \hat{V}_{nn} \quad 2.2$$

The Schrödinger equation can be solved easily for single-electron systems. However, for N -electron systems, the approximate solution is obtained by the iterative procedure until self-consistency is achieved. Hence, solving the time-independent Schrödinger equation is a laborious task. However, decoupling the electronic and nuclear motions by using several approximations simplify the problem. Thus, the first approximation which significantly suppressed this problem is Born-Oppenheimer approximation⁸⁵ which is discussed in the next section.

2.1 Born-Oppenheimer Approximation

As the mass of nuclei is ≈ 1900 times more than the mass of electrons, the motion of the nucleus can be assumed to be stationary in comparison to the motion of the electrons. Thus, kinetic energy term for nucleus becomes zero according to the Born-Oppenheimer Approximation.^{84,85} This decoupling of electronic degrees of freedom from the nuclei degree of freedom, simplify the complex Schrödinger equation. Thus, two sets of Schrödinger equations are produced, one for electrons and other for the nuclei. Under this approximation, the internuclear repulsion is taken as a constant and so does the \hat{V}_{nn} . Thus, electronic Hamiltonian can be written as,

$$\hat{H}_e = - \sum_{i=1}^N \frac{1}{2} \nabla_i^2 - \sum_{i=1}^N \sum_{a=1}^M \frac{Z_a}{r_{ia}} + \sum_{i=1}^N \sum_{j>i}^N \frac{1}{r_{ij}} \quad 2.3$$

Using electronic Hamiltonian, the electronic Schrödinger equation can be written as,

$$H_e \Psi_e = E_e \Psi_e \quad 2.4$$

The electronic wave functions Ψ_e describing the motion of electrons is explicitly as function of electronic coordinates $\{x_i\}$ and depends only parametrically on the nuclear coordinates $\{R_A\}$. In the first step, the electronic energy, E_e is obtained by solving the Schrödinger equation for a many-electron wave function, Ψ_e for the fixed position of the nuclei. Then, the equation is solved for the nuclear motion in the average electronic field until self-consistency is obtained. Thus, the complete solution is obtained by writing the total energy of the molecule (E_{tot}) as the sum of electronic energy (E_e) and the constant internuclear repulsion energy, \hat{V}_{nn} , i.e.

$$E_{\text{tot}} = E_e + \hat{V}_{\text{nn}} \quad 2.5$$

\hat{V}_{nn} terms are independent of the position of electrons and remain constant for all values of the electronic term. As a significant number of chemical phenomena mainly depend on the electronic wave function, the main aim of quantum chemists is to solve the electronic Schrödinger equation.

2.2 Theoretical model chemistry

In theoretical model chemistry, general considerations are needed to calculate the molecular properties and describe the chemical process of interest to decide the suitable model.⁸⁶ Thus, a theoretical model can be viewed as a precise computer-simulation based mathematical procedure carried out by using a software. Then, this procedure can approximately describe a chemical process. Further, such models are used to calculate chemical and molecular properties of interest. It is worth mentioning that, in most cases, a single model is not sufficient for a

particular scientific investigation. Thus, to address and study large classes of chemical phenomena various sets of related models are used. Each set of data obtained at a particular model may compete with data obtained applying another model. Thus, some general requirements and a judgment must be made on the examination the property of interest to finalize the given model. In 1931, John Pople, mentioned the five stages in the development and use of a model. First, (a) determining the level of accuracy of the systems predicted, (b) second, precisely formulating an approximate mathematical procedure to describe a system, while making the formulation as general and continuous as possible, (c) third, implementing the formulated method as efficient and easily used computer programs, (d) fourth, verifying the model against experimental data; and (e) last, using the model to predict unknown chemical problems.

These models can be broadly classified as semi-empirical and ab initio, based on the parameters used in the models. In semi-empirical methods, the empirical parameters are used. However, the ab initio methods use fundamental constants of physics to define a system and do not depend on any empirical values. Electronic structure theory deals with the description of electrons in atoms or molecules and Hartree Fock (HF) theory is the fundamental basis of the most of electronic structure theory.

2.3 Hartree-Fock Approximation

The variational principle is the most important theoretical principle used in quantum mechanics for an approximation of the ground state. This principle states that, *for a well-behaved normalized trial wave function, $\tilde{\Psi}$, the expectation value of the Hamiltonian operator, \hat{H} corresponding to $\tilde{\Psi}$ will be an upper bound to the true energy of ground state, E_0 .*^{84,85} This true

energy of ground state E_0 , is obtained using the exact ground state wave functions, Ψ_0 . So, this condition can be written as,

$$\langle \tilde{\Psi} | \hat{H} | \tilde{\Psi} \rangle = E_{\text{trial}} \geq E_0 = \langle \Psi_0 | \hat{H} | \Psi_0 \rangle \quad \text{if } \langle \tilde{\Psi} | \tilde{\Psi} \rangle = 1 \quad 2.6$$

The energy estimate is equal to the exact ground state energy if and only if the variationally determined trial function matches the ground state wave functions. As the Schrödinger wave equation can be solved exactly only for one-electron systems, finding approximate solutions to the electronic Schrödinger equation motivates the development of the ab initio techniques for many-electrons systems or molecules.

So, the Hartree-Fock (HF) approximation is briefly discussed which is the core of all ab initio techniques for many-electron systems. Using the orthonormality of the spin orbitals and variational method, the HF equations can be derived and so as the Slater determinant with minimum energy. A ‘trial’ Slater determinant wave functions can be written as,

$$|\tilde{\Psi}\rangle = \left\{ (N!)^{-\frac{1}{2}} \sum_{n=1}^{N!} (-1)^n P_n \{ \chi_i(\vec{x}_1) \chi_j(\vec{x}_2) \dots \chi_k(\vec{x}_N) \} \right\} \quad 2.7$$

Where P represents an operator generating n^{th} permutation of the N electrons and P_n is the number of interchanges required to obtain essential permutation. Using the orthonormality of the spin orbitals and few mathematical manipulations the equation obtained is as follows,

$$\langle \tilde{\Psi} | \hat{H} | \tilde{\Psi} \rangle = \sum_i^N \langle i | \tilde{h} | i \rangle - \sum_i^N \sum_{j>i}^N ((\langle ij | ij \rangle - \langle ij | ji \rangle)), \quad 2.8$$

Here, the ket and bra notations refer to,

$$\langle i|\hat{h}|i\rangle = \int d\vec{x}_1 \chi_i^*(\vec{x}_1) \hat{h} \chi_i(\vec{x}_1); \langle ij|ij\rangle = \int d\vec{x}_1 d\vec{x}_2 \chi_i^*(\vec{x}_1) \chi_j^*(\vec{x}_2) r_{12}^{-1} \chi_i(\vec{x}_1) \chi_j(\vec{x}_2); \quad 2.9$$

and,

$$\langle ij|ji\rangle = \int d\vec{x}_1 d\vec{x}_2 \chi_i^*(\vec{x}_1) \chi_j^*(\vec{x}_2) r_{12}^{-1} \chi_j(\vec{x}_1) \chi_i(\vec{x}_2) \quad 2.10$$

By applying the variational principle for true ground state ket $|\Psi_0\rangle$ we get, $E_0 = \langle \Psi_0 | \hat{H} | \Psi_0 \rangle \leq \langle \tilde{\Psi} | \hat{H} | \tilde{\Psi} \rangle$, considering, $|\Psi\rangle = |\Psi_0\rangle$, the HF ground state energy can be written as,

$$E_0^{\text{HF}} = \sum_i^N \langle i|\hat{h}|i\rangle - \sum_i^N \sum_{j>i}^N ((\langle ij|ij\rangle) - \langle ij|ji\rangle), \quad 2.11$$

Consequently, by varying the spin orbitals using the constraint of their orthonormality i.e. $\int d\vec{x} \chi_i^*(\vec{x}) \chi_j(\vec{x}) = \langle i|j\rangle = \delta_{ij}$ the $E_0^{\text{HF}}[\{\chi_i\}]$ is minimised. Using the Lagrange multipliers equation $L_0[\{\chi_i\}]$ of spin orbitals. The non-canonical form of HF equation can be written as

$$\hat{F}(\vec{x}) \chi_i(\vec{x}) = \sum_j^N \epsilon_{ij} \chi_j(\vec{x}), \quad (i = 1, 2, \dots, N), \quad 2.12$$

Where, ϵ_{ij} are the Lagrange multipliers the ‘Fock operator’ $\hat{F}(\vec{x})$ is an effective one-electron operator given as

$$\hat{F}(\vec{x}) = \hat{h} + \hat{V}^{\text{HF}}(\vec{x}), \quad 2.13$$

The first term represents the kinetic energy of the single-particle and potential of the i^{th} electron, while $V^{\text{HF}}(\vec{x})$, the average potential perceived by the i^{th} electron due to remaining $N-1$ electrons is represented by Hartree-Fock potential (\hat{V}^{HF}). Due to this average potential, the HF theory is considered as a *mean field theory*.^{84,85}

The noncanonical HF equation (2.12) are converted to the standard canonical form to unitary transformations of the spin orbitals yields

$$\hat{F}(\vec{x})\chi_i(\vec{x}) = \epsilon_i\chi_i(\vec{x}) \quad (i = 1, 2, \dots, N) \quad 2.14$$

This is actually a pseudo eigenvalue problem. This equation is needed to be solved iteratively using the self-consistent field (SCF) procedure. The orbitals are initially derived from their own effective potential which involves finding the energy minimum. Initially, some trial orbitals are used to construct the Fock operators. These trial orbitals are used to obtain improved orbitals which serve as input for a new Fock operator. The iterative procedure is continued until self-consistency is reached where effective potential, $V^{\text{HF}}(\vec{x})$ no longer changes.

Despite the impressive results, the HF approximation has a drawback as it neglects the electron correlation. Though the HF wave functions account for ~99% of the total energy, the remaining ~1% largely influences the chemical properties of the molecules. This difference between the exact ground state energy E_0 of the system and the HF energy in a given basis set is the electron correlation energy (E_{corr}),

$$E_{\text{corr}} = E_0 - E_0^{\text{HF}} \quad 2.15$$

Since, both E_{tot} and E_0^{HF} are less than zero and $|E_0| > |E_0^{\text{HF}}|$, the E_{corr} is a negative quantity.

^{84,85} It is because; the electrons feel an instantaneous repulsion as they are often too close to each other. To consider the electron correlation in the molecular systems the Post HF methods are discussed in upcoming sections.

2.4 Post HF methods

The post-HF methods like the configuration interaction (CI), coupled-cluster (CC) theory, Møller-Plesset (MP) perturbation theory etc. are proposed to incorporate the electron correlation effects in the molecular systems.^{84,85} But these methods are expensive and these post-HF methods can be used only for small and medium-sized molecular systems. In the next section, Møller-Plesset (MP) perturbation theory is discussed briefly.

2.4.1 Møller-Plesset (MP) perturbation theory

Møller-Plesset (MP) perturbation theory^{84,85} is a particular case of Rayleigh-Schrödinger perturbation theory. In this theory, the zeroth-order Hamiltonian is chosen to be the Hartree-Fock Hamiltonian. The perturbation operator \hat{V} is thus the difference between the electron-electron interaction and the Hartree-Fock exchange energy. The second-order energy correction, which is called the second-order Møller-Plesset (MP2) correlation energy is always negative. The MP2 total energy is simply defined as, $E_{\text{MP2}} = E_{\text{HF}} + E_{\text{c}}^{\text{MP2}}$. Since it is not a variational theory, the MP2 total energy is not necessarily above the exact ground-state total energy. The MP2 method can be considered as the computationally cheapest post-HF method and is thus widely used. In the next section, a more accurate post-Hartree Fock method, Coupled Cluster theory is discussed briefly.

2.5 Coupled Cluster Theory

The coupled-cluster theory^{84,85} is one of the important post-Hartree-Fock for describing many-body systems. The coupled-cluster wavefunction can be written as, $|\Psi_{\text{cc}}\rangle = e^{\hat{T}}|\Phi_0\rangle$, where $\hat{T} = \hat{T}_1 + \hat{T}_2 + \hat{T}_3 \dots + \hat{T}_N$ where Φ_0 is the HF wave function, and \hat{T} is the cluster

operator which is the sum of cluster operators of different excitation levels. The truncation of the cluster operator at \hat{T}_1 and \hat{T}_2 is known as coupled-cluster singles doubles (CCSD).

CCSD and MP2 both neglect static correlation effects since both use a single reference wavefunction. However, the quality of energy is different. CCSD energy is correct up to third-order while MP2 is correct up to second order. This is because the cluster operator includes only singles and doubles, via unlinked amplitudes of higher excitation that contribute up to second-order to CCSD function. Thus, the energies given by CCSD method are much better than the ones given by MP2 Methods. Although, both MP2 and CCSD are size consistent, CCSD is computationally more expensive

To deal with difficulties of time consumption, disk memory and space, the density functional theory (DFT) provides an alternative. It incorporates the electron correlation with no substantial increase in the computational cost. DFT treats charge density as a basic variable for the ground state description. The electron density is less complicated than the many particles wave function of the systems. Hence, DFT provides an alternative computational tool with a remarkable quality/cost ratio.⁸⁷ In the next sections, a brief overview of developments in DFT has been discussed.

2.6 Density Functional Theory

The Hohenberg and Kohn theorems (HK theorems) form the basis of DFT. The first HK theorem states that the external potential applied on a system, in ground state, is defined as a unique functional of electron density. The external potential determines the Hamiltonian, \hat{H} axiomatically making it a unique functional of density. The second HK theorem states that the

approximate electron density associated with an external potential is always greater than or equal to the exact ground state energy.

Thus, the ground state energy of the system can be expressed as:

$$E_0 = T[\rho_0] + E_{ee}[\rho_0] + E_{Ne}[\rho_0] \quad 2.16$$

T is the kinetic energy, E_{ee} is the electron-electron interaction energy and E_{Ne} is the nucleus-electron interaction energy. The first two terms are independent of number of electrons, electron-nucleus distance and nuclear charge and are universally valid while the E_{Ne} depends on those variables and is therefore system dependent. The independent parts of the above equation is the Hohenberg-Kohn functional, $F_{HK}[\rho]$. The exact HK functional is not known. The E_{ee} term can be written as the sum of coulomb term and a term containing all non-classical contributions to the electron-electron interaction. The energy is then determined using variational principle. To improve the results obtained, Kohn-Sham orbitals have been developed. Here, the hypothetical system consists of non-interacting electrons, having ρ equivalent to the real system, which experiences average repulsion field from other electrons. The total energy is then written as:

$$E[\rho] = T_s[\rho] + \int [\hat{V}_{ext}(r) + \hat{J}(r)]\rho(r)dr + E_{XC}[\rho] \quad 2.17$$

where, $T_s[\rho]$ is the electron kinetic energy of the hypothetical system, $\hat{J}(r)$ gives the classical coulomb interaction between electrons and $\hat{V}_{ext}(r)$ is the potential due to the nuclei.

Kinetic energy is computed in terms of one electron function:

$$T_s[\rho] = \frac{1}{2} \sum_{i=1}^N \langle \phi_i | \nabla^2 | \phi_i \rangle \quad 2.18$$

$$\hat{V}_{\text{ext}} = \sum_A \frac{Z_A}{|\mathbf{R}_A - \mathbf{r}|} \quad 2.19$$

$$\hat{J}(\mathbf{r}) = \int \frac{\rho(\mathbf{r}')}{|\mathbf{r}' - \mathbf{r}|} d\mathbf{r}' \quad 2.20$$

\mathbf{r} and \mathbf{r}' are the coordinates of the two electrons and Z_A is the nuclear charge. E_{XC} contains all the other contributions to energy such as electron exchange, correlation energy, correction for self-interaction and the difference in kinetic energy between interacting and non-interacting system. The Hamiltonian for the non-interacting system is:

$$\hat{H}_s = -\frac{1}{2} \sum_i \nabla_i^2 + \sum_i V_{S(\mathbf{r}_i)} \quad 2.21$$

The non-interaction fictitious system is represented by Kohn-Sham orbitals, ϕ_i . They are determined using one-electron Kohn-Sham operator, \hat{f}^{KS} .

$$\hat{f}^{\text{KS}} \phi_i = \epsilon_i \phi_i \quad 2.22$$

$$\hat{f}^{\text{KS}} = -\frac{1}{2} \nabla^2 + V_{S(\mathbf{r})} \quad 2.23$$

V_s is the effective potential of non-interacting system.

The major part of kinetic energy can thus be computed and the residual part is merged with non-classical E_{XC} term. E_{XC} is the unknown term and different approximations for its determination have led to the development of several density functionals.

2.6.1 Local Density Approximations (LDA), Generalized Gradient Approximation Functional (GGA), Hybrid Functionals

The simplest approximations for the exchange-correlation energy used in DFT is the “Local Density Approximations” which state that exchange-correlations energy is a function of the electron density in the immediate vicinity of the point at a given position. However, for atoms and molecular exhibiting rapid attenuation in the electron density in the asymptotic region results obtained are not satisfactory. Hence, for better results generalized gradient approximation’ (GGA) based methods are used because in these methods energy density is incorporated with the gradient of the density $\vec{\nabla}\rho$ at that given position. The meta-GGA functionals are more accurate than the GGA functionals as they take into consideration the Laplacian (∇^2) i.e. second derivative of the electron density and the quantities such as thermodynamic energies and metal-metal interactions can be accurately described. In general LDAs, GGAs and meta-GGAs are local functionals. So, for obtaining better agreement with the experimental the hybrid exchange-correlation functionals are developed. The problem of the electronic self-interaction results in a very poor description of the exchange part in the LDAs, GGAs and meta-GGAs functionals.

In hybrid functionals, the exchange-correlation energy is obtained from a portion of exact exchange from Hartree–Fock theory with the rest of the exchange–correlation energy from other sources (ab initio or empirical). Becke proposed the three parameters for hybrid functionals by introducing a small fraction of exact exchange component in the DFT exchange-

correlation functional ensuring better results. The popular B3LYP (or Becke3LYP) hybrid functional uses semi-empirical, $a = 2.0$, $b = 0.72$, and $c = 0.82$ as specified by the Becke. These parameters, determined by fitting atomisation energies, ionisation potentials, proton affinities and total atomic energies give good fit to experimental molecular atomization energies for first-row elements.^{88,89}

$$E_{xc}^{B3LYP} = (E_x^{LSDA} + E_c^{VWN3}) + a_0(E_x^{exact} + E_x^{LSDA}) + a_x \nabla E_x^{B88} + a_c(E_c^{LYP} - E_c^{VWN3}) \quad 2.24$$

E_x^{LSDA} and E_c^{LSDA} respectively are the exchange and correlation energy from LSDA approximation, E_x^{exact} is the HF exchange, ∇E_x^{B88} , and E_c^{LYP} are the exchange and correlation terms due to Becke, Lee, Yang And Parr, respectively. The E_c^{VWN3} , is VWN3 local spin density correlation functional. The B3LYP functional gained popularity due to its extensive applicability and works quite well for the covalently bonded systems. However, its aptness is being questioned especially for non-covalent interactions like van der Waals interactions, aromatic-aromatic stacking etc.⁹⁰ Furthermore, recent studies also indicated that B3LYP method showed inaccuracy in envisaging heats of formation in organic molecules^{91,92} as well as gives incorrect trends in binding energies of organometallic catalytic systems.⁹³ However, dispersion corrected B3LYP functionals are now available. This covers the shortfalls of the B3LYP method by adding the D^{94} or $D3^{95}$ Grimme's dispersion corrections empirically. A range-separated DFT functional ω -B97XD⁹⁶ is developed by Head-Gordon and co-workers which is capable of capturing both short-range and long-range interactions.

2.7 Basis Sets

Molecular orbitals are approximated as the linear combination of basis functions, which are one particle functions. A complete basis set is not an approximation. However, for a complete

basis set, infinite number of basis functions must be used, which is not practical. A finite basis set defines the components of molecular orbitals in the direction of the selected basis functions. As the computational cost for *ab initio* methods scales as M^4 , where M is the number of basis functions, there is a trade-off between expense and accuracy. There are mainly two types of basis functions: the Slater Type Orbital and the Gaussian Type Orbital.⁹⁷ The STO is of the type:

$$\chi_{\zeta,n,l,m}(r,\theta,\phi) = NY_{l,m}(\theta,\phi)r^{n-1}e^{-r\zeta} \quad 2.25$$

where, N is the normalization constant, $Y_{l,m}$ is the spherical harmonic function, r is the radial function and ζ controls the width of the orbital. STOs do not have radial nodes. Radial nodes are introduced by taking linear combination of STOs. But, analytical calculation of three and four-centre two-electron integrals cannot be done in case of STOs. Hence the much more popular GTOs are used which are easier to calculate. GTOs are represented as:

$$\chi_{\zeta,n,l,m}(r,\theta,\phi) = NY_{l,m}(\theta,\phi)r^{2n-2-l}e^{-r^2\zeta} \quad 2.26$$

The r^2 in the exponential causes the GTO to poorly represent proper behavior near the nucleus and also at the tail of the wave function. Hence, a combination of GTOs, i.e., Contracted type GTOs (CGTO) are mostly used, which mimics the STOs but are easy to calculate.

Depending on the combination of the GTOs there are several classifications of basis sets like the minimal basis sets, which contain just one basis function for each atomic orbital in the atom; the split valence basis sets which treat the core and valence orbitals differently; Pople basis sets⁹⁸, Dunning's correlation-consistent basis sets^{99,100}, which are optimized using

correlated wave functions, etc. There are also the plane wave basis sets, which are used to describe periodic systems.

2.8 Self-Consistent Reaction Field theories: Effect of Solvation

Two types methods are used for evaluating the solvent effect: (a) one considering the individual solvent molecules and (b) regarding the solvent as continuous medium⁹⁷ so as to account for the “macroscopic” or “long range” effects, i.e. solvent polarization, resulting in the generation of altered dielectric constant. The modelling of long-range solvation can be carried out using several approaches that apply the concept of a “reaction field” in one way or another. The Self-Consistent Reaction Field theory (SCRF) model is one such method that considers a uniform polarizable solvent having dielectric constant ϵ along with a solute M placed in an appropriately shaped hole in this medium.¹⁰¹ Creating a cavity in the medium leads to destabilisation as it involves breaking of the uniform solvent field which requires energy, whereas, the dispersion interactions between the solvent and solute lead to stabilization. Electrostatic results on account of electric charge distribution of solute molecule polarizing the medium which then acts back on the molecule. The solvation (free) energy can consequently be written as

$$\Delta G_{\text{solvation}} = \Delta G_{\text{cavity}} + \Delta G_{\text{dispersion}} + \Delta G_{\text{electrostatic}} \quad 2.27$$

The stabilization resulting from van der Waals interactions between M and the solvent as well as the energy required for creating are generally assumed to be proportional to surface area of the solute. The corresponding energy term is proportional to the total surface area or is parameterized by having a constant ξ which is specific for each type of atom. The shape of the cavity thus becomes significant. The ξ parameters are determined by fitting to experimental

solvation data. The influence between a solute with its surrounding medium can most simply be described using the Onsager reaction field model.¹⁰² The basic assumption made in this model is that the solute is placed in spherical cavity inside the solvent. The Kirkwood model employs the general multipole expansion while the Kirkwood-Westheimer model considers an elliptical cavity. The Polarizable Continuum Model (PCM)¹⁰³ is one of the most commonly used and reliable solvation procedures which defines the cavity as a series of interlocking atomic spheres.

SMD^{104,105} model is a continuum solvation model based on the quantum mechanical charge density of a solute molecule interacting with a continuum description of the solvent. The model is called SMD, where the “D” stands for “density” to denote that the full solute electron density is used without defining partial atomic charges. “Continuum” denotes that the solvent is not represented explicitly but rather as a dielectric medium with surface tension at the solute-solvent boundary. SMD is a universal solvation model, where “universal” denotes its applicability to any charged or uncharged solute in any solvent or liquid medium for which a few key descriptors are known (in particular, dielectric constant, refractive index, bulk surface tension, and acidity and basicity parameters).

2.9 Geometry Optimization and Hessian calculations

Optimization in general refers to determining stationary points of a function, where the first derivative of energy with respect to the geometric coordinates of the system, is zero. Geometry optimization essentially predicts the minimum energy structure of a system. The minimum energy configuration of a system is determined iteratively, by minimizing the force on the comprising atoms in each step. Several procedures are available to locate minimum energy

structures, like Steepest Descent (SD) method, Conjugate Gradient (CG) method, Newton-Raphson (NR) method etc.

In SD method, the search direction is defined along the negative gradient.

$$d_i = -g_i \quad 2.28$$

Though there is a guarantee to approach a minimum, there is an oscillation around the minimum path. Also the rate of convergence drops as the minima is reached.

The CG method improves on this by performing the search along a line that is conjugate to the direction of the previous search.

$$d_i = -g_i + \beta_i d_{i-1} \quad 2.29$$

β values can be chosen in several ways, depending on the method. CG method is not suitable for non-linear surfaces.

In the NR method, the function is approximated as a quadratic surface and minimum is determined. The true function is expanded about the current position, x_0 up to second order and its gradient is made zero.

$$f(x) = f(x_0) + g(x - x_0) + \frac{1}{2} H(x - x_0)^2 \quad 2.30$$

$$(x - x_0) = -H^{-1}g \quad 2.31$$

$$\Delta x' = \sum_i \Delta x'_i = -\frac{f_i}{\epsilon_i} \quad 2.32$$

where Hessian, H , is the diagonal in the coordinate system (x'). f_i is projection of gradient along Hessian Eigen vector with Eigen value ϵ_i . Since the real function may have terms beyond second order, the NR method iteratively approaches towards stationary point. NR method always converges to the nearest local minimum. Hence care should be taken in preparing the initial geometries to get the correct configuration. Many optimization algorithms in quantum chemical software packages use some variant of the NR method. One such is the “Berny algorithm developed by Bernhard Schlegel¹⁰⁶, which is used in the present study.

In Berny optimization, the local minimum on the potential energy surface is located using the forces on the atoms as well as the Hessian matrix. Since explicit calculation of the Hessian is costly, an approximated Hessian is constructed at the beginning, applying valence force field and is updated during each iteration, using the energies and gradients calculated in each step.

The optimized geometry can be a local/global minimum or a saddle point on the potential energy surface. The first (gradient) and second (Hessian) derivatives of energy of the system with respect to geometrical parameters, provides information about the nature of the minima. The negative of the gradient gives the vector of forces on the atoms. The eigenvectors of the mass-weighted Hessian matrix gives the normal modes of vibration. A minimum in the potential energy surface has zero gradient and all positive vibrational frequencies. A first order saddle point (Transition State) has maximum in one direction and minimum in all other directions in the potential energy surface. Thus, it has zero gradient and one negative vibrational frequency. Similarly, n th order saddle point will have zero gradient and n imaginary frequencies.

2.10 Molecular Orbitals

Molecular orbital (MO) is a one-electron orbital wave function which is used to describe the region of space in which the function has a significant amplitude. This amplitude gives an estimate of the probability of finding an electron in any specific region. These molecular orbitals are formed as linear combinations of atomic orbitals (LCAO). In the LCAO method, it is assumed that the molecular orbital wave function Ψ_i can be written as a simple weighted sum of the n constituent atomic orbitals.

$$\Psi_i = \sum_{i=1}^N c_{ij} \chi_i \quad 2.33$$

One can get c_{ij} coefficients numerically by substituting this equation into the Schrödinger equation and applying the variational principle. The molecular orbitals obtained from this method are highly delocalised in nature. Thus, to get a localized set of molecular orbitals the Natural Bond Orbitals (NBO) are used. In NBO analysis, the input atomic orbital basis set is transformed via natural atomic orbitals (NAOs) and natural hybrid orbitals (NHOs) into natural bond orbitals (NBOs). The NBOs obtained in this fashion correspond to the widely used Lewis picture, in which two-center bonds and lone pairs are localized. These approximations are widely applied in the density functional theory (DFT) or Hartree–Fock (HF) models to the Schrödinger equation.

2.11 Time-dependent density functional theory

TDDFT⁹⁷ can be viewed as the extension of density functional theory (DFT), to show that the time-dependent wave function is equivalent to the time-dependent electronic density, and then

to derive the effective potential of a fictitious non-interacting system which returns the same density as any given interacting system. The foundation of TDDFT is done by Runge-Gross which state that in its Runge-Gross theorem that, there exist is a unique mapping between the time-dependent external potential of a system and its time-dependent density, for a given initial wavefunction. This implies that the many-body wavefunction, depending upon $3N$ variables, is equivalent to the density, which depends upon only three, and that all properties of a system can thus be determined from knowledge of the density alone. The most popular application of TDDFT is in the calculation of the energies of excited states of isolated systems and, less commonly, solids. Such calculations are based on the fact that the linear response function that is, how the electron density changes when the external potential changes have poles at the exact excitation energies of a system.

2.12 Periodic Boundary Calculations for Band gap and Band structure

Band gap and band structure calculations take advantage of the periodic nature of a crystal lattice, thus an infinite size system is converted in the finite size systems by imposing the certain PBC condition¹⁰⁷ with maintaining its overall symmetry. Thus, the general formalism for doing this is taking a crystal lattice in real space framework (having dimensions of wavelength) and then converting this real space framework into the reciprocal space framework (having dimensions of reciprocal of the wavelength). The reciprocal space framework elegantly reserved all the information of real space. After that, the Wigner-Seitz cell is drawn with the help of Bragg planes which further classified the segment formed into the various Brillouin Zone. When the wave vector touches the Bragg's planes, the diffraction will occur. When diffraction occurs, the relationship between E vs K is distorted. This gives rise the leftover ranges of energy not covered by any band, a result of the finite widths of the energy bands are

produces. The energy gap between leftover ranges is generally termed as band gap. Thus, a band gap is defined as “*the difference of energy between the valence band and the conduction band*”. Thus, the band gap represents the minimum energy required to jump an electron from valence band up to a conduction band state so that the electron can participate in conduction in the systems. The band gap of a semiconductor is of two types, a direct band gap or an indirect band gap. The minimal-energy state in the conduction band and maximal-energy state in valence band are characterized by a certain crystal momentum (k-vector) in the Brillouin zone. If the crystal momentum of electrons and holes is the same in both the conduction band and the valence band; an electron can directly emit a photon. This band gap is called direct band gap. If the k vectors are different, band gap is called indirect band gap. However, this gap exists for a large (infinite) size polymer, oligomer system. Therefore, some set of boundary conditions are used in computer simulations for approximating a large system by using a small part called a unit cell. These boundary conditions are nothing but the previously mentioned Periodic boundary conditions (PBCs). Further, electronic band structure describes the range of energies an electron may not have. Determining theoretical band gaps before synthesis or experiment can save valuable lab time.

CHAPTER 3

Structures, Stability and Spectral Properties of Thia[n]helicene (n=1-10) and their Corresponding Radical Cations

3.1 Introduction

This chapter presents studies on sulfur-based helical systems and their corresponding radical cations in the quest of the potential candidate for electronic devices. Continuous growth in the research interest of oligothiophene systems is observed due to their wide range of applications as organic photoelectric devices.^{5,108} Thiophene based materials make significant contributions in the field of organic light-emitting diodes,^{109,110} photovoltaics,^{111,112} and organic field-effect transistors^{113,114}. The wide variety of thiophene-based materials such as polymers, oligomers, oligohelices, and oligoacenes fulfil these requirements of molecular systems for finding applications in efficient photoelectric devices. Synthesis and characterizations of α -oligothiophenes and α -polythiophenes are well reported in the literature.¹¹⁻¹⁵ Depending on the nature of fusion of the thiophene rings, four different types of conformers are possible. It is reported that these conformers can be synthesized by altering the nature of condensation (syn and anti) of the thiophene rings. At present, thiophene-based [n]helicenes, where n is the total number of thiophene rings present in these systems are considered and studied in detail applying first principle-based electronic structure theory. Some recent studies show considerable enhancement in the electronic properties of these thia[n]helicenes.⁶⁶ As discussed in section 1.5, the single-crystal X-ray structural data of thia[n]helicenes, [3]TH and [7]TH are reported in the literature.⁶⁵ These thia[n]helicenes show strong chiro-optical properties and

have large optical bandgap (~ 3.5 eV).⁶⁶ However, there is no systematic study on these thia[n]helicenes to examine the effect of size on the structure and electronic properties.

It is reported in the literature that the stable radical cation of thia[7]helicene, [7]TH^{•+} can be generated via electrochemical oxidations in DCM solvent and an inert atmosphere at room temperature.⁶⁷ This *ortho*-annulated thiophene based radical cation can have extensive applications as NIR (near-infrared region) detector. However, there is no report in the literature of such studies on radical cation of different size thia[n]helicenes. It is also expected that material based on thia[n]helicenes can be of great choice for producing stable radical cations that can be used as NIR detectors. The experimental characterization of the radical cations of these type of thia[n]helicenes can be performed by UV-Vis spectroscopy. The transient optical absorption maximum (λ_{max}) is being used as an indicator for the presence of these radical cationic systems of thia[n]helicenes in a non-polar solvent. Based on EPR spectra of thia[7]helicene, [7]TH radical cation, it is reported that [7]TH^{•+} is stable up to a few minutes. It is expected that the radical cations of thia[n]helicenes, [n]TH^{•+} for $n > 7$ can be more stable than thia[7]helicene, [7]TH^{•+} in DCM solvent. Thus, a comprehensive understanding of electronic structures as well as spectral properties of these radical cations of thia[n]helicenes is needed for finding applications of these systems as organic electronic devices. Although some scattered experimental studies are available for neutral thia[n]helicenes and their corresponding radical cations of thia[n]helicenes,^{62–67} to the best of the knowledge, no systematic theoretical studies are available for these helicenes. Moreover, no study is reported on the possibility of dimerization of these systems. Such information is crucial as dimerization often leads to a significant change in electronic properties and may make the system unsuitable for application as electronic devices.

This chapter deals with the first principle-based quantum chemical study on neutral and radical cation of thia[n]helicenes, [n]TH, n=1-10. Various molecular properties like structures, ionization energies, energy gap and UV-Vis spectral properties of these systems are reported in the gas phase as well as in DCM solvent. Moreover, calculations have been performed to find out the possibility of dimerization in both unsubstituted and substituted thia[7]helicene in DCM solvent as a case study.

3.2 Theoretical Methods

In this section, the theoretical methods used for calculating the electronic structures for neutral thia[n]helicenes and their corresponding radical cations are discussed. The ortho β -annulation scheme of thiophene rings are used to produce all conformer for neutral thia[n]helicenes (n=1-10) and their corresponding radical cations of thia[n]helicenes, [n]TH^{•+} (n=1-10). The conformers for neutral and radical cations of thia[n]helicenes are optimized using the B3LYP functional^{88,89} along with 6-311++G(d,p) basis set to get the most stable structure in the gas phase and also in DCM solvent. Most stable structures of neutral and radical cations of thia[n]helicenes obtained at the B3LYP level of theory are re-optimized applying dispersion corrected B3LYP-D⁹⁴ method. The solvation model based on solute density (SMD)^{104,105} is used to introduce macroscopic solvent effect for all calculations in the solvent phase. Hessian calculations are carried out in the gas phase and also in DCM solvent to characterize the most stable structure of neutral and radical cation of thia[n]helicenes as the true minima and to compute thermodynamic parameters. The most stable structures obtained at B3LYP-D level are being used for single point energy calculations at B3LYP-D3⁹⁵ and MP2 levels. For neutral thia[n]helicenes, the restricted shell formalism (RHF) is used, and for radical cations of thia[n]helicenes, the restricted open-shell formalism (ROHF) is used. Excited-state

calculations are carried out applying TDDFT procedure and considering CAM-B3LYP functional along with 6-311++G(d,p) basis set for neutral as well as the radical cation of thia[n]helicenes for the lowest fifty excited states in DCM solvent. CAM-B3LYP is a long-range corrected hybrid exchange-correlation functional designed to give a good description of electronic excitations and charge transfer processes.^{115,116} All the possible structures of unsubstituted and substituted π -dimer of neutral thia[7]helicene, as well as radical cation of thia[7]helicene, are optimized at B3LYP-D level of theory using 6-311++G(d,p) basis set to get the most stable structure in DCM solvent. Hessian calculations are also carried out to characterize the most stable structure of these systems as the true minima in DCM solvent and to compute thermodynamic parameters. All theoretical calculations are performed using the GAUSSIAN 16 program.¹¹⁷

3.3 Results and Discussions

3.3.1 Structure for thia[n]helicenes, [n]TH, n=1-10 in DCM solvent

It is reported in the literature that the structure of neutral thia[3]helicene, [3]TH is non-planar spacer type and that of neutral thia[7]helicene, [7]TH is cross-conjugated and annelated into a helix.⁶⁵ Sequential addition of a thiophene unit to thia[1]helicene, [1]TH in a syn manner is performed to produce thia[2]helicene, [2]TH. This procedure is repeated to produce larger thia[n]helicenes, [n]TH, n=3-10. Table 3.1 summarizes the molecular properties of neutral thia[n]helicenes, [n]TH, n=1-10 of fully optimized structures at B3LYP-D level with 6-311++G(d,p) basis set in the gas phase and in DCM solvent. At the B3LYP-D level, the planar structure is obtained for thia[1]helicene in DCM (see Figure 3.1a). On moving further, for thia[2]helicene also a planar structure is obtained at the present level of theory in DCM (See Figure 3.1b). In case of thia[3]helicene the structure is nearly planar in DCM solvent and the

dihedral angles $\delta(\text{Br1C2C3Br2})$ and $\delta(\text{Br2C3C2C4})$ are calculated as 1.4° and -178.6° respectively (Figure 3.1c). Based on single-crystal X-ray analysis, it is reported that the dihedral angles, $\delta(\text{Br1C2C3Br2})$ and $\delta(\text{Br2C3C2C4})$ in thia[3]helicene are 13.3° and -164.3° .⁶⁵ Thus to improve geometrical parameters of thia[3]helicene, [3]TH in DCM solvent calculated at B3LYP-D level of theory, the optimized structure at B3LYP-D level is re-optimized at MP2 level of theory considering DCM solvent. Calculated r_{Br1Br2} distance and spacer distance, $r_{\text{C2-C7}}$ at the MP2 level of theory in DCM are 3.53 \AA and 3.70 \AA respectively. Calculated dihedral angles $\delta(\text{Br1C2C3Br2})$ and $\delta(\text{Br2C3C2C4})$ at this level are 11.3° and -168.9° respectively (see Figure 3.1d).

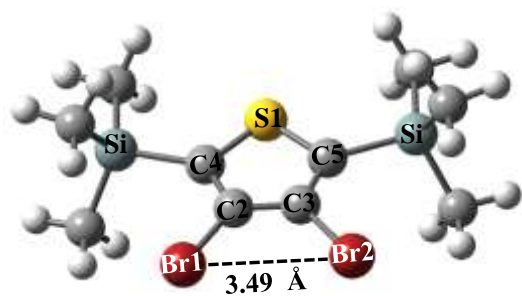
The non-planar structure obtained for thia[3]helicene at MP2 level is in good agreement with experimentally reported structure.⁶⁵ Calculated Mulliken charges on Si and Br atoms are 0.56 and -0.13 a.u. respectively in thia[3]helicene. Thus, two bulky Br groups present at C2 and C3 not only create a geometrical steric hindrance but also create an electronic steric hindrance. This makes thia[3]helicene to have a non-planar structure. It may be noted that ω -B97XD⁹⁶ density functional also produces a planar structure for thia[3]helicene in DCM solvent with the same. In case of thia[4]helicene the structure obtained is non-planar (see Figure 3.1e) and the distance between the two Br atoms is found to be 3.51 \AA . Moreover, the calculated dihedral angles $\delta(\text{Br1C2C3Br2})$ and $\delta(\text{Br2C3C2C4})$ in DCM solvent at MP2 level are -65.6° and 78.4° respectively. Calculated distances, $r_{\text{Br1-Br2}}$, $r_{\text{C2-C3}}$, $r_{\text{C4-C8}}$ are 3.53 , 4.24 and 6.97 \AA respectively at MP2 level which is comparable to the corresponding values obtained at B3LYP-D level of theory. Thus, the structure obtained at B3LYP-D and MP2 level in DCM solvent are very close in thia[4]helicene in DCM solvent.

Geometry optimization is also carried out for thia[1]helicene and thia[2]helicene at MP2 level

Table 3.1 Selected [#]geometrical parameters of neutral thia[n]helicenes, [n]TH n=1-10 calculated at B3LYP-D /6-311++G(d,p) level of theory in gas phase. Values in the braces show corresponding geometrical parameters neutral thia[n]helicenes, n=1-10 in DCM solvent. Bold-faced values in third braces are calculated at B3LYP/6-311++G(d,p) level of theory in DCM solvent.

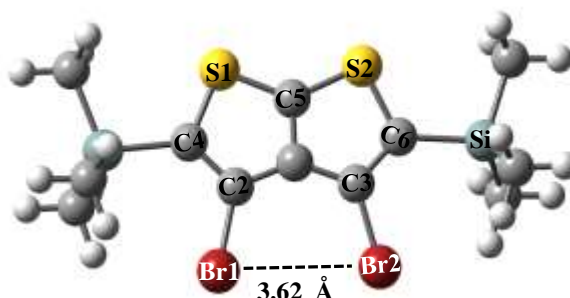
n	1	2	3	4	5	6	7	8	9	10
r_{C4-C5} (Å)	2.57, (2.57)	2.51, (2.51)	2.49, (2.49)	2.50, (2.50)	2.51, (2.51)	2.50, (2.50)	2.50, (2.50)	2.50, (2.50)	2.51, (2.51)	2.50, (2.50)
r_{C5-C6} (Å)	-	2.51, (2.51)	2.42, (2.42)	2.43, (2.43)	2.44, (2.45)	2.44, (2.44)	2.43, (2.43)	2.44, (2.44)	2.43, (2.45)	2.43, (2.43)
r_{C7-C8} (Å)	-	-	-	2.50, (2.50)	2.44, (2.45)	2.43, (2.43)	2.43, (2.42)	2.44, (2.44)	2.43, (2.45)	2.43, (2.42)
r_{C8-C9} (Å)	-	-	-	-	2.50, (2.50)	2.44, (2.44)	2.43, (2.44)	2.44, (2.44)	2.43, (2.43)	2.43, (2.43)
r_{Br1-Br2} (Å)	3.49, (3.49), [3.49]	3.61, (3.62), [3.61]	3.50, (3.51), [3.51]	3.48, (3.51), [3.50]	3.53, (3.52), [3.52]	3.68, (3.65), [3.69]	4.20, (4.09), [4.19]	5.08, (4.94), [5.10]	5.78, (5.82), [5.79]	6.17, (5.73), [6.18]
δ(Br1C2C3Br2) (degree)	0, (0), [0]	0, (0), [0]	0, (1.4), [2.0]	-60.6, (-65.9), [-61.4]	-107.3, (-112.4), [-112.4]	-149.2, (-153.4), [-149.0]	-167.6, (-166.1), [-168.9]	-123.7, (-94.2), [-124.8]	-75.1, (-55.3), [-78.5]	-26.0, (-30.9), [-29.0]
δ(Br2C3C2C4) (degree)	180, (180), [180]	180, (180), [180]	-180.0, (-178.6), [-178.2]	78.2, (71.5), [77.4]	-10.1, (-14.5), [-14.1]	49.5, (51.6), [49.4]	81.5, (82.6), [80.7]	113.7, (141.9), [112.7]	-151.8, (-165.5), [-149.5]	-169.5, (-172.8), [-171.7]

[#]Figure 3.1 may be referred for identifying geometrical parameters.



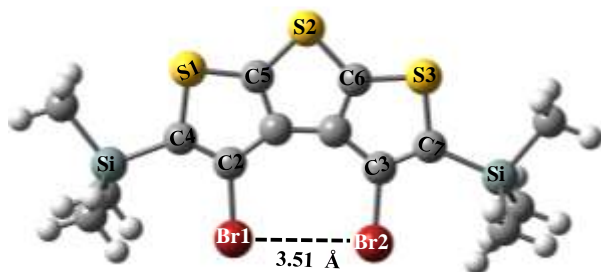
$r_{C2-C3} = 1.43 \text{ \AA}$, $r_{C4-C5} = 2.57 \text{ \AA}$
 $\delta(\text{Br1C2C3Br2}) = 0^\circ$, $\delta(\text{Br2C3C2C4}) = 180^\circ$
 $\angle C4S1C5 = 95.2^\circ$

a



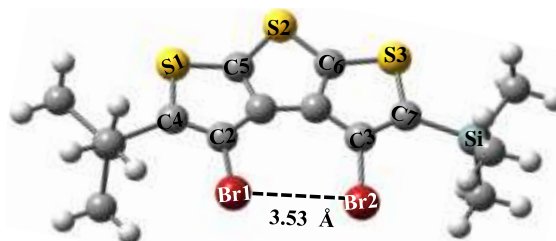
$r_{C2-C3} = 2.71 \text{ \AA}$, $r_{C4-C6} = 4.66 \text{ \AA}$
 $\delta(\text{Br1C2C3Br2}) = 0^\circ$, $\delta(\text{Br2C3C2C4}) = 180^\circ$
 $\angle C4S1C5 = 91.6^\circ$

b



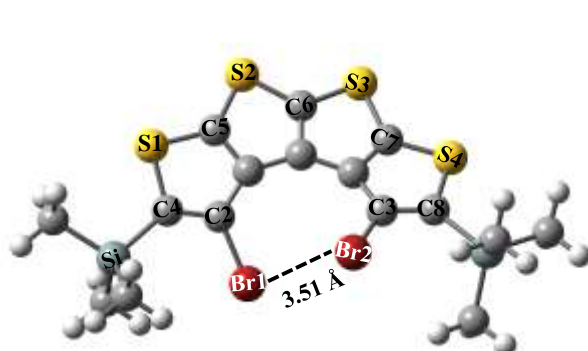
$r_{C2-C3} = 3.73 \text{ \AA}$, $r_{C4-C7} = 6.21 \text{ \AA}$
 $\delta(\text{Br1C2C3Br2}) = 1.4^\circ$, $\delta(\text{Br2C3C2C4}) = -178.6^\circ$
 $\angle C4S1C5 = 91.3^\circ$, $\angle C5S2C6 = 88.1^\circ$

c



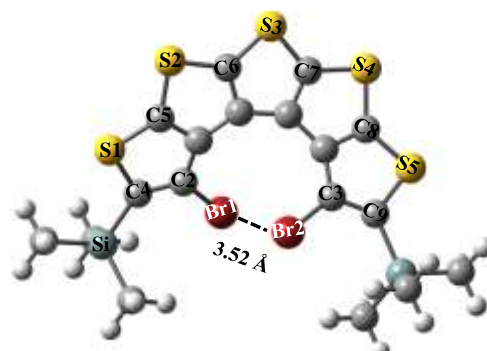
$r_{C2-C3} = 3.70 \text{ \AA}$, $r_{C4-C7} = 6.20 \text{ \AA}$
 $\delta(\text{Br1C2C3Br2}) = 11.3^\circ$, $\delta(\text{Br2C3C2C4}) = -168.9^\circ$
 $\angle C4S1C5 = 91.9^\circ$, $\angle C5S2C6 = 88.4^\circ$

d



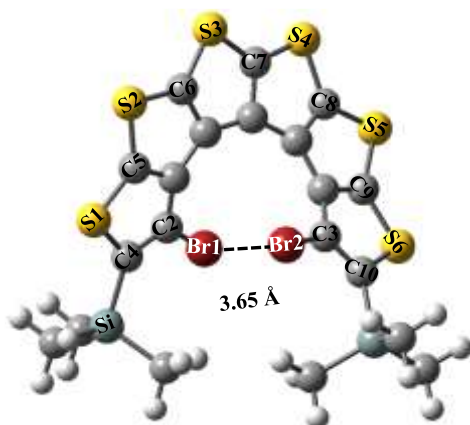
$r_{C2-C3} = 4.29 \text{ \AA}$, $r_{C4-C8} = 6.94 \text{ \AA}$
 $\delta(\text{Br1C2C3Br2}) = -65.9^\circ$, $\delta(\text{Br2C3C2C4}) = 71.5^\circ$
 $\angle C4S1C5 = 91.4^\circ$, $\angle C5S2C6 = 88.2^\circ$

e



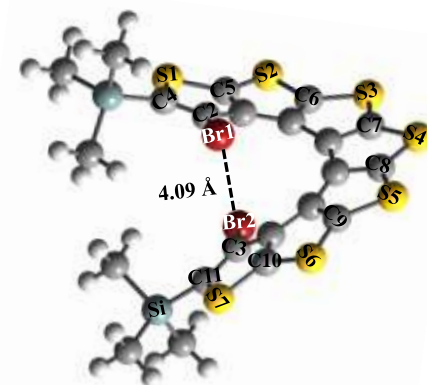
$r_{C2-C3} = 4.35 \text{ \AA}$, $r_{C4-C9} = 6.86 \text{ \AA}$
 $\delta(\text{Br1C2C3Br2}) = -112.4^\circ$, $\delta(\text{Br2C3C2C4}) = -14.1^\circ$
 $\angle C4S1C5 = 91.5^\circ$, $\angle C6S3C7 = 88.4^\circ$

f



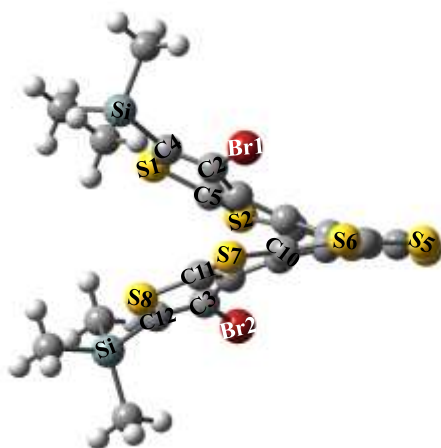
$r_{C2-C3} = 4.23 \text{ \AA}$, $r_{C4-C10} = 6.17 \text{ \AA}$
 $\delta(Br1C2C3Br2) = -153.4^\circ$, $\delta(Br2C3C2C4) = 51.6^\circ$
 $\angle C4S1C5 = 91.5^\circ$, $\angle C5S2C6 = 88.2^\circ$

g



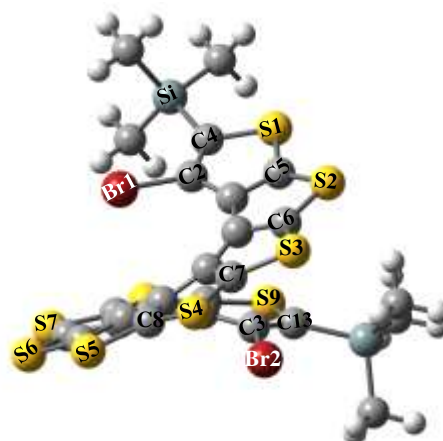
$r_{C2-C3} = 4.12 \text{ \AA}$, $r_{C4-C11} = 5.75 \text{ \AA}$
 $\delta(Br1C2C3Br2) = -166.1^\circ$, $\delta(Br2C3C2C4) = 82.6^\circ$
 $\angle C4S1C5 = 91.4^\circ$, $\angle C5S2C6 = 88.1^\circ$

h



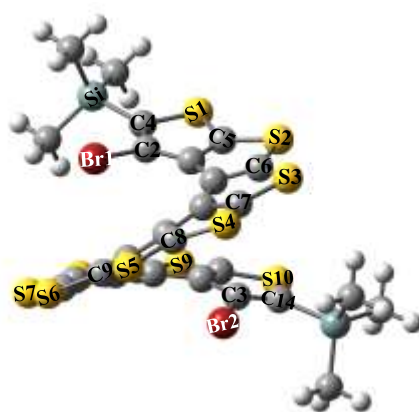
$r_{Br1-Br2} = 4.94 \text{ \AA}$, $r_{C2-C3} = 3.90 \text{ \AA}$, $r_{C4-C12} = 4.88 \text{ \AA}$
 $\delta(Br1C2C3Br2) = -94.2^\circ$, $\delta(Br2C3C2C4) = 141.9^\circ$
 $\angle C4S1C5 = 91.5^\circ$, $\angle C5S2C6 = 88.1^\circ$

i



$r_{Br1-Br2} = 5.82 \text{ \AA}$, $r_{C2-C3} = 4.31 \text{ \AA}$, $r_{C4-C13} = 5.33 \text{ \AA}$
 $\delta(Br1C2C3Br2) = -55.3^\circ$, $\delta(Br2C3C2C4) = -165.5^\circ$
 $\angle C4S1C5 = 91.5^\circ$, $\angle C5S2C6 = 88.3^\circ$

j



$$r_{\text{Br1-Br2}} = 5.73 \text{ \AA}, r_{\text{C2-C3}} = 5.05 \text{ \AA}, r_{\text{C4-C14}} = 6.55 \text{ \AA}$$

$$\delta(\text{Br1C2C3Br2}) = -30.9^\circ, \delta(\text{Br2C3C2C4}) = -172.8^\circ$$

$$\angle \text{C4S1C5} = 91.5^\circ, \angle \text{C5S2C6} = 88.2^\circ$$

k

Figure 3.1 Most stable structures of neutral thia[n]helicenes, [n]TH, n=1-10 a) [1]TH, b) [2]TH, c) [3]TH (B3LYP-D), d) [3]TH (MP2), e) [4]TH, f) [5]TH, g) [6]TH, h) [7]TH, i) [8]TH, j) [9]TH and k) [10]TH, with selected geometrical parameters calculated at B3LYP-D/6-311++G(d,p) level of theory in DCM solvent. d) is the most stable structure of thia[3]helicene calculated at MP2 is /6-311++G(d,p) level of theory in DCM solvent.

to examine the performance of B3LYP-D functional. Geometrical parameters obtained for these thia[n]helicenes at MP2 level are very close to those obtained at B3LYP-D level of theory. Thus, for the rest of the systems, geometry optimization is carried out by applying B3LYP-D functional. For thia[5]helicene the non-planar structure is displayed in Figure 3.1f. In the case of the next larger system, thia[6]helicene the same kind of non-planar structure is obtained as shown in Figure 3.1g. It may be noted that the helical structure obtained for thia[7]helicene, [7]TH (see Figure 3.1h) is consistent with the experimentally reported structure of thia[7]helicene, [7]TH.⁶⁵ Calculated Mulliken charges on sulfur atoms labeled as S1, S2, S3, and S4 are 0.12 a.u., -0.36 a.u., -0.28 a.u. and -0.30 a.u. respectively. In case of thia[8]helicene, eight thiophene rings are fused to make a coil type structure as shown in Figure 3.1i. The structures of thia[n]helicenes, [n]TH, n=9-10 are also fully optimized considering DCM solvent at B3LYP-D level and shown in Figure 3.1j and Figure 3.1k respectively. One can easily note

from Table 1 that only a very small change is obtained in the listed geometrical parameters for these thia[n]helicenes with addition of thiophene rings except for dihedral angle as the systems loose planarity for larger size ($n \geq 3$) helicenes. Table 3.1 indicates that calculated dihedral angles for thia[n]helicenes, $n=3-8$ at B3LYP-D level are considerably different than those at B3LYP level showing the effect of dispersion in the geometry. However, no difference in the calculated distance between the two Br atoms is observed. In short, it is predicted that the structures of [1]TH to [3]TH systems are planar at B3LYP-D/6-311++G(d,p) level of theory in gas phase and in DCM solvent. However, the structure of neutral thia[3]helicene, [3]TH is not planar when the calculation is carried out at the MP2 level of theory in gas phase as well as in DCM solvent Except for [3]TH system, calculated geometrical parameters of these neutral helicenes at B3LYP-D and MP2 levels of theory for thia[n]helicenes, [n]TH, $n=1-10$ are very close in the gas phase as well as in DCM solvent.

3.3.2 Ionization energies for thia[n]helicenes, [n]TH, $n=1-10$ in DCM solvent

Ionization energy is a significant molecular parameter, as it gives an account of the stability of the molecular systems. Thus, ionization energy must be considered to get the energy required to convert neutral molecular systems to their corresponding positive charged systems. Also, the additional benefits of positively charged systems can behave as p-type semiconductor and transport properties may be significantly enhanced. Thus, ionization energies of these thia[n]helicenes systems are reported to investigate the suitability of these systems for finding applications as organic electronic devices. The ionization energies (IE) for thia[n]helicenes,

Table 3.2 Calculated ionization energy (in eV) of thia[n]helicenes, [n]TH, n=1-10 in gas phase applying different theoretical methods. Values in the braces are the corresponding energy in DCM solvent.

Ionization energy (in eV) of thia[n]helicenes, [n]TH, n = 1-5					
Method	[1]TH	[2]TH	[3]TH	[4]TH	[5]TH
i)	7.9, (6.5)	7.5, (6.2)	7.3, (6.1)	7.2, (5.9)	7.0, (5.7)
ii)	8.5, (6.5)	7.5, (6.2)	7.3, (6.1)	7.2, (5.9)	7.0, (5.7)
iii)	8.5, (6.5)	7.5, (6.2)	7.3, (6.1)	7.2, (5.9)	7.0, (5.7)
iv)	8.6, (7.2)	7.3, (5.9)	7.1, (5.8)	7.5, (6.2)	7.2, (5.8)
Ionization energy (in eV) of thia[n]helicenes, [n]TH, n = 6-10					
Method	[6]TH	[7]TH	[8]TH	[9]TH	[10]TH
i)	7.0, (5.8)	6.9, (5.8)	6.8, (5.6)	6.8, (5.7)	6.8, (5.7)
ii)	7.0, (5.8)	6.9, (5.8)	6.8, (5.6)	6.8, (5.7)	6.8, (5.7)
iii)	7.0, (5.8)	6.9, (5.8)	6.8, (5.6)	6.8, (5.7)	6.8, (5.7)
iv)	7.3, (6.0)	6.7, (5.5)	6.6, (5.7)	6.6, (5.5)	7.2, (6.1)

i) B3LYP, ii) B3LYP-D, iii) B3LYP-D3, and iv) MP2 with 6-311++G(d,p) basis set

[n]TH, n=1-10 are calculated as the difference of energy for the most stable structures of neutral and their corresponding radical cations in gas phase and The most stable structures obtained for neutral and their corresponding radical cations at B3LYP-D level of theory are being used to calculate the IE at B3LYP-D3 and MP2 levels of theory. One can see from the Table 3.2 that IE values calculated at different levels of theory for each size of thia[n]helicenes, [n]TH in the gas phase are very close at the DFT level. It is also observed that IE values calculated at the MP2 level show both positive and negative deviation with respect to DFT values. Again, IE values calculated including the medium effect of DCM solvent following a macroscopic

solvent model are significantly lower than those in the gas phase for all thia[n]helicenes. The observation is consistent at MP2 and all the DFT levels considered at present. This suggests that cations of thia[n]helicenes are more stable in DCM solvent compared to gas phase. Table 3.2 also indicates that ionization energy value of these systems in gas phase calculated at DFT levels decreases with the addition of each ring to saturate at 6.8 eV. However, the calculated values are within 0.4 eV except for thia[1]helicene. Table 3.2 also indicates that ionization energy value of these systems in gas phase calculated at DFT levels decreases with the addition of each ring to saturate at 6.8 eV. However, when the same parameter is calculated including solvent effect at the same levels of theory, ionization energy value leads to 5.7 eV for thia[10]helicene. It is also noted that IE values increase on addition of a ring to neutral thia[5]helicene and thia[8]helicene. At MP2 level, calculated IE values show a different trend on addition of a ring; however, the calculated values are within 0.4 eV except for thia[1]helicene.

3.3.3 HOMO-LUMO gap for thia[n]helicenes, [n]TH, n=1-10 in DCM solvent

For a large conjugated system, small highest occupied molecular orbital (HOMO) to unoccupied molecular orbital (LUMO) gaps lead to mobile π electrons which make it easy for the electron to jump to a higher energy level that is close in energy. Thus, the greater the mobility of the π electrons in large conjugated π -orbital systems leads to greater stabilization of molecules as the distribution of the energy throughout the molecule. Hence, smaller HOMO-LUMO gaps correspond to better stability. This mobility of the π -electron also contributes to its conductivity. Moreover, HOMO-LUMO gaps also indicates the minimum energy requirement for an electronic transition. Thus, it is an essential molecular parameter for these helicenes for finding applications as organic electronic devices in a suitable energy range. The

energy separation between the highest occupied molecular orbital (HOMO) and the lowest unoccupied molecular orbital (LUMO) has been used as a simple indicator of kinetic stability of a molecular system. A large HOMO-LUMO gap implies high kinetic stability and low chemical reactivity, because it is energetically unfavourable to add electrons to a high-lying LUMO, to extract electrons from a low-lying HOMO, and so to form the activated complex of any potential reaction. Moreover, HOMO-LUMO gap also indicates the minimum energy requirement for an electronic transition. Thus, it is an important molecular parameter for these helicenes for finding applications as organic electronic devices in a suitable energy range.

Table 3.3 Calculated HOMO-LUMO energy gap (in eV) of thia[n]helicenes, [n]TH, n=1-10 in the gas phase. Values in the braces are the corresponding energy gaps of neutral thia[n]helicenes in DCM solvent. Data shown in bold faces are the experimental values from the literature.

HOMO-LUMO energy gap (in eV) of thia[n]helicenes, [n]TH, n = 1-5					
Method	[1]TH	[2]TH	[3]TH	[4]TH	[5]TH
i)	5.3, (5.3)	5.0, (5.1)	4.9, (4.9)	4.7, (4.7)	4.5, (4.6)
ii)	5.3, (5.3)	5.0, (5.1)	4.9, (4.9)	4.7, (4.7)	4.5, (4.6)
iii)	5.3, (5.3)	5.0, (5.1)	4.9, (4.9), 4.9	4.7, (4.7)	4.5, (4.6)
HOMO-LUMO energy gap (in eV) of thia[n]helicenes, [n]TH, n = 6-10					
Method	[6]TH	[7]TH	[8]TH	[9]TH	[10]TH
i)	4.6, (4.6)	4.5, (4.6)	4.4, (4.2)	4.3, (4.3)	4.3, (4.3)
ii)	4.6, (4.6)	4.5, (4.6)	4.4, (4.2)	4.3, (4.3)	4.3, (4.3)
iii)	4.6, (4.6)	4.5, (4.6), 5.0	4.4, (4.2)	4.3, (4.3)	4.3, (4.3)

i) B3LYP, ii) B3LYP-D, and iii) B3LYP-D3 with 6-311++G(d,p) basis set

Table 3.3 summaries calculated HOMO-LUMO gap of thia[n]helicenes, [n]TH, n=1-10 at B3LYP, B3LYP-D, B3LYP-D3 levels of theory using 6-311++G(d,p) basis set in the gas phase and in DCM solvent. This energy parameter has been calculated considering the most stable structure of the respective helicene. Table 3.3 indicates that on the addition of each ring the calculated energy gap systematically decreases to saturate at 4.3 eV in the gas phase. This behaviour is consistent at all the three levels of DFT considered at present and the calculated values are also the same. Incidentally, when the energy gap is calculated considering the most stable structures of thia[n]helicenes obtained in DCM solvent, the values are the same as in gas phase except a few cases. The energy gap for [3]TH and [7]TH are reported in the literature as 4.9 eV and 5.0 eV respectively, calculated based on experimental UV-Vis spectra.⁶⁵

The present calculated value for [3]TH is exactly the same as the literature data at all the three levels of theory.⁶⁵ However, present calculated data for [7]TH system is 0.4 eV lower than the literature data. Overall, the calculated HOMO-LUMO gap of thia[n]helicenes, [n]TH, n=1-10 shown in Table 3 should be reliable. In short, for neutral thia[n]helicenes, n=1-10 the calculated HOMO-LUMO gap belongs to UV-region of the electromagnetic spectrum.

3.3.4 Structure for radical cations of thia[n]helicenes, [n]TH^{•+}, n=1-10 in DCM solvent

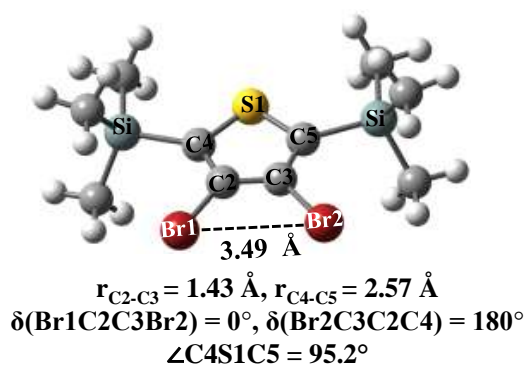
It is reported in the literature based on electrochemical experiments that stable radical cation of thia[7]helicene, [7]TH^{•+} can be generated at room temperature in the presence of counter ion PF₆⁻ in DCM solvent.⁶⁷ Geometrical parameters of radical cation of thia[n]helicenes, n=1-10, [n]TH^{•+} are optimized considering the corresponding neutral structure as the initial input. For the sake of simplicity, calculations are performed without using counterion. Table 3.4 shows selected geometrical parameters of the fully optimized structures of radical cations of thia[n]helicenes, [n]TH^{•+}, n=1-10 at B3LYP-D functional considering 6-311++G(d,p) basis set

in the gas phase and DCM solvent. The optimized molecular structures of radical cations of thia[n]helicenes, $[n]\text{TH}^{+\bullet}$ for $n=1-10$ in DCM solvent are provided in Figure 3.2(a-j). Table 3.4 reveals that no significant change occurs for the geometrical parameters ongoing from gas phase to solvent DCM except for a few larger size helicenes. It may also be noted from Figure 3a that the radical cation of thia[1]helicene is planar. The spin densities are equally populated over carbon atoms labeled as C4 and C5 with 0.3 a.u. and that on sulfur atom (S1) is 0.01 a.u. In case of radical cation of thia[2]helicene, a planar structure (see Figure 3.2b) is obtained. The spin densities are equally (0.16 a.u.) populated over sulfur atoms, S1 and S2 and the same at C4 and C6 is 0.07 a.u. In contrast, for the radical cation of thia[3]helicene, a non-planar structure (see Figure 3.2c) is obtained in DCM solvent. Mulliken charges on Si and Br atoms are obtained as 0.46 and -0.03 respectively. The spin densities at sulfur atoms labeled as S1 and S2 are 0.05 and 0.2 a.u. respectively and for carbon atoms labeled as C4 and C7 the value of spin density is 0.12 a.u. Closer proximity of two bulky Br atoms present at carbon atoms labeled as C2 and C3 may be the source of geometrical and electronic steric hindrances. This makes the planar structure of radical cation of thia[3]helicene unstable and converts it into a stable non-planar helical structure. Thus, to produce helical shape in radical cation of thia[3]helicene, the presence of TMS groups at carbon atoms labeled as C4 and C7 atoms and Br groups at carbon atoms labeled as C2 and C3 atoms is necessary. For thia[4]helicene radical cation, the dihedral angles $\delta(\text{Br1C2C3Br2})$ and $\delta(\text{Br2C3C2C4})$ are calculated as -66.2° and 76.2° respectively showing it as a non-planar structure (see Figure 3.2d). In the case of the optimized structure of radical cation of thia[4]helicene, Mulliken charges over Si and Br atoms are -0.49 a.u. and -0.01 a.u. respectively. The spin densities at sulfur atoms labeled as S1 and S2 are 0.12 a.u. and 0.06 a.u. respectively and for carbon atoms labeled as C4 and C8 the same is obtained as -0.01 a.u. For thia[5]helicene radical cation, the

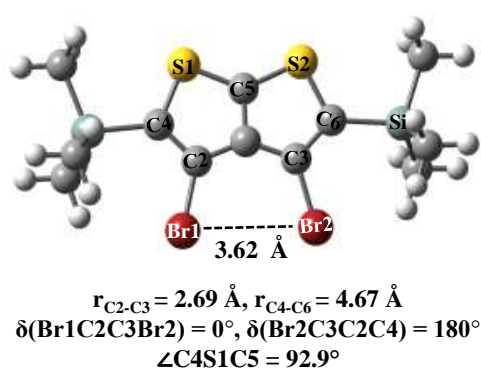
Table 3.4 Selected [#]geometrical parameters for radical cations of thia[n]helicenes, [n]TH⁺ n=1-10 calculated at B3LYP-D /6-311++G(d,p) level of theory in gas phase. Values in the braces show corresponding geometrical parameters for radical cations of thia[n]helicenes, n=1-10 in DCM solvent. Bold-faced values in third braces are calculated at B3LYP/6-311++G(d,p) level of theory in DCM solvent.

N	1	2	3	4	5	6	7	8	9	10
r_{C4-C5} (Å)	2.55, (2.55)	2.50, (2.50)	2.48, (2.47)	2.50, (2.50)	2.50, (2.50)	2.49, (2.50)	2.50, (2.50)	2.50, (2.50)	2.50, (2.50)	2.50, (2.50)
r_{C5-C6} (Å)	-	2.50, (2.50)	2.43, (2.42)	2.42, (2.42)	2.45, (2.42)	2.43, (2.43)	2.43, (2.44)	2.43, (2.44)	2.43, (2.43)	2.43, (2.43)
r_{C7-C8} (Å)	-	-	-	2.50, (2.50)	2.45, (2.45)	2.42, (2.42)	2.43, (2.43)	2.42, (2.44)	2.41, (2.41)	2.43, (2.43)
r_{C8-C9} (Å)	-	-	-	-	2.43, (2.43)	2.43, (2.42)	2.41, (2.41)	2.42, (2.43)	2.42, (2.42)	2.42, (2.41)
r_{Br1-Br2} (Å)	3.51, (3.52), [3.48]	3.60, (3.60), [3.59]	3.54, (3.55), [3.55]	3.48, (3.49), [3.48]	3.55, (3.55), [3.58]	3.71, (3.67), [3.72]	4.30, (4.10), [4.30]	5.14, (5.10), [5.10]	5.74, (5.77), [5.77]	6.20, (6.21), [6.21]
δ(Br1C2C3Br2) (degree)	0, (0), [0]	0, (0), [0]	0, (18.3), [12.9]	-65.7, (-66.2), [-62.5]	-114.5, (-113.2), [-108.1]	-147.4, (-151.9), [-147.0]	-166.5, (-165.9), [-167.9]	-124.4, (-124.8), [-124.8]	-59.9, (-66.0), [-82.3]	-27.4, (-11.6), [-29.8]
δ(Br2C3C2C4) (degree)	180, (180), [180]	180, (180), [180]	-161.1, (-162.6), [-166.4]	71.6, (71.2), [76.1]	-12.8, (-11.7), [-7.3]	46.9, (48.7), [46.5]	80.8, (81.5), [79.9]	99.2, (112.2), [112.7]	-147.1, (-161.8), [-146.4]	-170.8, (-159.7), [-172.3]

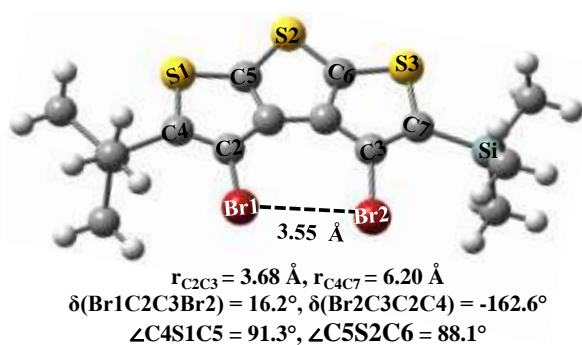
[#]Figure 3.2 may be referred for identifying geometrical parameters.



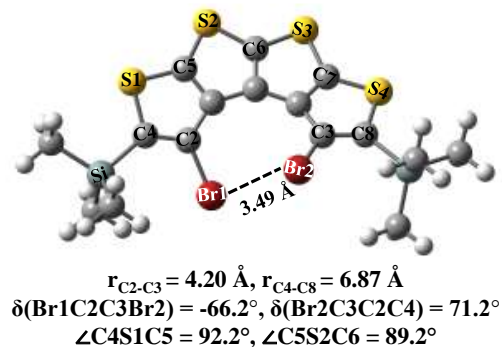
a



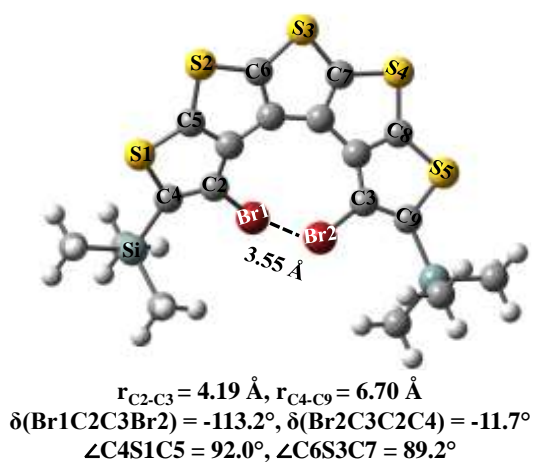
b



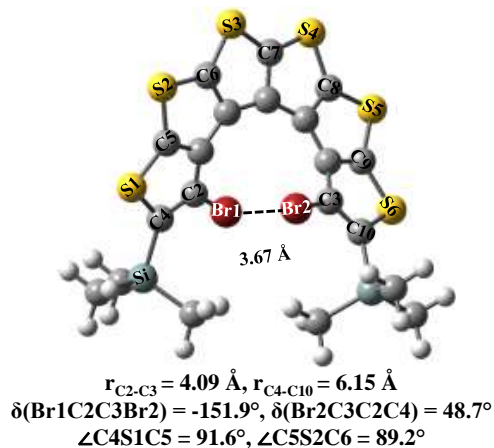
c



d



e



f

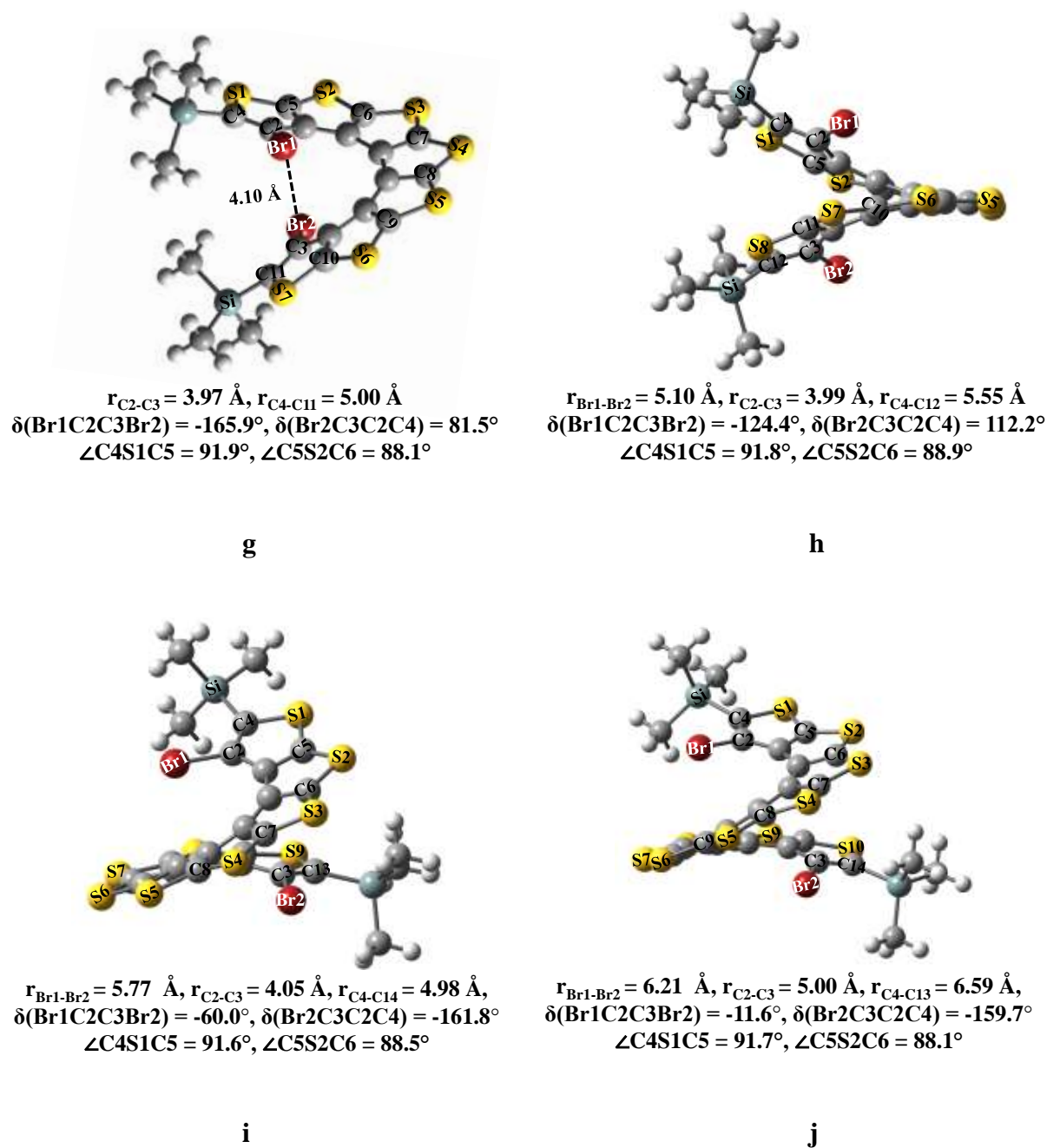


Figure 3.2 Most stable structures for (a-j) radical cation of thia[n]helicenes, $[n]TH^{+}$, $n=1-10$ a) $[1]TH^{+}$, b) $[2]TH^{+}$, c) $[3]TH^{+}$, d) $[4]TH^{+}$, e) $[5]TH^{+}$, f) $[6]TH^{+}$, g) $[7]TH^{+}$, h) $[8]TH^{+}$, i) $[9]TH^{+}$, and j) $[10]TH^{+}$ with selected geometrical parameters calculated at B3LYP-D/6-311++G(d,p) level of theory in DCM solvent.

dihedral angles $\delta(\text{Br1C2C3Br2})$ and $\delta(\text{Br2C3C2C4})$ are calculated as -113.2° and -11.7° respectively showing it as a helical structure (see Figure 3.2e). Spin densities on sulfur atoms labeled as S1, S2 and S3 are 0.07, 0.13 and 0.01 a.u. respectively and for carbon atoms labeled as C4 and C9 the value obtained is 0.01 a.u. The dihedral angles $\delta(\text{Br1C2C3Br2})$ and $\delta(\text{Br2C3C2C4})$ the radical cation of thia[6]helicene (see Figure 3.2f) are obtained as -151.9 and 48.7° respectively showing largely non-planar helical structure. The calculated spin densities over sulfur atoms labeled as S1, S2, and S3 are 0.02, 0.12 and 0.01 a.u. respectively. In the case of radical cation of thia[7]helicene in DCM solvent, the dihedral angles $\delta(\text{Br1C2C3Br2})$ and $\delta(\text{Br2C3C2C4})$ are -165.9 and 81.5° respectively (see Figure 3.2g). Spin densities on sulfur atoms labeled as S1, S2, S3, and S4 are 0.05, 0.04, 0.04 and 0.16 a.u. respectively and the same for C4 and C11 atoms is -0.01 a.u.. The structure obtained for radical cation of thia[8]helicene is also of coil type. The one complete turn in this coil type structure requires eight fused thiophene rings for radical cation of thia[8]helicene. For the radical cations of thia[8]helicene, thia[9]helicene and thia[10]helicene coil type helical structures (see Figure 3.2(h-j)) are obtained in DCM solvent. Table 3.4 indicates that calculated dihedral angles for thia[n]helicenes radical cations, $n=3-8$ at B3LYP-D level are considerably different than those at B3LYP level showing the effect of dispersion in the geometry. However, no difference in the calculated distance between the two Br atoms is observed.

In short, the stepwise addition of thiophene rings in these radical cations produces planar structures in radical cations of thia[n]helicenes, $[\text{n}]\text{TH}^{++}$ for $n=1-2$ in the gas phase and in DCM solvent. For the radical cations of thia[n]helicenes, $[\text{n}]\text{TH}^{++}$ for $n=3-6$ the non-planar structures are obtained in the gas phase as well as in solvent. In the case of radical cations of thia[n]helicenes, $[\text{n}]\text{TH}^{++}$ for $n=7-10$, the coil type helical structures are obtained in the gas phase as well as in DCM solvent. The Si and Br atoms are found to be positively and negatively

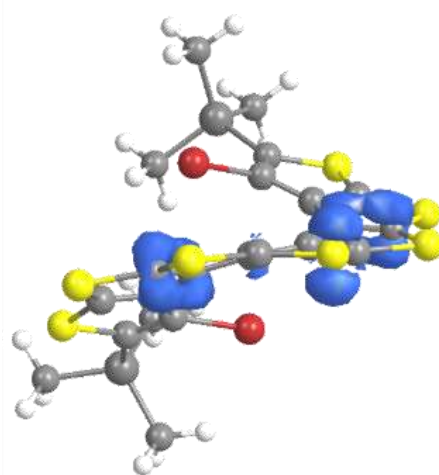


Figure 3.3 Spin density plot for thia[7]helicenes radical cation calculated at B3LYP-D/6-311++G(d,p) level of theory in DCM solvent with contour cutoff= 0.002 a.u.

charged respectively. In case of thia[n]helicenes, $[n]\text{TH}^{*+}$ for $n=1-6$.

Spin density in the most stable structure of these thia[n]helicenes ($n=1-10$) radical cation is calculated at B3LYP-D/6-311++G(d,p) level including the macroscopic effect of DCM solvent following ROHF (Restricted Open-shell Hartree Fock) formalism to avoid any spin contamination. Calculated spin density is plotted to understand the pattern of location of the odd electron in these systems. Figure 3.3 shows the spin density plot of thia[7]helicenes radical cation, $[7]\text{TH}^{*+}$ with a contour cut-off value of 0.002 a.u. It is observed that a significant amount of spin density is always present on heavy atoms. Thus it is expected that high g value may be obtained in the EPR spectra of thia[n]helicenes radical cation, $[n]\text{TH}^{*+}$. In fact, based on EPR study it is reported that g value for thia[7]helicene radical cation is ~ 2.006 which is comparable to the g value of free electron.⁶⁷

3.3.5 HOMO-LUMO energy gap for thia[n]helicenes radical cation, [n]TH^{•+}, n=1-10 in DCM solvent

Energy gaps between two selected orbitals in radical cations of thia[n]helicenes, [n]TH^{•+}, n=1-10 are calculated at B3LYP, B3LYP-D and B3LYP-D3 levels based on the optimized structures in DCM solvent applying respective functional. In these odd electron radical cation helicenes, the highest occupied orbital is singly occupied and it is referred as the lowest singly occupied molecular orbital or LSOMO. Optical absorption band may be observed when an electron makes a transition from the highest doubly occupied molecular orbital or HDOMO to LSOMO. Table 3.5 provides the calculated HDOMO-LSOMO gap for the radical cations of

Table 3.5 Calculated HDOMO-LSOMO energy gap (in eV) for radical cations of thia[n]helicenes, [n]TH^{•+}, n=1-10 in DCM solvent. Values in the braces are the corresponding LSOMO-LUMO gaps for radical cations of thia[n]helicenes in DCM solvent. HDOMO refers to the highest doubly occupied molecular orbital, LSOMO stands for the lowest singly occupied molecular orbital and LUMO stands for the lowest unoccupied molecular orbital

Energy gap (in eV) for thia[n]helicene radical cations, [n]TH ^{•+} , n = 1-5					
Method	[1]TH ^{•+}	[2]TH ^{•+}	[3]TH ^{•+}	[4]TH ^{•+}	[5]TH ^{•+}
i)	3.2, (1.9)	3.0, (2.3)	3.0, (2.1)	2.8, (1.8)	2.7, (1.7)
ii)	3.2, (1.9)	3.0, (2.3)	3.0, (2.1)	2.8, (1.8)	2.7, (1.7)
iii)	3.2, (1.9)	3.0, (2.3)	3.0, (2.1)	2.8, (1.8)	2.7, (1.7)
Energy gap (in eV) for thia[n]helicene radical cations, [n]TH ^{•+} , n = 6-10					
Method	[6]TH ^{•+}	[7]TH ^{•+}	[8]TH ^{•+}	[9]TH ^{•+}	[10]TH ^{•+}
i)	2.6, (1.7)	2.5, (1.9)	2.4, (2.0)	2.5, (1.9)	2.3, (1.8)
ii)	2.6, (1.7)	2.5, (1.9)	2.4, (2.0)	2.5, (1.9)	2.3, (1.8)
iii)	2.6, (1.7)	2.5, (1.9)	2.4, (2.0)	2.5, (1.9)	2.3, (1.8)

i) B3LYP, ii) B3LYP-D, and iii) B3LYP-D3 with 6-311++G(d,p) basis set

thia[n]helicenes and these values are in the range of 3.2 - 2.3 eV. It is observed that the values for each size helicene radical cation are the same at all these three DFT functionals. It is interesting to note that the HOMO-LSOMO energy gap decreases on the stepwise addition of the thiophene rings to the radical cation of thia[1]helicene, [1]TH^{•+} till [10]TH^{•+} with an exception for [9]TH^{•+}. The continuous decrease may be due to the increase in conjugation with the increase in the number of thiophene rings in the helicene radical cations. Moreover, the calculated HOMO-LSOMO energy gap lies in the visible region of the electromagnetic spectrum. Similarly, LSOMO-LUMO energy gaps in these thia[n]helicene radical cations are also calculated and listed in Table 3.5. These energy gaps are in the range of 2.1 - 1.7 eV and no systematic variation is seen. However, the change in energy gap is small (0.1 eV) for the large size helicenes. Interestingly, the calculated values are same again for the same size of helicene at all the three levels of DFT functionals. Calculated LSOMO-LUMO energy gap for radical cations of thia[n]helicenes, [n]TH^{•+} for n=4-6,10 lies in NIR region of the electromagnetic spectrum. In summary, these doublet radical cationic systems generated from their corresponding neutral systems have a suitable HOMO-LSOMO and LSOMO-LUMO energy gaps. Moreover, the helical structures provide flexibility for using these radical cationic doublet systems as IR detector.

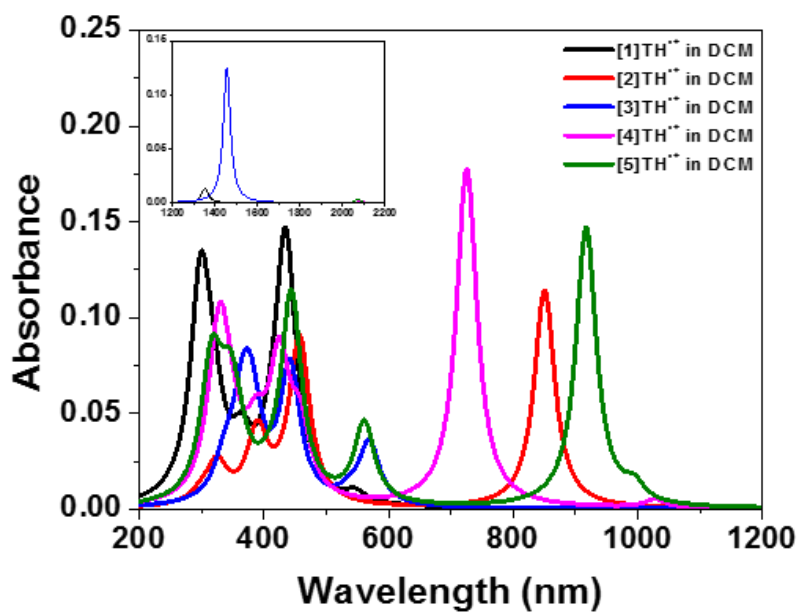
3.3.6 Excited state electronic spectra for radical cations of thia[n]helicenes, [n]TH^{•+}, n=1-10 in DCM

To obtain optical absorption bands (λ_{max}) for the radical cations of thia[n]helicene, [n]TH^{•+}, n=1-10, excited state electronic structure calculations are carried out following TDDFT procedure. CAM-B3LYP, DFT functional in conjunction with 6-311++G(d,p) basis set are considered for the excited state calculations in DCM solvent following macroscopic solvent model for all the radical cations of these thia[n]helicenes. Table 3.6 shows calculated λ_{max} ,

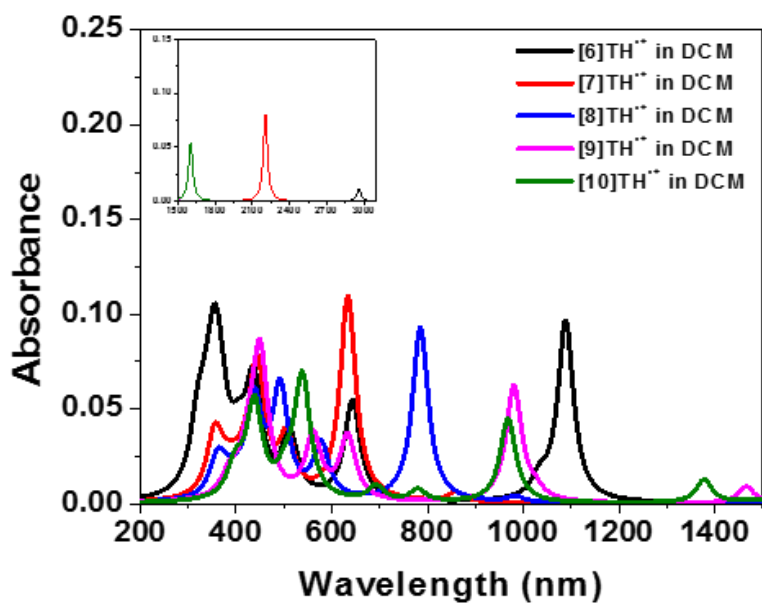
Table 3.6 Calculated excited state data for the radical cations of thia[n]helicenes, [n]TH^{•+} (n=1-10) in DCM solvent considering CAM-B3LYP/6-311++G(d,p) level of theory under TDDFT formalism.

N	λ_{max} (nm)	Oscillator strength (f)	Electronic Transitions [§]
1	1351	0.013	H → L (0.97)
	435	0.136	H-2 → L (0.92)
	413	0.010	H-4 → L (0.98)
2	850	0.114	H-1 → L (0.93)
	457	0.087	H-7 → L (0.71)
	387	0.023	H-6 → L (0.97)
3	1454	0.125	H-1 → L (0.74)
	442	0.070	H-4 → L (0.56), H-9 → L (0.56)
4	1028	0.004	H-1 → L (0.96)
	726	0.177	H-2 → L (0.96)
	425	0.003	H-4 → L (0.51), H-10 → L (0.51)
5	2071	0.003	H → L (0.86)
	994	0.001	H-2 → L (0.94)
	917	0.146	H-1 → L (0.79)
6	2961	0.012	H → L (0.71)
	1089	0.095	H-1 → L (0.72)
	643	0.052	H-3 → L (0.90)
7	2206	0.081	H-1 → L (0.86)
	634	0.107	H-4 → L (0.95)
	505	0.030	H-5 → L (0.90)
8	984	0.003	H-3 → L (0.92)
	785	0.092	H-4 → L (0.92)
	492	0.057	H-6 → L (0.94)
9	1466	0.009	H-2 → L (0.95)
	980	0.061	H-3 → L (0.96)
	450	0.073	H-7 → L (0.68)
10	1605	0.055	H → L (0.97)
	968	0.044	H-3 → L (0.74)
	780	0.007	H-4 → L (0.73)

[§]H = Highest doubly occupied molecular orbital (HDOMO) & L = Lowest singly occupied molecular orbital (LSOMO). Values in the braces show relative contribution of the transition for the optical band. Transitions with major contributions are only shown.



a



b

Figure 3.4 Simulated UV-Vis spectra for radical cations of thia[n]helicenes, $n[\text{TH}]^{\bullet+}$ a) $n=1-5$ and b) $6-10$ in DCM solvent following TDDFT procedure at CAM-B3LYP/6-311++G(d,p) level of theory. The figures are taken at isovalue of 0.002 a.u.

oscillator strength (f) and origin of corresponding electronic transitions for all these ten radical cations of thia[n]helicenes. Simulated electronic spectra of thia[n]helicene radical cations, [n]TH^{•+} (n=1-5) in DCM solvent are displayed in Figure 3.4a. It is interesting to note that [3]TH^{•+} has the stronger absorption band in the IR region ($\lambda_{\text{max}} = 1454$ nm) with the calculated oscillator strength of 0.125. It is also observed that thia[n]helicene radical cations, [1]TH^{•+} and [5]TH^{•+} have weak bands in this region. Similarly, simulated electronic spectra of thia[n]helicene radical cations, [n]TH^{•+} (n=6-10) in DCM solvent are displayed in Figure 3.4b. It may also be noted that radical cations of thia[7]helicene, [7]TH^{•+} and thia[10]helicene, [10]TH^{•+} have also strong absorption bands in the IR region ($\lambda_{\text{max}} = 2206$ and 1604 nm respectively). However, calculations suggest that optical absorption bands in IR region for thia[n]helicene radical cations, [6]TH^{•+}, [8]TH^{•+} and [9]TH^{•+} are relatively weak. Out of all these radical cationic systems studied at present the experimental absorption spectrum has been reported only for the radical cation of thia[7]helicene, [7]TH^{•+} having λ_{max} value at 510 nm.^[67] However, the optical spectrum has been reported only upto 1000 nm. Error may be due to the fact that the experimental UV-Visible spectrum of radical cation of thia[7]helicene, [7]TH^{•+} is reported having PF₆⁻ as the counter ion in DCM solvent. However, the present calculations have been carried out in DCM solvent considering a macroscopic solvent model without any counterion.

The selected MOs are plotted using the most stable structures of these radical cations of thia[n]helicenes, [n]TH^{•+}, n=1-10 in DCM solvent calculated applying B3LYP-D functional and 6-311++G(d,p) basis functions in Figure 3.5. For radical cation of thia[1]helicene, [1]TH^{•+}, the lowest energy band (1351 nm) is mainly due to the electronic transition of HOMO → LUMO (see Table 3.6); HOMO refers to the highest doubly occupied

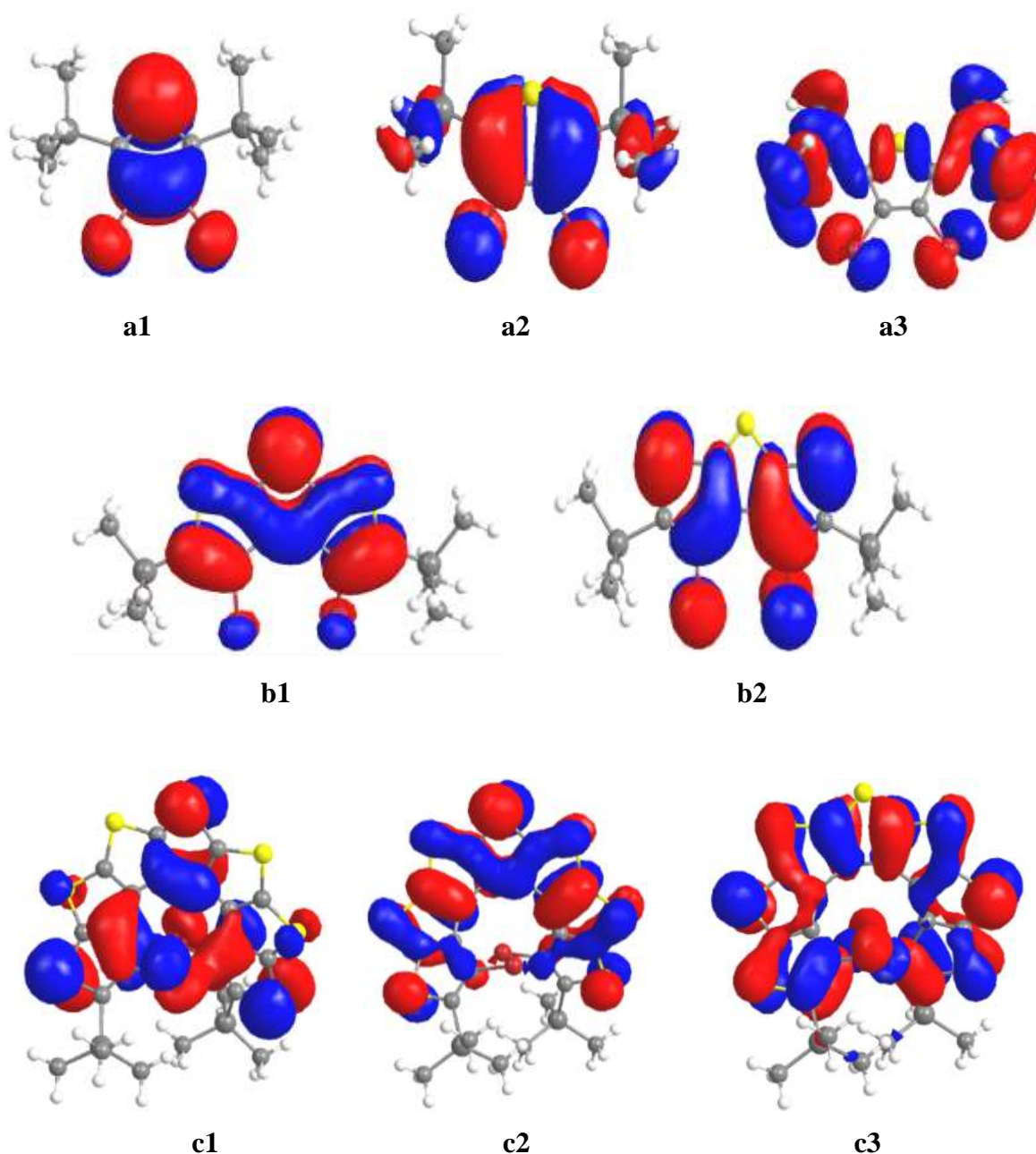


Figure 3.5 Selected molecular orbital plots (a1-c2) for radical cations of thia[n]helicenes, a1) H orbital of [1]TH^{•+}, a2) L orbital of [1]TH^{•+}, a3) H-2 orbital of [1]TH^{•+}, b1) H-1 orbital of [3]TH^{•+}, b2) L orbital of [3]TH^{•+} c1) H-4 orbital of [7]TH^{•+}, c2) L orbital of [7]TH^{•+}, and c3) H-1 orbital of [7]TH^{•+} based on most stable structures in DCM solvent.

molecular orbital (henceforth referred as H) and LSOMO refer to the lowest singly occupied molecular orbital (henceforth referred as L). These two orbitals are plotted in Figure 3.5a1 and Figure 3.5a2 respectively. From the orbital plots, it appears that it is a $\pi \rightarrow \pi^*$ (ring) electronic

transition. However, the strong band in the visible region at 435 nm is mainly due to H-2→L electronic transition. H-2 orbital is shown in Figure 3.5a3 and it appears to be a σ orbital. Thus, the strong optical absorption band of thia[1]helicene, [1]TH⁺⁺ is due to $\sigma \rightarrow \pi^*$. The assignment coefficients of atomic orbitals. In case of the radical cation of thia[2]helicene, [2]TH⁺⁺, the major optical absorption band at 850 nm is mainly due to H-1→L transition and orbital analysis suggests that it is a π - π^* transition. Similarly, for radical cation of thia[3]helicene, [3]TH⁺⁺, the strong optical absorption band at 1454 nm is mainly due to H-1→L transition. The orbitals, H-1 and L are displayed in Figure 3.5b1 and Figure 3.5b2 respectively and the transition as π - π^* . It is interesting to note that on successive addition of two thiophene rings to [1]TH⁺⁺, the major optical band undergoes large red shift from 435 nm to 850 nm for [2]TH⁺⁺ and 850 nm to 1454 nm for [3]TH⁺⁺ system. In case of radical cation of thia[4]helicene, [4]TH⁺⁺ the major optical band is largely blue shifted compared to [3]TH⁺⁺ and the band is originated due to n - π^* type electronic transition. On successive addition of two thiophene rings to [4]TH⁺⁺ systems, the strong optical band is predicted to be red shifted at 917 nm and 1089 nm in [5]TH⁺⁺ and [6]TH⁺⁺ systems. In case of the radical cation of thia[7]helicene, [7]TH⁺⁺, the major optical band is blue shifted to 634 nm compared to [6]TH⁺⁺ and it appears to be n - π^* type of electronic transition. As shown in Table 6, the corresponding orbitals are H-4 and L respectively. Orbital plots are shown in Figure 3.5c1 and Figure 3.5c2. However, it has also strong optical band in the IR region and this is due to π - π^* electronic transition. The corresponding orbitals involved are shown in Figure 3.5c2 and Figure 3.5c3. For thia[8]helicene, [8]TH⁺⁺, the absorption bands are predicted only in the visible range. In case of [9]TH⁺⁺ system a weak band is obtained in IR region. However, for radical cation of thia[10]helicene, [10]TH⁺⁺ a strong optical band is predicted at 1604 nm and this is due to π - π^* electronic transition.

3.3.7 Dimerization of neutral and radical cation of thia[7]helicene in DCM solvent

Few attempts have been made to study π -dimerization of radical cations of linearly conjugated oligothiophenes.^{32,118,119} However, the introduction of bulky substituents at the terminal end of the thiophene rings of these radical cationic systems reduces the probability of dimerization significantly.^{32,118,119} As intermolecular interactions is driven force for such dimerization process. Thus, one expects that this dimerization process can also be possible in unhindered neutral oligothiophene. As the present substituted thia[n]helicene systems have π -conjugated helical framework and there are significant intermolecular interaction between such systems. Therefore, the performance of a device made of such molecules can be affected due to such π -dimerization. Thus, a detailed theoretical study on the π -dimerization of neutral as well as radical cations of thia[n]helicenes would provide valuable guidance for the further development of these systems to be used as electronic devices.

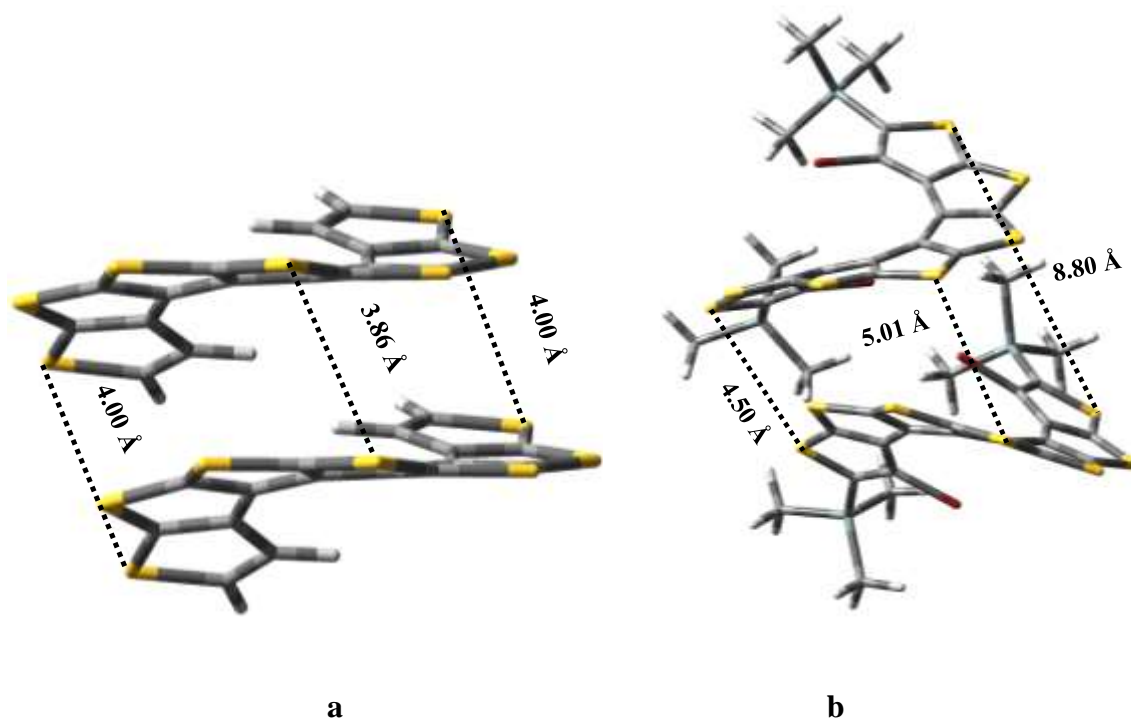
As a case study, DFT calculations are performed to elucidate the formation of π -dimers of neutral as well as radical cation of thia[7]helicene at the B3LYP-D/6-311++G(d,p) level of theory in DCM solvent. In case 1, the various possible structures for the unsubstituted and substituted π -dimer of neutral thia[7]helicene are optimized to get the most stable structures considering SMD model to include macroscopic solvent effect. In case 2, the various possible structures for the unsubstituted and substituted π -dimer of thia[7]helicene radical cation are optimized to get the most stable structures considering same SMD model. The present calculations are reported without counter anion. As the effect stabilization through electrostatic interactions may be small in solution because PF_6^- is a weakly coordinating anion.¹²⁰

3.3.7.1 Structure of π -dimers of neutral thia[7]helicene and radical cation of thia[7]helicene

The various possible structures of unsubstituted and end-substituted thia[7]helicene systems are considered in their neutral as well as radical cationic cases to get the most stable structures for these systems. At first, a structure having face-to-face π - π stacking between monomer units is considered as the initial input structure for optimization to have maximum intermolecular interaction. S-S bonded σ -type dimer system is also considered as initial geometries for neutral and radical cation of unsubstituted and end-substituted thia[7]helicene in DCM solvent. Out of these possible input structures, only the most stable structures obtained after geometries optimization are reported at present.

To study the effect of counter ion on the dimerization of unsubstituted and end-substituted thia[7]helicene radical cation, two PF_6^- anions are placed in several positions in the most stable structure of π -dimer of the thia[7]helicene radical cation. In first possible structure, the two PF_6^- counter anions are placed at the top and bottom parallel to the coil axis of π -dimer. In second possible structure, both the PF_6^- counter anions are placed perpendicular to coil axis of π -dimer. In these possible structures, the first PF_6^- anion is placed near to sulfur atoms of the central thiophene rings of the π -dimer and second PF_6^- anion is placed near to the carbon atoms of the terminal thiophene rings. In third possible structure, the two PF_6^- counter anions are placed near to sulfur atoms of the terminal thiophene rings of the π -dimer. Along with that the PF_6^- counter anions are placed several other possible positions in π -dimer of unsubstituted and end substituted thia[7]helicene radical cation to study the effect of counter anion on the dimerization and only the most stable structures obtained after geometries optimization are reported here.

Case 1: The most stable structure of unsubstituted π -dimer of neutral thia[7]helicene, ([7]TH)₂, the structure with fully π - π stacking of two [7]TH rings is observed at B3LYP-D level of theory in DCM solvent. Most stable structure of unsubstituted π -dimer of neutral ([7]TH)₂ is shown in **a**. In the most stable structure, π -dimer of neutral ([7]TH)₂, two monomer units are placed almost parallel to each other to give rise to a sandwich-type configuration. The minimum and maximum non-bonded distances obtained are 3.86 Å and 4.0 Å respectively (see Figure 3.6 a). In comparison, for substituted π -dimer of neutral thia[7]helicene, (s-[7]TH)₂, the most stable structure obtained is partial π - π stacked structure (see Figure 3.6 b). The minimum and maximum non-bonded distances obtained are 4.50 Å, and 8.80 Å respectively (see Figure 3.6b). This increase in non-bonded distances shows that partial π - π stacked structure of substituted π -dimer of neutral thia[7]helicene is destabilized from the substituted one end.



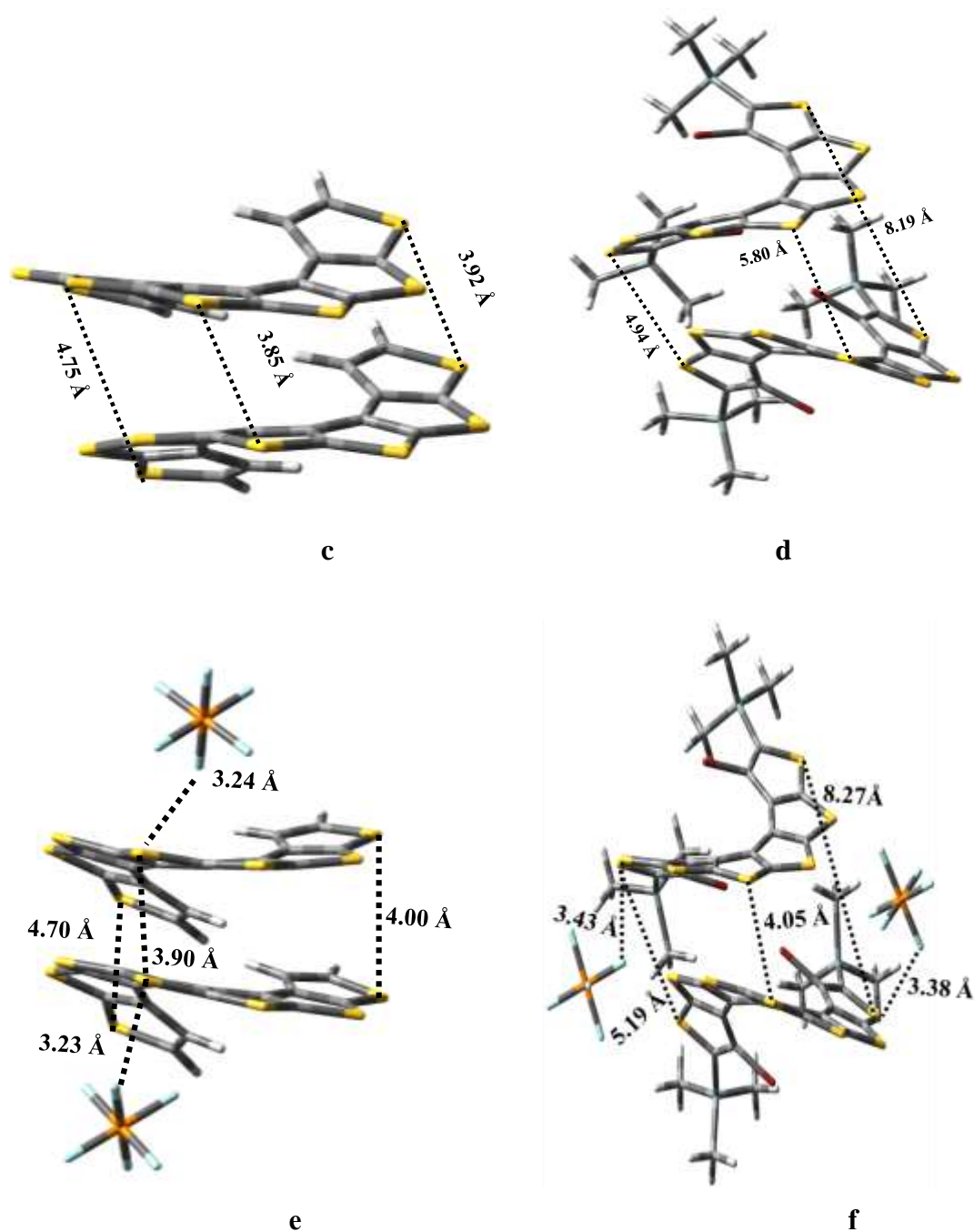


Figure 3.6 Most stable π -dimeric structure of a) neutral unsubstituted thia[7]helicene monomer, b) neutral substituted thia[7]helicene monomer, c) radical cation of unsubstituted thia[7]helicene monomer, d) radical cation of substituted thia[7]helicene monomer, e) unsubstituted thia[7]helicene monomer radical cation with PF_6^- counter ions, f) end substituted thia[7]helicene monomer radical cation with PF_6^- counter ions. Calculated at B3LYP-D/6-311++G(d,p) level of theory in DCM solvent.

Case 2: In case of unsubstituted charged π -dimer, $([7]TH)_2^{2+}$ the most stable structure obtained is fully π - π stacking of two units of the radical cation of thia[7]helicene (see Figure 3.6c). Though the slight increase in the non-bonded distance is observed from the one end, overall the most stable structure obtained is quite similar to most stable structure of unsubstituted neutral π -dimer, $([7]TH)_2^{2+}$. In comparison, the substituted π -dimer of radical cation of thia[7]helicene, the structure obtained is partly π - π stacking of two units of the radical cation in DCM solvent (see Figure 3.6d).

Case 3: In presence of two PF_6^- counter ions, the most stable structure obtained for the unsubstituted charged π -dimer, $([7]TH)_2^{2+}$, shows a π - π stacking of two units of the radical cation of thia[7]helicene with one PF_6^- counter ions being present at the top and the other at the bottom as shown in Figure 3.6e. In case of the most stable structure of the end-substituted charged π -dimer, $(s-[7]TH)_2^{2+}$ system, it is observed (see Figure 3.6f) that the each PF_6^- counter ions are present near to corner of each monomer unit.

3.3.7.2 Energy data for π -dimer of thia[7]helicene

Case 1: Dimerization energy is calculated as the difference of total energy of the π -dimer system and the sum of the total energy of the two dissociated monomer systems. The dimerization energy, ΔE_{dim} calculated for unsubstituted neutral π -dimer, $([7]TH)_2$ is -19.8 kcal/mol in DCM solvent. Thus, this indicates that the formation of π -dimer is a favourable process in unsubstituted neutral $([7]TH)_2$ from its two dissociated [7]TH monomer systems. As ΔE_{dim} is calculated from the internal energy. Thus, the hessian calculations are performed to produce thermochemical data. At STP, the Gibbs free energy of dimerization (ΔG_{dim}) calculated as -3.9 kcal/mol for the most stable structure of unsubstituted neutral π -dimer, $([7]TH)_2$. The negative value of ΔG_{dim} indicates that the formation of the π -dimer is a

favourable process for the above-mentioned system. For substituted π -dimer of neutral thia[7]helicene the ΔE_{dim} calculated is -16.3 kcal/mol in DCM solvent. This shows that the formation of the substituted π -dimer of neutral thia[7]helicene from its monomer units is again a favourable process. However, ΔG_{dim} calculated for the substituted π -dimer of neutral thia[7]helicene is +0.2 kcal/mol and it indicates that the formation of the π -dimer is not a favourable process.

Case 2: ΔE_{dim} calculated for unsubstituted π -dimer of radical cation of thia[7]helicene is -17.4 kcal/mol in DCM solution. However, calculated ΔG_{dim} for the same dimer at STP is +6.6 kcal/mol and this indicates that the dimerization process is the unfavourable process. ΔE_{dim} calculated for substituted π -dimer of radical cation of thia[7]helicene is -9.0 kcal/mol. Again, calculated ΔG_{dim} for substituted radical cation of thia[7]helicene is +14.1 kcal/mol which rules out the formation of the π -dimer in DCM solvent. The high positive value of ΔG_{dim} calculated for π -dimer of substituted radical cation of thia[7]helicene shows that substituted radical cation of thia[7]helicene does not indicate the dimerization at STP in DCM solvent. Hence, the present theoretical study on dimerization of radical cations of substituted thia[7]helicene supports the observed experimental EPR spectra of radical cation of thia[7]helicene to remains intense at low temperatures up to few minutes.

Case 3: The calculated ΔG_{dim} is -1.6 kcal/mol at STP for the most stable structure of unsubstituted radical cation of thia[7]helicene with two PF_6^- counter ions and this indicates a significant possibility of dimer formation in presence of two PF_6^- counterions. However, calculated ΔG_{dim} for the most stable structure of end substituted radical cation of thia[7]helicene with two PF_6^- counterion structure at STP is +2.8 kcal/mol. Thus the formation

of dimer from end substituted radical cation of thia[7]helicene in presence of counter ions is ruled out.

3.4 Conclusions

It is observed that B3LYP-D functional works quite well to predict molecular geometry of neutral and radical cations of thia[n]helicenes, [n]TH and [n]TH^{•+} in gas phase as well as in DCM solvent except for thia[3]helicene, [3]TH system. These substituted neutral and positively charged thia[n]helicene systems prefer flexible non-planar structure when the number of thiophene rings is three or more. HOMO-LUMO energy gap of neutral thia[n]helicene calculated applying B3LYP, B3LYP-D and B3LYP-D3 functionals are found to be very close both in gas phase and in DCM solvent. The ionization energies for thia[n]helicenes, [n]TH calculated applying B3LYP, B3LYP-D and B3LYP-D3 functionals are comparable with ionization energies obtained at MP2 level. The error in calculated ionization energies for neutral thia[n]helicenes, [n]TH at B3LYP, B3LYP-D, and B3LYP-D3 levels are in the range of 0.6-1.0 eV compared to the same calculated at MP2 level. High g value in EPR spectra is expected for thia[n]helicenes radical cation as spin density is calculated to be localized mostly on the heavy atoms. Excited-state study for radical cations of substituted thia[n]helicene, [n]TH^{•+} in DCM solvent elucidates that these systems strongly absorb in visible and near infrared region (NIR) of electromagnetic spectrum. Origin of optical absorption bands are assigned based on the plots of the molecular orbitals involved. It is inferred that the NIR bands are due to π - π^* electronic transition. The calculated ΔG_{dim} at STP for π -dimer of unsubstituted thia[7]helicene indicates that dimerization is possible and for π -dimer of substituted thia[7]helicene shows that dimerization is not favourable at STP in DCM solvent. Calculated ΔG_{dim} values for π -dimer of unsubstituted and substituted radical

cations of thia[7]helicene at STP do not indicate possibility of dimerization in DCM solvent. Free energy parameters on π -dimer of unsubstituted and end substituted radical cations of thia[7]helicene in presence of counter ion, PF_6^- in DCM solvent at STP decreases the possibility of dimerization. Overall, the present studies elucidate that thia[n]helicene may find applications as organic optoelectronic devices.

Effect of Size on Structures, Stability and Spectral Properties of Seleno[n]helicenes (n=1-10) and their Corresponding Radical cations[†]

4.1 Introduction

This chapter represents the Selenium-based analogues of thia[n]helicenes. They are the first reported selenophene β -helical systems of this type motivated from their corresponding thia[n]helicenes. In general, selenophene based materials are widely used as bulk heterojunction solar cells¹²¹, organic field-effect transistor³⁵, high-performance complementary metal-oxide circuits¹²², highly transmissive electrochromic polymer.³⁷ Selenium present in selenophene based materials improve the performance of these materials by tuning their energy gap and increasing the ability to harvest a large amount of solar flux in comparison to their thiophene based analogues.¹²³ In selenophene based materials these features can be achieved by controlling the combining ratio of selenium atoms with other atoms like oxygen and sulfur.¹²³ In comparison to thiophene based oligomers, the selenophene based oligomers have more π -conjugation and excellent transport properties due to the large size and polarizable nature of Se atom. The general synthesis, spectral properties, and theoretical studies on systems based on anti- α -[6]selenophene, syn- α -[6]selenophene, anti- β -seleno[6]acene are reported in literature.^{39,57,124–126} On the other hand, only a few reports are available in the literature on selenophene based helicene systems.^{13,68} As thiophene based helicenes have strong chiro-optical properties and very wide optical band gap (~ 3.5 eV)⁶⁷, thus it is expected that selenophene based helicene systems can show enhanced electronic feature due to large size and

[†]Kumar, R.; Maity, D. K. Structure, stability and spectral properties of seleno[n]helicenes (n = 1-10). *New J. Chem.* **2019**, 44 (2), 428–441.

polarizable nature of Se atom. The most important fact about thia[n]helicenes systems are that they show strong chiro-optical properties and have suitable optical bandgap. As seleno[n]helicenes have more π -conjugation than their corresponding thia[n]helicenes, it is expected to see considerable enhancement in chiro-optical properties in these systems. Moreover, seleno[n]helicenes are also expected to have optical bandgap in the NIR region. However, theoretical or experimental studies on such seleno[n]helicenes are at the early stages.⁷⁰ The stability of radical cations of seleno[n]helicenes is expected to be more than the corresponding radical cations of thia[n]helicenes due to large size and polarizable nature of Se atom. However, to the best of our knowledge, systematic theoretical studies on these seleno[n]helicenes radical cation are very few.⁷⁰ Moreover, a case study on possibility of dimerization of these neutral and radical cation seleno[n]helicene systems is recently reported.⁷⁰ Such information is fundamental as dimerization often leads to the significant change in electronic properties and may make them unsuitable for applications as electronic devices.

First principle-based quantum chemical methods are employed on neutral and radical cations of seleno[n]helicenes, [n]SH, n=1-10. Various molecular properties like structures, ionization energies, energy gap and UV-Vis spectral properties of these systems are reported in the gas phase as well as in DCM solvent. A first principle based DFT study on band gap is also provided for neutral seleno[n]helicenes using periodic boundary condition. Moreover, model calculations have been performed to find out possibility of dimerization in unsubstituted and substituted neutral seleno[7]helicene, [7]SH in DCM solvent. Model calculations are also carried out for unsubstituted and substituted seleno[7]helicenes, [7]SH^{•+} radical cation with and without PF₆⁻ counter anion in DCM solvent.

4.2 Theoretical Methods

Selenophene rings are fused stepwise in an ortho manner, known as ortho β -annulation scheme, to produce all possible structures of unsubstituted and end substituted neutral seleno[n]helicenes, $n=1-10$ and their corresponding radical cations. The minimum energy equilibrium structures of unsubstituted and end substituted neutral seleno[n]helicenes, $n=1-10$ and their corresponding radical cations are optimized using B3LYP^{88,89} functional and considering 6-311++G(d,p) basis set for all the atoms in the gas phase and in DCM solvent. Solvent DCM is considered for these calculations as it is reported that oligoselenophenes are fairly soluble in DCM.^{123,127} The macroscopic solvation model (SMD)^{104,105} considered for all the theoretical calculations at present is based on solute density. Most stable structures of unsubstituted and end substituted neutral seleno[n]helicenes [n]SH, $n=1-10$ and their corresponding radical cations obtained at the B3LYP level of theory are being further re-optimized applying functional B3LYP-D⁹⁴ in conjugation with the same basis set in the gas phase and in DCM solvent to improve geometrical parameters. To verify if the equilibrium structures obtained refer to the true minima or not, Hessian calculations are carried out in the gas phase as well as in DCM solvent for neutral and radical cation of seleno[n]helicenes. Most stable structures obtained at the B3LYP-D level are then used for single point energy calculations at B3LYP-D3⁹⁵ and MP2 levels in the gas phase and DCM solvent to improve energy parameters. Restricted open-shell Hartree Fock (ROHF) formalism is used to avoid any spin contamination in these Se based radical cationic doublet systems. Excited-state calculations are carried out applying TDDFT procedure and considering CAM-B3LYP^{115,116} functional along with 6-311++G(d,p) basis set for neutral as well as their radical cations of seleno[n]helicenes for the lowest 50 excited states in DCM solvent. Visualization of frontier

molecular orbitals have been carried out at B3LYP-D/6-311++G(d,p) level to get the information about the type of orbitals involved in electronic transitions. As a case study on the possibility of dimerization, all possible structures of unsubstituted and end substituted π -dimer of neutral seleno[7]helicene and its radical cation are optimized at B3LYP-D/6-311++G(d,p) level of theory in DCM solvent to predict the most stable structure. PF_6^- counter ion is also considered for geometry optimization of the radical cation in DCM solvent. All theoretical calculations are performed using the GAUSSIAN 16 program.¹¹⁷

4.3 Results and Discussions

4.3.1 Most stable structures of seleno[n]helicenes, [n]SH, n=1-10 in DCM solvent

The Stepwise addition of a selenophene unit to the substituted neutral seleno[1]helicene in a syn manner is carried out to produce seleno[2]helicene. This procedure is repeated to produce larger unsubstituted and end substituted seleno[n]helicenes, n=3-10. Table 4.1 provides selected geometrical properties of fully optimized structures of neutral seleno[n]helicenes, n=1-10 applying B3LYP-D density functional adopting 6-311++G(d,p) basis set for all the atoms in the gas phase and in DCM solvent. Though there are slight changes in geometrical parameters for neutral seleno[n]helicenes in solvent DCM, overall molecular geometries are almost same as the geometries in gas phase. Most stable structures for neutral seleno[n]helicenes, n=1-10 calculated at the present level of theory in DCM solvent are shown in Figure 4.1(a-j). In case of seleno[1]helicene and seleno[2]helicene planar structures are obtained as one may understand from the calculated dihedral angles for these systems. A non-planar structure is obtained as the most stable one for seleno[3]helicene in DCM solvent (see Figure 4.1c). Calculated dihedral angles, $\delta(\text{Br1C2C3Br2})$ and $\delta(\text{Br2C3C2C4})$ are 47.3° and -128.3° respectively. The calculated non-planarity for this seleno[3]helicene is more than the

corresponding thia[3]helicene as reported (dihedral angles are 13.3° and -164.3°) in the literature based on crystallography.⁶⁵ However, crystal structure is reported only for thia[3]helicene and thia[7]helicene. Calculated Mulliken charges on Si atom of TMS group and Br atoms are 0.09 a.u. and -0.11 a.u. respectively in seleno[3]helicene. Thus, two bulky Br groups present on C2 and C3 atoms make seleno[3]helicene to have a non-planar structure to minimize geometrical and electronic steric hindrances. In case of seleno[4]helicene, the structure obtained is non-planar (displayed in Figure 4.1d) as can be seen from the calculated dihedral angles and the distance between two Br atoms is found to be 3.48 Å which is more than that for seleno[3]helicene. Figure 4.1e shows the minimum energy structure of seleno[5]helicene in DCM solvent considering a macroscopic solvent model. The calculated dihedral angles, $\delta(\text{Br1C2C3Br2})$ and $\delta(\text{Br2C3C2C4})$ suggest that the non-planarity is further increased compared to seleno[4]helicene. The distance between the Br atoms in seleno[5]helicene is calculated as 3.93 Å which is longer than the lower helicenes. In case of the next higher system, seleno[6]helicene, same kind of structure is obtained with larger non-planarity as shown in Figure 4.1f. For seleno[7]helicene system, a helical structure is obtained as the most stable equilibrium structure (see Figure 4.1g). Present calculated dihedral angles, $\delta(\text{Br1C2C3Br2})$ and $\delta(\text{Br2C3C2C4})$ are -128.7° and 108.4° respectively compared to the reported dihedral angles, -170.1° and 83.1° for thia[7]helicene system based on crystallography.⁶⁵ Mulliken charges on selenium atoms labeled as Se1, Se2, Se3, and Se4 are 0.35 a.u., 0.18 a.u., 0.17 a.u., and 0.14 a.u. respectively. One turn in the helical structure is completed in case of seleno[8]helicene system and the corresponding most stable structure is shown in Figure 4.1h. Fully optimized structures of seleno[n]helicenes, n=9-10 are also

Table 4.1 Selected [#]geometrical parameters of neutral end substituted seleno[n]helicenes, n=1-10 calculated at B3LYP-D/6-311++G(d,p) level of theory in gas phase. Values in the first braces show corresponding geometrical parameters of neutral end substituted seleno[n]helicenes, n=1-10 in DCM solvent. Bold faced values in third braces are calculated at B3LYP/6-311++G(d,p) level of theory in DCM solvent.

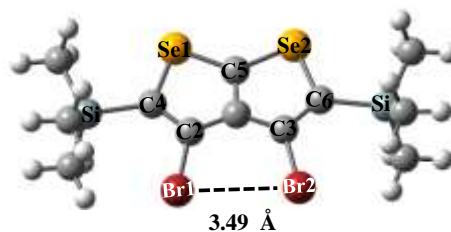
n	1	2	3	4	5	6	7	8	9	10
r _{C4-C5} (Å)	2.68, (2.70)	2.60, (2.61)	2.60, (2.59)	2.61, (2.60)	2.61, (2.61)	2.61, (2.60)	2.61, (2.61)	2.61, (2.60)	2.60, (2.61)	2.60, (2.61)
r _{C5-C6} (Å)	-	2.60, (2.61)	2.54, (2.55)	2.56, (2.56)	2.55, (2.55)	2.54, (2.54)	2.55, (2.55)	2.53, (2.53)	2.54, (2.54)	2.54, (2.54)
r _{C7-C8} (Å)	-	-	-	2.62, (2.61)	2.55, (2.55)	2.53, (2.53)	2.54, (2.54)	2.52, (2.52)	2.52, (2.52)	2.52, (2.52)
r _{C8-C9} (Å)	-	-	-	-	2.61, (2.62)	2.54, (2.54)	2.55, (2.55)	2.52, (2.52)	2.52, (2.52)	2.52, (2.52)
r _{Br1-Br2} (Å)	3.48, (3.48), [3.44]	3.49, (3.48), [3.48]	3.43, (3.43), [3.43]	3.48, (3.46), [3.49]	3.61, (3.63), [3.62]	4.14, (4.24), [4.16]	5.11, (5.10), [5.09]	5.40, (5.75), [5.74]	5.82, (6.09), [6.13]	6.09, (6.32), [6.36]
δ(Br1C2C3Br2) (degree)	0, (0), [0]	0, (0), [0]	43.8, (43.7), [39.7]	-93.1, (-91.5), [-87.7]	-134.5, (-135.4), [-128.6]	179.8, (178.2), [175.6]	-128.7, (-128.9), [-135.2]	-90.2, (-83.4), [-86.0]	-28.3, (-31.2), [-30.5]	-19.9, (-14.9), [-15.4]
δ(Br2C3C2C4) (degree)	180, (180), [180]	180, (180), [180]	-128.3, (-128.3), [-133.6]	19.1, (23.5), [25.6]	-34.2, (-32.9), [-30.9]	70.3, (70.1), [68.1]	108.4, (108.5), [104.1]	142.2, (145.8), [144.0]	-170.0, (-172.4), [-172.0]	-126.3, (-129.9), [-129.7]

[#]Figure 4.1 may be referred for identifying geometrical parameters.



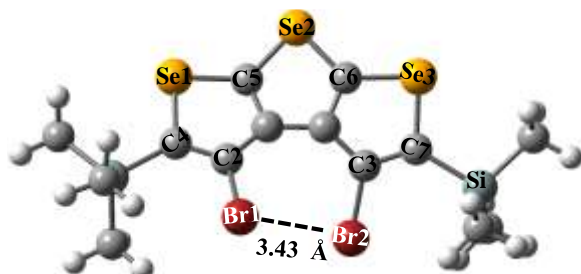
$r_{C2-C3} = 1.44 \text{ \AA}$, $r_{C4-C5} = 2.68 \text{ \AA}$
 $\delta(\text{Br1C2C3Br2}) = 0^\circ$, $\delta(\text{Br2C3C2C4}) = 180^\circ$
 $\angle C4\text{Se1C5} = 90.2^\circ$

a



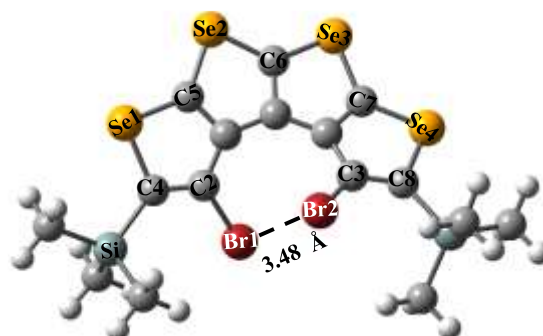
$r_{C2-C3} = 2.70 \text{ \AA}$, $r_{C4-C6} = 4.79 \text{ \AA}$
 $\delta(\text{Br1C2C3Br2}) = 0^\circ$, $\delta(\text{Br2C3C2C4}) = 180^\circ$
 $\angle C4\text{Se1C5} = 88.5^\circ$

b



$r_{C2-C3} = 3.62 \text{ \AA}$, $r_{C4-C7} = 6.19 \text{ \AA}$
 $\delta(\text{Br1C2C3Br2}) = 43.7^\circ$, $\delta(\text{Br2C3C2C4}) = -128.4^\circ$
 $\angle C4\text{Se1C5} = 87.2^\circ$, $\angle C5\text{Se2C6} = 86.0^\circ$

c



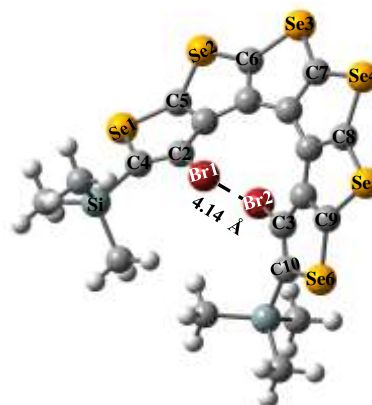
$r_{C2-C3} = 3.92 \text{ \AA}$, $r_{C4-C8} = 6.56 \text{ \AA}$
 $\delta(\text{Br1C2C3Br2}) = -93.1^\circ$, $\delta(\text{Br2C3C2C4}) = -19.1^\circ$
 $\angle C4\text{Se1C5} = 88.0^\circ$, $\angle C5\text{Se2C6} = 84.7^\circ$

d



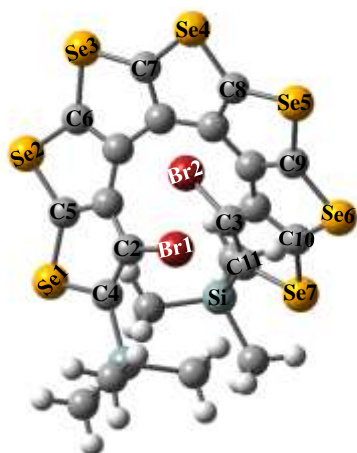
$r_{C2-C3} = 3.93 \text{ \AA}$, $r_{C4-C9} = 6.38 \text{ \AA}$
 $\delta(\text{Br1C2C3Br2}) = -134.5^\circ$, $\delta(\text{Br2C3C2C4}) = -34.2^\circ$
 $\angle C4\text{Se1C5} = 87.8^\circ$, $\angle C5\text{Se2C6} = 85.6^\circ$

e



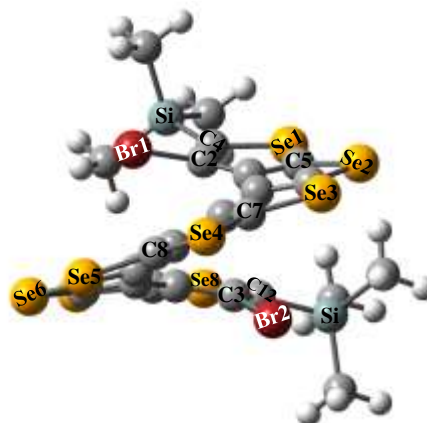
$r_{C2-C3} = 3.82 \text{ \AA}$, $r_{C4-C10} = 5.52 \text{ \AA}$
 $\delta(\text{Br1C2C3Br2}) = 179.8^\circ$, $\delta(\text{Br2C3C2C4}) = 70.4^\circ$
 $\angle C4\text{Se1C5} = 87.2^\circ$, $\angle C5\text{Se2C6} = 85.4^\circ$

f



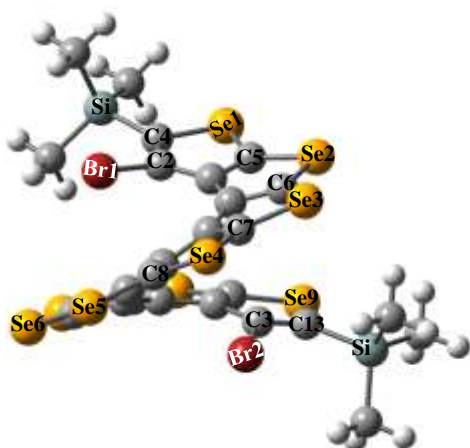
$r_{\text{Br1-Br2}} = 5.11 \text{ \AA}$, $r_{\text{C2-C3}} = 3.47 \text{ \AA}$, $r_{\text{C4-C11}} = 4.34 \text{ \AA}$
 $\delta(\text{Br1C2C3Br2}) = -128.9^\circ$, $\delta(\text{Br2C3C2C4}) = 108.5^\circ$
 $\angle\text{C4Se1C5} = 87.2^\circ$, $\angle\text{C5Se2C6} = 84.5^\circ$

g



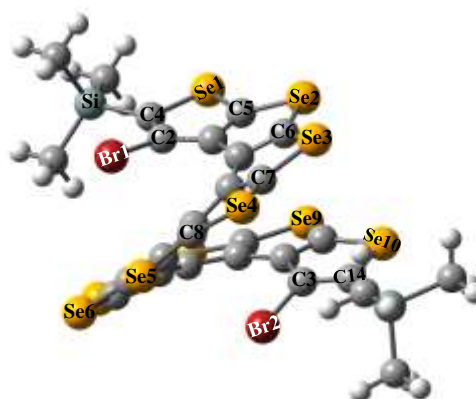
$r_{\text{Br1-Br2}} = 5.40 \text{ \AA}$, $r_{\text{C2-C3}} = 3.40 \text{ \AA}$, $r_{\text{C4-C12}} = 3.93 \text{ \AA}$
 $\delta(\text{Br1C2C3Br2}) = -90.2^\circ$, $\delta(\text{Br2C3C2C4}) = 142.2^\circ$
 $\angle\text{C4Se1C5} = 87.2^\circ$, $\angle\text{C5Se2C6} = 84.5^\circ$

h



$r_{\text{Br1-Br2}} = 5.84 \text{ \AA}$, $r_{\text{C2-C3}} = 4.22 \text{ \AA}$, $r_{\text{C4-C13}} = 5.41 \text{ \AA}$
 $\delta(\text{Br1C2C3Br2}) = -28.3^\circ$, $\delta(\text{Br2C3C2C4}) = 170.0^\circ$
 $\angle\text{C4Se1C5} = 87.1^\circ$, $\angle\text{C5Se2C6} = 84.4^\circ$

i



$r_{\text{Br1-Br2}} = 6.09 \text{ \AA}$, $r_{\text{C2-C3}} = 5.19 \text{ \AA}$, $r_{\text{C4-C13}} = 7.08 \text{ \AA}$
 $\delta(\text{Br1C2C3Br2}) = -26.9^\circ$, $\delta(\text{Br2C3C2C4}) = -126.3^\circ$
 $\angle\text{C4Se1C5} = 87.1^\circ$, $\angle\text{C5Se2C6} = 84.4^\circ$

j

Figure 4.1 Most stable structures (a-j) of neutral seleno[n]helicenes, n=1-10 a) [1]SH, b) [2]SH, c) [3]SH, d) [4]SH, e) [5]SH, f) [6]SH, g) [7]SH, h) [8]SH, i) [9]SH, and j) [10]SH, with selected geometrical parameters calculated at B3LYP-D/6-311++G(d,p) level of theory in DCM solvent

calculated considering DCM solvent at B3LYP-D level and these are shown in Figure 4.1(i-j). One can easily note from Table 4.1 that only a very small change is obtained in the listed geometrical parameters for seleno[n]helicenes with addition of selenophene rings.

In short, it is predicted that neutral [1]SH and [2]SH are planar in DCM solvent. However, the structure of seleno[n]helicenes, [n]SH, n=3-10 are non-planar. It is also predicted geometrical parameters of neutral seleno[n]helicenes, [n]SH, n=1-10 in the gas phase and in DCM solvent are very close. Table 4.1 indicates that calculated dihedral angles for seleno[n]helicenes, n=3-8 at B3LYP-D level are considerably different than those at B3LYP level showing the effect of dispersion in the geometry. However, no difference in the calculated distance between the two Br atoms is observed.

4.3.2 Ionization energies of seleno[n]helicenes, [n]SH, n=1-10 in DCM solvent

The importance of ionization energy is discussed in Chapter 3 at section 3.3.2. One can see from Table 4.2 calculated IE values at different levels of theory for seleno[n]helicenes, [n]SH in the gas phase are very close at the DFT level. The ionization energy (IE) for seleno[n]helicenes, n=1-10 are calculated as the difference of energy for the most stable structures of neutral and their corresponding radical cations. Table 4.2 provides calculated ionization energies for seleno[n]helicenes, [n]SH, n=1-10 at B3LYP, B3LYP-D, B3LYP-D3 and MP2 levels of theory using 6-311++G(d,p) basis set in the gas phase and in DCM solvent. The most stable structures obtained for neutral and their corresponding radical cations of seleno[n]helicenes at B3LYP-D level of theory are used to calculate the IE at other levels of theory. One can see from Table 4.2 that IE values calculated at MP2 level show both positive and negative deviation with respect to DFT values. IE values calculated including macroscopic medium effect in DCM solvent are significantly lower than those in gas phase for all

Table 4.2 Calculated ionization energies (in eV) of neutral seleno[n]helicenes, [n]SH, n=1-10 in the gas phase applying different theoretical methods. Values in braces are corresponding ionization energies in DCM solvent.

Ionization energies (in eV) of seleno[n]helicenes, [n]SH, n =1-5					
Method	[1]SH	[2]SH	[3]SH	[4]SH	[5]SH
i)	8.1, (6.7)	7.9, (5.9)	7.2, (5.6)	7.1, (5.8)	6.8, (5.3)
ii)	8.3, (6.6)	7.9, (6.0)	7.3, (5.7)	7.2, (5.7)	6.9, (5.4)
iii)	8.3, (6.6)	7.9, (5.9)	7.3, (5.7)	7.2, (5.7)	6.9, (5.4)
iv)	8.5, (6.4)	7.2, (5.7)	7.0, (5.7)	7.1, (5.6)	7.0, (5.5)
Ionization energies (in eV) of seleno[n]helicenes, [n]SH, n =6-10					
Method	[6]SH	[7]SH	[8]SH	[9]SH	[10]SH
i)	6.8, (5.5)	6.6, (5.4)	6.6, (5.2)	6.5, (5.1)	6.4, (5.1)
ii)	6.9, (5.4)	6.8, (5.3)	6.7, (5.3)	6.6, (5.2)	6.5, (5.1)
iii)	6.9, (5.4)	6.8, (5.3)	6.7, (5.3)	6.6, (5.2)	6.5, (5.1)
iv)	7.1, (5.6)	7.1, (5.5)	7.0, (5.4)	6.9, (5.4)	7.0, (5.5)

i) B3LYP, ii) B3LYP-D, iii) B3LYP-D3, and iv) MP2 with 6-311++G(d,p) basis set

seleno[n]helicene systems. This indicates that radical cations of seleno[n]helicenes are more stable in DCM solvent compared to gas phase. Table 4.2 also indicates that ionization energy of these systems in gas phase calculated at DFT levels decreases with the addition to each ring to saturate at 6.5 eV. However, ionization energy value leads to 5.1 eV when the same calculation is carried out including solvent effect.

4.3.3 Energy gap of seleno[n]helicenes, [n]SH, n=1-10 in DCM solvent

The importance of the energy gap is discussed in Chapter 3 at section 3.3.3. Table 3 summarizes at B3LYP, B3LYP-D and B3LYP-D3 levels of theory using 6-311++G(d,p) basis

Table 4.3 Calculated HOMO-LUMO energy gap (in eV) of neutral seleno[n]helicenes, [n]SH, n = 1-10 in gas phase. Values in braces are corresponding energy gap of neutral seleno[n]helicenes in DCM solvent.

HOMO-LUMO energy gap (in eV) of seleno[n]helicenes, [n]SH, n =1-5					
Method	[1]SH	[2]SH	[3]SH	[4]SH	[5]SH
i)	5.1, (5.2)	4.7, (4.7)	4.4, (4.5)	4.3, (4.3)	4.2, (4.2)
ii)	5.1, (5.2)	4.7, (4.7)	4.4, (4.5)	4.3, (4.3)	4.2, (4.2)
iii)	5.2, (5.2)	4.7, (4.7)	4.4, (4.5)	4.3, (4.3)	4.2, (4.2)
HOMO-LUMO energy gap (in eV) of seleno[n]helicenes, [n]SH, n =6-10					
Method	[6]SH	[7]SH	[8]SH	[9]SH	[10]SH
i)	4.2, (4.2)	4.0, (4.0)	4.0, (4.0)	3.9, (4.0)	3.9, (3.9)
ii)	4.2, (4.2)	4.0, (4.0)	4.0, (4.0)	3.9, (4.0)	3.9, (3.9)
iii)	4.2, (4.2)	4.0, (4.0)	4.0, (4.0)	3.9, (4.0)	3.9, (3.9)

i) B3LYP, ii) B3LYP-D, and iii) B3LYP-D3, with 6-311++G(d,p) basis set

set in the gas phase and in DCM solvent. This energy parameter has been calculated considering the most stable structure of the respective helicenes. Table 4.3 indicates that on the addition of each selenophene ring, the calculated energy gap systematically decreases to saturate at 3.9 eV in the gas phase. This observation is consistent at B3LYP level in the presence or absence of dispersion corrections. The calculated energy gap for seleno[n]helicenes in the DCM solvent is observed to be very close to those in the gas phase with some exception.

In short, for neutral seleno[n]helicenes, n=1-10 the calculated HOMO-LUMO gap belongs to UV-region of the electromagnetic spectrum.

4.3.4 Most stable structures of radical cations of seleno[n]helicenes, [n]SH^{•+}, n=1-10

Sequential addition of a selenophene unit to end substituted seleno[1]helicene radical cation, [1]SH^{•+} in a syn manner is performed to produce seleno[2]helicene radical cation, [2]SH^{•+}. This procedure is repeated to produce larger seleno[n]helicenes radical cation, [n]SH^{•+}, n=3-10.

Geometrical parameters for seleno[n]helicenes radical cation, $[n]SH^{+\bullet}$, $n=1-10$ are optimized considering the corresponding neutral structures as the initial input. Table 4.4 summarizes the geometrical parameters of fully optimized structures for $[n]SH^{+\bullet}$, $n=1-10$ using B3LYP-D functional and 6-311++G(d,p) basis set in the gas phase and in DCM solvent. Table 4 also reveals that no significant change occurs for most of the geometrical parameters on going from gas phase to solvent DCM for $[n]SH^{+\bullet}$, $n=1-10$.

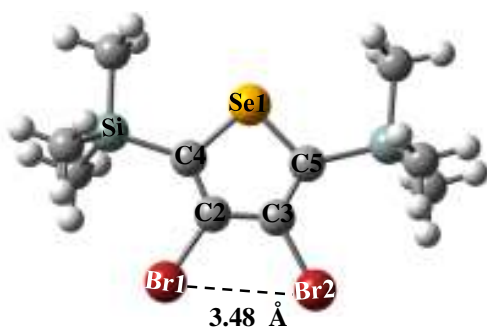
The most stable structures for seleno[n]helicenes radical cation, $n=1-10$ calculated considering DCM solvent are shown in Figure 4.2(a-j). For $[1]SH^{+\bullet}$ and $[2]SH^{+\bullet}$, planar structures are obtained at B3LYP-D level of theory in DCM solvent (see Figure 4.2(a-b)). In case of $[3]SH^{+\bullet}$, the most stable equilibrium structure is non-planar (see Figure 4.2c). Selected geometrical parameters are shown in the Figure 4.2c. Calculated dihedral angles, $\delta(Br1C2C3Br2)$ and $\delta(Br2C3C2C4)$ are 46.3° and -125.5° respectively. The distance between the two Br atoms is calculated to be 3.50 \AA . The calculated spin densities on selenium atoms labeled as Se1, Se2 and Se3 of seleno[3]helicene radical cation in DCM solvent are 0.08 a.u. 0.28 a.u. and 0.08 a.u. respectively. So, the odd electron spin density is mainly localized on central selenium atoms of $[3]SH^{+\bullet}$. The calculated spin densities on carbon atoms labeled as C2 and C4 are 0.10 a.u. and 0.07 a.u. respectively. Calculated Mulliken charges on Si and Br atoms are 0.06 and -0.02 a.u. respectively. Thus, two bulky Br groups present at C2 and C3 positions create both geometrical and electronic steric hindrances. Probably, this makes seleno[3]helicene radical cation to have a non-planar structure.

In case of $[4]SH^{+\bullet}$, the most stable structure obtained is non-planar as shown in Figure 4.2d and the distance between the two Br atoms is found to be 3.49 \AA . Calculated dihedral angles,

Table 4.4 Selected [#]geometrical parameters of end substituted seleno[n]helicenes radical cation, n=1-10 calculated at B3LYP-D/6-311++G(d,p) level of theory in gas phase. Values in the first braces show corresponding geometrical parameters of end substituted seleno[n]helicenes radical cation, n=1-10 in DCM solvent. Bold faced values in third braces are calculated at B3LYP/6-311++G(d,p) level of theory in DCM solvent.

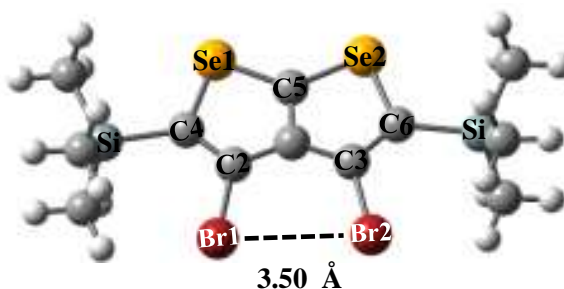
n	1	2	3	4	5	6	7	8	9	10
r_{C4-C5} (Å)	2.68, (2.70)	2.60, (2.60)	2.60, (2.60)	2.62, (2.61)	2.61, (2.61)	2.61, (2.61)	2.61, (2.61)	2.61, (2.61)	2.60, (2.61)	2.60, (2.61)
r_{C5-C6} (Å)	-	2.60, (2.60)	2.60, (2.58)	2.55, (2.54)	2.55, (2.55)	2.55, (2.55)	2.55, (2.53)	2.53, (2.53)	2.54, (2.53)	2.54, (2.53)
r_{C7-C8} (Å)	-	-	-	2.62, (2.61)	2.55, (2.55)	2.53, (2.53)	2.54, (2.54)	2.52, (2.52)	2.52, (2.52)	2.52, (2.52)
r_{C8-C9} (Å)	-	-	-	-	2.61, (2.62)	2.54, (2.54)	2.55, (2.55)	2.52, (2.52)	2.52, (2.52)	2.52, (2.52)
r_{Br1-Br2} (Å)	3.48, (3.31), [3.42]	3.50, (3.50), [3.47]	3.45, (3.45), [3.44]	3.49, (3.49), [3.48]	3.62, (3.63), [3.64]	4.11, (4.18), [4.23]	5.06, (4.93), [5.14]	5.42, (5.43), [5.78]	5.88, (5.90), [6.16]	6.12, (6.39), [6.45]
δ(Br1C2C3Br2) (degree)	0, (0), [0]	0, (0), [0]	43.9, (46.3), [42.6]	-92.1, (-91.2), [-86.6]	-133.0, (-132.7), [-128.7]	178.3, (178.9), [175.6]	-131.8, (-135.9), [-135.4]	-91.2, (-91.6), [-85.8]	-28.3, (-28.3), [-28.8]	-18.9, (-15.3), [-15.1]
δ(Br2C3C2C4) (degree)	180, (180), [180]	180, (180), [180]	-128.8, (-125.5), [-129.8]	20.4, (24.2), [29.6]	-33.7, (-31.3), [-28.6]	69.6, (68.1), [66.5]	106.4, (103.4), [103.0]	-144.0, (-140.8), [-143.5]	-177.0, (-170.2), [-171.1]	-127.3, (-129.9), [-129.9]

[#]**Figure 4.2** may be referred for identifying geometrical parameters



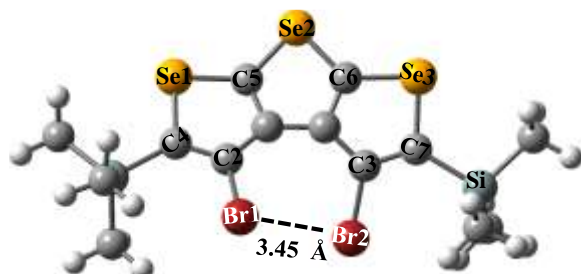
$r_{C2-C3} = 1.50 \text{ \AA}$, $r_{C4-C5} = 2.73 \text{ \AA}$
 $\delta(\text{Br1C2C3Br2}) = 0^\circ$, $\delta(\text{Br2C3C2C4}) = 180^\circ$
 $\angle C4\text{Se1C5} = 92.0^\circ$

a



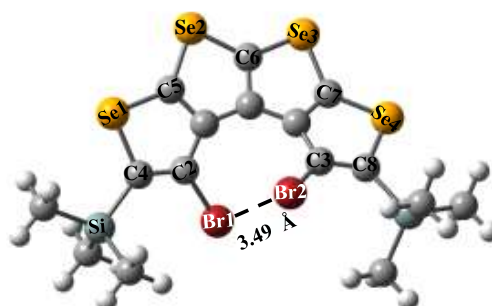
$r_{C2-C3} = 2.70 \text{ \AA}$, $r_{C4-C6} = 4.79 \text{ \AA}$
 $\delta(\text{Br1C2C3Br2}) = 0^\circ$, $\delta(\text{Br2C3C2C4}) = 180^\circ$
 $\angle C4\text{Se1C5} = 88.2^\circ$

b



$r_{C2-C3} = 3.62 \text{ \AA}$, $r_{C4-C7} = 6.19 \text{ \AA}$
 $\delta(\text{Br1C2C3Br2}) = 46.3^\circ$, $\delta(\text{Br2C3C2C4}) = -125.5^\circ$
 $\angle C4\text{Se1C5} = 87.2^\circ$, $\angle C5\text{Se2C6} = 86.0^\circ$

c



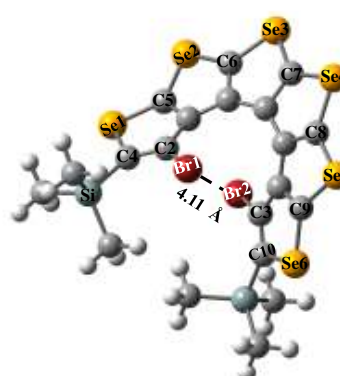
$r_{C2-C3} = 3.90 \text{ \AA}$, $r_{C4-C8} = 6.52 \text{ \AA}$
 $\delta(\text{Br1C2C3Br2}) = -91.2^\circ$, $\delta(\text{Br2C3C2C4}) = -24.2^\circ$
 $\angle C4\text{Se1C5} = 87.8^\circ$, $\angle C5\text{Se2C6} = 84.5^\circ$

d



$r_{C2-C3} = 3.89 \text{ \AA}$, $r_{C4-C9} = 6.17 \text{ \AA}$
 $\delta(\text{Br1C2C3Br2}) = -132.7^\circ$, $\delta(\text{Br2C3C2C4}) = -31.3^\circ$
 $\angle C4\text{Se1C5} = 87.8^\circ$, $\angle C5\text{Se2C6} = 85.2^\circ$

e



$r_{C2-C3} = 3.80 \text{ \AA}$, $r_{C4-C10} = 5.50 \text{ \AA}$
 $\delta(\text{Br1C2C3Br2}) = 178.9^\circ$, $\delta(\text{Br2C3C2C4}) = 68.1^\circ$
 $\angle C4\text{Se1C5} = 87.3^\circ$, $\angle C5\text{Se2C6} = 85.6^\circ$

f

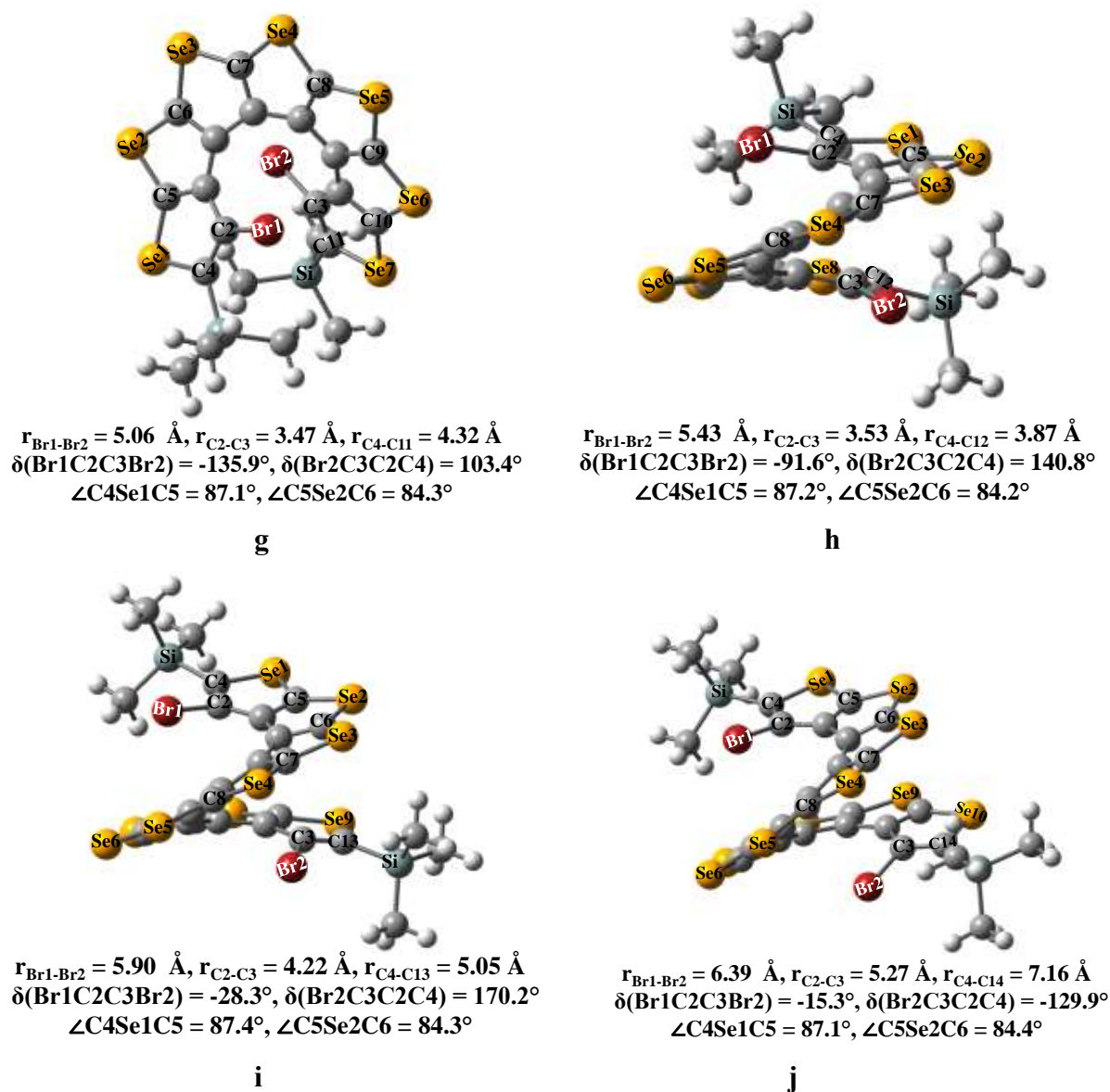


Figure 4.2 Most stable structures (a-j) for radical cation of end substituted seleno[n]helicenes $n=1-10$, a) [1]SH⁺, b) [2]SH⁺, c) [3]SH⁺, d) [4]SH⁺, e) [5]SH⁺, f) [6]SH⁺, g) [7]SH⁺, h) [8]SH⁺, i) [9]SH⁺, and j) [10]SH⁺, with selected geometrical parameters calculated at B3LYP-D/6-311++G(d,p) level of theory in DCM solvent.

$\delta(\text{Br1C2C3Br2})$ and $\delta(\text{Br2C3C2C4})$ are -91.2° and 24.2° respectively. Spin densities on selenium atoms labeled as Se1 and Se2 are 0.008 a.u. and 0.20 a.u. respectively. Calculated

spin densities on respective carbon atoms labeled as C2, C4 and C5 are 0.03, 0.10 and 0.06 a.u. Mulliken charges on selenium atoms labeled as Se1 and Se2 are 0.31 and 0.40 a.u. whereas the same on Si and Br atoms are 0.09 and -0.06 a.u. respectively. Figure 4.2e shows the most stable structure of [5]SH⁺⁺. The dihedral angles, $\delta(\text{Br1C2C3Br2})$ and $\delta(\text{Br2C3C2C4})$ indicate that non-planarity is increased in this system compared to seleno[4]helicene radical cation. Spin densities on selenium atoms labeled as Se1, Se2 and Se3 are obtained 0.08, 0.14, and 0.006 a.u. for [5]SH⁺⁺ in DCM solvent. The same on carbon atoms labeled as C2, C4, C5 and C6 are 0.03, 0.001, 0.01 and 0.14 a.u. respectively. Mulliken charges on selenium atoms labeled as Se1, Se2 and Se3 are obtained 0.36, 0.35, and 0.25 a.u. Mulliken charges on carbon atoms labeled as C2, C4, C5 and C6 are 0.04, -0.57, -0.74 and -0.50 a.u. respectively.

The most stable structure of [6]SH⁺⁺ is also non-planer as shown in Figure 4.2f. Spin densities on selenium atoms labeled as Se1, Se2 and Se3 are 0.03, 0.14, and 0.05 a.u. and the same on carbon atoms labeled as C2, C4, C5, C6, and C7 are 0.01, 0.008, 0.001 0.08 and 0.18 a.u. respectively. Mulliken charges on selenium atoms labeled as Se1, Se2 and Se3 are 0.30, 0.36, and -0.27 a.u. Mulliken charges are 0.10, -0.76, -0.93, -0.51 and -0.51 a.u. over C2, C4, C5, C6, and C7 carbon atoms respectively. As in case of neutral seleno[7]helicene, helical structure is obtained for radical cation of seleno[7]helicene, [7]SH⁺⁺ the in DCM solvent (see Figure 4.2g). Mulliken charges are 0.42, 0.28, 0.28, and 0.32 a.u. on Se1, Se2, Se3, and Se4 selenium atoms respectively. Spin densities are obtained as 0.06, 0.04, 0.04, and 0.18 a.u. on Se1, Se2, Se3, and Se4 atoms respectively. The one turn in helical structure is completed for radical cation of [8]SH⁺⁺ at present level of theory in DCM solvent. One complete turn in these radical cations of seleno[n]helicenes requires eight fused selenophene rings as in case of the neutral systems. Optimized structure of [8]SH⁺⁺ is shown in Figure 4.2h along with selected geometrical parameters. The coil type helical structures for [n]SH⁺⁺, n=9-10 are shown in

Figure 4.2 (i-j). Table 4.4 indicates that only a small change is occurred in the geometrical parameters in seleno[n]helicene radical cation on the addition of selenophene rings to seleno[n-1]helicene radical cation. It is summarized that the most stable structures of [1]SH^{•+} and [2]SH^{•+} in DCM solvent are planar. Structure of seleno[n]helicenes radical cation, n=3-10 in DCM solvent are non-planar. Table 4.4 shows that calculated dihedral angles for seleno[n]helicenes, n=3-8 radical cation at B3LYP-D level are considerably different than those at B3LYP level showing the effect of dispersion in the geometry. However, no difference in the calculated distance between the two Br atoms is observed.

To understand the pattern of the location of the odd electron in these doublet radical cation systems, spin density is calculated and plotted. Figure 4.3 shows the spin density plot of the seleno[7]helicene radical cation with a contour cut-off value of 0.004 a.u.

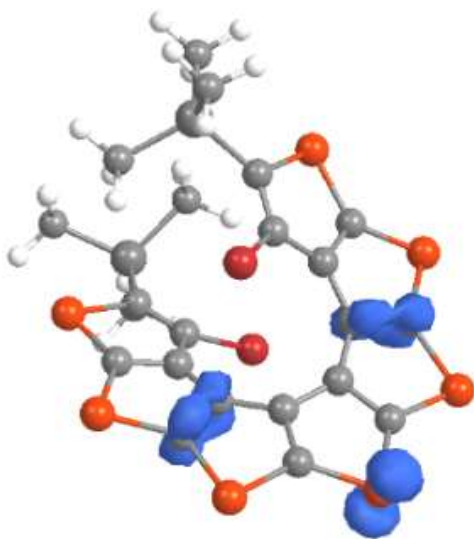


Figure 4.3 Spin density plot for the radical cation of end substituted seleno[7]helicene at the B3LYP-D/6-311++G(d,p) level of theory in DCM solvent with contour cutoff = 0.004 a.u.

It is observed that a significant amount of spin density is always present on heavy atoms. Spin densities on selenium atoms labeled as Se1, Se2, Se3, and Se4 are obtained 0.08 a.u., 0.03 a.u., 0.027 a.u., and 0.23 a.u. respectively in radical cation of [7]SH^{•+}. Similar plots on seleno[n]helicene radical cations systems also show significant amount of spin densities on selenium atoms. Thus, it is expected that a high g value may be obtained in the EPR spectra of these seleno[n]helicene radical cations.

4.3.5 Energy gap for radical cations of seleno[n]helicenes, [n]SH^{•+}, n=1-10

In these odd electron radical cation selenophene based helicenes, the highest occupied orbital is singly occupied and its referred as the lowest singly occupied molecular orbital or LSOMO. The optical band may be observed when electron makes transition from the highest occupied molecular orbital or HOMO to LSOMO. Thus, energy gaps between two selected orbitals of seleno[n]helicenes radical cation, [n]SH^{•+}, n=1-10 are calculated at B3LYP, B3LYP-D, and B3LYP-D3 functionals based on optimized structures in DCM applying respective functional. Table 4.5 summarizes the energy gap for seleno[n]helicenes radical cation, [n]SH^{•+}, n=1-10 at B3LYP, B3LYP-D, and B3LYP-D3 functionals in DCM solvent. Table 4.5 shows that the HOMO-LSOMO gap are same at B3LYP, B3LYP-D, and B3LYP-D3 functionals for seleno[n]helicenes radical cation, [n]SH^{•+} in DCM solvent. The value of HOMO-LSOMO gap for seleno[n]helicenes radical cation, [n]SH^{•+} are lies in the range 2.0-3.0 eV at B3LYP level of theory in DCM solvent (see Table 4.5). The value of HOMO-LSOMO gap for seleno[n]helicenes radical cation, [n]SH^{•+} are lies in the range 2.1-2.9 eV at B3LYP-D and B3LYP-D3 levels of theory in DCM solvent (see Table 4.5). It is to be noted that the HOMO-LSOMO gap varies only by 0.1-0.2 eV at B3LYP functional in comparison to B3LYP-D and B3LYP-D3 functionals for seleno[n]helicenes radical cation, [n]SH^{•+} in DCM solvent. Further,

Table 4.5 Calculated HOMO-LSOMO energy gap (in eV) for radical cations of seleno[n]helicenes, [n]SH^{•+}, n=1-10 in DCM solvent. Values in the braces are corresponding LSOMO-LUMO energy gap for radical cations of seleno[n]helicenes, [n]SH^{•+} in DCM solvent.

Energy gap (in eV) for seleno[n]helicene radical cations, [n]SH^{•+}, n = 1-5					
Method	[1]SH^{•+}	[2]SH^{•+}	[3]SH^{•+}	[4]SH^{•+}	[5]SH^{•+}
i)	2.6, (2.3)	3.0, (2.1)	2.9, (1.9)	2.0, (2.1)	2.6, (1.7)
ii)	2.8, (2.1)	2.9, (2.1)	2.7, (2.0)	2.3, (2.0)	2.4, (2.0)
iii)	2.8, (2.1)	2.9, (2.1)	2.7, (2.0)	2.3, (2.0)	2.4, (2.0)
Energy gap (in eV) for seleno[n]helicene radical cations, [n]SH^{•+}, n = 6-10					
Method	[6]SH^{•+}	[7]SH^{•+}	[8]SH^{•+}	[9]SH^{•+}	[10]SH^{•+}
i)	2.0, (2.0)	2.0, (1.9)	2.2, (1.7)	2.2, (1.8)	2.2, (1.8)
ii)	2.2, (2.0)	2.2, (1.9)	2.1, (2.0)	2.1, (1.9)	2.1, (1.9)
iii)	2.2, (2.0)	2.2, (1.9)	2.1, (2.0)	2.1, (1.9)	2.1, (1.9)

i) B3LYP, ii) B3LYP-D, iii) and B3LYP-D3 with 6-311++G(d,p) basis set

the HOMO-LSOMO gap systematically decreases as the number of selenophene rings increases and HOMO-LSOMO gap saturate at 2.1 eV for large size seleno[n]helicenes radical cation, [n]SH^{•+}. The energy gap for these [n]SH^{•+} lies in the visible region and in NIR region of electromagnetic spectrum in DCM solvent. Furthermore, LSOMO-LUMO gap are almost same at above-mentioned levels of theory in DCM solvent. The value of LSOMO-LUMO gap for seleno[n]helicenes radical cation, [n]SH^{•+} are lies in the range 2.1 eV-1.9 eV at B3LYP-D and B3LYP-D3 levels of theory in DCM solvent (see Table 4.5). The value of LSOMO-LUMO gap for thia[n]helicenes radical cation, [n]TH^{•+} are lies in the range 2.3 eV-1.7 eV at B3LYP-D and B3LYP-D3 levels of theory in DCM solvent (see Table 4.5). The energy gap for these [n]SH^{•+} lies in IR region of electromagnetic spectrum in DCM solvent. The energy gap is not decrease as regularly as the number of selenophene rings increases for these seleno[n]helicenes

radical cation, $[n]SH^{*+}$ in DCM solvent. This due to reason that as these radical cations systems not only have the π -electron delocalization and conjugation through the selenium atoms but also have high degree of helical distortion. Energy gap is found to be almost same at B3LYP, B3LYP-D, and B3LYP-D3 functionals for $[n]SH^{*+}$ (see Table 4.5)

In summary, these doublet radical cations systems generated from their corresponding neutral systems have suitable HOMO-LSOMO and LSOMO-LUMO energy gaps. Moreover, the helical structures provide flexibility for using these cationic doublet systems as IR detector.

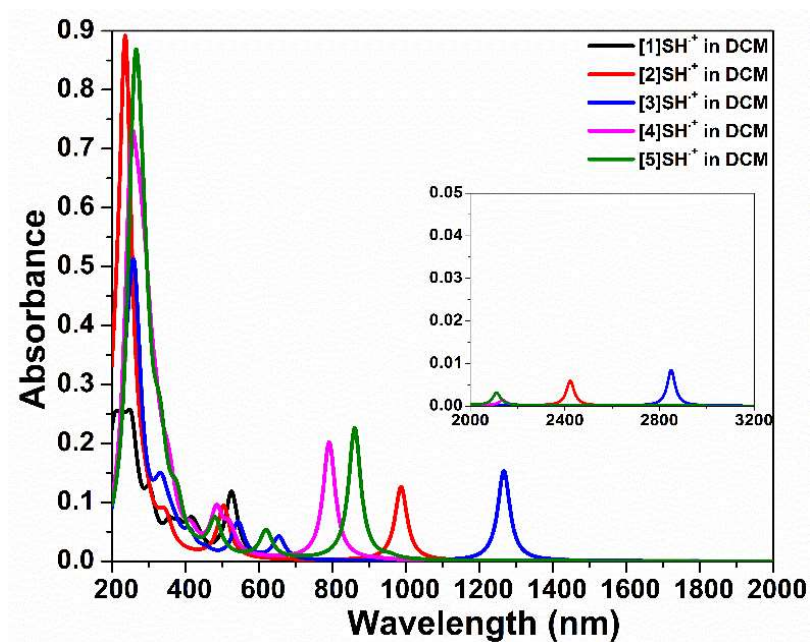
4.3.6 Excited state electronic spectra for radical cations of seleno[n]helicenes, $[n]SH^{*+}$, n=1-10 in gas phase and in DCM

TDDFT procedure is applied to study a few low lying excited states of seleno[n]helicenes radical cation, n=1-10 in DCM solvent and to simulate UV-Vis spectra adopting CAM-B3LYP/6-311++G(d,p) method. Table 4.6 presents λ_{max} of the absorption bands with corresponding oscillator strengths (f) and molecular orbitals involved in electronic transitions. The simulated UV-Vis spectra of $[n]SH^{*+}$, n=1-5 in DCM solvent are displayed in Figure 4.4a. Figure 4.4b shows simulated UV-Vis spectra of $[n]SH^{*+}$, n=6-10 in DCM solvent. It is interesting to note that $[2]SH^{*+}$ and $[3]SH^{*+}$ systems have one strong and one weak absorption band in NIR region. Simulated electronic spectrum of $[3]SH^{*+}$ shows a strong absorption band in DCM solvent at 1265 nm with oscillator strength of 0.152. It may be noted from Figure 4.4a that except for $[1]SH^{*+}$, all the radical cation systems $[n]SH^{*+}$ for n=2-6 have absorption bands in IR region. In case of $[7]SH^{*+}$ and $[8]SH^{*+}$ systems in DCM solvent, strong absorption bands in the visible region with $\lambda_{max} = 572$ and 516 nm respectively along with relatively weak absorption bands in IR region ($\lambda_{max} = 1279$ and 1077 nm) are predicted. Interestingly,

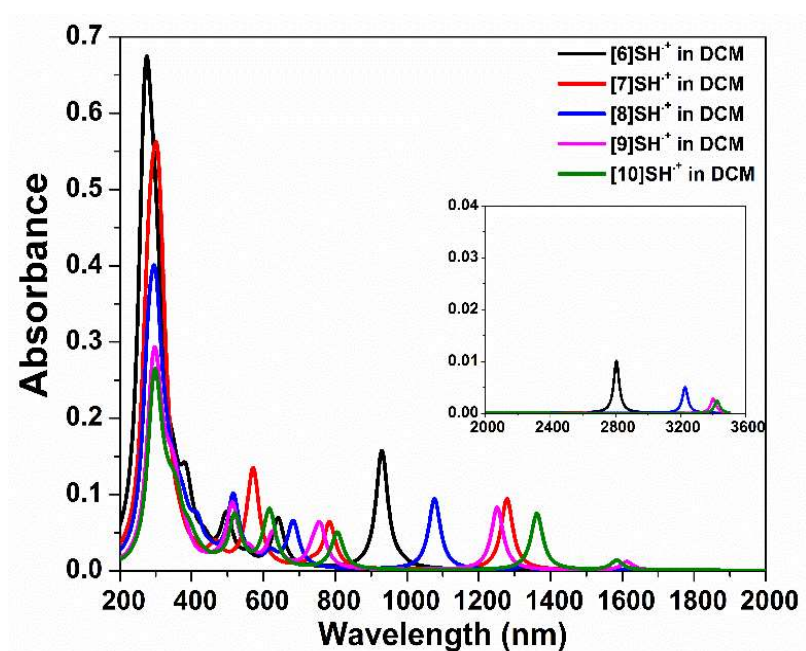
Table 4.6 Calculated excited state data for radical cations of seleno[n]helicenes [n]SH^{•+}, n=1-10 in DCM solvent considering CAM-B3LYP/6-311++G(d,p) level of theory under TDDFT formalism. Value in the braces are excited state data for radical cations of seleno[n]helicenes [n]SH^{•+}, n=1-10 in DCM solvent considering same level of theory.

[n]SH ^{•+}	λ_{\max} (nm)	Oscillator strength (f)	Electronic Transitions [§]
[1]SH ^{•+}	525	0.111	H-2 → L (0.68)
	415	0.042	H-2 → L (0.65)
[2]SH ^{•+}	2422	0.006	H → L (0.92)
	985	0.125	H-1 → L (0.92)
	503	0.088	H-3 → L (0.88)
[3]SH ^{•+}	2846	0.008	H-1 → L (0.79)
	1265	0.152	H → L (0.79)
	543	0.060	H-3 → L (0.74)
[4]SH ^{•+}	2138	0.001	H → L (0.98)
	790	0.198	H-2 → L (0.98)
[5]SH ^{•+}	2111	0.003	H → L (0.98)
	859	0.225	H-1 → L (0.96)
	619	0.046	H-3 → L (0.90)
[6]SH ^{•+}	2804	0.010	H → L (0.90)
	930	0.155	H-1 → L (0.90)
	641	0.062	H-3 → L (0.87)
[7]SH ^{•+}	1279	0.093	H-1 → L (0.94)
	784	0.060	H-4 → L (0.96)
	572	0.122	H-5 → L (0.83)
[8]SH ^{•+}	3228	0.005	H → L (0.80)
	1077	0.090	H-2 → L (0.83)
	683	0.060	H-4 → L (0.93)
	516	0.122	H-6 → L (0.83)
[9]SH ^{•+}	3401	0.003	H → L (0.69)
	1612	0.011	H-1 → L (0.94)
	1252	0.082	H-2 → L (0.73)
	626	0.044	H-3 → L (0.77)
[10]SH ^{•+}	3424	0.002	H-2 → L (0.98))
	1584	0.075	H-1 → L (0.93)
	1362	0.013	H-1 → L (0.71)
	618	0.068	H-6 → L (0.89)

[§]H=Highest doubly occupied molecular orbital (HDOMO) & L= Lowest singly molecular orbital (LSOMO). Values in the braces show relative contribution of the transition for the optical band. Transitions with major contributions are only shown.



a



b

Figure 4.4 UV-Vis spectra for radical cations of end substituted seleno[n]helicenes in DCM solvent, [1]SH⁺, a) $n=1-5$ and b) $n=6-10$ following TDDFT procedure at CAM-B3LYP/6-311++G(d,p) level of theory.

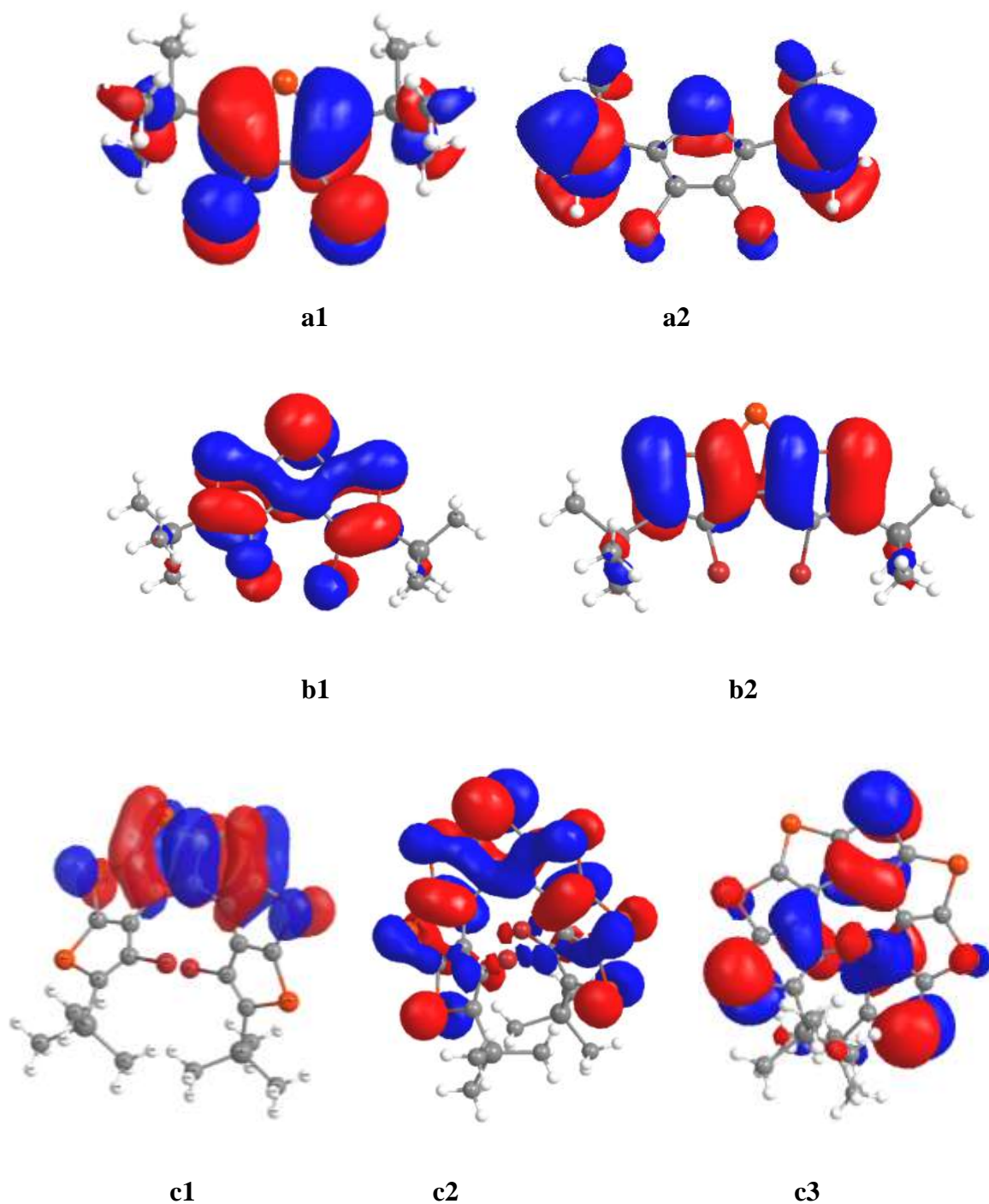


Figure 4.5 Selected molecular orbital diagram of most stable structures of seleno[n]helicenes, [n]SH⁺ n=1,3,7 a1) H-2 orbital of [1]SH⁺, a2) L orbital of [1]SH⁺, b1) H orbital of [3]SH⁺, b2) L orbital of [3]SH⁺, c1) H-5 orbital of [7]SH⁺, c2) L orbital of [7]SH⁺, and c3) H-1 orbital of [7]SH⁺ calculated at B3LYP-D/6-311++G(d,p) level of theory in DCM solvent. The figures are taken at isovalue of 0.002 a.u..

for [9]SH^{•+} and [10]SH^{•+} systems in DCM solvent, strong absorption bands are observed in the IR region. To examine the type electronic transitions in seleno[n]helicenes radical cation, n=1-10 selected MOs are plotted in Figure 4.5. These MOs are calculated considering the most stable structure of these radical cations in DCM solvent. Figure 4.5a1 and Figure 4.5a2 suggest that the optical absorption band at 525 nm for [1]SH^{•+} is due to $\pi \rightarrow \pi^*$ electronic transition. Similarly for [2]SH^{•+} system, the strong absorption band at 985 nm is mainly due to $\pi \rightarrow \pi^*$ transition. Again for [3]SH^{•+} system, the strong absorption band at 1265 nm is mainly due to $\pi \rightarrow \pi^*$ type transition and the corresponding orbitals are displayed in Figure 4.5b1 and Figure 4.5b2 respectively. It is interesting to note that on successive addition of selenophene rings to seleno[1]helicene radical cation, [1]SH^{•+}, the major optical absorption band undergoes large red shifts, $\Delta\nu=460$ nm for [2]SH^{•+} and $\Delta\nu=280$ nm [3]SH^{•+}. However, in case of [4]SH^{•+}, the major optical band is largely blue shifted compared to that in [3]SH^{•+} and the band is originated due to $n \rightarrow \pi^*$ type electronic transition. Again on successive addition of two selenophene rings to [4]SH^{•+} system, the strong optical band is predicted to be red shifted, $\Delta\nu=69$ nm for [5]SH^{•+} and $\Delta\nu=71$ nm [6]SH^{•+}. In case of seleno[7]helicene radical cation, [7]SH^{•+}, the major optical band is blue shifted to 572 nm and appears to be $n \rightarrow \pi^*$ type of electronic transition. Corresponding orbitals involved in the transition are displayed in Figure 4.5c1 and Figure 4.5c2 respectively. However, it has also a strong optical band in NIR region and this is due to $\pi \rightarrow \pi^*$ type of electronic transition. The corresponding orbitals involved are shown in Figure 4.5c1 and Figure 4.5c3. Strong absorption bands are predicted only in the visible region for [8]SH^{•+} system. In case of [9]SH^{•+} system, strong absorption bands in the IR as well as Visible regions are predicted. However, [10]SH^{•+} system has strong optical band in IR region and this is due to $\pi \rightarrow \pi^*$ type of electronic transition. Overall, based on excited-state studies, it may be

concluded that most of these seleno[n]helicenes radical cations, $[n]SH^{•+}$ may be important in making variety of detectors that can be used in far IR and near IR region.

4.3.7 Dimerization of neutral and radical cation of thia[7]helicene in DCM solvent

From the literature, it is found that the dimer formation is one of the probable processes in π -radical cations systems.¹²⁸ Thus, to produce persistent stable π -radical cations appropriate structural modifications are often needed. One such structural modifications is substituting the terminal ends of the systems by bulky substituents which can control the dimerization of reactive radical cations.^{32,118} Other methods to control the dimerization are steric control and increase the π -conjugation in the radical cationic systems.^{32,118,119} Thus, the control of such π -dimerizing self-association of reactive π -radical cations is always the subject of the interest. As this π -dimerization can significantly affect the performance of a device made of such molecules.

These seleno[n]helicenes systems represent the class of π -conjugated systems. Thus π -dimerization is always a possibility due to intermolecular interactions. However, it can be expected that the extent of intramolecular π -dimerization may not be significant due to the flexible shape and presence of large substituents at end positions. But, a theoretical model study on π -dimerization is always necessary before using these systems for the further development of electronic devices. Also, it can provide some valuable guidance to control of such π -dimerizing self-association in neutral as well as radical cations of seleno[n]helicenes. To the best of our knowledge, no systematic theoretical studies are available on the π -dimers of neutral and radical cations of seleno[n]helicenes in solution. In solution, the radical cations are always generated with some counter ion like PF_6^- , SbF_6^- etc. However, in literature, it is given that

this effect may be small in solution because PF_6^- counter anion is a weakly coordinating anion.

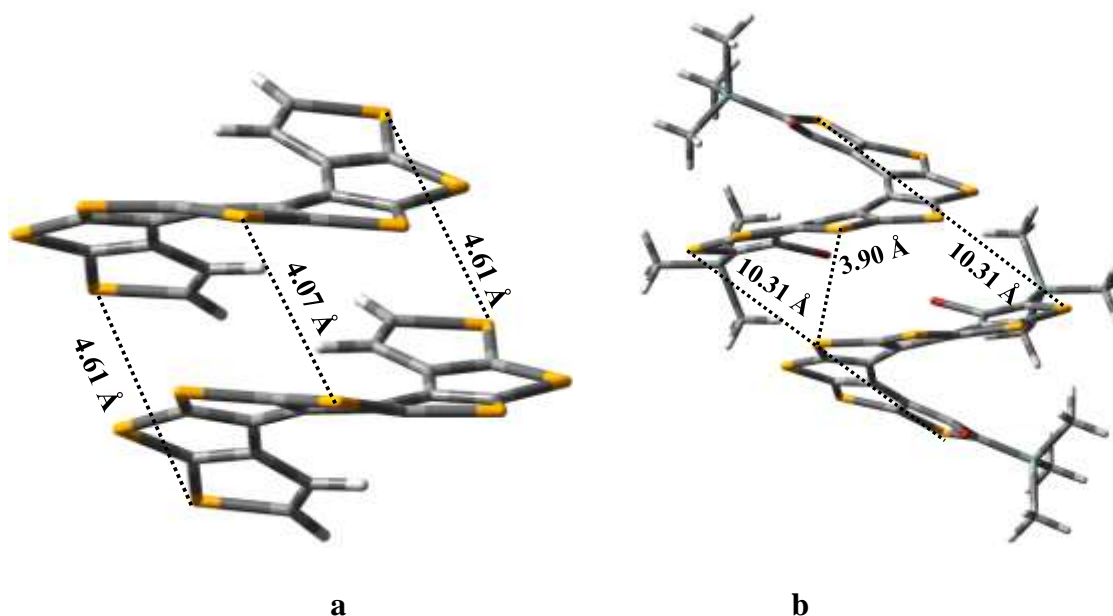
¹²⁰ But, the contribution of electrostatic stabilization should be considered in the solution.

Thus, a case study on the π -dimerization in neutral as well as radical cations of seleno[7]helicene is being performed at B3LYP-D/6-311++G(d,p) level of theory in DCM solvent. Structure of the π -dimer systems.

4.3.7.1 Structure of the π -dimer system

Similar to thia[7]helicenes systems, three different cases are considered as described below

Case 1: The most stable structure of unsubstituted π -dimer of neutral seleno[7]helicene, $([7]\text{SH})_2$, is fully π - π stacked structure arises due to Vander wall attraction two [7]SH at B3LYP-D level of theory in DCM solvent (see Figure 4.6a). Most stable structure of unsubstituted π -dimer of neutral $([7]\text{SH})_2$ suggests a sandwich-type configuration and the



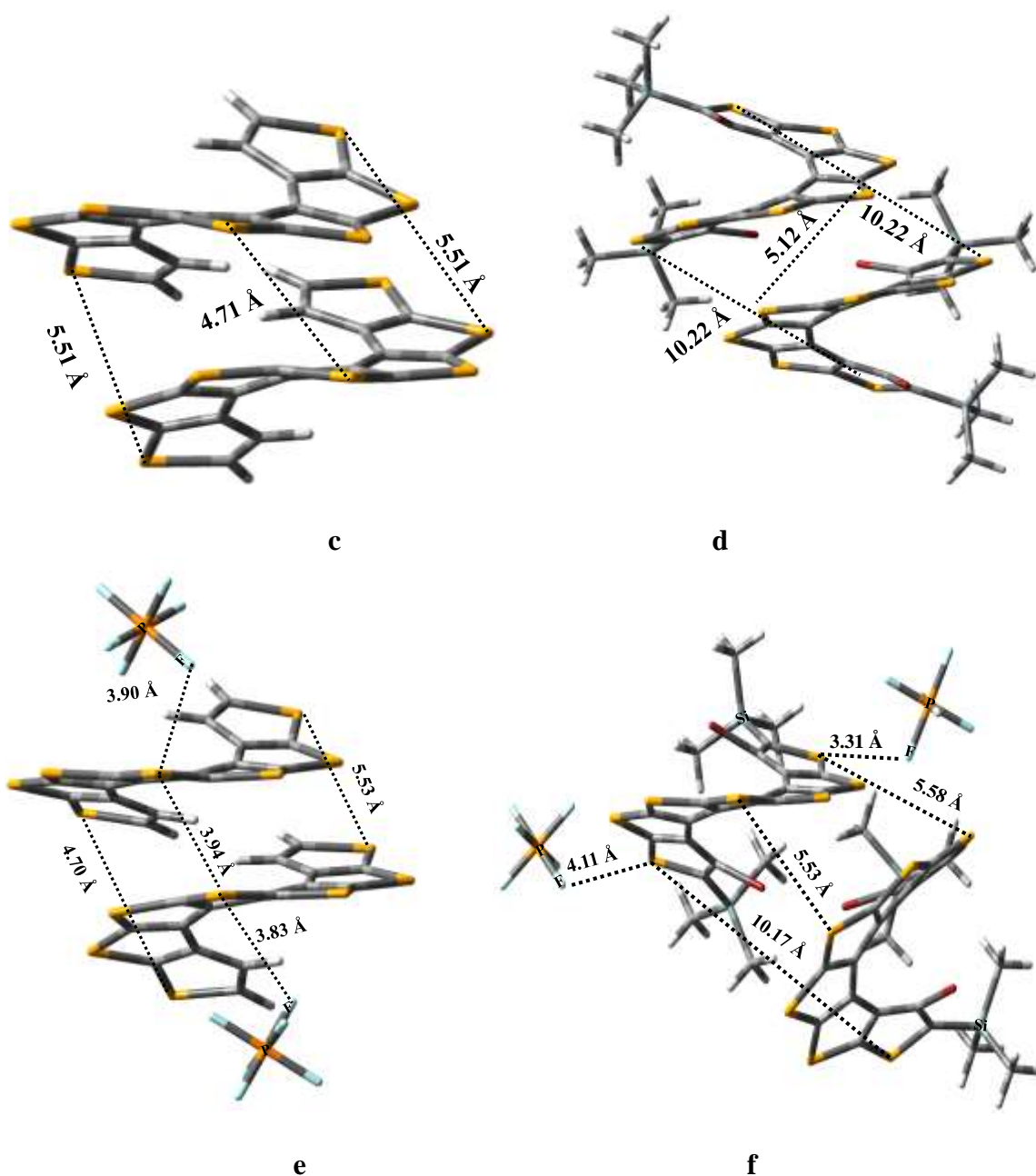


Figure 4.6 Most stable π -dimeric structure of a) neutral unsubstituted seleno[7]helicene monomer, b) neutral substituted seleno[7]helicene monomer, c) radical cation of unsubstituted seleno[7]helicene monomer, d) radical cation of substituted seleno[7]helicene monomer, e) radical cation of unsubstituted seleno[7]helicene monomer with PF_6^- counter anion, f) radical cation of substituted seleno[7]helicene monomer with PF_6^- counter anion. Calculated at B3LYP-D/6-311++G(d,p) level of theory in DCM solvent.

maximum and minimum non-bonded distances between two monomers [7]SH units are calculated as 4.61 Å and 4.07 Å respectively (see Figure 4.6a). In comparison, the most stable structure calculated for substituted π -dimer of neutral seleno[7]helicene, (s-[7]SH)₂ show partial π - π stacking of two monomer s-[7]SH structure (see Figure 4.6b), here s-represents the substitution of TMS at α and α' terminal ends, substitution of Br at β and β' terminal ends. The maximum and minimum non-bonded distances between two monomer s-[7]SH units are calculated as 10.31 Å, and 3.90 Å respectively at the present level of theory in DCM solvent (see Figure 4.6b). This increase in non-bonded distances shows that substituted π -dimer of neutral seleno[7]helicene formed is not stabilized from the one substituted end.

Case 2: For unsubstituted charged π -dimer, ([7]SH)₂²⁺ the most stable structure obtained is fully π - π stacking of two units of the radical cation of seleno[7]helicene (see Figure 4.6c). In comparison, the substituted π -dimer of radical cation of seleno[7]helicene, the structure obtained is partly π - π stacking of two units of the radical cation in DCM solvent (see Figure 4.6d).

Case 3: With two PF₆⁻ counter anion, for the unsubstituted charged π -dimer, ([7]SH)₂²⁺, the most stable structure obtained is showing a π - π stacking of two units of the radical cation of seleno[7]helicene with PF₆⁻ counter anion present in the top and below (see Figure 4.6e). For the most stable structure of the substituted charged π -dimer, (s-[7]SH)₂²⁺ the two PF₆⁻ counter anion shows that both the PF₆⁻ anion are interacting only to the one unit of the dimer (see Figure 4.6f).

4.3.7.2 Dimerization energy (ΔG_{dim}) for π -dimer system

Case 1: Dimerization energy is calculated as the difference of total energy of the π -dimer system and the sum of the total energy of the two dissociated monomer systems. Based on

Hessian calculations, followed by thermochemical analysis Gibbs free energy of dimerization, ΔG_{dim} is calculated for unsubstituted neutral π -dimer, $([7]\text{SH})_2$ as -7.0 kcal/mol. This indicates that the formation of the π -dimer is a favourable process for neutral unsubstituted seleno[7]helicene. In comparison, ΔG_{dim} calculated for the substituted π -dimer of neutral seleno[7]helicene is +2.5 kcal/mol and it indicates that the formation of the π -dimer is not a favourable process. Thus, the substitution of TMS at α and α' terminal ends, substitution of TMS Br at β and β' terminal ends significantly reduces the intermolecular interactions which is responsible for π -dimer formation.

Case 2: In case of π -dimer of unsubstituted radical cation of seleno[7]helicene, the calculated ΔG_{dim} at STP is -0.2 kcal/mol and this indicates that the dimerization process is the very less favourable process. In contrast, the calculated ΔG_{dim} for the substituted radical cation of seleno[7]helicene is +1.5 kcal/mol which rules out the formation of the π -dimer in DCM solvent. The positive value of ΔG_{dim} calculated for π -dimer of substituted radical cation of seleno[7]helicene shows that substituted radical cation of seleno[7]helicene does not indicate the dimerization at STP in DCM solvent.

Case 3: It is interesting to note that, calculated ΔG_{dim} is -3.0 kcal/mol at STP for the most stable structure of unsubstituted radical cation of seleno[7]helicene with two PF_6^- counteranion and this indicates that significant possibility of the dimer in the presence of two PF_6^- counterion. However, calculated ΔG_{dim} for the most stable structure of substituted radical cation of seleno[7]helicene with two PF_6^- counteranion structure at STP is 3.7 kcal/mol and this indicates that the dimer formed is not stabilized in the presence of counteranions.

4.4 Conclusions

It is observed that B3LYP-D functional works quite well to predict molecular geometry of neutral seleno[n]helicenes and their radical cation in DCM solvent following macroscopic SMD solvent model. It is also noted that B3LYP functional produces structures with different non-planarity for some of the systems. End substituted seleno[n]helicene systems prefer non-planar structure when the number of selenophene rings is three or more. Neutral end substituted seleno[n]helicenes, $n=1-10$ show the optical absorption bands in the ultraviolet region. However, their radical cations have strong absorption in the range of visible to IR. Origin of optical absorption bands of the end substituted seleno[n]helicenes radical cation in the IR regions are due to $\pi \rightarrow \pi^*$ type of electronic transition. Calculated free energy at STP in DCM solvent for π -dimer of unsubstituted seleno[7]helicene suggests that dimerization of the monomer unit is possible. However, the same calculated for π -dimer of end substituted seleno[7]helicene in DCM solvent shows that dimerization is not favorable at STP. Calculated free energy values for π -dimer of unsubstituted and end substituted radical cations of seleno[7]helicene in DCM solvent at STP do not indicate any possibility of dimerization. Free energy parameters on π -dimer of unsubstituted and end substituted radical cations of seleno[7]helicene in presence of counter ion, PF_6^- in DCM solvent at STP decreases the possibility of dimerization. Overall, these selenophene based helical systems may be useful in organic-electronic devices.

CHAPTER 5

Comparative Study on Band Gap of Chalcogen (S, Se and Te) based β -Helicenes and Spectral Properties of their Corresponding Radical Cations

5.1 Introduction

As discussed in the previous chapters, the thiophene and selenophene based linear and rigid π -conjugated systems are useful candidates in optical device applications. However, studies on thiophene and selenophene based flexible systems are at their early stages. Chapter 3 and Chapter 4 highlighted that the substituted thia[n]helicenes and seleno[n]helicenes systems have suitable energy gap and low probability of dimerization in DCM solvent. Also, they have strong absorption in NIR region in their radical cationic state in DCM solvent. Replacement of sulfur atom in thiophene with tellurium atom is expected to affect the electronic properties in thia[n]helicenes in their neutral and radical cationic state. Thus a systematic study on tellurium based helicenes systems may provide a novel molecular systems to be used as electronic devices.

Tellurophene is a tellurium-based analogue of thiophene/selenophene systems. The incorporation of the tellurophene-motif into π -extended molecules is observed to be a promising strategy to produce advanced materials.⁴⁷ Replacement of sulfur (S) atom in thiophenes with tellurium (Te) atoms can dramatically change the electronic properties of these compounds without significantly altering their electronic structures.⁴⁷⁻⁵¹ For instance, the experimentally reported HOMO-LUMO gap changes from 2.0 eV in polythiophene to 1.5 eV for polytellurophene.⁴⁶ The literature review reveals that the photon absorption in several

tellurophenes based conjugated systems increases due to strong interactions between tellurium atoms.⁴⁶ These increased strong interactions between tellurium atoms increase the importance of these systems in photovoltaic devices. Also, the tellurophene-based conjugated systems may exhibit efficient singlet to triplet intersystem crossing due to the heavy atom effect of tellurium, which can increase the lifetime of photoluminescence.⁴⁶ Though tellurophene-based conjugated systems have a great future in optoelectronic devices, in comparison to thiophene and selenophene π -conjugated systems, the studies on their tellurophene analogues are still at an early stage. It is due to the fact that the synthetic methods for tellurophene-based systems are not as much established in comparison to their thiophene and selenophene-based analogues.⁴⁶ Te is capable of showing several stable oxidation states and its sensitivity to oxidizing environments is always a matter of concern.¹²⁹

The thiophene, selenophene and tellurophene π -conjugated systems have planar and rigid structures with strong π -conjugation. Due to their planar/rigid shapes and strong π -conjugation, they are prone to π -dimerization in their neutral and radical cationic states.^{31,32} Again, it is known that the dimerization process strongly affects the electronic features of such systems which can affect their device performance. Despite the low degree of electronic delocalization in these helicenes systems, they have strong chiroptical properties and stability in the solid and in solution phase. It is discussed in the previous chapter, that thia- and seleno- [n]helicenes systems have wide energy gap and low probability of dimerization in DCM solvent. These systems not only have poor tendency to form π -dimers in neutral and radical cationic state but also have strong absorptions in NIR region in DCM solvent.⁷⁰

Motivated by thiophene and selenophene based [n]helicenes systems, their corresponding telluro[n]helicenes analogues are theoretically explored and presented in this chapter. These

telluro[n]helicenes systems are novel tellurophene based helical systems. The electronic features of these telluro[n]helicenes (n=1-10) are also compared with the reported thiophene and selenophene-based helicenes systems. The stability of radical cations of telluro[n]helicenes is expected to be more than those of the corresponding radical cations of sulfur and selenium-based analogues due to the large size and polarizable nature of Te atoms than Se and S atoms. Thus, a case study is also reported on the possibility of dimerization in unsubstituted and end substituted neutral and radical cations of telluro[7]helicene systems in DCM solvent.

This chapter provides theoretically calculated band gap of chalcogen (S, Se and Te) based neutral helicenes. The effect of increasing the number of ortho fused rings and the size of chalcogen atoms are studied and reported. HOMO-LUMO energy gaps of the radical cations of the tellurium based helicenes and the variation of energy gap are studied with the number of ortho fused rings. The calculated energy gaps are also compared for three different chalcogen based helicenes systems. The unique structures and reactivity of this class of chalcogen compounds, as well as their interesting optical and electronic properties, put them in the category of the materials of extensive potential applications. This study also provides finding suitable candidates for NIR detector from these chalcogen based helicenes systems. Dimerization study of unsubstituted and end substituted neutral telluro[7]helicene and its radical cation in the presence of a PF_6^- counter ion in DCM solvent is also studied as sample cased and reported.

5.2 Computational methods

Stepwise ortho-fusion of tellurophene rings are used to produce all possible structures of unsubstituted and end substituted neutral telluro[n]helicenes (n = 1-10) and their corresponding

radical cations. Geometry optimizations of telluro[n]helicenes are performed by using B3LYP^{88,89} and B3LYP-D⁹⁴ DFT functionals. As in the previous systems, 6-311++G(d,p) basis functions are considered for all the atoms except Te. For Te atoms, Los Alamos ECP, LanL2DZ^{130,131} and split valance triple zeta basis functions, Def2TZVP^{132,133} are tried. However, LANL2DZ and DEF2TZVP basis sets are found to be unsuitable due to problem in SCF convergence. Thus, the minimum energy equilibrium structures of unsubstituted and end substituted neutral telluro[n]helicenes ($n = 1-10$) and their corresponding radical cations are calculated using the B3LYP functional and dispersion corrected functional B3LYP-D in conjunction with 6-311++G(d,p) basis set for H, C, Si, and Br atoms and all electron 3-21G basis set for Te atoms in the gas phase and also in DCM solvent. It is reported that several oligotellurophenes systems are susceptible to oxidation in aqueous medium¹³⁴. Moreover, DCM solvent is considered for thia and seleno [n]helicenes. Thus, DCM solvent is considered for all solvent-based calculations with a macroscopic solvation model based on solute density (SMD).^{104,105} Most stable structures of unsubstituted and end substituted neutral telluro[n]helicenes [n]TeH ($n = 1-10$) and their corresponding radical cations obtained at the B3LYP level of theory is further reoptimized applying dispersion corrected functional B3LYP-D in conjunction with the same basis set in DCM solvent to examine the effect of dispersion and to improve geometrical parameters as in performed for thia- and seleno- [n]helicenes. To verify if the equilibrium structures obtained refer to the true minima or not, hessian calculations are carried out in DCM solvent for neutral and radical cations of telluro[n]helicenes. Most stable structures obtained at the B3LYP-D⁹⁴ level are then used for single point energy calculations at B3LYP-D3⁹⁵ functionals in DCM solvent to improve energy parameters. The restricted open-shell Hartree-Fock (ROHF) formalism is used to avoid any spin contamination in the radical cationic doublet systems. Excited-state calculations are carried out applying the

TDDFT procedure and considering the CAM-B3LYP functional along with 6-311++G(d,p) basis set for H, C, Si, and Br atoms and 3-21G basis set for Te atoms for neutral as well as the radical cations of Telluro[n]helicenes. The UV-visible spectra are reported with the lowest 50 excited states in DCM solvent. CAM-B3LYP is a long-range corrected hybrid exchange-correlation functional designed to predict reasonable spectra.^{115,116} Visualization of frontier molecular orbitals is carried out to gather information about the type of orbitals involved in electronic transitions. As a case study to find out the possibility of dimerization, Gibbs free energy data are reported for the unsubstituted and end substituted dimers of neutral telluro[7]helicene and its radical cation using most stable structures in DCM. B3LYP-D functional with 6-311++G(d,p) basis set for H, C, Si, and Br atoms and 3-21G basis set for Te atoms is considered to perform the case study on above-mentioned systems. Further, two PF₆⁻ counter anions are also considered for geometry optimization of the π -dimers of unsubstituted and end substituted telluro[7]helicene radical cations in DCM solvent.

5.3 Results and Discussions

5.3.1 Structure for neutral telluro[n]helicene, [n]TeH, n=1-10 in DCM solvent

Table 5.1 provides selected geometrical parameters of the fully optimized structures of neutral telluro[n]helicenes (n = 1-10) in DCM solvent. Table 5.1 indicates that calculated dihedral angles for telluro[n]helicenes, n=3-7 at the B3LYP-D level are considerably different than those at the B3LYP level showing the effect of dispersion. However, no difference in the calculated distance between the two Br atoms is observed. The most stable structures for neutral telluro[n]helicenes, n = 1-10 are calculated in DCM solvent are shown in Figure 5.1(a-j). The most stable structures of telluro[n]helicenes, n=1-2 are planar as suggested by their dihedral

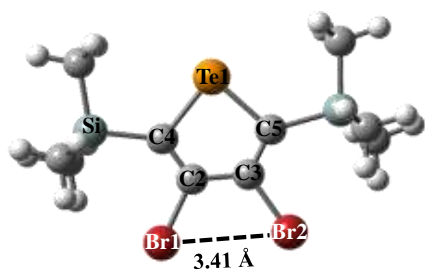
Table 5.1 Selected [#]geometrical parameters of neutral end substituted telluro[n]helicenes, n=1-10 calculated at B3LYP-D with 6-311++G(d,p) basis set for H, C, Si, and Br atoms and 3-21G basis set for Te atoms in DCM solvent. The value in the braces are calculated at B3LYP functional with the same basis set in DCM solvent.

n	1	2	3	4	5	6	7	8	9	10
r_{C2-C3} (Å)	1.45	2.70	3.42	3.63	3.61	3.25	3.27	4.22	5.20	5.85
^ar_{C4-C5+n} (Å)	2.81,	4.93	6.06	6.07	5.35	4.17	3.76	5.53	7.19	8.08
^br_{Te1-Te(n)} (Å)	-	3.79, (3.78)	6.86, (6.84)	8.46, (8.50)	8.43, (8.63)	6.92, (7.01)	4.32, (4.82)	4.08, (4.58)	6.57, (6.84)	8.98, (9.21)
r_{Br1-Br2} (Å)	3.41, (3.37)	3.37, (3.34)	3.43, (3.41)	3.56, (3.55)	4.15, (4.12)	4.97, (5.16)	5.53, (5.70)	5.96, (6.13)	6.16, (6.35)	6.30, (6.35)
δ(Br1C2C3Br2) (degree)	0, (0)	0, (0)	72.5, (69.9)	-113.7, (- 110.9)	-164.3, (-161.4)	-146.1, (-141.1)	-91.8, (-88.6)	-20.6, (-21.4)	33.4, (31.2)	79.7, (78.4)
δ(Br2C3C2C4) (degree)	180, (180)	180, (180)	-77.5, (-81.5)	-11.0, (-8.9)	-56.6, (-55.1)	95.1, (98.6)	141.7, (142.6)	-163.3, (-164.5)	-110.6, (-112.8)	-50.9, (-52.8)

[#]**Figure 5.1** may be referred for identifying geometrical parameters.

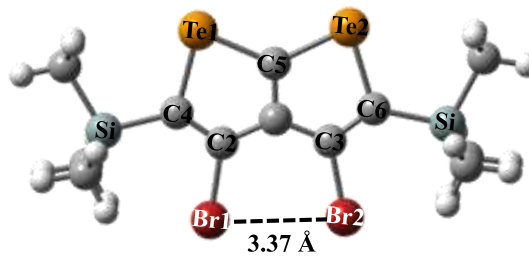
^ar_{C4-C5+n}, n=0 for telluro[1]helicene, n=1 for telluro[2]helicene and so on.

^br_{Te1-Te(n)}, n = 1 for telluro[1]helicene, n = 2 for telluro[2]helicene and so on.



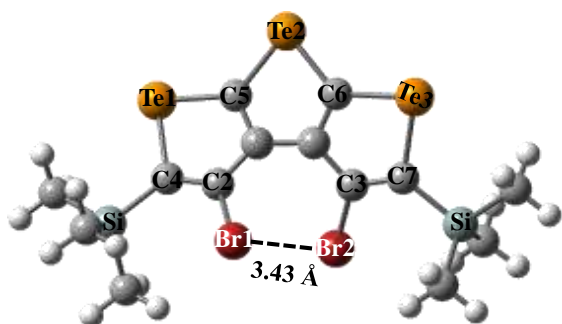
$r_{C2-C3} = 1.45 \text{ \AA}$, $r_{C4-C5} = 2.81 \text{ \AA}$,
 $\delta(Br1C2C3Br2) = 0^\circ$, $\delta(Br2C3C2C4) = 180^\circ$

a



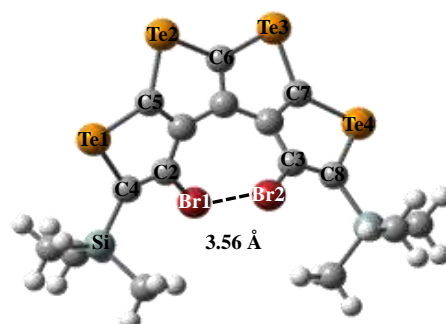
$r_{C2-C3} = 2.70 \text{ \AA}$, $r_{C4-C6} = 4.93 \text{ \AA}$,
 $\delta(Br1C2C3Br2) = 0^\circ$, $\delta(Br2C3C2C4) = 180^\circ$

b



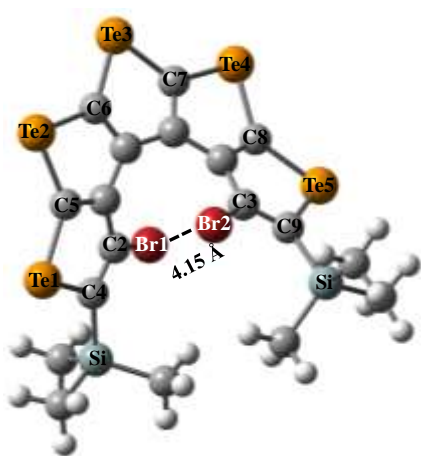
$r_{C2-C3} = 3.42 \text{ \AA}$, $r_{C4-C7} = 6.06 \text{ \AA}$,
 $\delta(Br1C2C3Br2) = 72.5^\circ$, $\delta(Br2C3C2C4) = -77.5^\circ$

c



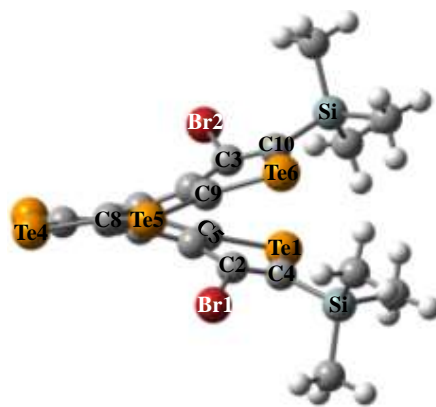
$r_{C2-C3} = 3.63 \text{ \AA}$, $r_{C4-C8} = 6.07 \text{ \AA}$,
 $\delta(Br1C2C3Br2) = -113.7^\circ$, $\delta(Br2C3C2C4) = -11.0^\circ$

d



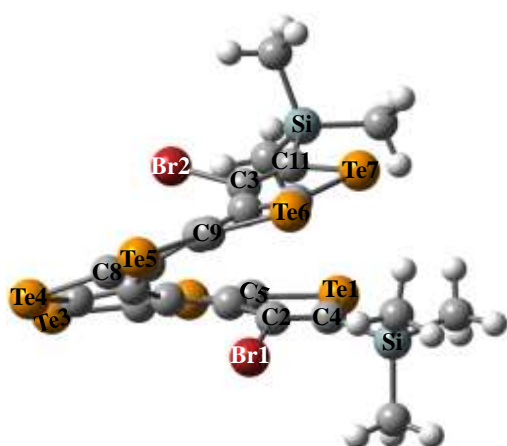
$r_{C2-C3} = 3.61 \text{ \AA}$, $r_{C4-C9} = 5.35 \text{ \AA}$,
 $\delta(Br1C2C3Br2) = -164.3^\circ$, $\delta(Br2C3C2C4) = -56.6^\circ$

e



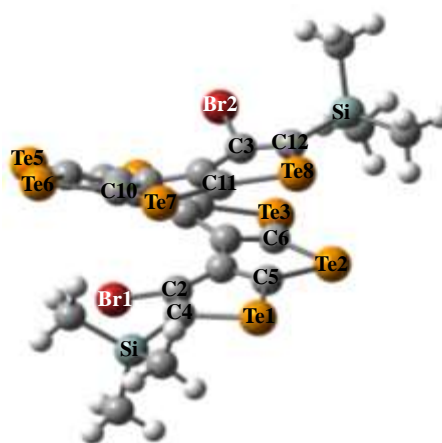
$r_{Br1-Br2} = 4.97 \text{ \AA}$, $r_{C2-C3} = 3.25 \text{ \AA}$, $r_{C4-C10} = 4.17 \text{ \AA}$,
 $\delta(Br1C2C3Br2) = -146.1^\circ$, $\delta(Br2C3C2C4) = 95.1^\circ$

f



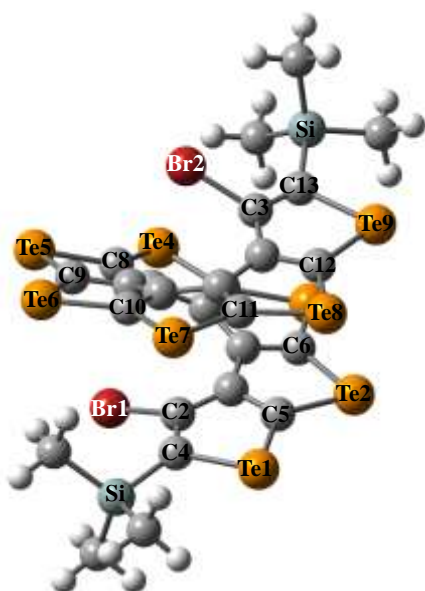
$r_{\text{Br1-Br2}} = 5.53 \text{ \AA}$, $r_{\text{C2-C3}} = 3.27 \text{ \AA}$, $r_{\text{C4-C11}} = 3.76 \text{ \AA}$,
 $\delta(\text{Br1C2C3Br2}) = -91.8^\circ$, $\delta(\text{Br2C3C2C4}) = 141.7^\circ$

g



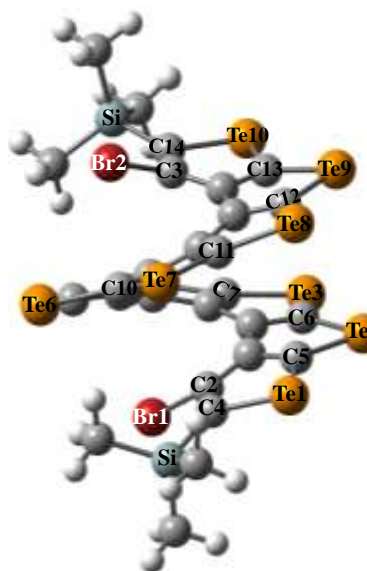
$r_{\text{Br1-Br2}} = 5.96 \text{ \AA}$, $r_{\text{C2-C3}} = 4.22 \text{ \AA}$, $r_{\text{C4-C12}} = 5.53 \text{ \AA}$,
 $\delta(\text{Br1C2C3Br2}) = -20.6^\circ$, $\delta(\text{Br2C3C2C4}) = -163.3^\circ$

h



$r_{\text{Br1-Br2}} = 6.16 \text{ \AA}$, $r_{\text{C2-C3}} = 5.20 \text{ \AA}$, $r_{\text{C4-C13}} = 7.19 \text{ \AA}$,
 $\delta(\text{Br1C2C3Br2}) = 33.4^\circ$, $\delta(\text{Br2C3C2C4}) = -110.6^\circ$

i



$r_{\text{Br1-Br2}} = 6.30 \text{ \AA}$, $r_{\text{C2-C3}} = 5.85 \text{ \AA}$, $r_{\text{C4-C14}} = 8.08 \text{ \AA}$,
 $\delta(\text{Br1C2C3Br2}) = 79.7^\circ$, $\delta(\text{Br2C3C2C4}) = -50.9^\circ$

j

Figure 5.1 Most stable structures of (a-j) telluro[n]helicenes, [n]TeH, n=1-10 a) [1]TeH, b) [2]TeH, c) [3]TeH, d) [4]TeH, e) [5]TeH, f) [6]TeH, g) [7]TeH, h) [8]TeH, i) [9]TeH, and j) [10]TeH, with with selected geometrical parameters calculated at B3LYP-D functional with 6-311++G(d,p) basis set for H, C, Si, Br atoms and 3-21G basis set for Te atoms in DCM solvent.

angles, $\delta(\text{Br1C2C3Br2})$ and $\delta(\text{Br2C3C2C4})$. A non-planar structure is obtained as the most stable one for telluro[3]helicene in DCM solvent (see Figure 5.1c). The calculated dihedral angles, $\delta(\text{Br1C2C3Br2})$ and $\delta(\text{Br2C3C2C4})$ are 72.5° and -77.5° respectively. The calculated non-planarity for this telluro[3]helicene is more than the corresponding thia- and seleno-[3]helicenes as presented in Table 3.1 and Table 4.1. Calculated non-bond distances, $r_{\text{S1-S3}}$, $r_{\text{Se1-Se3}}$ and $r_{\text{Te1-Te3}}$ are 5.82 Å, 6.62 Å, and 6.86 Å respectively thia[3]helicene, seleno[3]helicene and telluro[3]helicene systems. This suggests that the telluro[3]helicene is less conjugated than their corresponding thia[3]helicene and seleno[3]helicene systems. The non-planar structure obtained for telluro[3]helicene may be due to geometrical steric hindrances created because of two bulky Br groups present on C2 and C3 atoms. Figure 5.1(d-j) shows the minimum energy structures of telluro[n]helicenes, $n=4-10$ in DCM solvent considering a macroscopic solvent model. The calculated dihedral angles, $\delta(\text{Br1C2C3Br2})$ and $\delta(\text{Br2C3C2C4})$ suggest that, all the telluro[n]helicenes, $n \geq 3$ adopt non-planar structure at present level of theory in DCM solvent. For telluro[7]helicene system, a helical structure is obtained as the most stable equilibrium structure (see Figure 5.1g). Calculated non bonded distances $r_{\text{S1-S7}}$, $r_{\text{Se1-Se7}}$ and $r_{\text{Te1-Te7}}$ are 8.04 Å, 6.63 Å, and 4.32 Å respectively for thia[7]helicene, seleno[7]helicene and telluro[7]helicene. In case of telluro[7]helicene, calculated dihedral angles, $\delta(\text{Br1C2C3Br2})$ and $\delta(\text{Br2C3C2C4})$ are -91.8° and 141.7° respectively. However, the same calculated dihedral angles in case of thia[7]helicene and seleno[7]helicene are -168.9° , 80.7° and -135.2° and 104.1° respectively as provides in chapter 3 and chapter 4. This suggests that the telluro[7]helicene is more conjugated than their corresponding thia[7]helicene and seleno[7]helicene systems. Also, one turn in the helical structure is completed in case of telluro[7]helicene system and the corresponding most stable structure is shown in Figure 5.1g

as observed in case of thia- and seleno- [n]helicenes. But, for thia[n]helicenes and seleno[n]helicenes eight fused rings are required for one complete turn.

In short, it is predicted that neutral [1]TeH and [2]TeH are planar in DCM solvent. However, the structure of telluro[n]helicenes, n=3-10 are non-planar and helical as reported for its lower analogues.

5.3.2 Comparison of ionization energies (IE) of thia[n]helicenes, seleno[n]helicenes and telluro[n]helicenes (n=1-10) in DCM solvent

Calculated IE values at B3LYP, B3LYP-D, and B3LYP-D3 levels of theory with 6-311++G(d,p) basis set for H, C, Br, and Si atom and 3-21G for Te atom for telluro[n]helicenes (n=1-10) in DCM solvent are provided in Table 5.2.

Table 5.2 Calculated ionization energies (in eV) of telluro[n]helicenes, [n]TeH, n=10 in DCM solvent.

Ionization energies (in eV) of telluro[n]helicenes, [n]TeH, n = 1-5					
Method	[1]TeH	[2]TeH	[3]TeH	[4]TeH	[5]TeH
i)	6.0	5.5	5.2	5.1	4.9
ii)	6.0	5.5	5.3	5.1	4.9
iii)	6.0	5.5	5.3	5.1	4.9
Ionization energies (in eV) of telluro[n]helicenes, [n]TeH, n = 6-10					
Method	[6]TeH	[7]TeH	[8]TeH	[9]TeH	[10]TeH
i)	4.9	4.8	4.7	4.7	4.6
ii)	4.8	4.7	4.8	4.9	4.6
iii)	4.8	4.7	4.8	4.9	4.6

i) B3LYP, ii) B3LYP-D, iii) and B3LYP-D3, with 6-311++G(d,p) basis set for H, C, Br, Si, atoms and 3-21G basis set for Te atom.

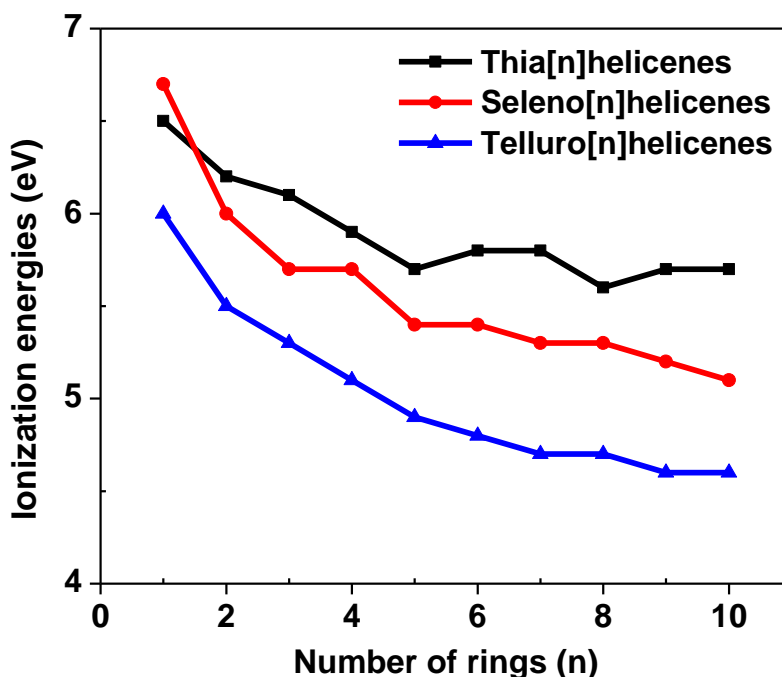


Figure 5.2 Comparison of the calculated ionization energies (in eV) of thia[n]helicenes, seleno[n]helicenes and telluro[n]helicenes at B3LYP-D level of theory in DCM solvent. 6-311++G(d,p) basis set for S, Se, H, C, Br, Si atoms and 3-21G basis set for Te atom is used for all calculations.

The ionization energies of telluro[n]helicenes are lower than thia[n]helicenes and seleno[n]helicenes at all mentioned DFT levels in DCM solvent. Table 3.2 and Table 4.2 in the previous chapters list the calculated IE values for thia and seleno- [n]helicenes respectively. The variation of ionization energies for thia[n]helicenes, seleno[n]helicenes and telluro[n]helicenes (n-10) with the increasing number of rings is shown in Figure 5.2. It may be noted that calculated IE follow the order, telluro[n]helicenes > seleno[n]helicenes > thia[n]helicenes for $n \geq 2$ at all DFT levels in DCM solvent. This is due to the reason that, size and polarizability of chalcogens follow the order, $\text{Te} > \text{Se} > \text{S}$. The conjugation follows the same order as the polarizability, telluro[n]helicenes > seleno[n]helicenes > thia[n]helicenes. As the size and polarizability of Te atom is more than that of S and Se atoms. Thus, Te atoms in telluro[n]helicenes can have stronger ability to hold positive charge as compared to S atoms

in thia[n]helicenes and Se atoms in seleno[n]helicenes. Thus, telluro[n]helicenes systems have much lower ionization energies than their corresponding thia[n]helicenes and seleno[n]helicenes in DCM solvent.

5.3.3 Comparison of HOMO-LUMO energy gap of thia[n]helicenes, seleno[n]helicenes and telluro[n]helicenes (n=1-10) in DCM solvent

HOMO-LUMO energy gap of telluro[n]helicenes (n=1-10) are calculated in DCM solvent applying different level of theory. The HOMO-LUMO energy gap values are provided in Table 5.3. The calculated HOMO-LUMO energy gap of thia[n]helicenes and seleno[n]helicenes are given in Table 3.3 and in Table 4.3 respectively. Figure 5.3 shows the variation of HOMO-LUMO gaps in thia[n]helicenes and seleno[n]helicenes and telluro[n]helicenes with the

Table 5.3 Calculated HOMO-LUMO energy gap (in eV) of neutral telluro[n]helicenes, [n]TeH (n=1-10) in DCM solvent.

HOMO-LUMO energy gap (in eV) of telluro[n]helicenes, [n]TeH, n = 1-5					
Method	[1]TeH	[2]TeH	[3]TeH	[4]TeH	[5]TeH
i)	4.6	3.9	3.7	3.7	3.6
ii)	4.6	3.9	3.7	3.7	3.6
iii)	4.6	3.9	3.7	3.7	3.6
HOMO-LUMO energy gap (in eV) of telluro[n]helicenes, [n]TeH, n = 6-10					
Method	[6]TeH	[7]TeH	[8]TeH	[9]TeH	[10]TeH
i)	3.5	3.4	3.3	3.3	3.3
ii)	3.4	3.4	3.3	3.2	3.2
iii)	3.4	3.4	3.3	3.2	3.2

i) B3LYP, ii) B3LYP-D, iii) and B3LYP-D3, with 6-311++G(d,p) basis set for H, C, Br, Si, atoms and 3-21G basis set for Te atom.

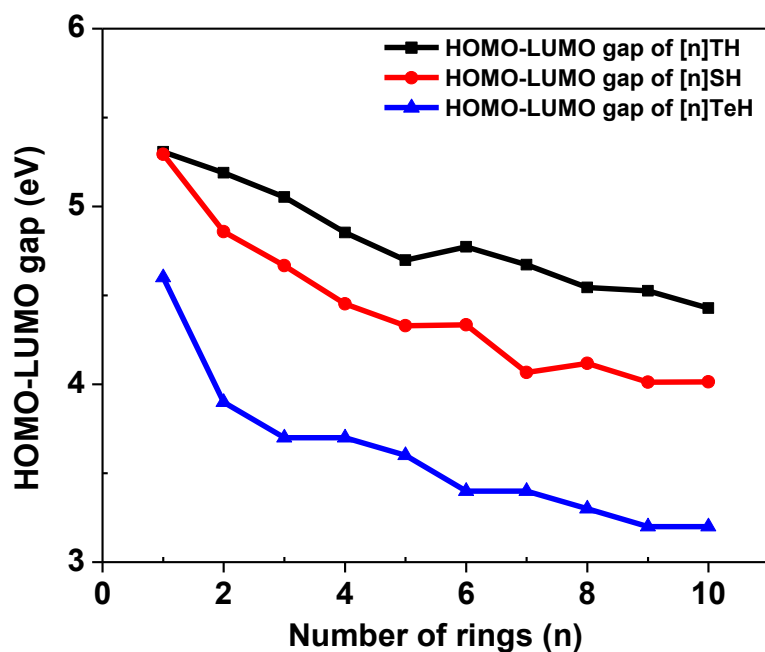


Figure 5.3 Comparison of calculated HOMO-LUMO energy gap (in eV) of thia[n]helicenes, seleno[n]helicenes and telluro[n]helicenes at B3LYP-D level of theory in DCM solvent. 6-311++G(d,p) basis set for S, Se, H, C, Br, Si atoms and 3-21G basis set for Te atom is used for the all calculations.

increasing number of rings at B3LYP-D level of theory in DCM solvent. The HOMO-LUMO gap follows the order telluro[n]helicenes < seleno[n]helicenes < thia[n]helicenes for $n \geq 2$ in DCM solvent. The HOMO-LUMO gap of telluro[n]helicenes in DCM solvent are lower than the same size thia[n]helicenes and seleno[n]helicenes at B3LYP-D level of theory. This may be due to fact that, the size and polarizability of chalcogen atoms follow order $\text{Te} > \text{Se} > \text{S}$.

5.3.4 Most stable structures of telluro[n]helicene radical cations, $[\text{n}]\text{TeH}^{++}$, $n=1-10$, in DCM solvent

Coordinates of all the atoms in the most stable structures of neutral telluro[n]helicenes are being as the initial input to get the most stable structures of telluro[n]helicene radical cations.

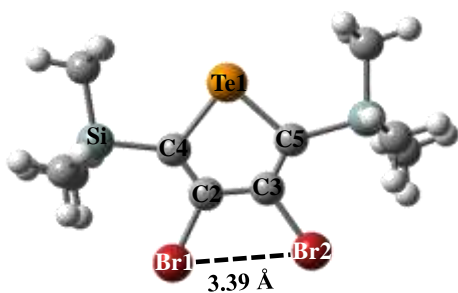
Table 5.4 Selected [#]geometrical parameters of neutral end substituted telluro[n]helicenes radical cation, n=1-10 calculated at B3LYP-D with 6-311++G(d,p) basis set for H, C, Si, and Br atoms and 3-21G basis set for Te atoms in DCM solvent. The value in the braces are calculated at B3LYP functional with same basis set in DCM solvent.

N	1	2	3	4	5	6	7	8	9	10
r_{C2-C3} (Å)	1.50	2.70	3.43	3.60	3.55	3.24	3.14	4.25	5.22	5.90
^ar_{C4-C5+n} (Å)	2.86	4.93	6.10	6.03	5.41	4.15	3.76	5.60	7.28	8.13
^br_{Te1-Te(n)} (Å)	-	3.78, (3.78)	6.86, (6.84)	8.37, (8.50)	8.45, (8.63)	6.89, (7.01)	4.12, (4.82)	3.96, (4.58)	6.79, (6.84)	9.07, (9.21)
r_{Br1-Br2} (Å)	3.39, (3.36)	3.36, (3.34)	3.41, (3.38)	3.57, (3.56)	4.10, (4.08)	4.96, (5.15)	5.56, (5.69)	5.98, (6.14)	6.01, (6.35)	6.33, (6.58)
δ(Br1C2C3Br2) (degree)	0, (0)	0, (0)	69.0, (66.2)	-113.2, (-110.2)	-161.2, (-158.7)	-146.8, (-142.5)	-89.6, (-88.9)	-15.8, (-21.4)	37.4, (31.9)	80.1, (78.7)
δ(Br2C3C2C4) (degree)	180, (180)	180, (180)	-82.8, (-86.5)	-7.9, (-5.7)	-53.7, (-52.4)	93.8, (96.8)	142.7, (142.1)	-160.2, (-164.6)	-106.2, (-111.8)	-50.3, (-51.7)

[#]**Figure 5.4** may be referred for identifying geometrical parameters.

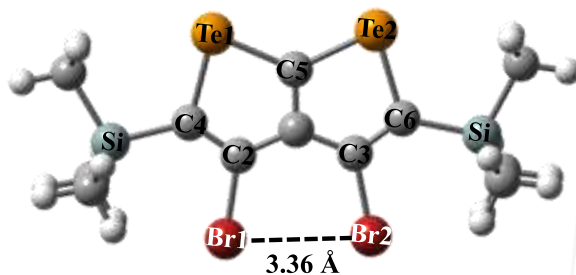
^ar_{C4-C5+n}, n = 0 for telluro[1]helicene radical cation, n = 1 for telluro[2]helicene radical cation and so on.

^br_{Te1-Te(n)}, n = 1 for telluro[1]helicene radical cation, n = 2 for telluro[2]helicene radical cation and so on



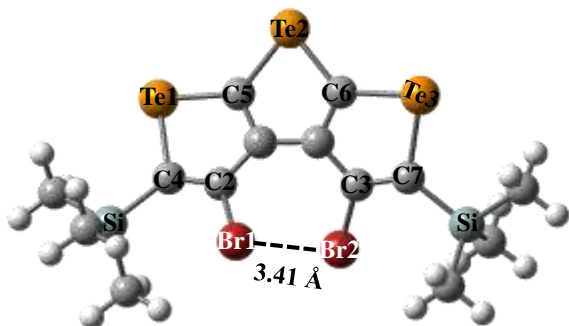
$$r_{C2C3} = 1.50 \text{ \AA}, r_{C4C5} = 2.86 \text{ \AA}, \\ \delta(Br1C2C3Br2) = 0^\circ, \delta(Br2C3C2C4) = 180^\circ$$

a



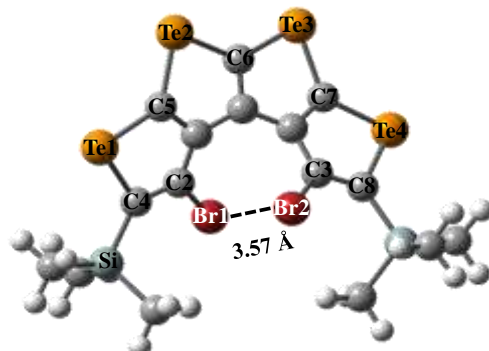
$$r_{C2-C3} = 2.70 \text{ \AA}, r_{C4-C6} = 4.93 \text{ \AA}, \\ \delta(Br1C2C3Br2) = 0^\circ, \delta(Br2C3C2C4) = 180^\circ$$

b



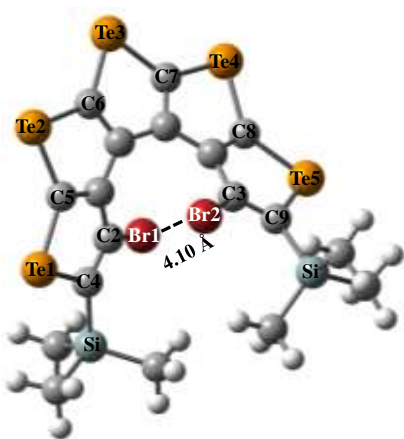
$$r_{C2-C3} = 3.43 \text{ \AA}, r_{C4-C7} = 6.03 \text{ \AA}, \\ \delta(Br1C2C3Br2) = 69.0^\circ, \delta(Br2C3C2C4) = -82.8^\circ$$

c



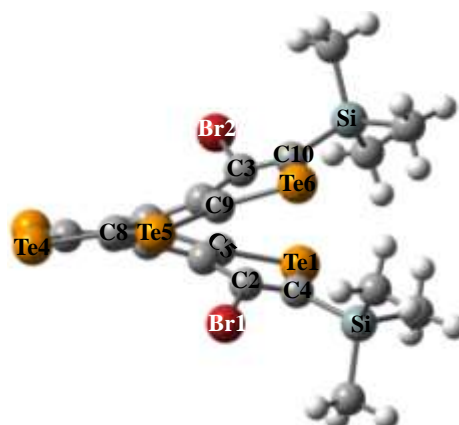
$$r_{C2-C3} = 3.60 \text{ \AA}, r_{C4-C8} = 6.03 \text{ \AA}, \\ \delta(Br1C2C3Br2) = -113.2^\circ, \delta(Br2C3C2C4) = -7.9^\circ$$

d



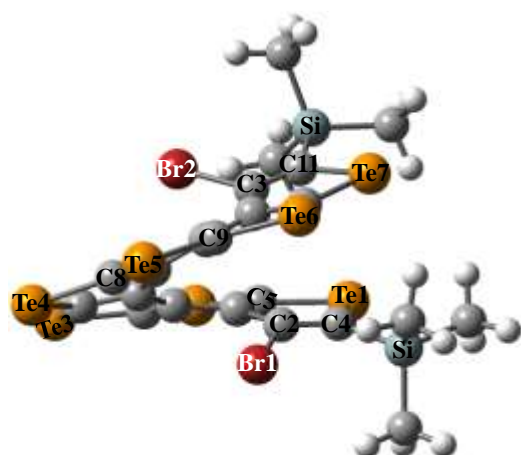
$$r_{C2-C3} = 3.55 \text{ \AA}, r_{C4-C9} = 5.41 \text{ \AA}, \\ \delta(Br1C2C3Br2) = -161.2^\circ, \delta(Br2C3C2C4) = -53.7^\circ$$

e



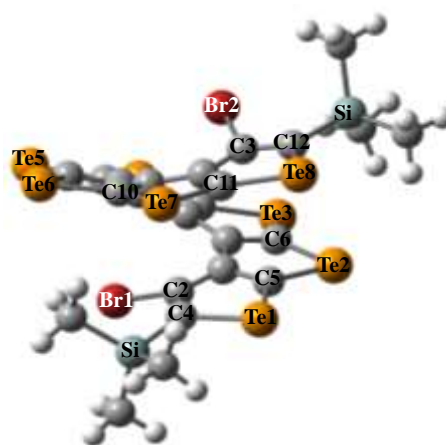
$$r_{Br1-Br2} = 4.96 \text{ \AA}, r_{C2C3} = 3.24 \text{ \AA}, r_{C4C10} = 4.15 \text{ \AA}, \\ \delta(Br1C2C3Br2) = -146.8^\circ, \delta(Br2C3C2C4) = 93.8^\circ$$

f



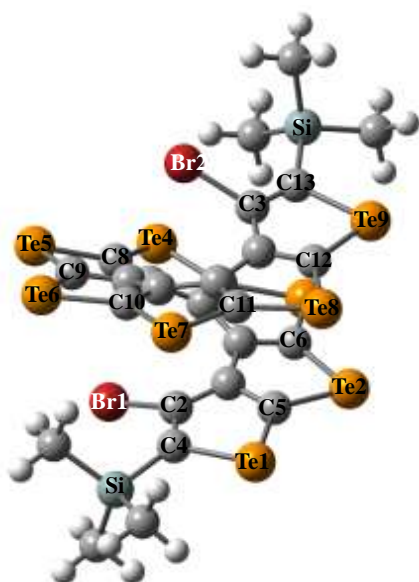
$r_{\text{Br1-Br2}} = 5.56 \text{ \AA}$, $r_{\text{C2-C3}} = 3.14 \text{ \AA}$, $r_{\text{C4-C11}} = 3.76 \text{ \AA}$,
 $\delta(\text{Br1C2C3Br2}) = -89.6^\circ$, $\delta(\text{Br2C3C2C4}) = 142.7^\circ$

g



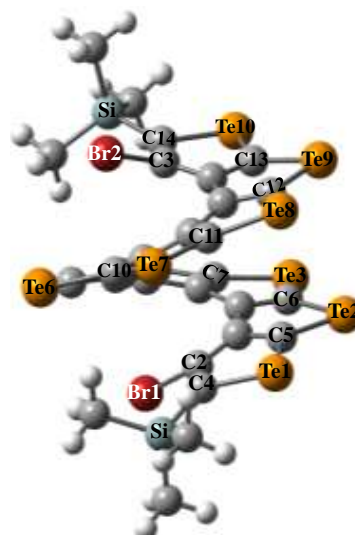
$r_{\text{Br1-Br2}} = 5.98 \text{ \AA}$, $r_{\text{C2-C3}} = 4.25 \text{ \AA}$, $r_{\text{C4-C12}} = 5.60 \text{ \AA}$,
 $\delta(\text{Br1C2C3Br2}) = -15.8^\circ$, $\delta(\text{Br2C3C2C4}) = -160.2^\circ$

h



$r_{\text{Br1-Br2}} = 6.01 \text{ \AA}$, $r_{\text{C2-C3}} = 5.22 \text{ \AA}$, $r_{\text{C4-C13}} = 7.28 \text{ \AA}$,
 $\delta(\text{Br1C2C3Br2}) = 37.4^\circ$, $\delta(\text{Br2C3C2C4}) = -106.2^\circ$

i



$r_{\text{Br1-Br2}} = 6.33 \text{ \AA}$, $r_{\text{C2-C3}} = 5.90 \text{ \AA}$, $r_{\text{C4-C14}} = 8.13 \text{ \AA}$,
 $\delta(\text{Br1C2C3Br2}) = 80.1^\circ$, $\delta(\text{Br2C3C2C4}) = -50.3^\circ$

j

Figure 5.4 Most stable structures (a-j) of telluro[n]helicenes radical cation, $[\text{n}]\text{TeH}^{+\bullet}$, $\text{n}=1-10$ a) $[\text{1}]\text{TeH}^{+\bullet}$, b) $[\text{2}]\text{TeH}^{+\bullet}$, c) $[\text{3}]\text{TeH}^{+\bullet}$, d) $[\text{4}]\text{TeH}^{+\bullet}$, e) $[\text{5}]\text{TeH}^{+\bullet}$, f) $[\text{6}]\text{TeH}^{+\bullet}$, g) $[\text{7}]\text{TeH}^{+\bullet}$, h) $[\text{8}]\text{TeH}^{+\bullet}$, i) $[\text{9}]\text{TeH}^{+\bullet}$, and j) $[\text{10}]\text{TeH}^{+\bullet}$ with selected geometrical parameters calculated at B3LYP-D with 6- 311++G(d,p) basis set for H, C, Si, and Br atoms and 3-21G basis set for Te atoms in DCM solvent.

Table 5.4 provides selected geometrical parameters of the fully optimized structures of telluro[n]helicene radical cations ($n = 1-10$) by applying the B3LYP-D functional in DCM solvent. 6-311++G(d,p) basis set for H, C, Si, and Br atoms and 3-21G basis set for Te atoms are considered for these calculations. Table 5.4 also indicates that calculated dihedral angles for telluro[n]helicenes radical cations, $n=3-7$ at B3LYP-D level are different than those at the B3LYP level showing the effect of dispersion in the geometry. However, no difference in the calculated distance between the two Br atoms is observed as in case of neutral helicenes. Most stable structures for telluro[n]helicene radical cations, ($n = 1-10$) calculated at the present level of theory in DCM solvent are shown in Figure 5.4(a-j). The most stable structure of obtained for telluro[n]helicene radical cations ($n = 1-10$) are very similar to their corresponding neutral telluro[n]helicene ($n = 1-10$ in DCM solvent. The calculated most stable structures of telluro[n]helicene radical cations, $n = 1-2$, are planar in DCM solvent. However, the structure of telluro[n]helicene radical cations, $[n]\text{TeH}^{+}$, $n=3-10$ are non-planar and helical in nature like neutral telluro[n]helicenes. In case of telluro[7]helicene radical cation, the non-bond distance $r_{\text{Te1-Te7}}$ is 4.12 Å. However, it can be recalled from chapter 3 and Chapter 4 the same calculated non bonded distances $r_{\text{S1-S7}}$ and $r_{\text{Se1-Se7}}$ are 8.00 Å and 6.52 Å respectively for thia[7]helicene and seleno[7]helicene radical cations. This suggests that the telluro[7]helicene radical cation is more conjugated than the corresponding thia[7]helicene and seleno[7]helicene radical cationic systems. Moreover, it is to noted that one turn in helical structure is completed in case of telluro[7]helicene radical cationic system and the corresponding most stable structure is shown in Figure 5.4h. It may be recalled that in case of thia- and seleno[n]helicene radical cationic systems eight fused rings are required for one complete turn.

5.3.5 PBC-DFT calculation for band gap of thia[n]helicenes, seleno[n]helicenes, and telluro[n]helicenes (n=1-10)

The maximum direct band gap of thia[n]helicenes and seleno[n]helicenes are calculated using local density functional, BLYP and 6-31G(d) basis set with periodic boundary condition (PBC). However, the maximum direct band gap of telluro[n]helicenes, [n]TeH are calculated using local density functional, BLYP and 6-31G(d) basis set for H, C, Br, and Si atoms and 3-21G for Te atom with periodic boundary condition (PBC).

Table 5.5 Direct Band gap (in eV) of thia[n]helicenes ([n]TH), seleno[n]helicenes ([n]SH), and telluro[n]helicenes ([n]TeH), n=1-10 calculated using PBC-BLYP method with periodic boundary condition. 3-21G basis set for Te atoms and 6-31G(d) basis set for all other atoms are considered.

Direct band gap (in eV) of chalcogen based [n]helicenes, n=1-10			
n	[n]TH	[n]SH	[n]TeH
1	3.79	3.62	3.33
2	3.63	3.37	2.72
3	3.40	3.20	2.15
4	3.35	3.06	2.18
5	3.20	2.87	2.08
6	3.15	2.60	2.04
7	3.21	2.41	1.95
8	3.13	2.82	1.84
9	3.05	2.51	1.76
10	3.00	2.74	1.84

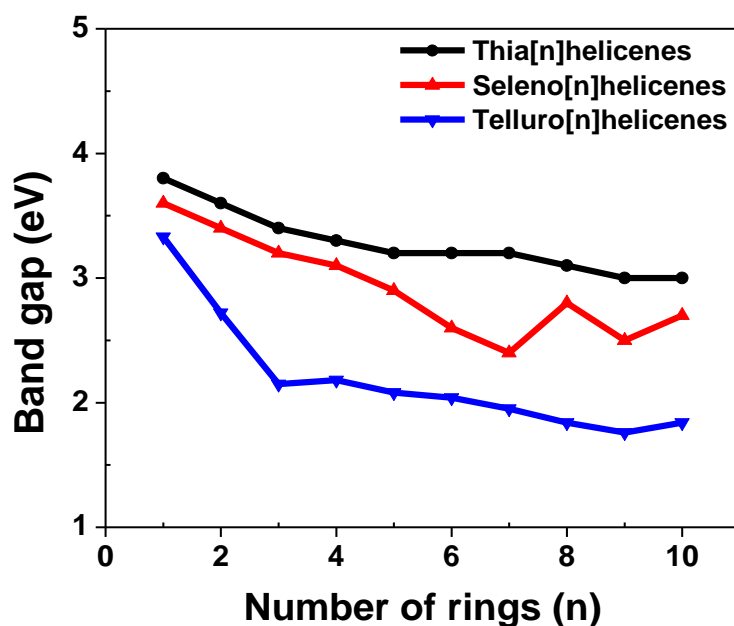


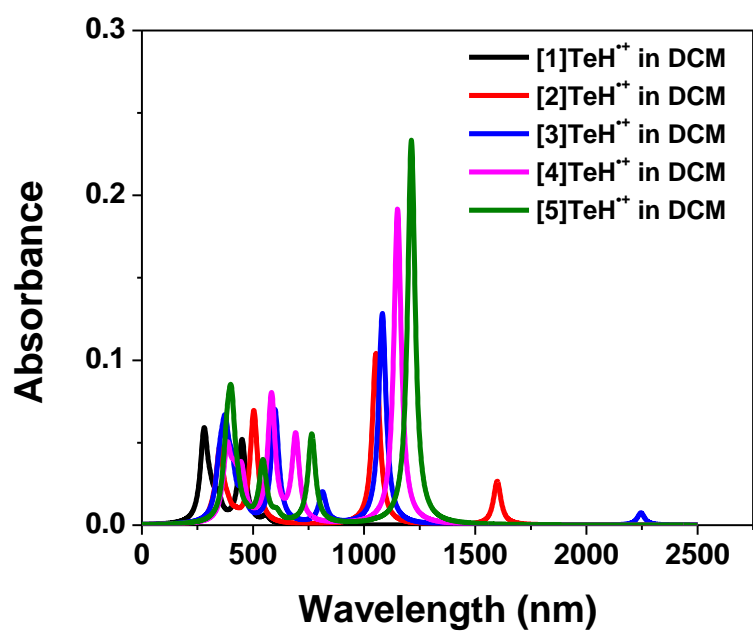
Figure 5.5 Comparison of calculated band gap for thia[n]helicenes, seleno[n]helicenes, and telluro[n]helicenes calculated using PBC-BLYP method with periodic boundary condition. 3-21G basis is for Te atoms and for all other atoms 6-31G(d) basis set is used with periodic boundary condition (PBC).

The direct band gap of thia[n]helicenes, [n]TH, $n=1-10$ at BLYP/6-31G(d) level of theory are calculated to be in the range of 3.8 to 3.0 eV (see Table 5.5). Calculated direct band gap of thia[n]helicenes decreases as the number of thiophene ring increases as shown in Figure 5.5. The direct band gap for seleno[n]helicenes is calculated to be in the range of 3.6 to 2.4 eV. Figure 5.5 clearly indicates that calculated direct band gaps are lower in seleno[n]helicenes as compared to the same in thia[n]helicenes for each size of seleno[n]helicenes like thia[n]helicenes. Calculated band gap increase slightly for [8]SH in comparison to [7]SH a zigzag variation is observed in the plot for [9]SH and [10]SH. These variations may be due to interplay of stability due to conjugations and strain due to increased size. Figure 5.5 clearly indicates that the calculated direct band gaps are lower in telluro[n]helicenes as compared to the same in thia- and seleno- [n]helicenes. The direct band gap for telluro[n]helicenes are

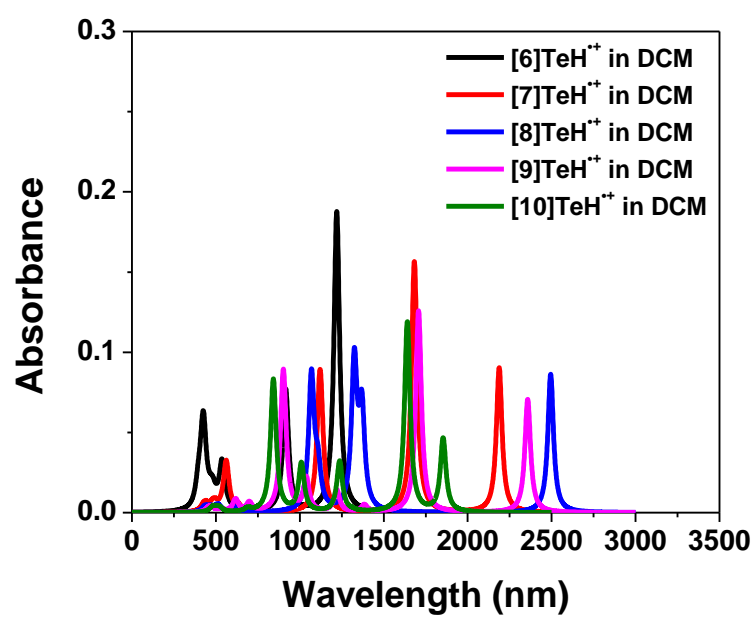
calculated to be in the range of 3.33 to 1.76 eV (see Table 5.5). The direct band gap of telluro[n]helicenes decreases as the number of tellurophene rings increases. Calculated direct band gap of follow the order, $[n]\text{TeH} < [n]\text{SH} < [n]\text{TH}$ for $n=1-10$. This order is same as the HOMO-LUMO gaps discussed in section 5.3.3. Overall, telluro[n]helicenes have the lowest band gap compared to their corresponding thia[n]helicenes and seleno[n]helicenes.

5.3.6 Excited-state electronic spectra for telluro[n]helicenes radical cation, $n=1-10$ in DCM solvent

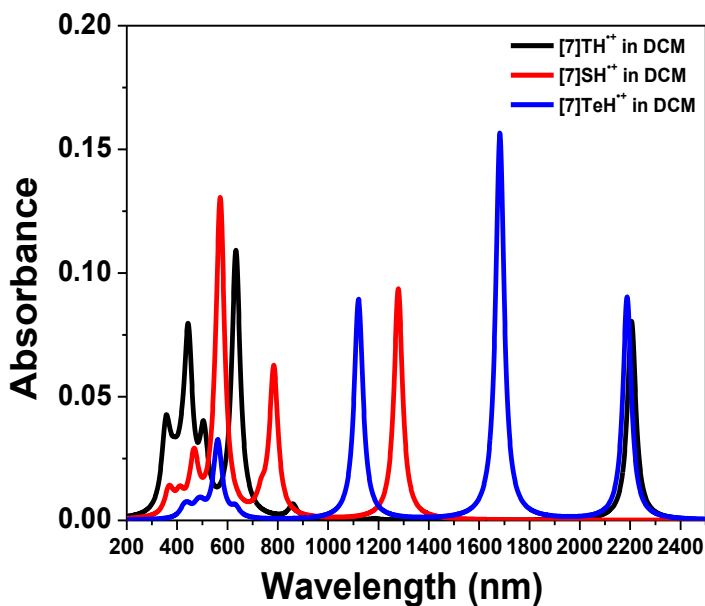
To simulate the UV-Vis spectra of telluro[n]helicenes radical cation, $[n]\text{TeH}^{*+}$, $n=1-10$, the TDDFT procedure is applied to study a few low lying excited states in DCM solvent using CAM-B3LYP functional with 6-311++G(d,p) basis set for H, C, Br, Si, atoms and 3-21G for Te atoms. The simulated UV-Vis spectra of telluro[n]helicenes radical cation, $n=1-5$ in DCM solvent are displayed in Figure 5.6a. Figure 5.6b shows simulated UV-Vis spectra of telluro[n]helicenes radical cation, $n=6-10$ in DCM solvent. Figure 5.6a and Figure 5.6a show that except for telluro[1]helicene radical cation, all the radical cation systems, $n=2-10$ have strong absorption bands in the visible region. Interestingly, these radical cationic systems even stronger absorption bands in NIR and far-infrared regions (FIR) are predicted in comparison to their absorption bands in the visible region. Comparison of UV-Vis spectra for all these helicenes show that the intensity of NIR peak for $[7]\text{TeH}^{*+}$ ($\lambda_{\text{max}} = 1682 \text{ nm}$, $f = 0.15$) is much



a



b



c

Figure 5.6 UV-Vis spectra for radical cations of end substituted telluro[n]helicenes, [n]TeH⁺ in DCM solvent, a) n=1-5 and b) n=6-10 c) comparison of calculated UV-Visible spectra of [7]TH⁺, [7]SH⁺ and [7]TeH⁺. TDDFT procedure is applied to generate the UV-Vis spectra calculated using CAM-B3LYP functional with 6-311++G(d,p) basis set for H, C, S, Se, Br, Si atoms and 3-21G for Te atoms.

higher than the NIR peak of [7]SH⁺ ($\lambda_{\max} = 1279$ nm, $f = 0.09$) and [7]TH⁺ ($\lambda_{\max} = 2206$ nm, $f = 0.02$) in DCM solvent as shown in Figure 5.6c. The orbital analysis suggests that the strong absorption peak in the NIR region is due to π - π^* type transition in telluro[7]helicenes radical cation.

Overall, based on excited-state studies, it may be concluded that most of these telluro[n]helicenes radical cations, [n]TeH⁺ may be important in making the varieties of detectors that can be used in far IR and near IR region.

5.3.7 Dimerization of neutral and radical cation of telluro[7]helicene in DCM solvent

Dimerization can significantly affect the performance of a device made of such helicenes molecules. A case study on the π -dimerization in neutral as well as radical cations of unsubstituted and end substituted telluro[7]helicene is performed in the absence and presence of PF_6^- counter ion as reported for thia[7]- and seleno[7]- helicene systems in the previous chapters.

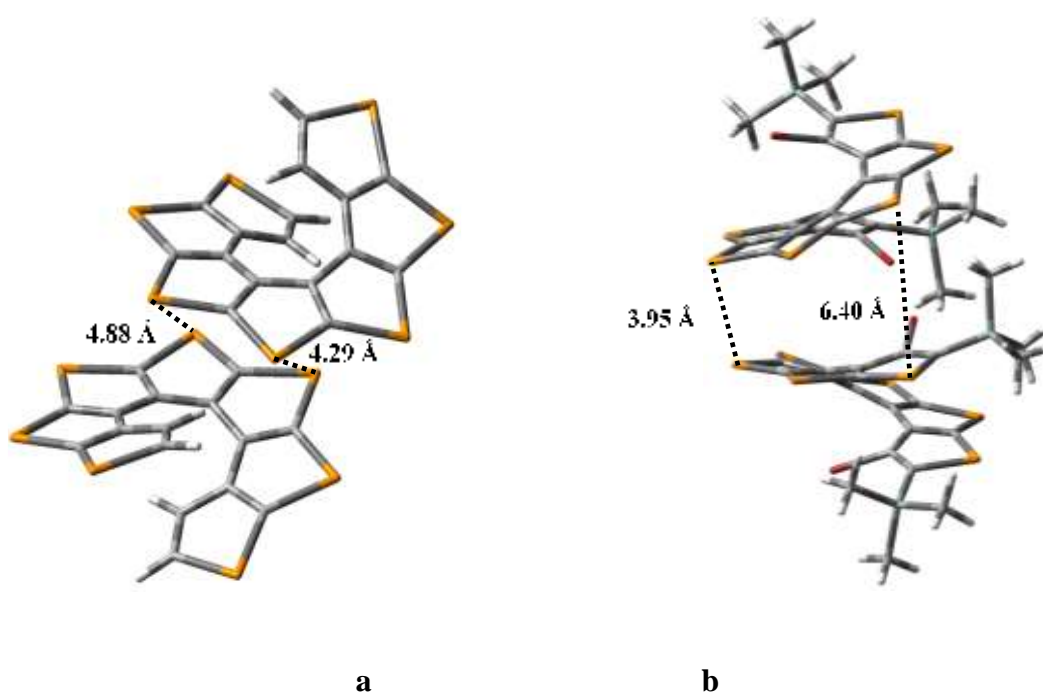
5.3.7.1 Structure and energy of the π -dimer systems

DFT calculations are performed on dimers of unsubstituted and end substituted neutral and radical cation of telluro[7]helicene applying B3LYP-D functional. The influence of electrostatic interaction of two PF_6^- counter ions is also considered on unsubstituted and end substituted telluro[7]helicene radical cation. Three situations are considered and discussed below.

Case 1: The most stable structure of unsubstituted π -dimer of neutral telluro[7]helicene, $([7]\text{TeH})_2$, is partly π - π stacked structure (see Figure 5.7a). Gibbs free energy of dimerization, ΔG_{dim} is calculated for unsubstituted neutral π -dimer, $([7]\text{TeH})_2$ as -26.9 kcal/mol. This indicates that the formation of the π -dimer is a favorable process for neutral unsubstituted telluro[7]helicene. The most stable structure calculated for end substituted π -dimer of neutral telluro[7]helicene, $(s-[7]\text{TeH})_2$ shows partial π - π stacking of two monomer $s-[7]\text{TeH}$ units (see Figure 5.7b). ΔG_{dim} calculated for π -dimer of neutral end substituted telluro[7]helicene is -16.6 kcal/mol and this clearly indicates that the formation of the π -dimer of end substituted system is a favorable process. However, a significant decreases in the value of ΔG_{dim} is observed in π -dimer of neutral end substituted telluro[7]helicene compared to unsubstituted telluro[7]helicene. ΔG_{dim} for neutral unsubstituted and substituted thia- and seleno[7]helicenes

are discussed in section 3.3.7 and section 4.3.7 respectively. It is to be noted that, the dimerization probability of neutral unsubstituted and substituted telluro[7]helicene is much higher than the corresponding neutral unsubstituted and substituted thia- and seleno[7]helicenes.

Case 2: The most stable structure of the unsubstituted π -dimer of telluro[7]helicene radical cation, $([7]\text{TeH})_2^{2+}$, is partly π - π stacked (see Figure 5.7c). Gibbs free energy of dimerization, ΔG_{dim} is calculated for unsubstituted π -dimer, $([7]\text{TeH})_2^{2+}$ as -28.5 kcal/mol. This indicates that the formation of the π -dimer is a favorable process for unsubstituted telluro[7]helicene radical cation. The most stable structure calculated for end substituted π -dimer of telluro[7]helicene, $(s\text{-}[7]\text{TeH})_2^{2+}$ shows partial π - π stacking of two monomer $s\text{-}[7]\text{TeH}$ units (see Figure 5.7d).



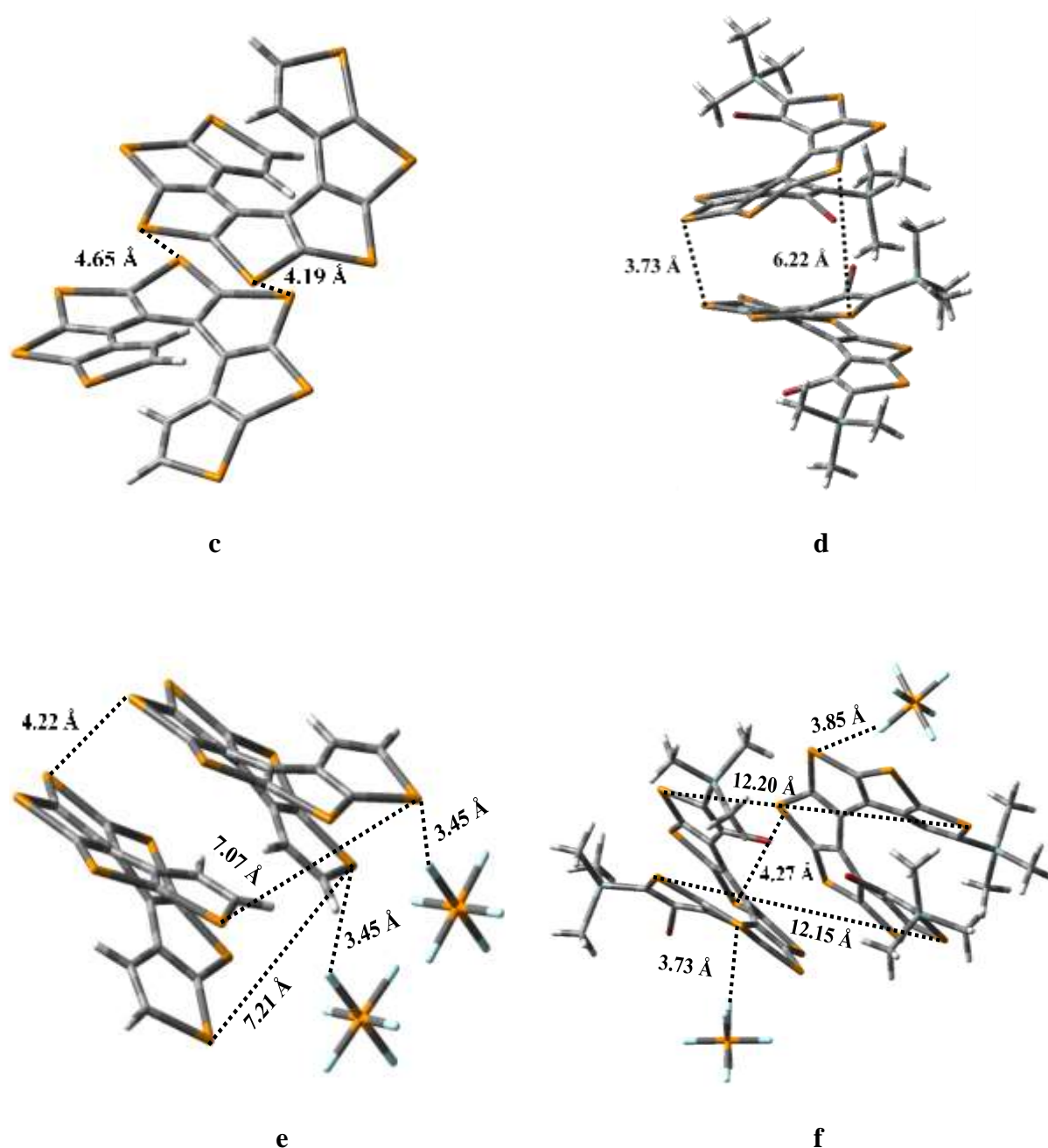


Figure 5.7 Most stable π -dimeric structure of a) neutral unsubstituted telluro[7]helicene monomer, b) neutral end substituted telluro[7]helicene monomer, c) unsubstituted telluro[7]helicene monomer radical cation, d) end substituted telluro[7]helicene monomer radical cation, e) unsubstituted telluro[7]helicene monomer radical cation with PF_6^- counter ions, f) end substituted telluro[7]helicene monomer radical cation with PF_6^- counter ions. Calculated at B3LYP-D functional with 6-311++G(d,p) basis set for H, C, Si, Br, P, F atoms and 3-21G basis set for Te atoms in DCM solvent.

ΔG_{dim} calculated for the π -dimer of end substituted telluro[7]helicene radical cation is +2.94 kcal/mol and this clearly suggests that the formation of the π -dimer of end substituted system is not a favorable process. Calculated ΔG_{dim} for π -dimer of unsubstituted and substituted thia- and seleno[7]helicene radical cations are more positive (see section 3.3.7 and section 4.3.7) than unsubstituted and substituted π -dimer of telluro[7]helicene radical cations. Thus, unsubstituted and substituted telluro[7]helicene radical cations have more probability of dimerization than their corresponding unsubstituted and substituted radical cations of thia- and seleno[7]helicenes.

Case 3: In presence of two PF_6^- counter ions, the most stable structure obtained for the unsubstituted π -dimer radical cation, $([7]\text{TeH})_2^{2+}$, shows a π - π stacking of two units of the radical cation of telluro[7]helicene with two PF_6^- counter ions are present near to only one ring as shown in (see Figure 5.7e). Gibbs free energy of dimerization, ΔG_{dim} is calculated for these systems is -30.1 kcal/mol. This indicates that the formation of the π -dimer is a favorable process for unsubstituted telluro[7]helicene radical cation even in the presence of two PF_6^- counter ions. In case of the most stable structure of the end substituted π -dimer radical cation, $(s-[7]\text{TeH})_2^{2+}$ system, it is observed (see Figure 5.7f) that one PF_6^- counter ions present at the top and the other at the bottom. Gibbs free energy of dimerization, ΔG_{dim} is calculated for this systems is -12.2 kcal/mol. This indicates that the formation of the π -dimer is decreased in the presence of counter anion in end substituted π -dimer, $(s-[7]\text{TeH})_2^{2+}$ radical cation system.

5.4 Conclusions

Effects of chalcogen atom substitution on structures and HOMO-LUMO energy gap of the chalco[n]helicenes $[n]\text{ChH}$, ($\text{Ch} = \text{S}, \text{Se}$ and Te , $n=1-10$) are investigated. In all the three cases,

three fused rings are necessary to produce non-planar structure irrespective of charge present in these systems. Eight fused rings are required for one complete turn in thia[n]helicene and seleno[n]helicene systems respectively. However, seven fused tellurophene rings are required to complete one turn in telluro[n]helicene systems. PBC-DFT calculations for band gap of thia[n]helicenes indicate that the value of band gap lies in the visible region for $n=3,6,8-10$. The band gap decreased as the number of thiophene rings increases in thia[n]helicenes and reached a value of 2.9 eV. The same calculations in seleno[n]helicenes suggest that the band gap of seleno[n]helicenes are lower than the band gap of thia[n]helicene. For telluro[n]helicenes systems also calculated band gap decreases with the increase in number of tellurophene rings. However, the calculated band gap are lowest for each size telluro[n]helicenes. Energy gap as well as band gap for chalcogen based [n]helicenes, follows the order, $[n]\text{TeH} < [n]\text{SH} < [n]\text{TH}$. Most of these telluro[n]helicenes radical cations have strong absorption in far IR and near IR region. Origin of optical absorption band of the end substituted telluro[n]helicenes radical cation in the IR regions is due to $\pi \rightarrow \pi^*$ type of electronic transition. Calculated free energy at STP in DCM solvent for π -dimer of neutral unsubstituted and end substituted telluro[7]helicene suggests that dimerization of the monomer units are possible. Calculated free energy values for π -dimer of end substituted radical cations of telluro[7]helicene in DCM solvent at STP do not indicate any possibility of dimerization. Free energy parameters on π -dimer of unsubstituted and end substituted radical cations of telluro[7]helicene in the presence of counter ion, PF_6^- in DCM solvent at STP decreases the possibility of dimerization. The neutral and radical cationic substituted and unsubstituted telluro[7]helicene systems have more chance of dimerization than their corresponding neutral unsubstituted and substituted thia- and seleno[7]helicenes Overall, these telluro[n]helicenes systems may be useful in optical devices.

CHAPTER 6

Effect of Excess Electron on Structure, Bonding and Spectral Properties of Diaryl Based Dichalcogen (S, Se and Te) Systems[†]

6.1 Introduction

This chapter deals with a study of antioxidant property of diaryl based dichalcogen (S, Se and Te) systems with an excess of electrons.¹³⁵ Chalcogens are present in amino acids, peptides, and proteins, essential for various biological redox reactions. Sulfur and selenium are present in amino acids, peptides, and proteins, essential for various biological redox reactions. Selenocystine and selenomethionine systems can act as an antioxidant by killing harmful peroxides in organisms, and these are also responsible for protection against inflammation and cancer.^{136–138} Diaryl dichalcogenides are eco-friendly oxidizing agents and demanding drugs in pharmaceutical chemistry mainly for their antioxidant properties.⁷¹ The diphenyl diselenides and diphenyl ditellurides have strong antioxidant activity and comparable toxicity. Their antioxidant activity can be modulated by inserting suitable ring substituents. The antioxidant nature of sulfur and selenium based diaryl dichalcogenides can be due to the ability to donate an electron in their anionic state in the solution phase.¹³⁵ Along with the ability to donate an electron, the anionic diaryl dichalcogenides should possess sufficient stability in the aqueous medium. One electron reduction of neutral dichalcogenides may lead to the formation of two-center three-electron (2c-3e) bonded radical anion systems.^{72–80}

The experimental characterization of 2c-3e bonding has often been indirect and transient optical absorption maximum (λ_{max}) is being used as an indicator for such bonding. Chalcogen centered 2c-3e bonded radical cation complexes are easily formed in aqueous (neutral or acidic)

[†]Kumar, R.; Maity, D. K. Effect of excess electron on structure, bonding, and spectral properties of sulfur/selenium based dichalcogen systems. *Int. J. Quantum Chem.* **2019**, *119* (7), e25855 (Cover page article).

and hydrocarbon solution which gives rise to extremely broad and structure-less UV-Visible absorption spectra with high extinction coefficient (ϵ) values. A similar absorption spectrum is also observed in case of transient disulfide radical anions formed on the reaction of the solvated electron with an aqueous solution of organic disulfides. Optical absorption spectra, and in particular the position of λ_{\max} and lifetimes ($t_{1/2}$) of these bands may be used to provide indirect information on the nature and strength of 2c-3e bonds of these complexes. Characterization of 2c-3e bond in sigma bonded radical cationic complexes can be done through optical absorption spectroscopy. Characterization of 2c-3e bond in cyclic dithia radical cations⁷², peptides¹³⁹, azoalkanes¹⁴⁰, transition metal complexes¹⁴¹ and other sigma bonded radical cationic complexes through optical absorption spectroscopy are reported in the literature. Absorption maximum (λ_{\max}) is described to correspond to the energy gap between the doubly occupied σ bonding orbital and singly occupied σ^* antibonding orbital and this is often being correlated to the strength of a 2c-3e -Ch \cdot :Ch- (Ch = S, Se and Te) bond. A λ_{\max} value in the blue region indicates a large separation between the doubly occupied σ and singly occupied σ^* orbitals due to a strong interaction of the corresponding p-orbitals resulting a strong 2c-3e bond and a λ_{\max} value in the red region for a small separation between the doubly occupied σ and singly occupied σ^* orbitals due to a weak interaction of the corresponding p-orbitals resulting a weak 2c-3e bond. A low-temperature matrix in combination with time-resolved pulse radiolysis is also used to characterize the optical absorption bands, λ_{\max} of such complexes. Electron Spin Resonance (ESR) provides valuable information on the nature of bonding in sulfur radical cation systems by probing the degree of localization of the excess electron.¹⁴² A direct measurement of the 2c-3e bond strengths is also made following mass spectroscopic studies of gas phase ion-molecule association equilibrium to measure the bond enthalpy in inter-

molecular 2c-3e bonded sulfur centered dimer radical cations. A real-time probing of 2c-3e bonded chalcogen system has also been performed following femtosecond laser spectroscopy. Recently, transient anion states of gas-phase diphenyl disulfide are characterized using electron transmission (ET) and dissociative electron attachment (DEA) spectroscopies. Electron capture dissociation (ECD) with Fourier transform ion cyclotron mass spectrometry (FTICR MS) has been used for direct measurement of sulfur and selenium centered 2c-3e bond complexes.¹³⁹

Quantum chemical calculations play a major role in understanding the nature of bonding in these radical anionic complexes. Mixing of two chalcogen valence p-orbitals from the respective radical anion, $R\text{Ch}^{\cdot-}$ and free radical, $R\text{Ch}^{\cdot}$ form dichalcogenides radical anion ($R\text{-Ch}:\cdot\text{Ch-R}$) $^{\cdot-}$ having a three electron bond between two chalcogen atoms. The transition of an electron from the highest doubly occupied molecular orbital (HDOMO) to the lowest singly occupied molecular orbital (LSOMO) of an organic radical anion system usually occurs by a visible photon. Bond strength of a 2c-3e bond is expected to depend on the combined effects of structural parameters, substitution patterns and electronic interactions. The combined effects are expected to control the extent of p-orbital interaction that in turn is expected to influence the strength of the newly formed bond.

The present chapter deals with the electron acceptor properties of dichalcogen systems, namely, diaryl dichalcogenides of the type $R\text{-Ch-CH-R}$ ($\text{Ch} = \text{S}, \text{Se}$ and Te ; $R = \text{Ph}, \text{PhCH}_2, o\text{-CH}_3\text{-Ph}, o\text{-HO-Ph}, o\text{-NO}_2\text{-Ph}$) and the newly formed 2c-3e bonds in their anionic ($R\text{-Ch-CH-R}$) $^{\cdot-}$ states. These studies may serve as a model for understanding the antioxidant behaviour of these dichalcogen systems. The geometry of radical, $R\text{-Ch}^{\cdot}$ and radical anion, $R\text{-Ch}^{\cdot-}$ states of ($R\text{-Ch-CH-R}$) $^{\cdot-}$ are also calculated at the same level of theory. Excited-state calculations are performed based on Time-Dependent Density Functional Theory (TDDFT) formalism to

simulate UV-Vis spectra of radical anion systems, $(\text{R}-\text{Ch}-\text{Ch}-\text{R})^{\cdot-}$. The effect of solvent water is introduced through macroscopic solvent model as well as through a discrete solvent model adding one water molecule to each of the chalcogen (Ch) atoms.

6.2 Theoretical Methods

The geometry of isolated neutral and negatively charged R-Ch-Ch-R systems (Ch = S, Se and Te; R = Ph, PhCH₂, o-CH₃-Ph, o-HO-Ph, o-NO₂-Ph) are fully optimized to find out the most stable structure applying density functional theory (DFT) and MP2 methods in conjunction with the 6-311++G(d,p) basis sets for C, H, O, N, S and Se atoms and 3-21G* for Te atom. DFT functionals B3LYP, B3LYP-D⁹⁴, B3LYP-D3⁹⁵, B3LYP-D3BJ¹⁴³ and ω -B97XD⁹⁶ are considered and geometries of all systems are fully optimized at all mentioned level of theory. Los Alamos ECP, LanL2DZ^{130,131} and split valance triple zeta basis functions, Def2TZVP^{132,133} are tried for Te atoms. However, both the basis sets are found to be unsuitable due to problem in SCF convergence. The effect of solvent water is introduced through a macroscopic solvent model based on solute density (SMD)¹⁰⁴ as well as through a discrete solvent model adding one water molecule to each of the Chalcogen (Ch) atoms. The energies of all these anionic systems are also calculated following Restricted Open-Shell Hartree-Fock (ROHF) formalism to avoid any spin contamination in these radical anionic doublet systems. Excited-state calculations on radical anion systems are performed for fifteen low lying excited states following TDDFT procedure considering CAM-B3LYP^{115,116} functional and 6-311++G(d,p) basis sets for C, H, O, N, S and Se atoms and 3-21G* for Te atom in the gas phase and water medium. CAM-B3LYP is a long-range corrected hybrid exchange-correlation functional designed to to predict reasonable spectra.^{115,116} Visualization of frontier molecular orbitals is carried out to get the information about the type of orbitals involved in electronic transitions.

6.3 Results and Discussions

Geometrical parameters of few neutral (PhS)₂, (PhSe)₂, and (PhTe)₂, systems are available in the Cambridge Structural Database (CSD) and also in some theoretical studies.^{144–148} However, detail ab initio studies on such systems that can give the structural as well as stability aspects in solution are at early stages. Geometrical parameters and binding energy of these dichalcogen systems are also reported based on theoretical calculations.⁷¹ Binding energy of H₃CSSCH₃ is also reported based on gas phase experiment and theoretical calculations.^{145,146} Geometrical parameters of neutral aliphatic selenium based dichalcogen system (H₃CSeSeCH₃) and binding energy are also reported in the literature based on gas phase experiments.^{149,150}

Benchmark analysis is performed to choose the optimal level of theory for the geometrical description of these species. Chalcogen-chalcogen and carbon-chalcogen bond lengths, carbon-chalcogen-chalcogen angle and carbon chalcogen-chalcogen-carbon dihedral angles are considered to decide the suitable level of theory for the present theoretical calculations. Selected geometrical parameters calculated at different levels of theory for neutral PhSSPh system are provided in Table 6.1 along with their anionic counterparts. Several initial geometries are considered for PhSSPh system to find out the most stable structure. The calculated bond distance values listed for PhSSPh system at B3LYP-D, B3LYP-D3, B3LYP-D3BJ, and ω -B97XD levels agrees well with that found at MP2 level. On geometry optimization, two minimum energy equilibrium structures are obtained for neutral systems and these structures differ mainly in spatial orientation of two phenyl rings. To calculate gas phase geometrical parameters of (PhS)₂ system more accurately, geometry optimization has also been carried out at the CCSD level of theory with the same basis functions. The r_{S1-S2} and r_{C1-S1} bond distances are calculated as 2.13 Å and 1.77 Å respectively. The bond angle, \angle C1S1S2,

dihedral angles, $\delta(\text{C1S1S2C2})$, $\delta(\text{S1S2C2C2}')$ and $\delta(\text{S2S1C1C1}')$ are predicted as 97.4° , 51.2° , 74.7° and -101.3° respectively at CCSD level of theory.⁷¹ It may be noted that these geometrical parameters are the same as MP2 values. The experimentally reported r_{S1S2} and r_{C1S1} bond distances in PhSSPh are 2.027 \AA and 1.789 \AA . Reported crystallographic data on the bond angle, $\angle\text{C1S1S2}$ and dihedral angle, $\delta(\text{C1S1S2C2})$ for PhSSPh system are 104.9 and 84.0° respectively. Thus, most stable structure obtained for PhSSPh system at MP2 and CCSD levels of theory is in close agreement with experimentally reported structure. Along with that, the reported deviations for the bond distances $r_{\text{S1-S2}}$ and $r_{\text{C1-S1}}$, bond angle, $\angle\text{C1S1S2}$, and dihedral angle, $\delta(\text{C1S1S2C2})$ are rather small in ω -B97XD functional and value obtained for these geometrical parameters are close to MP2 and CCSD levels of theory. On the basis of obtained results, ω -B97XD functional is a good functional for geometry optimizations.

To examine the change in geometrical parameters in same systems with Se and Te atoms in place of S, similar electronic structure calculations have been carried out. Geometrical parameters of neutral diphenyl dichalcogen system (PhSeSePh) are available in the Cambridge Structural Database (CSD).¹⁴⁴ Similar to $(\text{PhS})_2$ system discussed earlier, it is observed that again two minimum equilibrium structures are obtained which differ mainly in spatial orientation of two phenyl rings in case of $(\text{PhSe})_2$ and $(\text{PhTe})_2$ systems. Experimental bond distances, r_{Se1Se2} and r_{C1Se1} in neutral PhSeSePh system are 2.307 \AA and 1.946 \AA respectively. Based on crystallographic data, bond angle, $\angle\text{C1Se1Se2}$ and dihedral angle, $\delta(\text{C1Se1Se2C2})$ are 102.4° and 85.0° respectively for $(\text{PhSe})_2$.¹⁴⁶ For PhSeSePh system, the r_{Se1Se2} and r_{C1Se2} bond distances are 2.40 \AA and 1.92 \AA respectively at MP2 level of theory in gas phase. The calculated bond angle and dihedral angle are 102.4° and 85.0° respectively. Thus, most stable obtained for PhSeSePh system at MP2 and level of theory is similar to reported structure based

on crystallography. Similarly, the geometrical parameters obtained for the minimum energy structure of PhTeTePh system close to experimentally reported structure. It is also found that calculated bond distance and bond angles values listed for (PhSe)₂ and (PhTe)₂ systems at B3LYP-D, B3LYP-D3, B3LYP-D3BJ, and ω -B97XD levels agrees well with that found at MP2 level of theory. CCSD calculations are only limited to neutral (PhS)₂ system due to its computationally expensive nature.

It is interesting to mention that for (PhSe)₂ and (PhTe)₂ systems, it is possible to calculate chemical shift in the NMR spectra accurately from only these two equilibrium structures.¹⁵¹ Such observations are also reported in the literature for diphenyl dichalcogen systems including (PhTe)₂ based on conformation analysis.^{71,151,152} This certainly demonstrates that such above discussed theoretical methods have the predictive ability and can be very useful to interpret experimental results and to provide better insights.

6.3.1 Structures of (Ph-Ch)₂^{•−} radical anions (Ch = S, Se, & Te)

Table 6.1 summarizes the changes in selected geometrical parameters of (PhS)₂ produced upon the capture of an electron in the gas phase and in water medium. Several initial geometries of radical anion for diphenyl disulfide, (Ph-S)₂^{•−} are considered to find out the most stable structure. On optimization, two minimum energy structures are obtained and the structures are displayed in Figure 6.1 (a-b) along with relative stability and selected geometrical parameters. Two structures differ mainly in the spatial orientation of two phenyl rings. In the first case (see Figure 6.1a), one phenyl ring is displaced over the other phenyl ring. However, in the second case (see Figure 6.1b), two phenyl rings are in a molecular plane containing two sulfur atoms. Due to partial interactions of pi orbitals from two phenyl rings, the first structure (Figure 6.1a) is more stable than the second one by 3.8 kcal/mol as calculated at MP2/6-311++G(d,p) level

of theory in the gas phase. For the most stable structure of radical anion $(\text{PhS})_2^{\bullet-}$, the $r_{\text{S1-S2}}$ and $r_{\text{C1-S1}}$ bond distances are 2.83 Å and 1.76 Å respectively. The calculated gas phase bond angle, $\angle\text{C1S1S2}$ is 85.6° which is significantly smaller than DFT values. The calculated dihedral angle, $\delta(\text{C1S1S2C2})$ at MP2 level is 51.7° which is also significantly smaller than all the DFT values except ω -B97XD. Dihedral angle suggests that two phenyl rings are less displaced at MP2 level. To calculate these geometrical parameters more accurately, geometry optimization has also been carried out for $(\text{PhS})_2^{\bullet-}$ system in the gas phase at CCSD level of theory which is known to recover dynamic correlation accurately. The $r_{\text{S1-S2}}$ and $r_{\text{C1-S1}}$ bond distances are calculated as 2.87 Å and 1.77 Å respectively and these are very close to MP2 values. The bond angle, $\angle\text{C1S1S2}$, dihedral angles, $\delta(\text{C1S1S2C2})$, $\delta(\text{S1S2C2C2}')$ and $\delta(\text{S2S1C1C1}')$ are predicted as 91.6° , 41.8° and 78.8° and -99.8° respectively. It may be noted that the calculated bond angle is close to the MP2 value but the dihedral angles are different than MP2 values at CCSD level considering the same set of basis functions. Calculated distances C1-C2 and C3-C4 at MP2 level are 3.0 Å and 4.4 Å respectively (see Figure 6.1a). The solvent effect on the structure of the radical anion is also studied by applying SMD model for water medium and the structure obtained is very similar to the gas phase structure. Respective bond distances, $r_{\text{S1-S2}}$ and $r_{\text{C1-S1}}$ are 2.82 Å and 1.77 Å respectively. Bond angle, $\angle\text{C1S1S2}$ and dihedral angle, $\delta(\text{C1S1S2C2})$ are 87.2° and 49.8° respectively in water medium (see Figure 6.1c). It may be noted that in the water medium, displacement of the two phenyl rings in the radical anion, $(\text{PhS})_2^{\bullet-}$ is less as reflected in the calculated values of the dihedral angle, $\delta(\text{C1S1S2C2})$. The distance between C1 and C2 atoms 3.0 Å and the same between C3 and C4 atoms is 4.5 Å. Thus, MP2 results on geometrical parameters suggest that on attachment of an excess electron, the dichalcogen bond, S1-S2 elongates by 0.7 Å and C1-S1 bond distance remains practically unchanged in the gas phase and in water medium for $(\text{PhS})_2$ system. Along with that, bond

Table 6.1 Selected #geometrical and molecular parameters of diphenyl dichalcogenides, (PhS)₂ (Ch = Se and Te) in at the different levels of theory. Values in the braces show the parameters for the systems in presence of an excess electron (PhS)₂^{•-}.

Sr. no.	Method	r _{S1S2} (Å)	r _{C1S1} (Å)	∠C1S1S2 (degree)	δ(C1S1S2C2) (degree)	δ(S1S2C2C2') (degree)	δ(S2S1C1C1') (degree)
Neutral (PhS) ₂ and (PhS) ₂ ^{•-} radical anion in gas phase							
1.	i)	2.13, (2.89)	1.80, (1.76)	104.0, (103.9)	82.4, (80.8)	79.5, (91.6)	-103.5, (-88.6)
2.	ii)	2.13, (2.89)	1.80, (1.76)	104.0, (103.9)	82.4, (80.8)	79.5, (91.6)	-103.5, (-88.6)
3.	iii)	2.13, (2.89)	1.80, (1.76)	104.0, (103.9)	82.4, (80.8)	79.5, (91.6)	-103.5, (-88.6)
4.	iv)	2.13, (2.89)	1.80, (1.76)	104.0, (103.9)	82.4, (80.8)	79.5, (91.6)	-103.5, (-88.6)
5.	v)	2.11, (2.81)	1.78, (1.75)	101.2, (92.8)	69.3, (37.5)	84.0, (80.2)	-95.8, (-97.6)
6.	vi)	2.13, (2.83)	1.77, (1.76)	97.4, (85.6)	51.2, (51.7)	74.7, (68.4)	-101.3, (-111.1)
Neutral (PhS) ₂ and (PhS) ₂ ^{•-} radical anion in water medium							
1.	i)	2.14, (2.95)	1.80, (1.77)	104.1, (103.6)	82.4, (81.0)	84.2, (90.1)	-98.3, (-90.3)
2.	ii)	2.14, (2.95)	1.80, (1.77)	104.1, (103.6)	82.4, (81.0)	84.2, (90.1)	-98.3, (-90.3)
3.	iii)	2.14, (2.95)	1.80, (1.77)	104.1, (103.6)	82.4, (81.0)	84.2, (90.1)	-98.3, (-90.3)
4.	iv)	2.14, (2.95)	1.80, (1.77)	104.1, (103.6)	82.4, (81.0)	84.2, (90.1)	-98.3, (-90.3)
5.	v)	2.11, (2.91)	1.78, (1.76)	101.4, (94.5)	68.2, (28.7)	83.4, (86.5)	-95.9, (-92.4)
6.	vi)	2.13, (2.82)	1.77, (1.77)	97.7, (87.7)	47.8, (49.5)	74.5, (70.1)	-101.7, (-110.9)

#Methods: i) B3LYP; ii) B3LYP-D; iii) B3LYP-D3; iv) B3LYP-D3BJ; v) ω-B97XD; vi) MP2. Basis set: 6-311++G(d,p) for H, C, S, Se atoms and 3-21G* for Te atoms.

Table 6.2 Selected #geometrical and molecular parameters of diphenyl dichalcogenides, (PhCh)₂ (Ch = Se and Te) in at the different levels of theory. Values in the braces show the parameters for the systems in presence of an excess electron (PhCh)₂^{•-}.

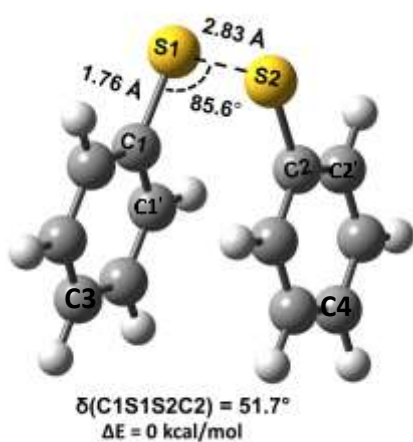
Sr. no.	Method	r _{Ch1Ch2} (Å)	r _{C1Ch1} (Å)	∠C1Ch1Ch2 (degree)	δ(C1Ch1Ch2C2) (degree)	δ(Ch1Ch2C2C2') (degree)	δ(Ch2Ch1C1C1') (degree)
Neutral (PhSe) ₂ and (PhSe) ₂ ^{•-} radical anion in water medium							
1.	i)	2.39, (3.14)	1.94, (1.92)	101.8, (100.3)	82.6, (72.7)	85.6, (85.1)	-96.9, (-95.0)
2.	ii)	2.39, (3.14)	1.94, (1.92)	101.8, (100.3)	82.6, (72.7)	85.6, (85.1)	-96.9, (-95.0)
3.	iii)	2.39, (3.14)	1.94, (1.92)	101.8, (100.3)	82.6, (72.7)	85.6, (85.1)	-96.9, (-95.0)
4.	iv)	2.39, (3.14)	1.94, (1.92)	101.8, (100.3)	82.6, (72.7)	85.6, (85.1)	-96.9, (-95.0)
5.	v)	2.35, (3.09)	1.92, (1.91)	98.4, (91.5)	67.2, (33.4)	84.3, (98.2)	-95.1, (-80.5)
6.	vi)	2.41, (3.05)	1.92, (1.93)	94.7, (92.4)	42.3, (22.1)	73.7, (47.3)	-102.6, (-131.7)
Neutral (PhTe) ₂ and (PhTe) ₂ ^{•-} radical anion in water medium							
1.	i)	2.76, (3.36)	2.15, (2.14)	100.0, (89.3)	84.1, (81.1)	86.5, (87.7)	-95.9, (-92.8)
2.	ii)	2.77, (3.41)	2.14, (2.14)	93.1, (82.9)	59.4, (44.5)	71.3, (68.6)	-79.1, (-112.2)
3.	iii)	2.77, (3.41)	2.14, (2.14)	94.4, (84.1)	66.2, (44.5)	89.9, (68.9)	-89.6, (-111.5)
4.	iv)	2.77, (3.41)	2.14, (2.14)	94.4, (84.1)	66.2, (44.5)	89.9, (68.9)	-89.6, (-111.5)
5.	v)	2.76, (3.35)	2.12, (2.13)	92.3, (84.9)	42.1, (43.1)	76.1, (70.5)	-102.9, (-110.1)
6.	vi)	2.79, (3.30)	2.12, (2.13)	89.9, (80.8)	38.1, (46.1)	78.2, (68.2)	-103.1, (-115.6)

#Methods: i) B3LYP; ii) B3LYP-D; iii) B3LYP-D3; iv) B3LYP-D3BJ; v) ω-B97XD; vi) MP2. Basis set: 6-311++G(d,p) for H, C, S, Se atoms and 3-21G* for Te atoms.

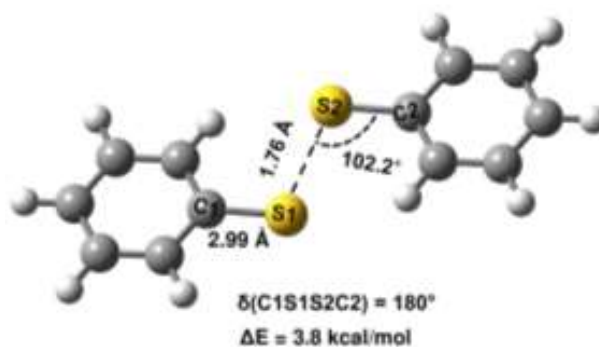
angle ($\angle C1S1S2$) and dihedral angle, $\delta(C1S1S2C2)$ remain unperturbed on electron attachment in $(PhS)_2$ in the gas phase as well as in water medium. It is clear from the above discussion that $(PhS)_2$ and its radical anion have peculiar structural features. Importantly, in solution the phenyl rings are almost free to rotate. This conformational motions of the phenyl rings not only observed experimentally¹⁴⁷ but also quantified through density functional theory (DFT) calculations in solution phase.¹³⁵ Though, all reported calculations are performed in the gas phase and in water medium, for the sake of convenience the structural and stability features discussions are limited only to water medium in upcoming discussions.

To examine the change in geometrical parameters in same systems with Se and Te atoms in place of S, similar electronic structure calculations have been performed. Table 6.2 provides the changes in selected geometrical parameters of $(PhCh)_2$ ($Ch = Se$ and Te) produced upon one electron reduction. Several initial geometries of $(Ph-Se)_2^{\bullet-}$ and $(Ph-Te)_2^{\bullet-}$ radical anions are considered to find out the most stable structure. Only the most stable structures of $(Ph-Se)_2^{\bullet-}$ and $(Ph-Te)_2^{\bullet-}$ radical anions are reported in Figure 6.1d and Figure 6.1e respectively at MP2 level of theory in water medium. The bond distances $r_{Se1-Se2}$ and r_{C1-Se1} are 3.05 Å and 1.93 Å respectively for $(Ph-Se)_2^{\bullet-}$ radical anion as shown in Figure 6.1d. The obtained bond angle, $\angle C1Se1Se2$ and dihedral angle, $\delta(C1Se1Se2C2)$ are 92.4° and 22.1° respectively in water medium. It may be noted that the calculated dihedral angle, $\delta(C1Se1Se2C2)$ is significantly smaller than the sulfur systems suggesting more pi-pi interaction in Se systems. The distance between the C1 and C2 atoms is 3.3 Å and that between C3 and C4 atoms is 3.8 Å. For the most stable structure of $(Ph-Te)_2^{\bullet-}$ radical anion, the $r_{Te1-Te2}$ and r_{C1-Te1} bond distances are calculated as 3.30 Å and 2.13 Å respectively at MP2 level of theory in a water medium (see Figure 6.1e). These bond distance are significantly larger than there sulfur and

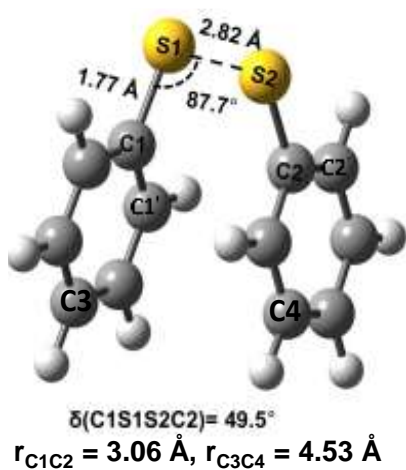
selenium analogues. The bond angle, $\angle \text{C1Te1Te2}$, dihedral angle, $\delta(\text{C1Te1Te2C2})$ are calculated as 80.5° , and 46.1° respectively. The distance between the C1 and C2 atoms is 3.1 \AA and that between C3 and C4 atoms is 4.3 \AA . The value of dihedral angle, $\delta(\text{C1Te1Te2C2})$ is significantly larger than the selenium systems and interestingly, the value obtained is close to it sulfur analogue.



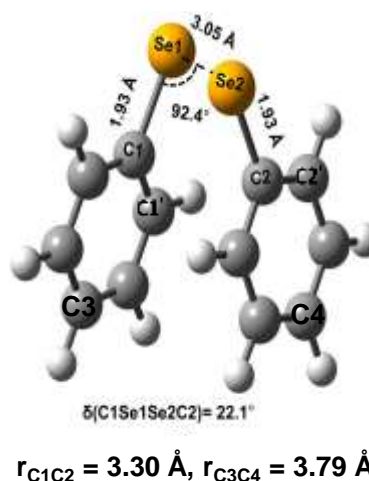
a



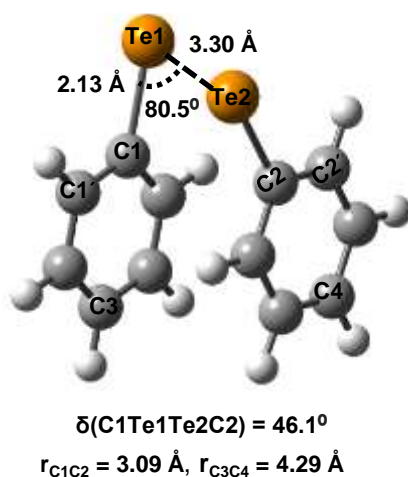
b



c



d



e

Figure 6.1 a) Most stable structure of $(\text{PhS})_2^{\bullet-}$ radical anion in the gas phase, b) second possible structure of $(\text{PhS})_2^{\bullet-}$ radical anion in the gas phase. c) $(\text{PhS})_2^{\bullet-}$ radical anion in water medium, d) $(\text{PhSe})_2^{\bullet-}$ radical anion in water medium calculated at MP2/6-311++G(d,p) level of theory. e) Most stable structures of $(\text{PhTe})_2^{\bullet-}$ radical anion in water medium. Method: MP2 level of theory with 6-311++G(d,p) basis set for H, C, S, Se atoms and 3-21G* basis set for Te atoms. ΔE represents the relative energy of the higher energy structure with respect to the most stable one.

This suggest that there is significant decrease in pi-pi interaction in Te systems compared to its selenium analogue. Calculated angle, $\angle \text{C1Ch1Ch2}$ and dihedral angles, $\delta(\text{C1Ch1Ch2C2})$, $\delta(\text{Ch1Ch2C2C2}')$ and $\delta(\text{Ch2Ch1C1C1}')$ are significantly larger at DFT level compared to MP2 data. It is also observed that the DFT functional, ω -B97XD produces these angles closer to MP2 values except for $\delta(\text{Ch1Ch2C2C2}')$ and $\delta(\text{Ch2Ch1C1C1}')$. ω -B97XD functionals is performing reasonably well and has the advantage of including the dispersion correction for phenyl rings are stacked close to each other along with long range correction. The calculated bond order for Ch-Ch bonds are 0.5 for $(\text{Ph-Ch})_2^{\bullet-}$ (Ch = Se, Se and Te) radical anions. Thus, the chalcogen atoms are bonded by 2c-3e bond in the most stable structures of these radical anions in water medium.

Inserting suitable ring substituents can modulate the antioxidant activity and affect the structural features of these diphenyl dichalcogenides. The next section provides the detail study on the most stable structures of diphenyl dichalcogenides substituted at ortho position by electron donating group.

6.3.2 Effect of electron-donating ortho-substituted groups: Structures of (o-R-PhCh)₂^{•-} radical anions (Ch = S, Se & Te; R= CH₃ & OH)

In order to gain insight into the overall molecular geometries of substituted diaryl dichalcogenides, electron donating group -CH₃ & -OH are substituted at one of the ortho-positions of the two phenyl rings (PhCh)₂ (Ch = S, Se & Te) and their corresponding radical anions. Structures with -CH₃ and -OH substitutions only in anti-positions of the most stable structure of diphenyl diselenide radical anion are considered as input geometries to locate equilibrium structure. Coordinates of all the atoms in the most stable structures of neutral (o-R-PhCh)₂ (R= CH₃ & OH) are used as the initial input to get the most stable structures of (o-R-PhCh)₂^{•-} radical anions.

Selected geometrical parameters calculated at different levels of theory for neutral (o-CH₃-PhCh)₂ and (o-CH₃-PhCh)₂^{•-} radical anionic systems are listed in Table 6.3. The most stable structure of (o-CH₃-PhCh)₂^{•-} radical anions calculated at MP2/6-311++G(d,p) level of theory including solvent effect following SMD model are shown in Figure 6.2 (a-c). The r_{S1-S2} and r_{C1-S1} bond distances are calculated as 2.92 Å and 1.79 Å respectively at present level of theory for (o-CH₃-PhS)₂^{•-} radical anion (see Figure 6.2a). Bond angle, ∠C1S1S2, dihedral angle, δ(C1S1S2C2) are predicted as 93.4° and 13.2° respectively. It is interesting to note that adding -CH₃ group to each phenyl ring in their ortho position has made the distance between two S atoms shorter by 0.1 Å in water medium. However, dihedral angle, δ(C1S1S2C2) is decreased

by $\sim 36^\circ$ indicating stronger pi-pi interaction. The minimum energy structure of (o-CH₃-PhSe)₂^{•-} radical anion is displayed in Figure 6.2b. On addition of -CH₃ group to the phenyl ring in (PhSe)₂^{•-} radical anion, no notable change in the bond distance are obtained. However, dihedral angle, (C1Se1Se2C2) is increased by 18° compared to that in the radical anion with unsubstituted phenyl rings. This increase in the dihedral angle reflects that the displacement between the two phenyl rings may be due to the bulky nature of -CH₃ groups. Distances between C3 and C4 atoms in -CH₃ group substituted radical anion and unsubstituted radical anion systems are 3.8 Å and 4.1 Å respectively. The $r_{\text{Te1-Te2}}$ and $r_{\text{C1-Te1}}$ bond distances are calculated as 3.34 Å and 2.14 Å respectively for (o-CH₃-PhTe)₂^{•-} radical anion (see Figure 6.2c). Bond angle, $\angle \text{C1Te1Te2}$ and dihedral angle, $\delta(\text{C1Te1Te2C2})$ are calculated as 83.8° and 41.8° respectively. It is worth to mention that adding -CH₃ group to each phenyl ring in their ortho position is marginally affecting the geometrical parameters compared to its unsubstituted Te-analogue. The spin densities over chalcogen atoms labelled are ~ 0.5 a.u. In sum, the methyl-substituted radical anion S, Se and Te based radical anion are forming stable 2c-3e bond.

Table 6.4 provides the changes in geometrical parameters of (o-OH-PhCh)₂ (Ch = S, Se & Te) and its anionic counterparts at MP2 level of theory in water medium. For (o-OH-PhCh)₂^{•-} radical anions, the most stable structures have pi-pi stacked structures like their ortho-methyl substituted and unsubstituted analogues (Figure 6.2(d-f)).

On addition of -OH group to the phenyl ring in (PhS)₂^{•-} radical anion, no notable change in the bond distances and bond angle are obtained. However, dihedral angle, (C1S1S2C2) is decreased by $\sim 9^\circ$ compared to that in the radical anion with unsubstituted phenyl rings

Table 6.3 Selected #geometrical and molecular parameters of diphenyl dichalcogenides, (o-CH₃-PhCh)₂ (Ch = S, Se and Te) in water medium at the different levels of theory. Values in the braces show the parameters for the systems in presence of an excess electron (o-CH₃-PhCh)₂^{•-}.

Sr. no.	Method	r _{Ch1Ch2} (Å)	r _{C1Ch1} (Å)	∠C1Ch1Ch2 (degree)	δ(C1Ch1Ch2C2) (degree)	δ(Ch1Ch2C2C2') (degree)	δ(Ch2Ch1C1C1') (degree)
Neutral (CH ₃ -PhS) ₂ and (CH ₃ -PhS) ₂ ^{•-} radical anion in water medium							
1.	i)	2.14, (3.08)	1.80, (1.76)	104.2, (101.1)	79.1, (5.2)	79.8, (89.7)	-103.2, (-90.7)
2.	ii)	2.15, (3.13)	1.79, (1.76)	100.4, (93.2)	62.2, (5.4)	81.2, (70.0)	-98.6, (-111.0)
3.	iii)	2.15, (3.14)	1.79, (1.76)	101.1, (94.3)	65.0, (6.1)	79.5, (70.4)	-99.8, (-109.1)
4.	iv)	2.15, (3.13)	1.79, (1.76)	100.2, (94.4)	61.3, (7.3)	79.5, (69.2)	-99.0, (-110.1)
5.	v)	2.11, (2.99)	1.78, (1.76)	101.0, (95.7)	64.3, (4.8)	80.9, (71.7)	-98.3, (-107.4)
6.	vi)	2.20, (2.92)	1.76, (1.79)	100.9, (93.4)	10.8, (13.2)	67.0, (61.8)	-112.7, (-120.6)
Neutral (CH ₃ -PhSe) ₂ and (CH ₃ -PhSe) ₂ ^{•-} radical anion in water medium							
1.	i)	2.39, (3.14)	1.95, (1.93)	102.4, (103.3)	78.9, (74.8)	76.4, (79.7)	-106.6, (-100.8)
2.	ii)	2.39, (3.14)	1.95, (1.93)	102.4, (103.3)	78.9, (74.8)	76.4, (79.7)	-106.6, (-100.8)
3.	iii)	2.39, (3.14)	1.95, (1.93)	102.4, (103.3)	78.9, (74.8)	76.4, (79.7)	-106.6, (-100.8)
4.	iv)	2.39, (3.14)	1.95, (1.93)	102.4, (103.3)	78.9, (74.8)	76.4, (79.7)	-106.6, (-100.8)
5.	v)	2.38, (3.11)	1.93, (1.91)	97.6, (91.7)	43.0, (30.9)	76.5, (80.9)	-100.8, (-98.0)
6.	vi)	2.41, (3.02)	1.92, (1.94)	96.6, (86.7)	37.8, (40.0)	77.0, (77.1)	-99.9, (-105.3)
Neutral (CH ₃ -PhTe) ₂ and (CH ₃ -PhTe) ₂ ^{•-} radical anion in water medium							
1.	i)	2.76, (3.39)	2.15, (2.15)	99.0, (88.9)	82.5, (66.0)	73.0, (78.8)	-109.9, (-102.9)
2.	ii)	2.80, (3.45)	2.15, (2.14)	91.8, (84.7)	37.1, (37.2)	75.6, (73.9)	-103.5, (-108.2)
3.	iii)	2.79, (3.43)	2.15, (2.14)	92.8, (85.6)	42.1, (38.8)	75.6, (75.2)	-101.9, (-106.3)
4.	iv)	2.79, (3.39)	2.14, (2.14)	92.2, (85.6)	37.6, (38.5)	76.0, (74.7)	-103.0, (-106.9)
5.	v)	2.76, (3.37)	2.13, (2.13)	93.0, (88.1)	37.4, (36.8)	77.8, (76.0)	-101.4, (-104.6)
6.	vi)	2.80, (3.32)	2.13, (2.14)	90.6, (82.1)	34.3, (42.3)	80.0, (76.0)	-101.6, (-109.9)

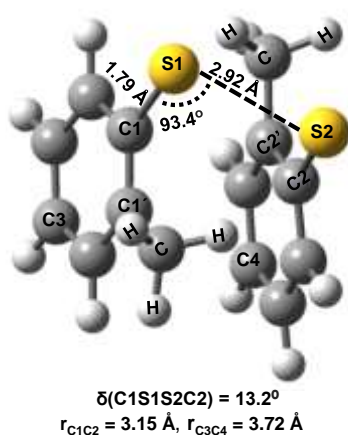
Table 6.4 Selected #geometrical and molecular parameters of diphenyl dichalcogenides, (o-HO-PhCh)₂ (Ch = S, Se and Te) in water medium at the different levels of theory. Values in the braces show the parameters for the systems in presence of an excess electron (o-HO-PhCh)₂^{•-}.

Sr. no.	Method	r _{Ch1Ch2} (Å)	r _{C1Ch1} (Å)	∠C1Ch1Ch2 (degree)	δ(C1Ch1Ch2C2) (degree)	δ(Ch1Ch2C2C2') (degree)	δ(Ch2Ch1C1C1') (degree)
Neutral (HO-PhS) ₂ and (HO-PhS) ₂ ^{•-} radical anion in water medium							
1.	i)	2.14, (3.05)	1.78, (1.76)	104.1, (98.1)	78.3, (30.2)	79.7, (90.5)	-103.3, (-89.3)
2.	ii)	2.19, (3.07)	1.78, (1.76)	99.9, (92.0)	44.9, (28.2)	79.1, (85.4)	-97.1, (-93.3)
3.	iii)	2.15, (3.07)	1.78, (1.75)	101.1, (92.9)	62.1, (27.1)	80.7, (85.1)	-98.0, (-93.5)
4.	iv)	2.16, (3.03)	1.78, (1.75)	100.3, (92.6)	57.4, (28.8)	79.9, (83.7)	-97.9, (-95.1)
5.	v)	2.12, (2.94)	1.77, (1.75)	101.0, (94.1)	61.8, (28.2)	80.9, (84.5)	-97.8, (-94.1)
6.	vi)	2.15, (2.92)	1.76, (1.76)	98.0, (89.3)	42.4, (40.3)	76.1, (77.8)	-100.4, (-103.5)
Neutral (HO-PhSe) ₂ and (HO-PhSe) ₂ ^{•-} radical anion in water medium							
1.	i)	2.40, (3.26)	1.93, (1.92)	102.2, (95.7)	79.7, (-4.3)	76.1, (80.3)	-106.7, (-99.7)
2.	ii)	2.47, (3.25)	1.92, (1.92)	98.9, (92.5)	11.9, (-0.3)	66.4, (72.7)	-112.3, (-107.7)
3.	iii)	2.47, (3.24)	1.92, (1.92)	99.7, (93.4)	12.8, (-0.7)	67.0, (73.4)	-111.8, (-106.2)
4.	iv)	2.47, (3.19)	1.92, (1.91)	99.2, (93.5)	12.4, (-0.1)	67.4, (73.1)	-111.6, (-106.7)
5.	v)	2.42, (3.14)	1.91, (1.91)	99.7, (94.2)	14.8, (-0.4)	67.5, (73.2)	-111.3, (-106.3)
6.	vi)	2.45, (3.08)	1.91, (1.94)	97.7, (91.7)	8.4, (11.0)	67.5, (62.2)	-113.5, (-119.5)
Neutral (HO-PhTe) ₂ and (HO-PhTe) ₂ ^{•-} radical anion in water medium							
1.	i)	2.77, (3.38)	2.14, (2.14)	99.1, (89.4)	82.0, (72.9)	72.2, (81.9)	-111.1, (-90.5)
2.	ii)	2.80, (3.44)	2.14, (2.14)	91.8, (84.2)	38.8, (40.4)	78.0, (74.0)	-101.8, (-108.1)
3.	iii)	2.80, (3.43)	2.14, (2.14)	92.0, (85.2)	42.6, (39.4)	77.3, (74.5)	-103.2, (-108.1)
4.	iv)	2.77, (3.39)	2.14, (2.13)	94.4, (85.4)	39.6, (40.2)	89.9, (73.1)	-107.3, (-111.5)
5.	v)	2.76, (3.37)	2.12, (2.12)	92.8, (86.4)	39.1, (38.2)	77.8, (74.1)	-101.5, (-106.3)
6.	vi)	2.80, (3.31)	2.12, (2.13)	90.3, (82.4)	35.1, (43.0)	79.6, (72.7)	-102.5, (-111.1)

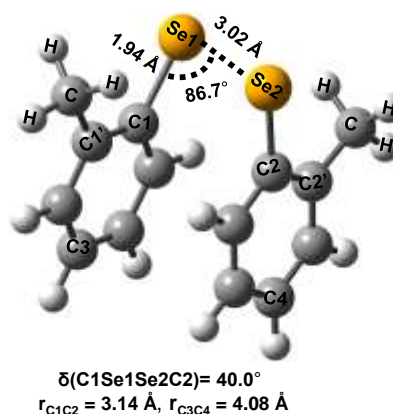
#Methods: i) B3LYP; ii) B3LYP-D; iii) B3LYP-D3; iv) B3LYP-D3BJ; v) ω-B97XD; vi) MP2. Basis set: 6-311++G(d,p) for H, C, S, Se atoms and 3-21G* for Te atoms.

indicating more pi-pi interaction in stacked phenyl rings. Moreover, two phenyl rings are less displaced in comparison to its methyl substituted analogue with almost similar values of bond distances and bond angle.

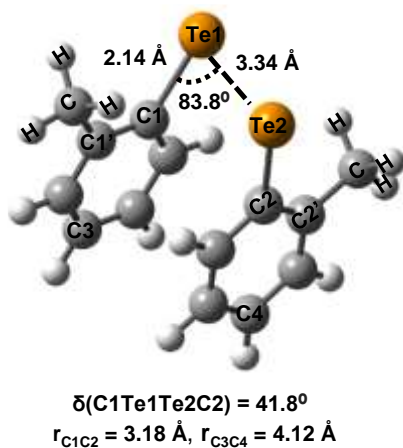
Figure 6.2e shows the most stable structure of $(o\text{-CH}_3\text{-PhSe})_2^{\bullet-}$ radical anion. It is now an obvious observation that the adding -OH group to each phenyl ring in their ortho position have



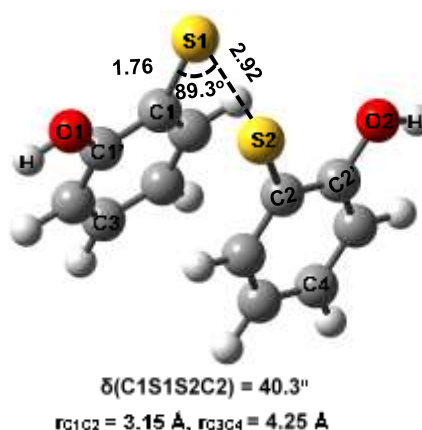
a



b



c



d

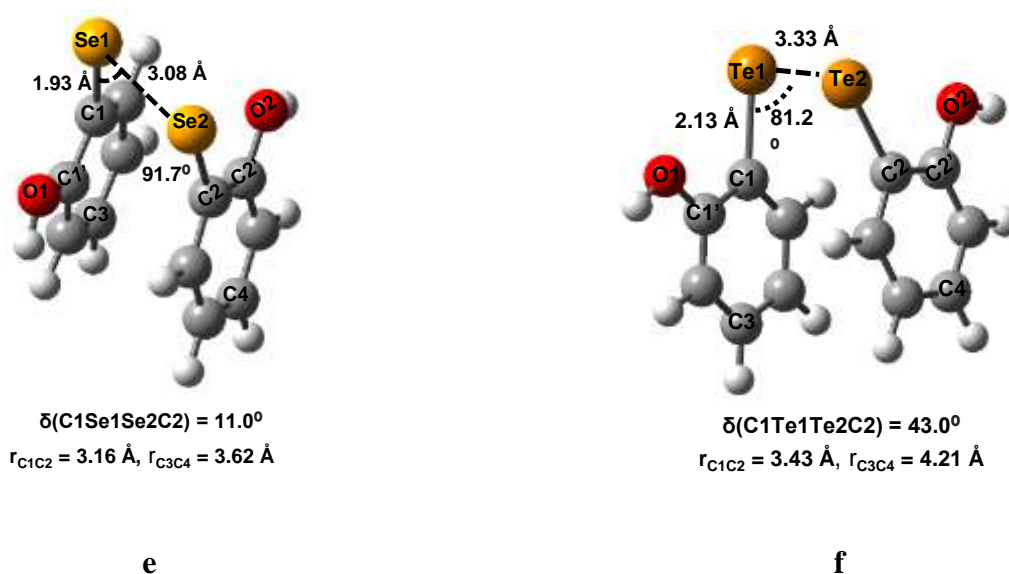


Figure 6.2 Most stable structures in water medium a) (o-CH₃-PhS)₂•⁻ radical anion, b) (o-CH₃-PhSe)₂•⁻ radical anion, c) (o-CH₃-PhTe)₂•⁻ radical anion, d) (o-HO-PhS)₂•⁻ radical anion, e) (o-HO-PhSe)₂•⁻ radical anion, and f) (o-HO-PhTe)₂•⁻ radical anion. Method: MP2 level of theory, Basis set: 6-311++G(d,p) for H, C, O, S, Se atoms and 3-21G* for Te atoms.

insignificant effect to bond distances and bond angle compared to unsubstituted and methyl substituted Se-analogues. However, dihedral angle, $\delta(\text{C1Se1Se2C2})$ is decreased by $\sim 11^\circ$ and \sim by 29° with respect to unsubstituted and methyl substituted Se-analogue respectively. This observation suggested that (o-OH-PhSe)₂•⁻ radical anion has more pi-pi stacking in two phenyl rings compared to unsubstituted and methyl substituted Se-analogues. It is interesting to note that adding -OH group to each phenyl ring in their ortho position is not significantly altering the geometrical parameters compared to its unsubstituted and methyl substituted Te-analogues. The spin densities over chalcogen atoms labelled are ~ 0.5 a.u. These ortho-hydroxyl-substituted dichalcogenides radical anions are forming hemi bonds.

It is also observed that the B3LYP, B3LYP-D, B3LYP-D3 and B3LYP-D3BJ functionals produced significantly larger bond angle and dihedral angles in comparison to MP2 level (see

Table 6.4). However, ω -B97XD produces these angles closer to MP2 values except for $\delta(\text{Ch1Ch2C2C2}')$ and $\delta(\text{Ch2Ch1C1C1}')$. The $(\text{o-R-Ph-Ch})_2^{\bullet-}$, $(\text{o-R-Ph-Ch})_2^{\bullet-}$ ($\text{Ch} = \text{S, Se and Te; R} = \text{CH}_3 \text{ and OH}$) radical anions are forming the stable 2c-3e bonds between their respective chalcogen atoms.

The next section provides the detail study on the most stable structures of diphenyl dichalcogenides substituted by electron withdrawing at ortho position in two phenyl rings.

6.3.3 Effect of electron-withdrawing ortho-substituted group: Structures of $(\text{o-R-Ph-Ch})_2^{\bullet-}$ radical anions ($\text{Ch} = \text{S, Se \& Te; R} = \text{NO}_2$)

It is already mention that inserting suitable ring substituents can modulate the antioxidant activity and affect the structural features of these diphenyl dichalcogenides. Next step is to see the effect of electron-withdrawing group on the structures of $(\text{Ph-Ch})_2^{\bullet-}$ ($\text{Ch} = \text{S, Se, \& Te}$). Nitro group is chosen for its varieties of well-known applications in synthetic as well as pharmaceutical chemistry.

Selected geometrical parameters calculated at different levels of theory for neutral $(\text{o-NO}_2\text{-PhCh})_2$ and corresponding radical anionic systems are displayed in Table 6.5. Structures with $-\text{NO}_2$ substitution only in anti-positions of the most stable structure of for neutral diphenyl dichalcogenides considered as input geometries to locate equilibrium structure. Coordinates of all the atoms in the most stable structures of neutral $(\text{o-NO}_2\text{-PhCh})_2$ are used as the initial input to get the most stable structures of $(\text{o-NO}_2\text{-PhCh})_2^{\bullet-}$ radical anions. For $(\text{o-NO}_2\text{-PhCh})_2^{\bullet-}$ radical anions, the most stable structures have pi-pi stacked structures like their substituted and unsubstituted analogues (Figure 6.3(a-c)). The $r_{\text{S1-S2}}$ and $r_{\text{C1-S1}}$ bond distances are calculated as 2.13 Å and 1.78 Å respectively for $(\text{o-NO}_2\text{-Ph-S})_2^{\bullet-}$ radical anion as shown in Figure 6.3a. It

is interesting to note that adding an electron withdrawing group like $-\text{NO}_2$ to each phenyl ring in their ortho position has made the distance between two S atoms significantly shorter as compared to its substituted and unsubstituted S-analogues. Not only that, the bond angle, $\angle \text{C1S1S2}$ is significantly larger with respect to substituted and unsubstituted S-analogues. Moreover, the two phenyl rings are more stacked than the unsubstituted and OH-substituted S-analogues as suggested by dihedral angles. But, two phenyl rings in $(\text{o-NO}_2\text{-Ph-S})_2^{\bullet-}$ radical anion show lesser pi-pi interaction compared to CH_3 -substituted S-analogue. Most stable structure of $(\text{o-NO}_2\text{-Ph-S})_2^{\bullet-}$ radical anion is displayed in Figure 6.3b. Bond distances $r_{\text{Se1-Se2}}$ and $r_{\text{C1-Se1}}$ are obtained as 2.41 and 1.95 Å, respectively. Bond angle, $\angle \text{C1Se1Se2}$ and dihedral angle, $\delta(\text{C1Se1Se2C2})$ are observed as 95.3° and 37.9° , respectively. It is interesting to note that adding an electron withdrawing group like $-\text{NO}_2$ to each phenyl ring in their ortho position has made the distance between two Se atoms shorter by 0.64 Å in water medium. However, dihedral angle, $\delta(\text{C1Se1Se2C2})$ is increased by 15.8° indicating less pi-pi interaction. Two phenyl rings in $(\text{o-NO}_2\text{-Ph-Se})_2^{\bullet-}$ radical anion show lesser pi-pi interaction compared to unsubstituted and OH-substituted Se-analogues. However, two phenyl rings are more stacked compared to and methyl-substituted Se-analogue as suggested by the dihedral angles values. The $r_{\text{Te1-Te2}}$ and $r_{\text{C1-Te1}}$ bond distances are calculated as 2.80 Å and 2.14 Å respectively for $(\text{o-NO}_2\text{-Ph-Te})_2^{\bullet-}$ radical anion as shown in Figure 6.3c. On addition of $-\text{NO}_2$ group to the phenyl ring in $(\text{PhTe})_2^{\bullet-}$ radical anion, the $r_{\text{Te1-Te2}}$ bond distance significantly decreased and bond angle obtained is $\sim 16^\circ$ larger than compared to unsubstituted and substituted Te-analogues. Not only that, two phenyl rings are less stacked in $(\text{o-NO}_2\text{-Ph-Te})_2^{\bullet-}$ radical anion compared to unsubstituted and substituted Te-analogues.

Table 6.5 Selected #geometrical and molecular parameters# of (o-NO₂-PhCh)₂ (Ch = S, Se and Te) in water medium at the different levels of theory. Values in the braces show the parameters for the systems in the presence of an excess electron (o-NO₂-PhCh)₂^{•-}.

Sr. no.	Method	r _{Ch1Ch2} (Å)	r _{C1Ch1} (Å)	∠C1Ch1Ch2 (degree)	δ(C1Ch1Ch2C2) (degree)	δ(Ch1Ch2C2C2') (degree)	δ(Ch2Ch1C1C1') (degree)
Neutral (o-NO ₂ -PhS) ₂ and (o-NO ₂ -PhS) ₂ ^{•-} radical anion in water medium							
1.	i)	2.13, (2.15)	1.80, (1.79)	103.6, (103.3)	92.3, (86.9)	86.5, (90.2)	-78.4, (-112.8)
2.	ii)	2.13, (2.15)	1.79, (1.79)	103.2, (100.1)	73.1, (63.5)	86.4, (96.5)	-80.3, (-107.6)
3.	iii)	2.13, (2.15)	1.79, (1.79)	103.5, (100.6)	75.8, (66.7)	86.4, (94.8)	-81.8, (-109.3)
4.	iv)	2.13, (2.15)	1.79, (1.79)	100.5, (99.8)	64.3, (64.4)	91.1, (92.9)	-105.7, (-107.6)
5.	v)	2.10, (2.11)	1.78, (1.78)	101.9, (101.0)	50.2, (66.1)	91.3, (95.3)	-96.3, (-108.5)
6.	vi)	2.17, (2.17)	1.76, (1.76)	99.6, (99.4)	33.7, (34.3)	86.4, (89.3)	-95.4, (-95.1)
Neutral (o-NO ₂ -PhSe) ₂ and (o-NO ₂ -PhSe) ₂ ^{•-} radical anion in water medium							
1.	i)	2.38, (2.40)	1.95, (1.95)	102.2, (102.2)	77.8, (78.9)	47.3, (60.8)	-131.6, (-112.0)
2.	ii)	2.38, (2.40)	1.95, (1.95)	102.2, (102.2)	77.8, (78.9)	47.3, (60.8)	-131.6, (-112.0)
3.	iii)	2.38, (2.40)	1.95, (1.95)	102.2, (102.2)	77.8, (78.9)	47.3, (60.8)	-131.6, (-112.0)
4.	iv)	2.38, (2.40)	1.95, (1.95)	102.2, (102.2)	77.8, (78.9)	47.3, (60.8)	-131.6, (-112.0)
5.	v)	2.37, (2.37)	1.93, (1.92)	96.4, (97.1)	44.5, (46.3)	67.6, (66.5)	-105.1, (-105.5)
6.	vi)	2.40, (2.41)	1.93, (1.95)	97.2, (95.3)	34.0, (37.9)	49.6, (75.1)	-123.1, (-101.1)
Neutral (o-NO ₂ -PhTe) ₂ and (o-NO ₂ -PhTe) ₂ ^{•-} radical anion in water medium							
1.	i)	2.78, (2.81)	2.16, (2.16)	99.5, (100.1)	82.8, (81.6)	76.8, (78.1)	-6.2, (-3.5)
2.	ii)	2.77, (2.80)	2.16, (2.16)	94.8, (95.6)	75.6, (75.7)	79.0, (79.2)	-1.4, (-2.1)
3.	iii)	2.77, (2.80)	2.16, (2.16)	95.7, (96.4)	77.0, (77.2)	78.9, (79.7)	-1.6, (-1.7)
4.	iv)	2.77, (2.80)	2.15, (2.15)	94.4, (95.4)	76.7, (76.9)	76.4, (76.4)	-0.8, (-1.6)
5.	v)	2.73, (2.76)	2.14, (2.14)	95.0, (95.8)	79.9, (80.5)	85.9, (87.2)	-0.6, (-0.6)
6.	vi)	2.80, (2.80)	2.12, (2.14)	92.2, (97.3)	31.0, (62.4)	85.3, (45.7)	-0.9, (-7.1)

#Methods: i) B3LYP; ii) B3LYP-D; iii) B3LYP-D3; iv) B3LYP-D3BJ; v) ω-B97XD; vi) MP2. Basis set: 6-311++G(d,p) for H, C, S, Se, N atoms and 3-21G* for Te atom.

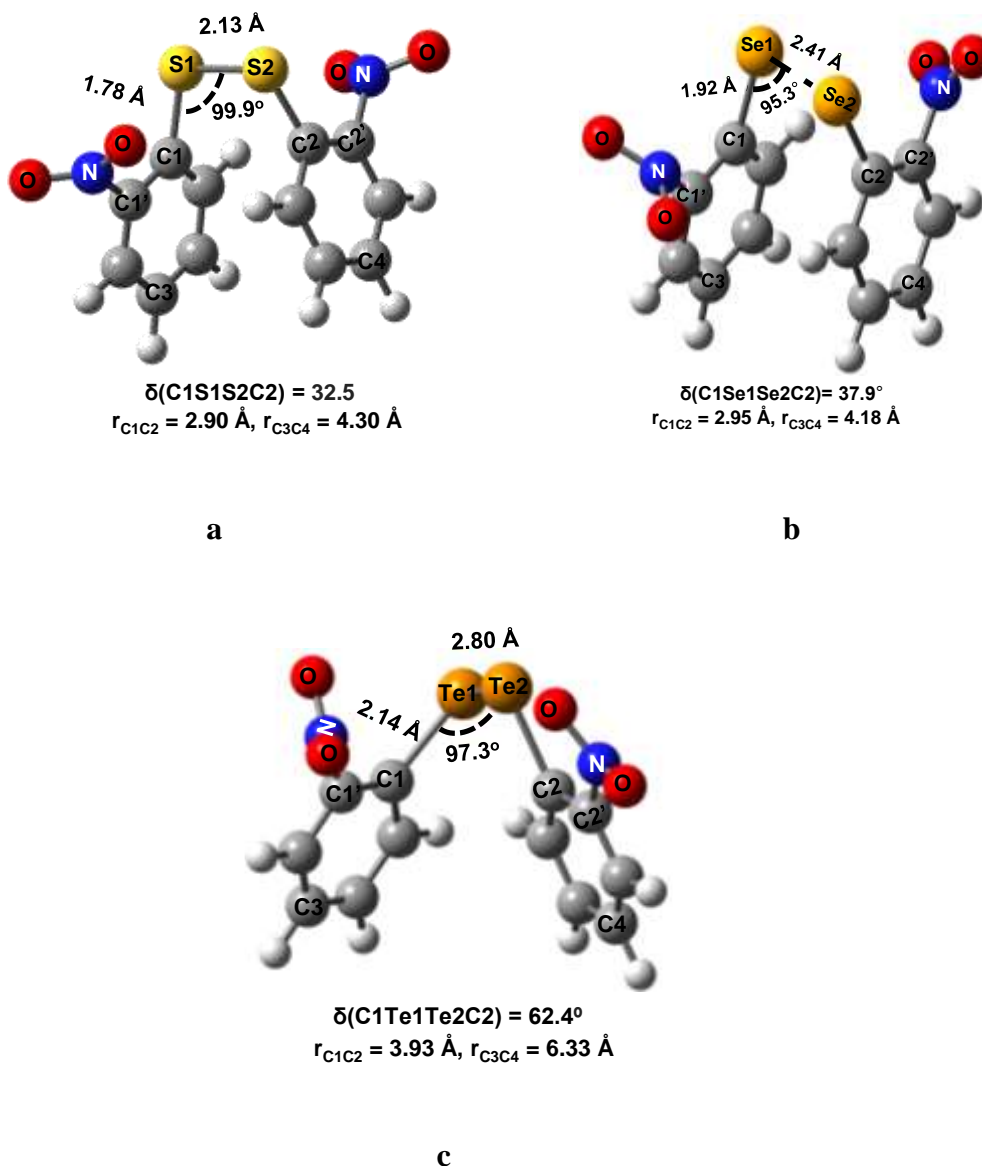


Figure 6.3 Most stable structures in water medium a) (o-NO₂-PhS)₂^{•-} radical anion, b) (o-NO₂-PhSe)₂^{•-} radical anion and, c) (o-NO₂-PhTe)₂^{•-} radical anion Method: MP2 level of theory, Basis set: 6-311++G(d,p) for H, C, N, O, S, Se atoms and 3-21G* for Te atoms.

Similar to electron donating group -CH₃ & -OH are substituted diphenyl dichalcogenides systems, the -NO₂ group substituted diphenyl dichalcogenides the DFT functional B3LYP, B3LYP-D, B3LYP-D3 and B3LYP-D3BJ produced significantly larger bond angle and dihedral angles in comparison to MP2 level. ω -B97XD functional works well for these angles

and results obtained are closer to MP2 values except for $\delta(\text{Ch1Ch2C2C2}')$ and $\delta(\text{Ch2Ch1C1C1}')$. The $(\text{o-NO}_2\text{-Ph-Ch})_2^{\bullet-}$ (Ch = S, Se and Te) radical anions are forming the 2c-3e bonds between their respective chalcogen atoms. Calculated bond orders between two S atoms in $(\text{o-NO}_2\text{-PhS})_2^{\bullet-}$ is 0.3 and between two Se atoms in $(\text{o-NO}_2\text{-PhSe})_2^{\bullet-}$ is 0.38. However, calculated bond order between two Te atoms in $(\text{o-NO}_2\text{-PhTe})_2^{\bullet-}$ is close to 0.4.

6.3.4 Effect of geometrical flexibility: Structures of $(\text{o-PhCH}_2\text{-Ch})_2^{\bullet-}$ radical anions (Ch = S, Se & Te)

Now a $-\text{CH}_2-$ group is added to the structure of radical anion $(\text{PhCh})_2^{\bullet-}$ (Ch = S, Se, & Te) between each phenyl ring and the chalcogen atom and the calculations are carried out for $(\text{PhCH}_2\text{Ch})_2^{\bullet-}$ radical anions. Table 6.6 provides the selected geometrical parameters calculated at different levels of theory for neutral $(\text{PhCH}_2\text{Ch})_2$ and corresponding radical anionic systems. Following the same approach, several initial geometries of this radical anion are considered for optimization and only two stable equilibrium structures are obtained at MP2 level of theory in water medium. However, the most stable structure for $(\text{PhCH}_2\text{Ch})_2^{\bullet-}$ radical anions are only reported in Figure 6.4(a-c). It is to be noted that the $(\text{o-PhCH}_2\text{-Ch})_2^{\bullet-}$ radical anion are not showing pi-pi stacking between the benzyl rings at MP2 level of theory in a water medium (see Figure 6.4(a-c)). It is due to the fact that the distance between the two phenyl rings are quite large and also their orientations do not allow any pi-pi interactions (see Figure 6.4(a-c)). For $(\text{PhCH}_2\text{-S})_2^{\bullet-}$ radical anion, the $r_{\text{S1-S2}}$ and $r_{\text{C1-S1}}$ bond distances are calculated as 2.78 Å and 1.83 Å respectively as displayed in Figure 6.4a. The dihedral angle, $\delta(\text{C1S1S2C2})$ is 71.8° at MP2 level of theory in a water medium (see Figure 6.4a). Bond distances $r_{\text{C1-C2}}$ and $r_{\text{C3-C4}}$ are 3.5 Å and 9.1 Å respectively at present level of theory. Thus, adding $-\text{CH}_2-$ group in phenyl ring increase the $r_{\text{C3-C4}}$ distance in $(\text{PhCH}_2\text{S})_2^{\bullet-}$ radical anion so that two benzyl rings

Table 6.6 Selected #geometrical and molecular parameters of diphenyl disulfide, (PhCH₂Ch)₂ (S, Se and Te) in water medium at the different levels of theory. Values in the braces show the parameters for the systems in presence of an excess electron (Ph CH₂Ch)₂^{•-}.

Sr. no.	Method	r _{Ch1Ch2} (Å)	r _{C1Ch1} (Å)	∠C1Ch1Ch2 (degree)	δ(C1Ch1Ch2C2) (degree)	δ(Ch1Ch2C2C2') (degree)	δ(Ch2Ch1C1C1') (degree)
Neutral (PhCH ₂ S) ₂ and (PhCH ₂ S) ₂ ^{•-} radical anion in water medium							
1.	i)	2.09, (2.92)	1.87, (1.85)	103.1, (94.8)	85.4, (76.8)	-179.0, (-177.5)	-179.0, (-177.5)
2.	ii)	2.09, (2.92)	1.87, (1.85)	103.1, (94.8)	85.4, (76.8)	-179.0, (-177.5)	-179.0, (-177.5)
3.	iii)	2.09, (2.92)	1.87, (1.85)	103.1, (94.8)	85.4, (76.8)	-179.0, (-177.5)	-179.0, (-177.5)
4.	iv)	2.09, (2.92)	1.87, (1.85)	103.1, (94.8)	85.4, (76.8)	-179.0, (-177.5)	-179.0, (-177.5)
5.	v)	2.07, (2.82)	1.84, (1.84)	101.9, (91.9)	85.5, (73.2)	178.0, (-132.1)	178.0, (-132.1)
6.	vi)	2.07, (2.78)	1.83, (1.8)	74.4, (90.5)	81.2, (71.8)	-178.0, (-141.6)	-177.9, (-141.6)
Neutral (PhCH ₂ Se) ₂ and (PhCH ₂ Se) ₂ ^{•-} radical anion in water medium							
1.	i)	2.36, (3.10)	2.02, (2.01)	101.3, (93.9)	85.1, (78.8)	178.5, (-179.9)	178.5, (-179.9)
2.	ii)	2.36, (3.10)	2.02, (2.01)	101.3, (93.9)	85.1, (78.8)	178.5, (-179.9)	178.5, (-179.9)
3.	iii)	2.36, (3.10)	2.02, (2.01)	101.3, (93.9)	85.1, (78.8)	178.5, (-179.9)	178.5, (-179.9)
4.	iv)	2.36, (3.10)	2.02, (2.01)	101.3, (93.9)	85.1, (78.8)	178.5, (-179.9)	178.5, (-179.9)
5.	v)	2.33, (3.04)	1.98, (1.98)	99.8, (91.6)	81.3, (66.0)	177.3, (-130.6)	177.3, (-130.6)
6.	vi)	2.35, (2.97)	1.98, (1.99)	99.3, (90.3)	81.1, (69.9)	-177.1, (-133.6)	-177.1, (-133.4)
Neutral (PhCH ₂ Te) ₂ and (PhCH ₂ Te) ₂ ^{•-} radical anion in water medium							
1.	i)	2.73, (3.34)	2.22, (2.22)	100.5, (86.1)	85.7, (160.2)	63.1, (106.6)	63.1, (106.6)
2.	ii)	2.72, (3.40)	2.22, (2.22)	98.5, (83.2)	73.1, (67.2)	26.6, (95.5)	26.6, (95.5)
3.	iii)	2.72, (3.38)	2.22, (2.22)	99.5, (85.8)	75.3, (66.7)	27.5, (92.7)	27.5, (92.7)
4.	iv)	2.72, (3.35)	2.22, (2.21)	98.9, (85.3)	77.0, (68.6)	24.7, (92.5)	24.7, (92.5)
5.	v)	2.70, (3.32)	2.19, (2.18)	99.7, (86.8)	73.0, (66.4)	27.7, (94.0)	27.7, (94.0)
6.	vi)	2.72, (3.29)	2.20, (2.19)	98.0, (84.4)	77.4, (69.2)	21.4, (93.7)	21.4, (93.7)

Methods: i) B3LYP; ii) B3LYP-D; iii) B3LYP-D3; iv) B3LYP-D3BJ; v) ω-B97XD; vi) MP2. Basis set: 6-311++G(d,p) for H, C, S, Se atoms and 3-21G* for Te atoms.

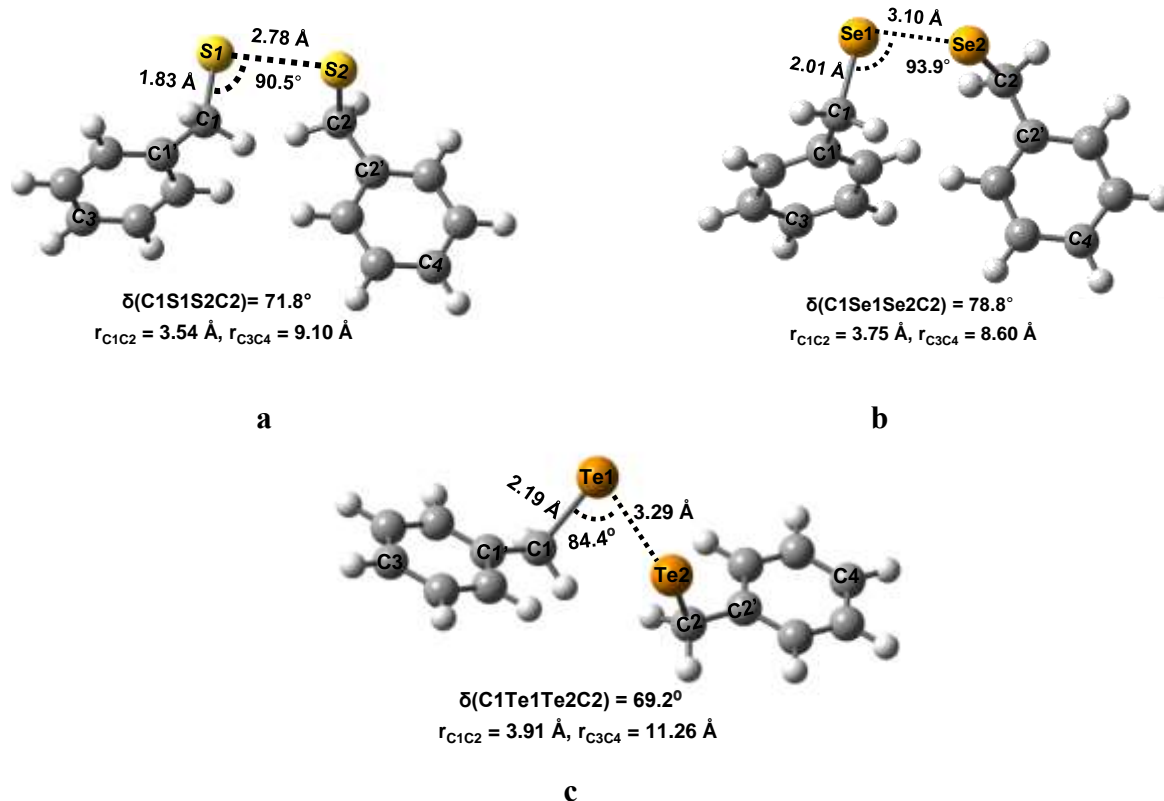


Figure 6.4 Most stable structures in water medium a) $(\text{PhCH}_2\text{S})_2^{\bullet-}$ radical anion, b) $(\text{PhCH}_2\text{Se})_2^{\bullet-}$ radical anion, and c) $(\text{PhCH}_2\text{Te})_2^{\bullet-}$ radical anion, Method: MP2 level of theory, Basis set: 6-311++G(d,p) for H, C, S, Se atoms and 3-21G* for Te atoms.

do not have any pi-pi interaction. Structure and selected geometrical parameters of the most stable structure of $(\text{PhCH}_2\text{Se})_2^{\bullet-}$ radical anion as calculated in water medium is given in Figure 6.4b. Calculated $r_{\text{Se1-Se2}}$ and $r_{\text{C1-Se1}}$ bond distances are 3.10 and 2.01 Å, respectively. It may be noted that $r_{\text{Se1-Se2}}$ bond is longer in $(\text{PhCH}_2\text{Se})_2^{\bullet-}$ by 0.07 Å than that in $(\text{PhSe})_2^{\bullet-}$. The obtained bond angle, $\angle \text{C1Se1Se2}$ and dihedral angle, $\delta(\text{C1Se1Se2C2})$ are 93.9° and 78.8° , respectively. Calculated data suggests that on the addition of $-\text{CH}_2-$ group, two phenyl rings are far apart and their orientations do not allow any pi-pi interaction to stabilize the radical anion system. For the most stable structure of $(\text{PhCH}_2\text{Te})_2^{\bullet-}$ radical anion, the $r_{\text{Te1-Te2}}$ and $r_{\text{C1-Te1}}$ bond distances are calculated as 3.29 Å and 2.13 Å respectively (see Figure 6.4c). The obtained bond angle,

$\angle \text{C1Te1Te2}$ and dihedral angle, $\delta(\text{C1Te1Te2C2})$ are 84.4° and 69.2° respectively. Two phenyl do not have any pi-pi interaction to stabilize this radical anionic system. The odd electron spin is calculated to be equally localized on two chalcogen atoms. Calculated bond order between two chalcogen atoms in all these systems having an excess electron is also close to 0.5., thus a stable 2c-3e bond is formed between their respective chalcogen atoms.

The chalcogen-chalcogen bond strength is an important parameter for the reactivity of these diaryl dichalcogenides radical anionic systems. As chalcogen-chalcogen bond strength gives the measure of stability of diaryl dichalcogenides anionic in aqueous medium. Also, their corresponding neutral systems should have suitable electron affinity to accept the extra electron. The next section aim to discuss the electron affinity and binding energies of neutral diaryl dichalcogenides and effect of adding an extra electron on their stability in water medium.

6.3.5 Stability of $(\text{R}-\text{Ch})_2^{\bullet-}$ radical anions ($\text{Ch} = \text{S}, \text{Se} \ \& \ \text{Te}$; $\text{R}=\text{Ph}, \text{o}-\text{CH}_3\text{-Ph}, \text{o}-\text{HO-Ph}, \text{o}-\text{NO}_2\text{-Ph}, \text{and PhCH}_2$) in water medium

In previous section it is highlighted that chose of different functionals have marginal effect on the chalcogen-chalcogen and carbon-chalcogen bond lengths, and carbon-chalcogen-chalcogen angle in these diaryl dichalcogenides. However, to produce appropriate carbon chalcogen-chalcogen-carbon dihedral angles the choice of dispersion correction functionals are necessary to consider the dispersion interaction of two stacked phenyl rings. Also, the DFT functional ω -B97XD produces the dihedral angles comparable to MP2 level of theory. One can expect that these functional can appropriately predict the electron affinity and binding energies of neutral diaryl dichalcogenides and binding energies of their corresponding radical anionic systems.

Table 6.7 provides the binding energies and electron affinity of neutral $(\text{R}-\text{Ch})_2$ ($\text{Ch} = \text{S}, \text{Se}, \ \& \ \text{Te}$; $\text{R}=\text{Ph}, \text{o}-\text{CH}_3\text{-Ph}, \text{and o-HO-Ph}$) and binding energies of their corresponding radical

anionic systems in water medium. The calculations are performed at various DFT functionals and MP2 level of theory in conjunction with 6-311++G(d,p) basis set for C, H, O, N, S and Se atoms and 3-21G* for Te atom. Table 6.8 shows the binding energies and electron affinity for neutral (R-Ch)₂ (Ch = S, Se & Te; R= o-NO₂-Ph and PhCH₂) systems and binding energies of radical anionic counterparts. Binding energies are calculated by the energy cost associated to the generation of two radical monochalcogenides, Ph-Ch• (homolytic dissociation) in the neutral compounds. The heterolytic dissociation of radical anionic systems is considered to calculate their binding energies. This dissociation of radical anion systems produces the Ph-Ch• and Ph-Ch^{•-} fragments. Binding energy is decreased by 70% when an extra electron is added to the neutral (PhS)₂ system at MP2 level of theory in water medium. This decrease in binding energies are 75 % and 52 % for neutral (PhSe)₂ and (PhTe)₂ systems for the one electron attachment process. The binding energy of (PhS)₂^{•-} radical anion is lower by 2.7 kcal/mol compared to (PhSe)₂^{•-} radical anion in the water medium. Binding energy of (PhSe)₂^{•-} radical anion 7.3 kcal/mol lower than the (PhTe)₂^{•-} in the water medium. In the literature it is reported that the binding energies of neutral (PhSe)₂ system is more than the (PhTe)₂ system in non-polar solvent.⁷¹ Table 6.7 shows that this order of binding energies for neutral (PhSe)₂ and (PhTe)₂ systems persists even in polar solvent like water with the choice of ω -B97XD functional and MP2 level of theory. Table 6.7 also shows that the binding energies of Te based radical anionic systems are greater than their S/Se based analogues.

Table 6.7 #Energy data for neutral (o-R-Ph-Ch)₂ (Ch = S, Se and Te; R = H, CH₃, and OH; Ch = S, Se and Te) in water medium at the different levels of theory. Values in the braces show the energy data for the systems in presence of an excess electron.

Sr. no.	Method	Electron Affinity (eV)	Binding Energy (kcal/mol)	Electron Affinity (eV)	Binding Energy (kcal/mol)	Electron Affinity (eV)	Binding Energy (kcal/mol)
		Neutral (PhS) ₂ and (Ph-S) ₂ ^{•-} radical anion		Neutral (PhSe) ₂ and (Ph-Se) ₂ ^{•-} radical anion		Neutral (PhTe) ₂ and (Ph-Te) ₂ ^{•-} radical anion	
1.	i)	-3.3	54.5, (18.1)	-3.3	38.3, (18.6)	-2.9	54.0, (18.5)
2.	ii)	-3.2	58.0, (20.2)	-3.2	59.6, (17.8)	-3.0	58.8, (25.5)
3.	iii)	-3.2	58.3, (21.0)	-3.3	60.2, (20.5)	-3.3	49.9, (24.8)
4.	iv)	-3.2	43.2, (13.5)	-3.3	57.2, (20.8)	-3.0	62.5, (28.9)
5.	v)	-3.2	43.2, (13.2)	-3.3	56.4, (19.9)	-2.9	53.6, (21.8)
6.	vi)	-2.5	68.8, (20.5)	-3.0	92.4, (23.2)	-2.7	63.9, (30.5)
		Neutral (o-CH ₃ -PhS) ₂ and (o-CH ₃ -Ph-S) ₂ ^{•-} radical anion		Neutral (o-CH ₃ -PhSe) ₂ and (o-CH ₃ -Ph-Se) ₂ ^{•-} radical anion		Neutral (o-CH ₃ -PhTe) ₂ and (o-CH ₃ -Ph-Te) ₂ ^{•-} radical anion	
1.	i)	-3.2	33.0, (6.5)	-3.3	37.7, (8.2)	-2.9	51.1, (16.3)
2.	ii)	-3.4	38.4, (15.8)	-3.2	55.2, (17.2)	-2.9	57.7, (25.2)
3.	iii)	-3.4	39.2, (15.8)	-3.2	55.9, (17.2)	-3.0	57.7, (25.2)
4.	iv)	-3.3	41.8, (17.8)	-3.2	58.1, (21.4)	-3.0	61.5, (28.5)
5.	v)	-3.2	43.4, (14.8)	-3.2	56.0, (20.1)	-2.9	55.6, (22.4)
6.	vi)	-2.9	57.8, (24.3)	-3.0	94.9, (26.5)	-2.7	68.9, (33.0)
		Neutral (o-HO-PhS) ₂ and (o-HO-Ph-S) ₂ ^{•-} radical anion		Neutral (o-HO-PhSe) ₂ and (o-HO-Ph-Se) ₂ ^{•-} radical anion		Neutral (o-HO-PhTe) ₂ and (o-HO-Ph-Te) ₂ ^{•-} radical anion	
1.	i)	-3.3	31.0, (6.3)	-3.3	50.0, (14.0)	-2.9	52.4, (17.1)
2.	ii)	-3.4	35.4, (12.9)	-3.3	54.6, (22.2)	-2.9	57.7, (24.9)
3.	iii)	-3.4	36.2, (13.5)	-3.3	54.4, (22.4)	-2.9	57.5, (24.9)
4.	iv)	-3.3	38.8, (15.5)	-3.4	57.4, (24.7)	-3.0	61.3, (28.1)
5.	v)	-3.3	40.5, (12.4)	-3.4	55.0, (20.8)	-3.3	48.3, (21.6)
6.	vi)	-2.4	58.0, (13.6)	-3.0	62.9, (25.5)	-2.7	64.9 (30.7)

Table 6.8 #Energy data for neutral (o-NO₂-Ph-Ch)₂ (Ch = S, Se and Te), and (PhCH₂Ch)₂ in water medium at the different levels of theory. Values in the braces show the energy data for the systems in presence of an excess electron.

Sr. no.	Method	Electron Affinity (eV)	Binding Energy (kcal/mol)	Electron Affinity (eV)	Binding Energy (kcal/mol)	Electron Affinity (eV)	Binding Energy (kcal/mol)
		Neutral (o-NO ₂ -PhS) ₂ and (o-NO ₂ -Ph-S) ₂ ^{•-} radical anion		Neutral (o-NO ₂ -PhSe) ₂ and (o-NO ₂ -Ph-Se) ₂ ^{•-} radical anion		Neutral (o-NO ₂ -PhTe) ₂ and (o-NO ₂ -Ph-Te) ₂ ^{•-} radical anion	
1.	i)	-3.6	36.8, (9.5)	-3.7	32.4, (10.0)	-3.7	41.8, (31.2)
2.	ii)	-3.8	40.1, (15.6)	-3.9	39.9, (15.8)	-3.7	48.6, (37.5)
3.	iii)	-3.8	40.4, (16.1)	-3.7	40.1, (16.2)	-3.7	48.0, (37.1)
4.	iv)	-3.7	42.0, (18.1)	-3.7	40.2, (17.9)	-3.7	51.1, (40.5)
5.	v)	-3.7	46.3, (20.3)	-3.6	44.6, (20.7)	-3.6	50.4, (39.6)
6.	vi)	-2.9	63.9, (7.3)	-2.9	60.7, (21.0)	-2.9	58.0, (29.6)
		Neutral (PhCH ₂ S) ₂ and (PhCH ₂ S) ₂ ^{•-} radical anion		Neutral (PhCH ₂ Se) ₂ and (PhCH ₂ Se) ₂ ^{•-} radical anion		Neutral (PhCH ₂ Te) ₂ and (PhCH ₂ Te) ₂ ^{•-} radical anion	
1.	i)	-2.7	53.2, (15.7)	-3.0	55.6, (17.6)	-2.7	53.7, (17.6)
2.	ii)	-2.6	56.4, (18.0)	-4.2	59.1, (20.8)	-2.5	62.0, (21.8)
3.	iii)	-2.6	56.3, (18.4)	-4.2	59.5, (20.6)	-2.5	61.6, (21.3)
4.	iv)	-2.7	62.0, (21.5)	-4.2	61.2, (22.3)	-2.5	65.4, (21.2)
5.	v)	-2.7	55.2, (19.4)	-2.9	58.6, (18.9)	-2.5	62.2, (19.8)
6.	vi)	-2.3	61.6, (16.3)	-2.7	61.7, (21.1)	-2.2	65.3, (21.8)

Methods: B3LYP; 2) B3LYP-D; 3) B3LYP-D3; 4) B3LYP-D3BJ; 4) ω-B97XD; and 6) MP2, Basis set: 6-311++G(d,p) for C, H, O, N, S, Se atoms and 3-21G* for Te atom.

On adding $-\text{CH}_3$ groups at the ortho position of the two phenyl rings in $(\text{PhS})_2^{\bullet-}$ radical anion, the binding energy is increased by 3.8 kcal/mol compared to the unsubstituted S-analogue at MP2 level of theory in water medium. However, when the substituting group is $-\text{OH}$, the increase of 6.9 kcal/mol is observed with respect to $(\text{PhS})_2^{\bullet-}$ radical anion. In the case of $(o\text{-NO}_2\text{-PhS})_2^{\bullet-}$ system, the binding energy is decreased by 13.2 kcal/mol compared to unsubstituted S-analogue. The electron affinity of sulfur systems follows the order, $(o\text{-CH}_3\text{-PhS})_2 \approx (o\text{-NO}_2\text{-PhS})_2 > (o\text{-PhS})_2 > (o\text{-OH-PhS})_2$ at present level of theory. DFT functionals are not giving the correct account of electron affinity for these diaryl disulfides.

On substituting $-\text{CH}_3$ and $-\text{OH}$ groups at the ortho position of the two stacked phenyl rings in $(\text{PhSe})_2^{\bullet-}$ radical anion, the binding energies of the radical anions are increased by 3.3 kcal/mol and 2.3 kcal/mol respectively compared to the unsubstituted Se-based analogue. However, for $-\text{NO}_2$ substitution the decrease of 2.2 kcal/mol is observed with respect to unsubstituted Se-based analogue. The electron affinity of these neutral diaryl diselenides systems follows the order, $(o\text{-CH}_3\text{-PhSe})_2 \approx (o\text{-OH-PhSe})_2 \approx (o\text{-PhSe})_2 > (o\text{-NO}_2\text{-PhS})_2$ at MP2 level of theory in water medium. For these selenium based systems, $\omega\text{-B97XD}$ functional produces the electron affinity values comparable to MP2 level of theory. The calculated binding energies and electron affinity values are lower in sulfur based systems compared to the same selenium based systems at MP2 and $\omega\text{-B97XD}$ level of theory.

The binding energies of the $(o\text{-CH}_3\text{-PhTe})_2^{\bullet-}$ and $(o\text{-HO-PhTe})_2^{\bullet-}$ radical anions are increased by 2.5 kcal/mol and 0.2 kcal/mol respectively compared to the unsubstituted $(\text{PhTe})_2^{\bullet-}$ radical anion. In the case of $(o\text{-NO}_2\text{-PhTe})_2^{\bullet-}$ system, the binding energy is decreased only by 0.9 kcal/mol with respect to unsubstituted Te-based analogue. The electron affinity of these neutral

diaryl ditellurides systems follows the order, $(o\text{-NO}_2\text{-PhTe})_2 > (o\text{-CH}_3\text{-PhTe})_2 \approx (o\text{-OH-PhTe})_2 \approx (o\text{-PhTe})_2$ at MP2 level of theory in water medium. ω -B97XD functional produces the electron affinity values comparable to MP2 level of theory for these tellurium based systems. The calculated binding energies values are greater in tellurium based systems compared to the same sulfur/selenium based systems at MP2 and ω -B97XD level of theory. Electron affinities values of tellurium based systems shows more negative values than their sulfur based systems, but significantly have less negative values with respect selenium based systems at MP2 level of theory.

The binding energies of $(\text{PhCH}_2\text{S})_2^{\bullet-}$, $(\text{PhCH}_2\text{Se})_2^{\bullet-}$ and $(\text{PhCH}_2\text{Te})_2^{\bullet-}$ radical anions are calculated to be lower by 4.2 kcal/mol, 4.4 kcal/mol and 8.2 kcal/mol respectively compared to their phenyl based analogues (see Table 6.8). These observations indicate that geometrical flexibility incorporated by adding a $-\text{CH}_2-$ group does not play a significant role to stabilize these radical anions and electronic effects are expected to play a major role to stabilize/destabilize these systems.

Overall, the $(o\text{-CH}_3\text{-Ph-Te})_2^{\bullet-}$ radical anionic system has the highest binding energy among all the (radical anionic systems. Its neutral system $(o\text{-CH}_3\text{-Ph-Te})_2$ has the highest electron affinity among reported dichalcogen neutral systems. The presence of $-\text{NO}_2$ at ortho position in $(\text{Ph-Te})_2^{\bullet-}$ radical anionic system marginally affect the binding energy in comparison to their sulfur/selenium based analogues. In sum, the binding energies and electron affinities calculated using ω -B97XD functional gives the values comparable to MP2 level of theory in water medium. It is to be noted that the combination of binding energy and electron affinity of the neutral systems suggested that $(o\text{-CH}_3\text{-Ph-Te})_2^{\bullet-}$ radical anionic system is the best suitable antioxidant among all radical anionic systems.

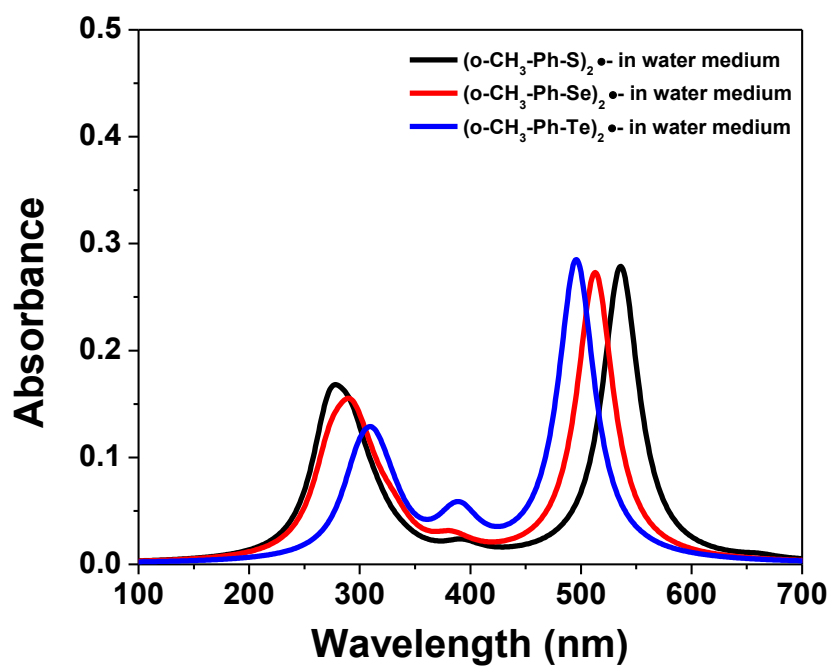
6.3.6 Excited state for (R-Ch)₂^{•-} radical anions (Ch = S, Se & Te; R=Ph, o-CH₃-Ph, and o-HO-Ph) systems

Excited-state calculations are carried for radical anions of (R-Ch)₂^{•-} (Ch = S, Se & Te; R=Ph, and o-CH₃-Ph,) systems applying TDDFT procedure considering CAM-B3LYP functional and for H, C, O, S, Se atoms basis sets used are 6-311++G(d,p) for Te atom basis set used is 3-21G* to find out a few low lying optical absorption bands. Table 6.9 presents the λ_{max} of the absorption bands with corresponding oscillator strengths (*f*) and molecular orbitals involved in electronic transitions. Figure 6.5a shows in the UV-Vis spectra of (Ph-S)₂^{•-} radical anion, the strong absorption band is produced at 509 nm in water medium. The origin of this band is mainly due to transition from H-1 → L orbitals. A relatively weak intensity band is also observed at 290 nm. In case of UV-Vis spectra of (Ph-Se)₂^{•-} radical anion, a strong absorption band is obtained at 482 nm and a weak intensity band at 304 nm (see Figure 6.5a). The origin of strong absorption band is mainly due to transition from H-2 → L orbitals. For (Ph-Te)₂^{•-} radical anion, Similarly, in the UV-Vis spectra of (Ph-Te)₂^{•-} radical anion, a strong and a weak absorption bands are produced at 488 nm and 308 nm respectively. The origin strong absorption band is mainly due to transition from H-1 → L orbitals. Ongoing from (Ph-S)₂^{•-} to (Ph-Se)₂^{•-} the strong absorption band undergoes blue shift of 21 nm and ongoing from (Ph-Se)₂^{•-} to (Ph-Te)₂^{•-} the strong absorption band undergoes red shift of 4 nm in the

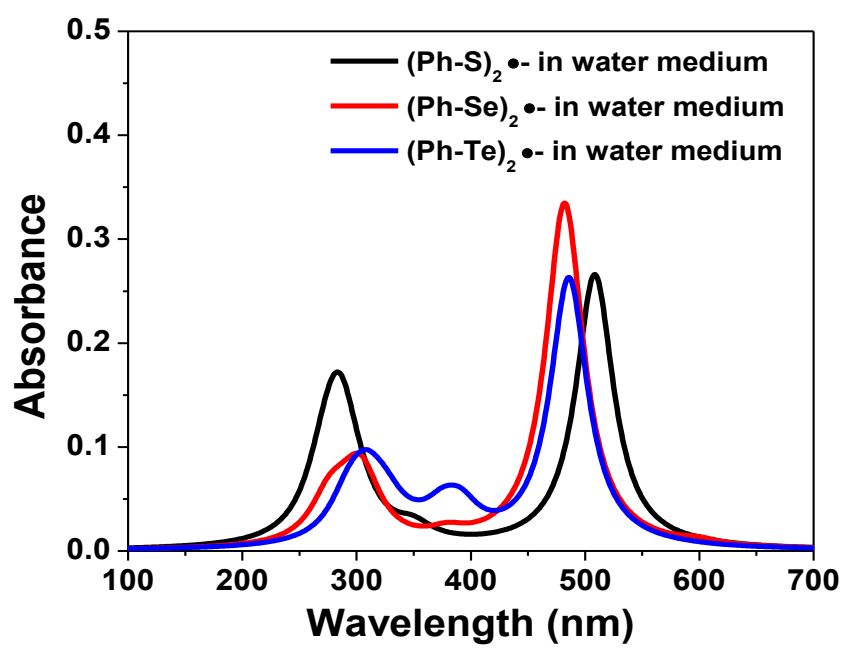
Table 6.9 #Excited state data for (RCh)₂^{•-} (Ch = S, Se & Te: R = Ph, and o-CH₃-Ph) and (PhCh)₂^{•-}.2H₂O radical anions in water medium.

	(PhS) ₂ ^{•-} radical anion			(PhSe) ₂ ^{•-} radical anion			(PhTe) ₂ ^{•-} radical anion		
Sr. no.	λ_{\max} (nm)	Oscillator strength (<i>f</i>)	Transitions involved	λ_{\max} (nm)	Oscillator strength (<i>f</i>)	Transitions involved	λ_{\max} (nm)	Oscillator strength (<i>f</i>)	Transitions involved
1.	509	0.264	H-1 → L (0.86)	482	0.333	H-2 → L (0.94)	486	0.260	H-1 → L (0.96)
2.	326	0.025	H-4 → L (0.55)	304	0.057	H-4 → L (0.78)	391	0.027	L → L+2 (0.60)
	(o-CH ₃ -PhS) ₂ ^{•-} radical anion			(o-CH ₃ -PhSe) ₂ ^{•-} radical anion			(o-CH ₃ -PhTe) ₂ ^{•-} radical anion		
1.	534	0.277	H-2 → L (0.80)	513	0.271	H-1 → L (0.97)	496	0.282	H-1 → L (0.73)
2.	272	0.107	H → L+7 (0.55)	291	0.071	L → L+7 (0.56)	392	0.024	L → L+2 (0.52)
	(PhS) ₂ ^{•-} .2H ₂ O radical anion			(PhSe) ₂ ^{•-} .2H ₂ O radical anion			(PhTe) ₂ ^{•-} .2H ₂ O radical anion		
1	764	0.007	H → L (0.83)	811	0.008	H → L (0.92)	839	0.001	H → L (0.99)
2	496	0.258	H-1 → L+2 (0.83)	495	0.240	H-1 → L (0.92)	483	0.211	H-1 → L (0.92)

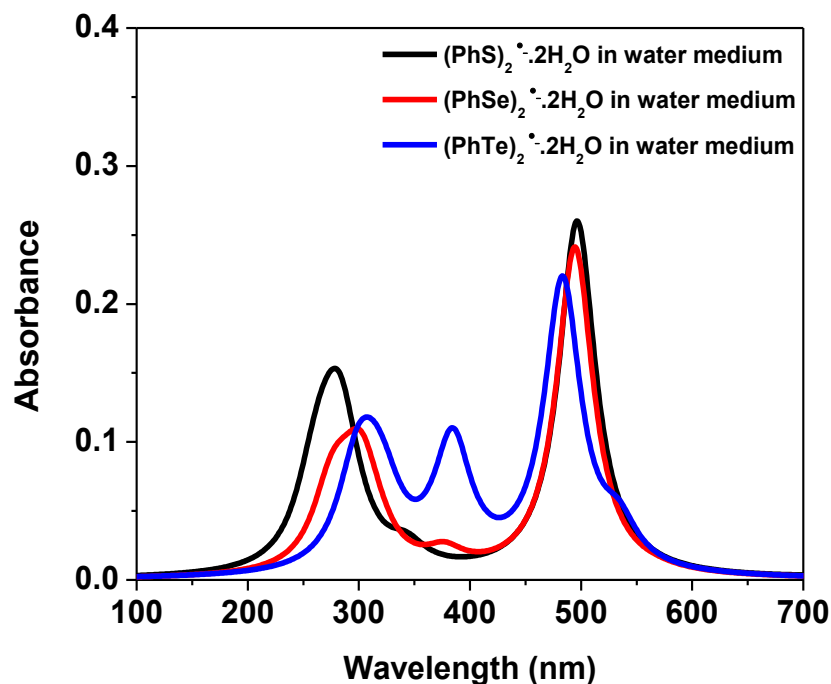
#Method: i) CAM-B3LYP Functional, ii) Basis set: 6-311++G(d,p) for H, C, O, S, and Se and iii) For Te atom 3-21G* basis set is used.



a



b



c

Figure 6.5 UV-Vis spectra calculated at CAM-B3LYP level of theory for 23 (a) $(\text{PhCh})_2^{\bullet-}$ (Ch = S, Se & Te) radical anions in water medium (b) $(o\text{-CH}_3\text{-PhCh})_2^{\bullet-}$ (Ch = S, Se & Te) radical anions in water medium, c) $(\text{PhCh})_2^{\bullet-} \cdot 2\text{H}_2\text{O}$ (Ch = S, Se & Te) Basis set: 6-311++G(d,p) for C, H, O, S and Se atoms and 3-21G* for Te atoms.

water medium. The weaker band in the UV-Vis spectra of $(\text{Ph-S})_2^{\bullet-}$ radical anion undergoes red shift compared to Se/Te based analogues as the size of chalcogen atom increases. The UV-Vis spectra of ortho-methyl substituted analogues of $(\text{Ph-Ch})_2^{\bullet-}$ (Ch = S, Se & Te) is shown in Figure 6.5b. It shows that, one strong and one weak intensity peak are obtained at 534 nm and 272 nm in the water medium. The origin of weak and strong absorption peak are mostly due to transition from $\text{H} \rightarrow \text{L}+1$ orbitals and $\text{H}-1 \rightarrow \text{L}$ orbitals respectively. In case of $(o\text{-CH}_3\text{-Ph-Se})_2^{\bullet-}$, one weak intensity peak is at 291 nm and one strong absorption peak is at 513 nm in water medium. The origin of weak and strong absorption peak are mostly due to transition from

$L \rightarrow L+7$ orbitals and $H-2 \rightarrow L$ orbitals respectively. For $(o\text{-CH}_3\text{-Ph-Te})_2^{\bullet-}$, one weak intensity peak is at 312 nm and one strong absorption peak is at 496 nm in the water medium. The origin of weak and strong absorption peaks are mostly due to transition from $L \rightarrow L+6$ orbitals and $H-1 \rightarrow L$ orbitals respectively. So as the size of chalcogen atom increases in the order $S < Se < Te$, the weaker band undergoes red shift and strong absorption band undergoes blue shift for $(o\text{-CH}_3\text{-Ph-Ch})_2^{\bullet-}$ ($Ch = S, Se \text{ \& } Te$). Further, the two water are explicitly added at 2.5 Å on $(Ph\text{-}Ch)_2^{\bullet-}$ ($Ch = S, Se \text{ \& } Te$) and then all possible structures are optimized at MP2/6-311++G(d,p) level of theory in water medium for $(Ph\text{-}Ch)_2^{\bullet-} \cdot 2H_2O$ ($Ch = S \text{ \& } Se$).

However, for $(Ph\text{-}Te)_2^{\bullet-} \cdot 2H_2O$, the two water are explicitly added at 2.5 Å on $(Ph\text{-}Ch)_2^{\bullet-}$ ($Ch = O, S, Se \text{ \& } Te$) and then all possible structures are optimized at MP2 level of theory with 6-311++G(d,p) basis set for H, C atoms and 3-21G basis set for Te atom in water medium. The most stable structures obtained are being used for UV-spectral calculations for $(Ph\text{-}Ch)_2^{\bullet-} \cdot 2H_2O$ ($Ch = S, \text{ \& } Se$) using CAM-B3LYP functional (as shown in Figure 6.5c). It is found that the, as the size of chalcogen atom increases in the order, $S < Se < Te$, the strong absorption band undergoes blue shift and weak absorption band undergoes red shift for $(Ph\text{-}Ch)_2^{\bullet-} \cdot 2H_2O$ ($Ch = S, Se \text{ \& } Te$) in the water medium.

6.3.7 Frontier molecular orbital for the $(o\text{-CH}_3\text{-Ph-Te})_2^{\bullet-}$ radical anionic system

Visualizations of selected molecular orbitals for the most stable $(o\text{-CH}_3\text{-Ph-Te})_2^{\bullet-}$ radical anion are important to understand the bonding features and molecular orbital involved electronic transitions. Selected molecular orbitals involved in the electronic transition of the major optical band of the $(o\text{-CH}_3\text{-Ph-Te})_2^{\bullet-}$ radical anion systems studied at present are displayed in

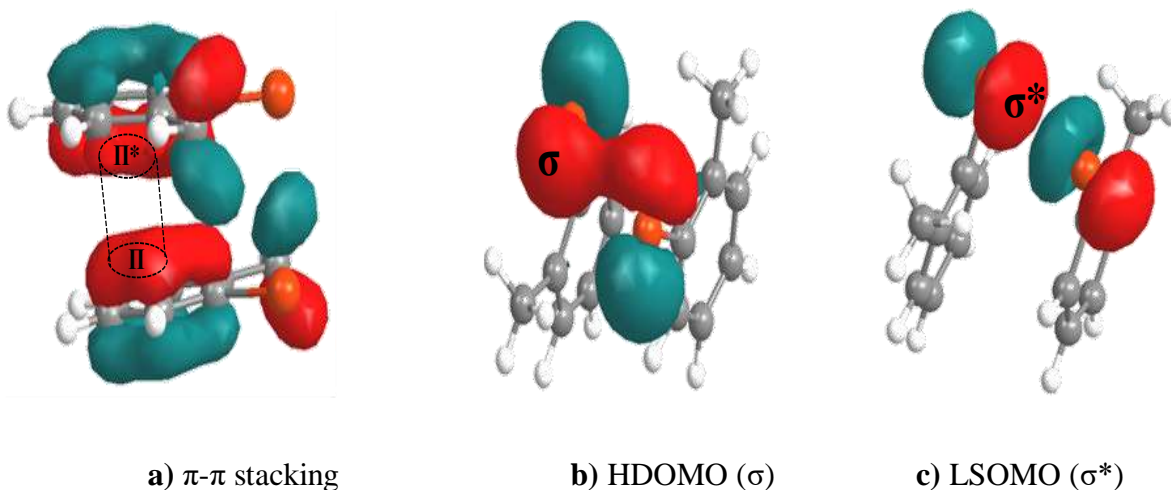


Figure 6.6 Molecular orbital diagrams for $(o\text{-CH}_3\text{-PhTe})_2^{\bullet-}$ calculated at MP2 level of theory with 3-21G* basis for Te atoms and 6-311++G(d,p) for all other atoms in water medium. (HDOMO = highest doubly occupied molecular orbital and LSOMO = lowest singly occupied molecular orbital. Molecular orbital diagrams are plotted with contour cut-off value of 0.04 a.u..

Figure 6.6(a-c). These orbitals are based on the most stable structures of the radical anions in water medium calculated at MP2 level with 6-311++G(d,p) basis set for C, H atoms and 3-21G* for Te atoms in water medium. Molecular orbital diagram for most stable structure of $(o\text{-CH}_3\text{-Ph-Te})_2^{\bullet-}$ shows π - π stacking of two phenyl rings (Figure 6.6a). Figure 6.6b clearly shows the head-on mixing of two p-orbitals of two Te atoms and results into sigma σ type bonding orbital. This σ type bonding orbital clearly shows the 2c-3e bond present in the most stable structure of $(o\text{-CH}_3\text{-Ph-Te})_2^{\bullet-}$ in the water medium. However, two p-orbitals of opposite symmetry are orientated towards each other indicating the presence of an antibonding sigma (σ^*) orbital Figure 6.6c. So the origin of most intense transition are labelled as $\sigma \rightarrow \sigma^*$ type transition for $(o\text{-CH}_3\text{-Ph-Te})_2^{\bullet-}$ in the water medium. Not only that, the most intense transitions for all other sulfur, selenium and Tellurium based radical anionic systems are also originating from $\sigma \rightarrow \sigma^*$ type transition.

6.4 Conclusions

The effect of an excess electron on geometry, nature of bonding and stability of diaryl dichalcogenides, namely, $(RCh)_2^{\bullet-}$ (Ch = S, Se & Te; R = Ph, o-CH₃-Ph, o-HO-Ph & PhCH₂) is studied. Calculated dihedral angle, $\delta(CXXC)$ at B3LYP level and B3LYP-D level including dispersion parameters (D and D3) are found to be significantly larger than MP2 data in both neutral and anionic diaryl dichalcogenides systems. However, the same calculated applying ω -B97XD functional has less errors. The dihedral angle calculated at CCSD level is smaller than MP2 value indicating less displacement of phenyl rings in case of systems with an excess electron. However, the said dihedral angles calculated for neutral systems are same at the two post-HF levels. Dispersion corrections are found to be essential for S, Se, Te based dichalcogen systems for binding energy calculations. These dichalcogenides have high electron affinity in water medium and should be able to capture electron efficiently suggesting their antioxidant property in water medium. The (o-CH₃-Ph-Te)₂^{•-} radical anionic system has highest binding energy among all the (o-R-Ph-Ch)₂^{•-} radical anionic systems. Its neutral system (o-CH₃-Ph-Te)₂ has highest binding energy and electron affinity among all neutral systems at MP2 level of theory in water medium. It is shown that in the presence of an excess electron, these diaryl dichalcogen systems are bound by two-centre three-electron bond between two chalcogen (S/Se/Te) atoms. Visualization of frontier molecular orbital of the most stable equilibrium structures suggests that sulfur and selenium valence p-orbitals are mixed head-on indicating sigma character of the two center three electron bond between two S/Se/Te atoms in these radical anions. The origin of the strong absorption bands in the visible region are assigned to be electronic transition from σ bonding orbital to antibonding σ^* orbital.

Theoretical studies on selected organic chalcogen systems

In this study, selected chalcogens (S, Se, and Te) based organic systems are studied in detail using first principle based electronic structure calculations. This work includes the chalcogen based π -conjugated helical systems which may be very important in future as organic optoelectronic devices. Further, the present study also provides a model system to find suitable antioxidant based on diaryl dichalcogenides radical anions.

The theoretical calculations predict that the chalcogen based β -helicenes systems are non-planar and flexible when the number of fused rings are three or more. As expected, HOMO-LUMO energy gap decreases as the number of fused ring increases. Further, band gap calculated applying periodic boundary conditions (PBC) for neutral chalcogen based $[n]$ helicenes shows that band gap decreases as the number of fused rings increases. Comparative studies on chalcogen based β -helicenes (chalcogen = S, Se and Te) show that energy gap of these systems decreases as the size and polarization of chalcogen atoms increases. Excited-state studies show that the radical cations generated from chalcogen based $[n]$ helicenes have strong absorption in near infrared region (NIR) region. IR peaks obtained in UV-Visible spectra for telluro[7]helicene radical cation have stronger absorption compared to the IR peaks obtained for thia[7]helicene and seleno[7]helicene radical cations in DCM solvent. A case study on unsubstituted thia[7]helicene radical cation shows that the radical cation generated from its corresponding neutral thia[7]helicene system has a very low probability of dimerization in non-polar solvent. In addition, case study on seleno[7]helicene radical cation shows that the extent of dimerization is less in comparison to thia[7]helicene radical cation. This dimerization probability is less in the presence of counter ion PF_6^- . A case study on telluro[7]helicene radical cation shows that these systems have a lower tendency for dimerization.

The present work also includes model systems based on diaryl dichalcogenides radical anions in search of a suitable antioxidant system. The effect of an excess electron on geometry, nature of bonding and stability of diaryl dichalcogenides, namely, $(\text{RCh})_2^{\bullet -}$ (Ch = S, Se & Te: R = Ph, PhCH_2 , o- NO_2 -Ph, o- HO -Ph, & o- CH_3 -Ph,) radical anions is studied. One electron reduction of neutral diaryl dichalcogenides leads to the formation of two-center three-electron (2c-3e) bonded radical anionic systems. These diaryl dichalcogenides radical anions show π - π stacking of two phenyl rings in water medium. They have high electron affinity in water medium and their corresponding neutral systems have a strong ability to capture electron efficiently suggesting their antioxidant property. Present calculations indicate that among all $(\text{RCh})_2^{\bullet -}$ radical anions, the (o- CH_3 -Ph-Te) $_2^{\bullet -}$ and (o- CH_3 -Ph-Se) $_2^{\bullet -}$ systems are suitable antioxidant in water medium. The UV-Vis spectral studies show that in water medium diaryl dichalcogenides radical anions strongly absorb in visible region. The origin of the strong absorption bands in the visible region are assigned to the $\sigma \rightarrow \sigma^*$ type electronic transition.



Homi Bhabha National Institute

Report of Ph.D. Viva-Voce

Board of Studies in Chemical Sciences

A. General Details:

1. **Name of the Constituent Institution:** Bhabha Atomic Research Centre

2. **Name of the Student:** Shri Rahul Kumar

3. **Enrolment Number:** CHEM01201404024

4. **Date of Enrolment in HBNI:** 01/08/2014

5. **Date of Submission of Thesis:** 14/02/2020

6. **Title of the Thesis:** Theoretical Studies on Selected Organic Chalcogen Systems

7. **Number of Doctoral Committee Meetings held with respective dates:**

Review Period	Date	Review Period	Date
1. 01/08/2015-31/07/2016	06/08/2016	2. 01/08/2016-31/07/2017	16/10/2017
3. 01/08/2017-31/07/2018	27/08/2018	4.	
5.		6.	

8. **Name and Affiliation of the Thesis Examiner 1:** Prof. Michio Iwaoka, Tokai University

Recommendations of the Examiner 1 (Thesis Evaluation) (i) accepted, (ii) accepted after revisions, or (iii) rejected: Accepted

9. **Name and Affiliation of the Thesis Examiner 2:** Prof. Raghavan B. Sunoj, Department of Chemistry, IIT

Recommendations of the Examiner 2 (Thesis Evaluation) (i) accepted, (ii) accepted after revisions, or (iii) rejected: Accepted

B. Record of the Viva-Voce Examination

- 1. Date of Viva Voce Examination:** 27/05/2020
- 2. Name and affiliation of External Examiner:** Raghavan B. Sunoj, Department of Chemistry, IIT
- 3. Whether there were other experts / faculty/students present ? Please enclose a soft copy of attendance sheet indicating participation in person/over video as per proforma given below at (5)**
- 4. Recommendations for the award of the Ph.D. degree:** Recommended
- 5. Attendance at Viva Voce (Doctoral Committee, External Examiner, others):**

Sr No	Composition	Name	Attended in person or through video; if in person, signature
1.	Chairman	Prof. A. K. Arya	
2.	Convener (Guide)	Prof. D. K. Maity	
3.	External Examiner	Prof. R. B. Sunoj	
4.	Member	Prof. C. Majumder	
5	Member	Prof. Musharaf Ali	
6.	Member	Prof. KRS. Chandrakumar	

(Convener, Viva Voce Board)



Homi Bhabha National Institute

CHECK LIST FOR 11 CRITERIA AS PER UGC (MINIMUM STANDARD AND PROCEDURE FOR AWARD OF PH.D. DEGREE) REGULATION 2009¹

1. Name of the Student: *Shri Rahul Kumar*
2. Name of the Constituent Institution: *BARC*
3. Enrolment No.: *CHEMO1201404024*
4. Board of Studies: *Chemical Sciences*

Sr. No.	Particular	Remark (Tick the appropriate one)
1.	Mode of selection for Ph.D. Programme	Written Test / Interview / Both ✓
2.	Number of Ph.D. students under the guide ≤ 8 during the period	Yes / No ✓
3.	Reservation Policy applied for selection	Yes / No ✓
4.	Course work done	Yes / No ✓
5.	Reviews of Annual Progress held	Yes / No ✓
6.	Test on Research Methodology held	Yes / No ✓
7.	Pre-synopsis presentation held	Yes / No ✓
8.	At least 1 journal paper published	Yes / No ✓
9.	At least of 2 papers in conference / seminar presented	Yes / No ✓
10.	Evaluation reports of Ph.D. Thesis from guide and two experts (one expert is out of state) received	Yes / No ✓
11.	Soft copy of Thesis submitted to HBNI	Yes / No ✓

Dean-Academic

To
Dean, HBNI

¹Ph.D. student has to fulfill all the 11 criteria laid by UGC to meet eligibility criteria for employment in Indian Universities. HBNI will issue required certificate only if a student meets all the eleven criteria.



Homi Bhabha National Institute

Training School Complex, 2nd Floor, Anushaktinagar, Mumbai 400 094

Tel. : 022-25597627

e-mail: registrar@hbni.ac.in

20th August 2018

No. HBNI/ RO-(1)/ 2018

CIRCULAR

The University Grants Commission, vide its Gazette notification No. 287, dated 31st July 2018 issued guidelines on promotion of academic integrity and prevention of plagiarism in higher education institutions. As per these guidelines, the thesis submitted by students shall be certified to be plagiarism-free, using tools that can detect plagiarism. The guidelines also prescribe penalty for plagiarism.

The guidelines have been displayed on the HBNI website and also circulated to all CIs for necessary action, vide Circular dated 6th August 2018.

Meanwhile, the HBNI Central Office is receiving queries for processing of PhD thesis for award of the degree, until such time that the software for plagiarism detection is procured and commissioned by the CIs/OCC. After deliberations and due processes, the following course of action is suggested:

1. All CIs/OCC shall immediately initiate necessary action to procure and commission the software for detection of plagiarism on or before Dec. 31st 2018. (It is also noted that few CIs have already procured such software and is in use).
2. Starting 1st January 2019, every thesis, at the time of submission to the Dean (Academic), shall be accompanied by a certification from the student and the supervisor as required by Clause no. 6 (a & b) and Clause no. 6 (c, d & f) of the UGC guidelines.
3. Pending procurement of the software, the thesis will be accompanied by the certificate from the student, duly endorsed by the supervisor, as given in the format enclosed, Annexure 1.
4. Deans (Academic) are requested to ensure that theses are forwarded to HBNI for processing only if they are accompanied by the Certificate. Effective from 1st September 2018, thesis not accompanied by the Certificate will not be processed by the Central Office for award of the degrees.

This is issued with the approval of Competent Authority.

Dr. Chandrasekar
REGISTRAR

All the Deans (Academics), CIs/ OCC
The Vice Chancellor, HBNI
The Dean, HBNI
Prof. D.K. Maity, Associate Dean, HBNI

CERTIFICATION ON ACADEMIC INTEGRITY

1. I Shri Rahul Kumar (name of student) HBNI Enrolment No. CHEM01201404024 hereby undertake that, the Thesis titled Theoretical studies on selected organic chalcogen systems is prepared by me and that the document reports the original work carried out by me and is free of plagiarism.

2. I am aware and undertake that if plagiarism is detected in my thesis at any stage in future, suitable penalty will be imposed as per the applicable guidelines of the Institute/ UGC.

Rahul Kumar
15/06/2020

Signature of the Student
(with date)

Endorsed by the PhD Supervisor

Signature (with date)

Name:

Designation:

Department/ Centre:

Name of the CI/ OCC:



Homi Bhabha National Institute

SYNOPSIS OF Ph. D. THESIS

1. **Name of the Student:** Rahul Kumar
2. **Name of the Constituent Institution:** Bhabha Atomic Research Centre
3. **Enrolment No. :** CHEM01201404024
4. **Title of the Thesis:** Theoretical studies on selected organic chalcogen systems
5. **Board of Studies:** Chemical Sciences

SYNOPSIS

The chalcogens are the elements that belong to the 16th group of the periodic table. These elements are oxygen (O), sulfur (S), selenium (Se), tellurium (Te), and polonium (Po). As Po is highly radioactive metal, the Po-based systems are scarcely known. Chalcogens exist in wide range of oxidation states from -2 to +6. Due to available d orbitals in S, Se and Te, they have increased flexibility of valence and can easily form bonds with other atoms. Due to this reason, the variety of conjugated organic materials are found based on these elements. These materials are essential and finding their application as electronic devices, antioxidant, catalysis, biologically active compounds, and medicine.¹⁻⁵

The band gap of thiophene lies in the ultraviolet region of the electromagnetic spectrum. To use thiophene based systems in organic electronic devices the fine tuning of band gap is always required to get a suitable energy gap (in semiconductor region).⁵ Based on literature survey, various types of methods can achieve the fine-tuning of band gap. These methods involve linear coupling or fusion of thiophene rings, doping, and changing their shape (e.g. converting a film into nanotubes) etc.⁵⁻⁷ But, the most convenient methods for tuning the band gap involves the linear coupling or fusion of thiophene subunits. These systems produced by above schemes have planar and rigid structures with strong π -conjugation. The spectral studies of α -oligothiophenes show that these systems absorb mainly in UV region and their corresponding radical cations have strong absorption in the UV-visible range in non-polar solvent.⁸ The ESR studies on the radical cations of unsubstituted α -oligothiophenes show radical cations generated are stable only at very low temperature.⁸ The π -conjugation leads to strong intermolecular interactions in the solution and solid-state. Several studies suggested that due to these intermolecular interactions, the π -dimerization become an inherent property of conjugated α -oligothiophenes and their corresponding radical cations.^{8,9} It is worth mentioning that

the dimerization affects the spectral features, energy gap and stability, which limits the utility and performance of these systems. However, this problem can be resolved by using the flexible systems of cross-conjugated fused thiophenes. After, the successful synthesis of thia[3]helicene and thia[7]helicene these systems attracted recent attention because of their flexible shape and unusually strong optical properties.^{10,11} Thia[7]helicene system has relatively large optical band gap, ~ 3.5 eV.¹¹ Not only that, [7]helicene is fairly stable at room temperature (~ 11 h).¹¹ Later on, a configurationally stable radical of thia[7]helicene is generated via electrochemical oxidation in DCM solvent.¹² The generated thia[7]helicene radical cation is stable up to ~ 15 min at room temperature.¹² The reason for this extraordinary stability of thia[7]helicene radical cation may lie in its helical structure. The generated radical cation has strong absorption in near-infrared region (NIR) in DCM solvent.¹² Thus, it is a critical system for making detector in the NIR region, which further may be useful in military applications. However, no systematic study available that provide the information of effect of size of thia[n]helicenes systems. In addition, one can expect larger ring size radical cations produced from their corresponding neutral thia[n]helicenes may also be stable in DCM solvent. Not only that, as size and polarizability of follows the order, $\text{Te} > \text{Se} > \text{S}$ the replacing sulfur from selenium or tellurium provide novel systems which may have enhanced electronic and structural features that may attract the interest of the theoretical as well as experimental chemists. Therefore, a theoretical investigation is performed on neutral as well as radical cation of chalcogens based [n]helicenes (S, Se and Te) in the quest of novel systems to be used in organic electronic devices.

Based on the above discussion, the present thesis deals with a theoretical study on structure, ionization energies, and energy gaps of the chalcogens (S, Se and Te) based [n]helicenes ($n=1-10$) using *ab initio* quantum chemistry-based methods. The direct band gap of chalcogens based [n]helicenes is also being calculated using PBC-DFT

methods. This systematic theoretical study is further extended to the radical cations generated from their corresponding neutral chalcogens based [n]helicenes. As UV-Visible spectral reports for thia[3]helicene and thia[7]helicene are available in DCM solvent. So, DCM is used for all solvent-based calculations in conjunction with solvation model based on the solute density (SMD). Besides, structures, energy gaps, electronic spectral properties are being reported for radical cations of chalcogens based [n]helicenes (n=1-10) in DCM solvent. The frontier molecular orbital diagrams are also calculated for radical cations of chalcogens based [n]helicenes (n=1-10) in DCM solvent. The types of molecular orbital involved in NIR transitions are also being labeled using the analysis of LCAO-MO orbitals using their coefficients of atomic orbitals. Further, a case study on the π -dimer of the unsubstituted and substituted, neutral and radical cation of thia[7]helicene and seleno[7]helicene are also being carried out to understand the dimerization process in DCM solvent. Overall, this study explores the structural and electronic properties of neutral and radical cations of chalcogens based [n]helicenes in search of optical material for applications in wide energy gap systems and NIR devices.

The antioxidant activity of diphenyl diselenides is due to electron donating nature of its corresponding radical anion system. Further, its activity can be modulated by inserting suitable substituents on phenyl rings. Later on, it is found that diphenyl ditellurides also has the antioxidant activity and surprisingly it is not significantly more toxic than organoselenium analogues.¹³ Thus, aim of this work is to prepare a model system to find out the dichalcogen based efficient antioxidant considering following points, 1) the effect of chalcogen (S, S, and Te) atoms, 2) effect of electron donating and electron withdrawing substituents on suitable aryl (phenyl) ring, and 3) effect of water medium. The extra electron in diaryl based dichalcogen radical anionic systems is accommodated in the lowest unoccupied molecular orbital, which is often an antibonding sigma orbital. Having two electrons in the highest bonding sigma

orbital and one electron in the lowest antibonding sigma orbital results in the formation of a half bond (bond order = 0.5) and hence these 2c-3e bond is also known as hemi bond or half bond.¹⁴

Based on the above discussion, this thesis also includes a theoretical study on the antioxidant properties of chalcogen (S, Se and Te) based dichalcogen systems with an excess of electrons. These chalcogens having exciting structural properties, stability with high antioxidant activity in water medium. This work deals with the electron acceptor properties of dichalcogen systems, of the type R-Ch-Ch-R (Ch = S, Se and Te; R= Ph, PhCH₂, o-NO₂-Ph, o-HO-Ph, and o-CH₃-Ph) and the newly formed 2c-3e bonds in their anionic (R-Ch-Ch-R)⁻ states. Bond strength of a 2c-3e bond is expected to depend on the combined effects of structural parameters, substitution patterns and electronic interactions. The combined effects are expected to control the extent of p-orbital interaction that in turn is expected to influence the strength of the newly formed bond. These studies may serve as a model for understanding the antioxidant behaviour of these dichalcogen systems.

This thesis is organized in 7 chapters. A brief description of each chapter is given below:

Chapter 1: It is the introductory chapter of the thesis. It provides a general description of chalcogen (S, Se and Te) based organic systems. Based on available experimental and theoretical studies, the gap areas are identified and discussed. Further, this chapter gives the objective, organization and scope of the present thesis.

Chapter 2: This chapter introduces the computational methods used in the electronic structure calculations in present work. Various aspects of quantum chemistry like Density Functional Theory (DFT), Perturbation Theory (PT), Coupled-Cluster Theory (CC) and Time-dependent Density Functional Theory (TDDFT) are discussed briefly.

The solvation model based on solute density (SMD) is explained in details. Further, the basis sets, various geometry optimization techniques, frontier molecular orbital calculations and band gap calculations are explained briefly in this chapter.

Chapter 3: This chapter deals with the structures, stability, ionization energies, energy gap of thia[n]helicenes (n=1-10) in the gas phase and DCM solvent. The benchmarking done to decide upon a suitable level of theory is provided in this chapter. The minimum energy structures of thia[n]helicenes radical cation are also calculated in the gas phase as well in DCM solvent. Geometrical parameters for the minimum energy structures are compared with available single crystal X-Ray data. Excited state study for radical cations of thia[n]helicene shows that these systems strongly absorb in NIR region in DCM solvent. UV-visible spectral data generated are also compared with available spectral data. A case study on π -dimers of neutral and radical cation of thia[7]helicene is also performed considering both unsubstituted and end substituted case to check the extent of π -dimerization process in DCM solvent. Overall, the present studies may be useful to get various systems based on these thia[n]helicenes to find applications as organic electronic devices.

Chapter 4: This chapter represents the selenium-based analogues of thia[n]helicenes. They are the first reported selenophene β -helical systems of this type motivated from their corresponding thia[n]helicenes. Due to unavailability of single X-Ray and spectral data the methods used for thia[n]helicenes systems are used to get structures, stability, ionization energies, energy gap and UV-Visible spectra of seleno[n]helicenes (n=1-10) in the gas phase and DCM solvent. Excited state study for radical cations of seleno[n]helicenes shows that these systems strongly absorb in NIR region in DCM solvent. A case study on π -dimers on π -dimer unsubstituted and substituted radical cations of seleno[7]helicene without and with counter anion PF_6^-

are also being performed to understand the extent of π -dimerization process in DCM solvent. Overall, these selenophene-based systems may be useful in organic electronic devices.

Chapter 5: These chapter deals with first reported telluro[n]helicenes systems motivated from their corresponding thia[n]helicenes. This chapter mainly deals with the effects of size chalcogen atom on ionization energies, energy gap and band gap of neutral chalcogen (chalcogen= S, Se and Te) based β -helicenes (n=1-10). Due to unavailability of X-Ray and spectral data the methods used for thia[n]helicenes systems are extended to get structures, stability, ionization energies, energy gap and UV-Visible spectra of telluro[n]helicenes (n=1-10) in the gas phase and DCM solvent. PBC-DFT calculations are performed to get the direct band gap for chalcogen based [n]helicenes. Excited state study for radical cations of telluro[n]helicene in DCM solvent shows that these systems absorb strongly than their corresponding radical cationic systems of thia[n]helicenes and seleno[n]helicenes in NIR region of electromagnetic spectrum. Overall, these tellurophene based systems are identified as potential candidate to be used in organic electronic devices.

Chapter 6: This chapter provides a model system for understanding the antioxidant behavior of dichalcogen systems the benchmarking is done to decide upon a suitable level of theory. The minimum energy structures for neutral and diaryl dichalcogenides radical anions are calculated in the gas phase as well in water medium. Geometrical parameters for the minimum energy structures are compared with available X-Ray data and microwave structural data. Based on the stability and have high electron affinity (corresponding neutral) in water medium the high antioxidant systems are identified. Excited state spectra of diaryl dichalcogenides radical anions show the

strong absorption bands in the visible region. These studies may serve as a model for understanding the antioxidant behaviour of these dichalcogen radical anionic systems.

Chapter 7: In this chapter, the conclusions drawn from the work carried out in the present thesis and future scope related to this topic of research is thoroughly discussed. In future, the band structures and phonon calculations can be done for all chalcogens based β -helicenes. Synthesis of seleno[n]helicenes and telluro[n]helicenes & spectral measurement should also be carried out to generate the experimental data to validate the theoretical results. The studies on measurement of antioxidant activity should be carried to get the kinetics of reaction between free radicals dichalcogen based antioxidant systems.

References

- 1 A. Mishra, C. Ma and P. Ba, *Chem. Rev.*, 2009, **109**, 1141-1276.
- 2 M. J. Sung, A. Luzio, W. T. Park, R. Kim, E. Gann, F. Maddalena, G. Pace, Y. Xu, D. Natali, C. de Falco, L. Dang, C. R. McNeill, M. Caironi, Y. Y. Noh and Y. H. Kim, *Adv. Funct. Mater.*, 2016, **26**, 4984-4997.
- 3 F. Zaccaria and L. P. Wolters, *J. Comput. Chem.*, 2016, **37**, 1672-1680.
- 4 F. Asuka, W. Dandan, *Chem. Sci.*, 2017, **8**, 2667-2670.
- 5 M. E. Cinar and T. Ozturk, *Chem. Rev.*, 2015, **115**, 3036-3140.
- 6 F. Böttger-Hiller, A. Mehner, S. Anders, L. Kroll, G. Cox, F. Simon and S. Spange, *Chem. Commun.*, 2012, **48**, 10568-10570.
- 7 K. Miyaura, Y. Miyata, B. Thendie, K. Yanagi, R. Kitaura, Y. Yamamoto, S. Arai, H. Kataura and H. Shinohara, *Sci. Rep.*, 2018, **8**, 2-7.
- 8 R. M. Osuna, M. C. Ruiz Delgado, V. Hernández, J. T. López Navarrete, B. Vercelli, G. Zotti, J. J. Novoa, Y. Suzuki, S. Yamaguchi, J. T. Henssler and A. J. Matzger, *Chem. Eur. J.*, 2009, **15**, 12346-12361.
- 9 M. Tateno, M. Takase, M. Iyoda, K. Komatsu and T. Nishinaga, *Chem. Eur. J.*, 2013, **19**, 5457-5467.
- 10 A. Rajca, H. Wang, M. Pink and S. Rajca, *Angew. Chem. Int. Ed.*, 2000, **112**, 4655-4657.
- 11 A. Rajca, M. Miyasaka, M. Pink, H. Wang and S. Rajca, *J. Am. Chem. Soc.*, 2004, **126**, 15211-15222.
- 12 J. K. Zak, M. Miyasaka, S. Rajca, M. Lapkowski and A. Rajca, *J. Am. Chem. Soc.*, 2010, **132**, 3246-3247.
- 13 C. Biot, W. Castro, C. Y. Botté and M. Navarro, *Dalton Trans.*, 2012, **41**, 6335-6349.
- 14 D. K. Maity, *J. Am. Chem. Soc.*, 2002, **124**, 8321-8328.

Thesis Highlight

Name of the Student: Shri Rahul Kumar

Name of the CI/OCC: Bhabha Atomic Research centre **Enrolment No.:** CHEM01201404024

Thesis Title: Theoretical studies on selected organic chalcogen systems

Discipline: Chemical Sciences

Sub-Area of Discipline: Theoretical chemistry

Date of viva voce: 27th May, 2020

Chalcogens (S, Se, and Te) based systems are widely used in organic electronics and medicinal chemistry. This work reports the in-depth studies on selected chalcogens based organic systems using electronic structure theory-based calculations. It includes the chalcogen based flexible π -conjugated helical systems which may be important in future as organic optoelectronic devices. The work also provides a model system to find suitable antioxidant based on diaryl dichalcogenides radical anions. The theoretical calculations predict that the thia[n]helicenes systems become helical when the number of thiophene rings are three or more. HOMO-LUMO energy gap decreases as the number of thiophenes ring increases.

Further, band gap calculated applying periodic boundary conditions (PBC) for neutral thia[n]helicenes shows that band gap decreases as the number of thiophene rings increases. Excited-state studies show that the radical cations generated from thia[n]helicenes have strong absorption in near infrared region (NIR) region (see Figure 1a). A case study

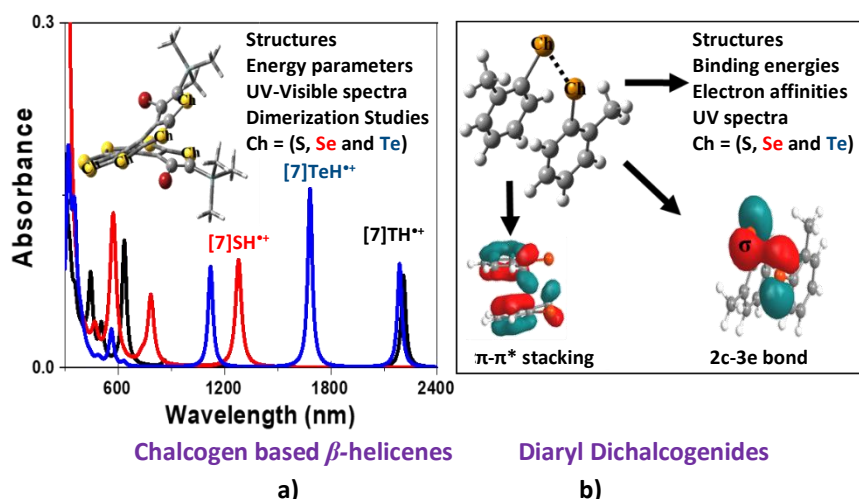


Figure 1. a) Comparison of the UV-visible spectra of [7]TH^{•+}, [7]SH^{•+} and [7]TeH^{•+} in DCM solvent, and b) Equilibrium structure of (o-CH₃Ph-Ch)₂^{•-} and MO diagrams showing 2c-3e bond and π - π stacking of aromatic rings.

on unsubstituted thia[7]helicene radical cation shows that the radical cation generated from its corresponding neutral thia[7]helicene system has a very low probability of dimerization in non-polar solvent. This dimerization probability is further reduced in the presence of counter ion PF₆⁻. Similar studies are extended to Se and Te based β -helicenes.

The present thesis also reports studies on effect of an excess electron on geometry, nature of bonding and stability of diaryl dichalcogenides, namely, (RCh)₂^{•-} (Ch = S, Se & Te; R : Ph, PhCH₂, o-NO₂-Ph, o-HO-Ph, & O-CH₃-Ph,) radical anions. One electron reduction of neutral diaryl dichalcogenides leads to the formation of two-center three-electron (2c-3e) bonded radical anionic systems (see Figure 1b). These diaryl dichalcogenides radical anions show π - π stacking of two phenyl rings in water medium. These systems have high electron affinity in water medium and their corresponding neutral systems have a strong ability to capture electron efficiently suggesting their antioxidant property. Overall, this work presents an exhaustive theoretical study on these complex organic chalcogen systems.